Modeling Alternating Hemiplegia of Childhood with iPSC-Derived Neurons

By

John Patrick Snow

Dissertation

Submitted to the Faculty of the

Graduate School of Vanderbilt University

in partial fulfillment of the requirements

for the degree of

DOCTOR OF PHILOSOPHY

in

Cell and Developmental Biology

May 31, 2020

Nashville, Tennessee

Approved:

Kevin C. Ess, M.D., Ph.D.

Ian Macara, Ph.D.

Aaron B. Bowman, Ph.D.

Vivian Gama, Ph.D.

Ethan Lee, M.D., Ph.D.

ACKNOWLEDGEMENTS

The majority of this work was supported by funding from the Alternating Hemiplegia of Childhood Foundation (to KCE). Additional funding was provided by Association Française de l'Hémiplégie Alternante (to KCE), the Vanderbilt Institute for Clinical and Translational Research (VR52630 pilot grant to JPS), and Public Health Service award T32GM007347 from the National Institute of General Medical Studies for the Vanderbilt Medical Scientist Training Program.

I would like to thank my research mentor, Kevin Ess, for his guidance in my research endeavors and support in career development, all while encouraging productivity and positivity during my graduate school experience. Thank you to the researchers and clinicians I also consider mentors in medicine and science during my graduate school years: Rob Carson, Cary Fu, Al George, Howard Kirshner, and Diana Neely. I would like to thank current and former members of the Ess, Fu, Carson, and Bowman laboratories for keeping my experiments going if I was out of lab and encouraging me to be a better student and researcher, particularly: Grant Westlake, Brittany P. Short, Christine Simmons, Mark Grier, Laura Armstrong, Lindsay Klofas, Anna Pfalzer, and Mary Chalkley.

Thank you to my undergraduate scientific mentors including Bruce Carter and Brad Kraemer for instilling in me sound research approaches and motivations. To the undergraduate students I have worked with throughout my graduate school years, thank you for your contribution to my science and training, and thank you for always being interested and engaged in the work we were performing. I hope you continue finding passion and success in your research endeavors in the years to come.

To my committee listed on the title page, thank you for your engagement in my graduate school training and willingness to share and collaborate in experiments and ideas. I truly appreciate your collective guidance and thoughtful challenges to my research approaches, data collection, and analyses. I would like to thank the present and past leadership and administers of the Vanderbilt Medical Scientist Training Program (MSTP), Department of Cell and Developmental Biology (CDB), and Program in Developmental Biology (PDB) along with my classmates, collaborators, and colleagues. These groups have provided an incredible and diverse community for a growing physician scientist throughout my training.

Thank you to the AHC patient, family, and research communities for continual inspiration and motivation as progress towards a cure continues. Finally, thank you to my friends, family, and fiancée for your encouragement, laughter, support, and understanding over the past five years.

TABLE OF CONTENTS

LIST OF TABLES

Page

SUPPLEMENTAL TABLES

LIST OF FIGURES

Page

SUPPLEMENTAL FIGURES

LIST OF ABBREVIATIONS

AHC	Alternating hemiplegia of childhood
ASD	Autism spectrum disorder
CAPOS	Cerebellar ataxia, areflexia, pes cavus, optic nerve atrophy, sensorineural hearing loss
CBD	Cannabidiol
COS	Child onset schizophrenia
CRISPR	Clustered regularly interspaced short palindromic repeats
CSF	Cerebrospinal fluid
ECAR	Extracellular acidification rate
eCB	Endocannabinoid
EEG	Electroencephalography
EIEE	Early infantile epileptic encephalopathy
ESC	Embryonic stem cell
FIPWE	Fever-induced paroxysmal weakness and encephalopathy
gNDM	GABAergic neural differentiation media
iPSC	Induced pluripotent stem cell
mcNDM	Mixed cortical neural differentiation media
MEA	Microelectrode array
MELAS	Mitochondrial encephalopathy, lactic acidosis, and stroke-like episodes
MRI	Magnetic resonance imaging
NIM	Neural induction media
NKA	Na^+, K^+-ATPase ion transporter
NMM	Neural maintenance media
NPC	Neural progenitor cell
OCR	Oxygen consumption rate
oRG	Outer radial glia
RDP	Rapid onset dystonia-parkinsonism
RECA	Relapsing encephalopathy with cerebellar ataxia
SERCA	Sarcoplasmic / endoplasmic reticulum calcium ATPase
TALEN	Transcription activator-like effector nuclease
vRG	Ventricular radial glia
VZ	Ventricular zone
wMFR	Weighted mean firing rate
ZFN	Zinc finger nuclease

INTRODUCTION

Alternating hemiplegia of childhood (AHC) is a rare and devastating neurodevelopmental disorder caused by heterozygous missense mutations in *ATP1A3*, the gene encoding the α3 subunit of the Na,K-ATPase (NKA) ion transporter (Heinzen et al., 2012). The NKA complex is responsible for exchanging three cytoplasmic sodium ions for two extracellular potassium ions, thus establishing electrochemical gradients essential for crucial cellular functions and membrane potential (Benarroch, 2011; Clausen et al., 2017; Dobretsov and Stimers, 2005). Patients with AHC present early in life with a constellation of symptoms including abnormal eye movements, seizures, dystonia, and characteristic spells of alternating hemiplegia or full "bilateral" quadriplegia (Bourgeois et al., 1993; Heinzen et al., 2014). Episodes in AHC are often triggered by external stimulation including temperature changes, physical exertion, or exposure to certain foods, among other triggers (Kansagra et al., 2013; Sweney et al., 2009). Over time, AHC patients manifest developmental delay and acquire intellectual disabilities.

AHC is the best studied to date of an expanding spectrum of neurological conditions associated with *ATP1A3* mutations (Sweney et al., 2015), including RDP (rapid-onset dystonia parkinsonism), CAPOS (cerebellar ataxia, areflexia, pes cavus, optic nerve atrophy, and sensorineural hearing loss), RECA (relapsing encephalopathy with cerebellar ataxia), EIEE (early infantile epileptic encephalopathy), and FIPWE (fever-induced paroxysmal weakness and encephalopathy) (de Carvalho Aguiar et al., 2004; Demos et al., 2014; Heinzen et al., 2014; Paciorkowski et al., 2015; Rosewich et al., 2014b). While these syndromes share symptomatic profiles including triggered episodes, strong genotype-to-phenotype correlations exist within this spectrum. In fact, 60% of patients worldwide diagnosed clinically as AHC have one of three unique heterozygous missense mutations in *ATP1A3*, leading to amino acid changes D801N, E815K, or G947R in the NKA-α3 subunit (Heinzen et al., 2012; Viollet et al., 2015). Unfortunately, only symptomatic and anecdotal treatment options exist for patients diagnosed with AHC, including benzodiazepines, antiepileptic drugs, and other agents.

While the NKA-α1 subunit is ubiquitously expressed across cell types, expression of the NKA-α3 subunit is generally restricted to neurons (Clausen et al., 2017; Richards et al., 2007). A critical component of neuronal functionality, the α3 subunit has a comparably lower affinity for sodium ions allowing the rapid expulsion of positive ions following neuronal activity and depolarization, particularly in dendrites and axons (Azarias et al., 2013; Blom et al., 2011; Kim et al., 2007). Common AHC-causing mutations in the α3 subunit result in impaired ion transporting ability without impacting protein trafficking to the plasma membrane (Heinzen et al., 2014; Koenderink et al., 2003; Li et al., 2015). Recent studies have demonstrated the ability to model *ATP1A3*-related diseases including AHC using animal models, often using external stressors to trigger phenotypes. Unfortunately, data from human-based model systems remain sparse (DeAndrade et al., 2011; Helseth et al., 2018; Holm and Lykke-Hartmann, 2016; Isaksen et al., 2017; Palladino et al., 2003; Simmons et al., 2018; Sugimoto et al., 2014).

To better understand the impacts of AHC-causing mutations on human neurons, we generated a patient-specific induced pluripotent stem cell (iPSC)-derived neuronal model of disease. First, fibroblasts collected from control and AHC patients were induced to pluripotency. CRISPR/Cas9 genetic editing technology was employed to create isogenic corrected iPSC clones to be used in parallel with unrelated wildtype controls to increase the confidence in our findings. Lineage-specific iPSC-derived cortical neurons generated from patient and control iPSCs were then used to study AHC pathophysiology, phenotypes, and potential treatment approaches *in vitro*. The following chapters explore what we have learned from our patient specific iPSC-derived neuronal model of AHC. Chapter I will discuss the current understanding of AHC clinical presentation, pathophysiology, treatment options, and disease modeling within the laboratory setting. Chapter II provides the methods, validation, and experimental rationale for the iPSC-derived

neuronal model used in the majority of this work. Chapter III describes our findings of NKA-subunit protein and RNA expression in this disease model, along with exploration of a trigger-induced hyperactivity phenotype and the impact of a commonly used drug for AHC, flunarizine, on this model. Chapter IV details the search for other phenotypes within this model system and its application for the study of alternative treatment routes and rationale in AHC. Chapter V catalogues our attempts to generate a more specific NKA-α3 antibody for use in field of *ATP1A3*-related diseases. Finally, Chapter VI will summarize our findings and provide a broader context for what the implications of this work mean in the development of future research directions and translational studies.

CHAPTER I

ALTERNATING HEMIPLEGIA OF CHILDHOOD: PRESENTATION, PATHOPHYSIOLOGY, AND DISEASE MODELING

Clinical Characteristics and Natural History of AHC

Alternating hemiplegia of childhood (AHC) is a rare neurodevelopmental disease initially described in 1971 by a case report detailing eight patients with "an unusual symptom complex of intermittent, alternating hemiplegia" (Verret and Steele, 1971). While still an early report of AHC, the symptomatic profile outlined by Verret and Steele has generally held true for today's diagnostic criteria. All eight patients described had symptoms beginning in early childhood, often appearing before the age of one. Hemiplegic spells, or weakness involving one side of the body, began in these patients following a brief prodrome and lasted from several hours to days, alternating from one side of the body or the other. Structural abnormalities were absent on imaging and while electroencephalogram (EEG) data showed no consistent abnormalities, seizures were common. The authors reported that although the hemiplegic spells were less frequent with aging, "residual neurological signs" including neurodevelopmental delay and dystonia became fixed. At the time, these symptoms were considered a complication of migraine or unappreciated vascular abnormalities. During the ensuing decade, subsequent case reports continued to build the clinical profile of children with alternating hemiplegia and associated symptoms as a migraine subtype (Golden and French, 1975; Hockaday, 1979; Hosking et al., 1978).

In 1980, Krageloh and Aicardi focused the diagnostic criteria and importantly isolated a separate syndrome from migraine in a case report of 5 individuals with symptoms characteristic of AHC. By tracing common characteristics from the previous reports, the authors concluded that "alternating hemiplegia in infants constitutes a clinically well-defined and easily recognizable syndrome" (Krageloh and Aicardi, 1980). After considerably increasing the patient population being characterized, a condensed list of more clear diagnostic criteria defining this condition was outlined in 1993. The seven diagnostic criteria now known eponymously as "Aicardi Criteria" (**Table 1.1**) and include: symptom onset before 18 months of age, repeated attacks of alternating hemiplegia including one or both sides of the body, other paroxysmal or autonomic symptoms including dystonia or oculomotor abnormalities, episodes of bilateral hemiplegia or quadriplegia, improvement of symptoms with sleep and recurrence upon awakening, evidence of developmental delay or other neurologic abnormalities, and the absence of symptom attribution to other disorders (Brashear et al., 2018; Masoud et al., 2017; Sweney et al., 2009). While atypical profiles are not uncommon, the majority of patients fall completely within these criteria.

Table 1.1: Updated Aicardi Diagnostic Criteria for Alternating Hemiplegia of Childhood

1	Symptom onset prior to 18 months of age
2	Repeated attacks of hemiplegia involving one or both sides of the body
3	Other paroxysmal symptoms including autonomic disturbances or dystonia
4	Episodes of bilateral hemiplegia or quadriplegia
5	Improvement of symptoms with sleep and recurrence upon awakening
6	Developmental delay or other neurologic abnormalities
7	Absence of another causative disease

In 2000, Mikati and colleagues further described a larger group of AHC patients and defined three phases involved in the natural history of disease. The first phase of disease is characterized by abnormal eye movements and dystonia, which are common initial symptoms in AHC patients. In fact, the most frequent symptoms at presentation across several recent cohort studies included abnormal ocular movements (80%) and dystonia (60%) while hemiplegic events were less common at initial diagnosis. These presenting symptoms were commonly present within the first 3 months of life, often in the early neonatal period. The second phase of disease includes the beginning of hemiplegic spells and often a loss of developmental milestones during early childhood. Seizures become a common and devastating symptom in up to half of AHC patients. The third phase of disease occurs around in mid-childhood and is described by a decrease in the frequency of hemiplegic and dystonic attacks, but the persistence of developmental delay and other neurological abnormalities. Ataxia and cognitive impairment are present in close to 100% of patients. (Kansagra et al., 2013; Mikati et al., 2000; Sweney et al., 2009). AHC patients also experience neuropsychiatric symptoms including deficits in language, memory, and attention, along with increased impulsivity and other behavioral disorders (Neville and Ninan, 2007; Panagiotakaki et al., 2015; Shafer et al., 2005; Sweney et al., 2009). Although the frequency of AHC has been estimated at 1 in 1,000,000 births, this number may be artificially suppressed by variability in symptomatic presentation, difficulty of initial diagnosis, and lack of disease awareness (Neville and Ninan, 2007).

The clinical evaluation for patients presenting with this symptomatic profile should involve an initial diagnostic workup to exclude alternative diagnoses. Brain magnetic resonance imaging (MRI) studies generally show normal appearing tissue and vascular anatomy or nonspecific changes with the absence of a clear pathology relating to other neurodevelopmental disorders. A minority of AHC patients with severe symptoms may have developmental brain abnormalities on an initial MRI including diffuse polymicrogyria, while imaging in other patients can demonstrate cerebellar, cerebral, or hippocampal atrophy years after presentation (Ghusayni et al., 2020; Sasaki et al., 2017; Severino et al., 2020). While many patients have seizures, EEG studies acquired during hemiplegic events or at baseline are normal and do not provide alternative explanations for symptoms. CSF assessment, muscle biopsy samples, and metabolic studies are generally normal or nonspecific (Brashear et al., 2018; Kansagra et al., 2013; Vila-Pueyo et al., 2014). Even with a clearly defined symptomatic profile, patients presenting with these symptoms and their families are often subjected to a long and complex diagnostic journey prior to official diagnosis. Sweney et al. (2009) report that around 15% of patients in their large study were over three years of age before a diagnosis of AHC was considered, although that number has improved compared to previous decades.

AHC symptoms emerge similarly to those of other neurodevelopmental conditions, further complicating the diagnostic process. Complicated migraines can present with weakness in extremities but are not usually accompanied by developmental delay in children. If the dominant symptom profile in an AHC patient includes seizures, epileptic conditions are often considered before AHC. While some epileptic patients experience limb weakness and dystonia, these symptoms do not improve in AHC patients following treatment with antiepileptic drugs. Moyamoya disease and other vascular conditions can mimic some symptoms of alternating hemiplegia but are associated with pathologic findings on imaging. Certain mitochondrial diseases including pyruvate dehydrogenase deficiency and mitochondrial encephalopathy with lactic acidosis and stroke-like episodes (MELAS) can also share symptomatic profiles with AHC but have clear pathological correlates on brain imaging. Other genetic causes on the differential may include inborn errors of neurotransmitter biosynthesis and metabolism, familial hemiplegic migraine, and other hereditary ataxias (Brashear et al., 2018; Kansagra et al., 2013; Sweney et al., 2009).

Causative *ATP1A3* Mutations in AHC and Related Diseases

In recent years, the continued revolution of cost-effective genomic testing has resulted in the etiologic characterization of numerous neurodevelopmental diseases and other genetic conditions. Through

independent studies, Heinzen et al. (2012) and Rosewich et al. (2012) almost simultaneously published findings of heterozygous missense mutations in the *ATP1A3* gene causing the majority of AHC cases. This gene encodes the α3 subunit of the sodium-potassium ATPase ion transporter (NKA-α3), a protein crucial to neuronal function. Heinzen et al. reported on 82 patients with typical AHC, identifying 19 unique heterozygous mutations in *ATP1A3*, generally *de novo* in origin. In total, 74% of patients clinically diagnosed as AHC in this study had confirmed mutations in *ATP1A3* on analysis. Rosewich et al. described such mutations in all of the 24 unrelated AHC patients they studied. A follow up study by Yang et al. (2014) confirmed these findings in a separate analysis of 47 AHC patients. Three mutation "hotspots" become obvious from these studies, including mutations causing D801N, E815K, and G947R protein variants, in total making up at least half of AHC patients depending on the population studied (Capuano et al., 2020; Heinzen et al., 2012; Panagiotakaki et al., 2015; Rosewich et al., 2012; Yang et al., 2014). A retrospective analysis of the AHC Foundation (AHCF) Registry in the United States (Viollet et al., 2015) further described causative mutations in a larger population. Out of 187 AHC patients, a mutation in *ATP1A3* was reported in 154 patients (82%). In general, mutations clustered around exons 17 and 18 of the *ATP1A3* gene, and the larger cohort highlighted the same protein variants as the most common recurrent hotspots including D801N (58 patients, 40%), E815K (38 patients, 26%), and G947R (11 patients, 8%).

Within these common mutation groupings, some phenotypic trends have been reported across multiple publications. Ishii et al. (2013) first reported in a small cohort that the E815K mutation was associated with a more severe phenotype than the D801N variant and other missense mutations in their study group. Patients with the E815K mutation in *ATP1A3* experienced more severe neurological symptoms including respiratory failure and status epilepticus. A larger follow-up study by Sasaki et al. (2014) solidified these results, confirming that the E815K mutation was described by earlier symptomatic onset in the neonatal period, more significant changes to motor function, increased frequency of status epilepticus, and higher rates of respiratory failure. While many patients with the D801N mutation were able to walk without assistance during the study period (7/10 individuals), none of the E815K patients (0/12) were able to achieve this milestone. Viollet et al. (2015) repeated a similar analysis in the AHCF Registry cohort and also reported a more severe phenotype in the E815K group including earlier age of onset, more severe motor impairment, and a higher frequency and prevalence of status epilepticus. Across these reports, patients harboring the G947R mutation often segregate into a phenotype comparable to D801N patients rather than the more severe E815K group. While these trends of genotype-to-phenotype correlations have become apparent, it is important to also note that each patient's case is individual and there is significant overlap between phenotypic profiles of each mutation site (Ishii et al., 2013; Sasaki et al., 2014; Viollet et al., 2015).

Although *ATP1A3* variants can be found in the majority of AHC patient cases (>80%), there is nevertheless a subset of clinically diagnosed patients with no identifiable mutations in this gene. While sequencing errors in the presence of duplications or microdeletions could result in an initial negative result, newer screening modalities nonetheless identify *ATP1A3* mutation-negative cases. Often, these are assumed to classify into another monogenic *de novo* disorder and patients will receive further targeted genetic tests to assess for an alternate diagnosis of familial hemiplegic migraine, episodic ataxia, or other related conditions. Common genes investigated include *CACNA1A*, *ATP1A2*, *EAAT1*, *SLC2A1*, and *SCN1A*. While these tests may be revealing for some patients and families, there is often a lack of etiologic clarity even after continued testing (de Vries et al., 2008; Jen et al., 2005; Rosewich et al., 2014a; Viollet et al., 2015; Vuillaumier-Barrot et al., 2010).

The association of *ATP1A3* mutations with striking neurological conditions was not new at the time of its discovery as causative in AHC. Over the past two decades, genetic testing has revealed a continually expanding spectrum of *ATP1A3*-related diseases (**Table 1.2**). While these diseases share common profiles including triggered symptoms, there is a very strong genotype-to-phenotype correlation where recurrent

mutations very close in the genetic sequence and protein structure result in strikingly unique phenotypes. Although these diseases share a common genetic etiology, their overlapping descriptions can pose a diagnostic challenge for even experienced pediatric neurologists (Dard et al., 2015; Heinzen et al., 2014; Mencacci, 2016; Paciorkowski et al., 2015).

Table 1.2: ATP1A3 Associated Diseases

Disease Acronym	Full Disease Name	Age of Onset	Symptomatic Profile	Associated *ATP1A3* Mutations
EIEE	Early infantile epileptic encephalopathy	Neonatal	Epilepsy, prolonged apnea, microcephaly, severe developmental disability	G358V, I363N E815K
AHC	Alternating hemiplegia of childhood	< 18 months	Ocular abnormalities, hemiplegic events, dystonia, seizures, autonomic changes, ataxia, developmental delay	D801N, E815K, G947R
CAPOS	Cerebellar ataxia, areflexia, pes cavus, optic atrophy, sensorineural hearing loss	> 6 months	Ataxia, dystonia, visual impairment, symmetric flaccid paresis, disturbances of consciousness	E818K
FIPWE	Fever-induced paroxysmal weakness and encephalopathy	Childhood	Infrequent fever-induced symptoms with slow improvement but persistent neurological deficits, sometimes with stepwise regression	R756H; R756L
RECA	Relapsing encephalopathy with cerebellar ataxia	Childhood	Acute trigger-related onset of encephalopathy and paroxysmal ataxia	R756C
RDP	Rapid onset dystonia parkinsonism	Early Adulthood	Abrupt onset of permanent dystonia and other parkinsonian features after a stressful trigger	T613M

Rapid onset dystonia-parkinsonism (RDP) was the first of these diseases associated with mutations in *ATP1A3*. In 2004, de Carvalho Aguiar and colleagues reported six unique mutations in *ATP1A3* across seven unrelated families with RDP. In subsequent studies, it has become clear that although many mutation sites across *ATP1A3* can result in RDP, the T613M heterozygous missense mutation is most common and can occur in both *de novo* and familial cases. Symptomatic individuals within these families generally present between the ages of 15 and 45, with studies confirming that the majority of patients present in young adulthood. Diagnostic criteria include the acute onset of dystonia with parkinsonian features, a generally rostro-caudal gradient of symptom evolution, prominent bulbar findings, symptom unresponsiveness to L-dopa administration, and often a family history of similar symptoms. Many of these patients experience symptom onset following a trigger event that may include excessive exercise, childbirth, alcohol binges, or significant emotional stress. Symptoms may stabilize within a month or so of onset, but fixed neurological deficits remain with minimal improvement over time. Nonmotor aspects of RDP include a high prevalence of mood disorders and other neuropsychiatric conditions, with some impairment in memory and learning compared with control groups (Brashear et al., 2018; de Carvalho Aguiar et al., 2004; Heinzen et al., 2014; Sweney et al., 2015).

AHC as described above was associated with *ATP1A3* mutations in 2012 with studies by Heinzen et al. and Rosewich et al. The three most common mutations associated with AHC remain D801N, E815K, and G947R. Compared to RDP, AHC patients present by definition before the age of 18 months with a unique constellation of symptoms. Although triggers such as fever, infection, medications, excessive stimulation, and water exposure play a key role in symptomatic expression and hemiplegic spell frequency, it is not commonly reported that triggers initiate the first onset of symptoms as seen in RDP (Sweney et al., 2015). Intriguingly, many AHC patients experience symptomatic improvement upon sleeping though can relapse within the minutes after awakening. Whereas RDP tends to stabilize over time, AHC patients and families often experience a frustrating "waxing and waning" of symptom severity and frequency throughout early childhood. Impaired cognition along with behavioral disorders become more dominant and clinically concerning symptoms of AHC by late childhood and adolescence, though there is often a reduction in hemiplegic spells (Brashear et al., 2018; Heinzen et al., 2014).

First described clinically in 1996, CAPOS (cerebellar ataxia, areflexia, pes cavus, optic atrophy, and sensorineural hearing loss) was associated with mutations in *ATP1A3* in 2014. The limited number of children presenting with this disease have sought care between six months and five years of age after presenting with symptoms following a febrile illness with recurrent fever-related episodes of ataxia and neurological deterioration including altered awareness. The *ATP1A3* variant associated with CAPOS in all reported cases is a recurring *de novo* heterozygous missense mutation, E818K, that can subsequently be passed to offspring in an autosomal dominant pattern (Demos et al., 2014). While CAPOS patients present with a specific constellation of symptoms compared to AHC and RDP, it is clear that the genetic variants involved, the abrupt onset of symptoms, and trigger-associated phenotypic expression connect these unique diseases.

A severe form of *ATP1A3*-associated disease, early infantile epileptic encephalopathy (EIEE) has been reported in a number of cases over the past several years and can be traced to heterozygous mutations in *ATP1A3* causing G358V and I363N variants of the NKA-α3 subunit. These patients have catastrophic seizures in the neonatal period along with apneic events, microcephaly, and significant developmental disability. Prolonged periods of ventilation and other severe clinical interventions are necessary to maintain survival as a result of these symptoms. While seizures are rare in RDP, some AHC patients present with neonatal seizures before the condition evolves to a more classic symptomatic profile with hemiplegic events (Paciorkowski et al., 2015). Seizures are especially common and more severe in the E815K subgroup of AHC patients, as noted above.

Fever-induced paroxysmal weakness and encephalopathy (FIPWE) and relapsing encephalopathy with cerebellar ataxia (RECA) are newly introduced clinical descriptions within the spectrum of *ATP1A3*-associated disease. Both FIPWE and RECA are strongly if not exclusively related to mutations at the R756 residue of the NKA-α3 protein in the limited amounts of case reports published to date. FIPWE presents in childhood with fever-triggered episodes of encephalopathy and weakness associated with "slowly improving but persistent deficits" (Yano et al., 2017). While some FIPWE patients have near-normal neurological function, others experience stepwise regression resulting in persistent dysphagia, cognitive deficits, and severe ataxia. RECA is characterized in pediatric patients by recurring periods of hypotonia and ataxia triggered by febrile episodes. Most individuals present with symptoms before the age of 5 years old, although initial presentation in adulthood is possible. In RECA patients, there is often a familial history of similar fever-triggered ataxia (Dard et al., 2015; Sabouraud et al., 2019). Compared to AHC, the dominant and consistent symptoms in these two unique syndromes are recurrent fever-triggered ataxia and encephalopathy with a subsequent finding of an R756 variant. These symptoms can resemble those seen with mitochondrial oxidative phosphorylation defects and thus can result in extended diagnostic journeys for patients and families.

With whole genome sequencing and whole exome screening being performed more commonly in hospitals and laboratories around the world, new associations of *ATP1A3* with various diseases are becoming increasingly more frequent. Recent reports highlight the connection of *ATP1A3* variants with neuropsychiatric conditions including both adult-onset and childhood-onset schizophrenia (COS) (Chaumette et al., 2018; Purcell et al., 2014; Smedemark-Margulies et al., 2016) along with genetic risks involving *ATP1A3* and associated protein subunit genes for autism spectrum disorder (ASD) (Takata et al., 2018; Torres et al., 2018). Intriguingly, patients with *ATP1A3*-variant-associated COS or ASD can present with motor impairments in addition to the more common symptoms of the diagnosed neurodevelopmental condition (Shrivastava et al., 2018). Impaired cellular energetics, oxidative stress, and disease-related inhibition or downregulation of the NKA-α3 subunit may also play a part in neurodegenerative conditions, including Alzheimer's and Parkinson's disease (Ohnishi et al., 2015; Shrivastava et al., 2015; Shrivastava et al., 2019). Undoubtedly, the role of *ATP1A3* mutations resulting in NKA-α3 subunit dysfunction is likely underappreciated in areas outside of the "classical" *ATP1A3*-related disease spectrum.

A further discussion of RDP, CAPOS, and other non-AHC *ATP1A3*-associated diseases remains outside the scope of this text. However, it is important to note that mechanistic interrogation and therapeutic discovery in the central *ATP1A3* spectrum disorder AHC may provide important insights into related conditions, including for disorders and treatment approaches yet to be associated with *ATP1A3* and the NKA-α3 protein. As noted in a 2018 commentary, "Assigning overly exact phenotype-genotype relationships could promote inaccurate interpretation of the overlapping phenotypes within the broad phenotypic spectrum of *ATP1A3*-related disorders" (Sival et al., 2018). Indeed, while this document will serve as an investigation of specific mutations in an *in vitro* disease model of AHC, it is important to interpret findings and conclusions in the full setting of *ATP1A3* disease.

AHC Treatment Approaches and Prognosis

Parents of AHC patients report a variety of triggers that may induce spells in their children. While commonly shared circumstances may trigger hemiplegic events, seizures, or dystonia in multiple patients, each case often presents a unique profile. Reported triggers in AHC include extreme stress or excitement, bright lights, heat or cold, bathing or swimming, food dyes, strenuous exercise, illness and fever, or irregular sleep patterns (Heinzen et al., 2014; Kansagra et al., 2013). While avoidance is recommended to reduce events, strict adherence to these instructions is often impossible given the diverse and sometimes random nature of trigger characteristics. Notably, a clear juxtaposition exists between symptomatic exacerbation with stressful triggers and subsequent resolution upon sleeping that may provide pathophysiological clues and potential treatment routes for clinicians and researchers. The prognosis for individuals diagnosed with AHC remains poor given the lack of disease-specific treatment options. Genotype-phenotype correlations have been reported suggesting that individuals with the G947R mutation have a more favorable prognosis than patients with D801N and E815K, although each patient presents a unique case (Panagiotakaki et al., 2015). The natural course of the disease includes decreased frequency of hemiplegic attacks and abnormal ocular movements over time, while developmental delay and neurological disabilities tend to remain constant with age. Sudden death can occur in a minority of patients with severe episodes and seizures, although many individuals live into adulthood with persistent neurological deficits (Kansagra et al., 2013; Panagiotakaki et al., 2010).

Management of AHC includes treatment of acute disease manifestations and prevention of symptom onset and exacerbation. Acute symptoms such as seizures and dystonia are often treated with standard antiepileptic drugs including benzodiazepines, while muscle relaxants provide relief for dystonic pain. Some medications including chloral hydrate and phenobarbital can be utilized during AHC associated events to induce sleep and temporarily resolve acute symptoms. Motor phenotypes in AHC and other

ATP1A3-related diseases are generally not responsive to classic Parkinsonian treatments such as levo-dopa. Physical therapy for ataxia and neuropsychiatric interventions for developmental disabilities and behavioral and mood disturbances are frequently used to the benefit of patients and families (Brashear et al., 2018; Kansagra et al., 2013; Sweney et al., 2015).

Given the unique presentation of AHC patients, various pharmacologic approaches have been attempted as prophylaxis for hemiplegic spells. The most common prophylactic treatment for primary manifestations of AHC is flunarizine, a nonspecific sodium and calcium channel antagonist that has been reported for decades in uncontrolled studies to reduce hemiplegic attack frequency and severity. Since an original investigation in 1987 of 12 patients, flunarizine has been labeled "the first truly promising drug" in AHC (Casaer, 1987). Previous reports have documented flunarizine efficacy in epilepsy and migraine, but definitive mechanisms and the impact on AHC-specific symptoms remains controversial. While some patients report improvement following flunarizine administration, many do not see significant changes to episode burden (Bourgeois et al., 1993; Pisciotta et al., 2017; Sasaki et al., 2001; Silver and Andermann, 1993; Sweney et al., 2015). Another migraine-associated voltage-dependent sodium channel blocker, topiramate, has also been reported as a successful prophylactic treatment option in AHC, but lacks the depth of investigation seen with flunarizine (Aishworiya et al., 2011; Jiang et al., 2006; Kasinathan et al., 2017). Anecdotal trials of other drugs including niaprazine, SSRIs, gabapentin, acetazolamide, cyproheptadine, haloperidol, coenzyme Q, nifedipine, melatonin, olanzapine, carnitine, cannabidiol, and oral ATP administration have been reported briefly by investigators without consistent rationale or efficacy (Ju et al., 2016; Kansagra et al., 2013; Pisciotta et al., 2017). Non-pharmacologic interventions including ketogenic diet trials have gained recent popularity and are being promoted as potential prophylactic treatments for AHC episodes, but have yet to be studied on a large enough scale to yield reproducible or broadly actionable changes to treatment guidelines (Roubergue et al., 2015).

Na,K-ATPase Basics: Structure, Function, and Physiology

The majority of AHC cases are caused by mutations in *ATP1A3*, a gene which encodes the α3 subunit of the sodium (Na^+), potassium (K^+)-adenosine triphosphatase ion transporter (Na,K-ATPase, NKA). The NKA complex is an integral protein across all cell types. This transporter actively shuttles three sodium ions from the cytoplasm to the extracellular space in return for two potassium ions thus completing a charge translocation process against ionic concentration gradients (**Figure 1.1A**). The NKA is so crucial to membrane biology that in some active brain regions the energetic requirements of this protein complex alone can be over half of an entire cell's energy usage (Attwell and Laughlin, 2001; Shrivastava et al., 2018). Transport of ions by the NKA pump is powered by hydrolysis of an ATP molecule and occurs in a well characterized sequence of events known as the Post-Albers cycle (**Figure 1.1B**). This process is critical for many cellular functions including the establishment and maintenance of a negative membrane potential, the control of cell volume and osmotic balance, and the regulation of ion gradients necessary to drive various types of ion-coupled transporters (Albers, 1967; Kaplan, 2002; Pivovarov et al., 2018; Post et al., 1972). The discovery and initial investigation of the Na,K-ATPase culminated in the awarding of the 1997 Nobel Prize in Chemistry to Danish researcher Jens Skou and collaborators studying ATPase enzymes (Clausen and Persson, 1998; Skou, 1957). This section will briefly discuss the normal function and localization of Na,K-ATPase subunits and how each major isoform is involved in human disease.

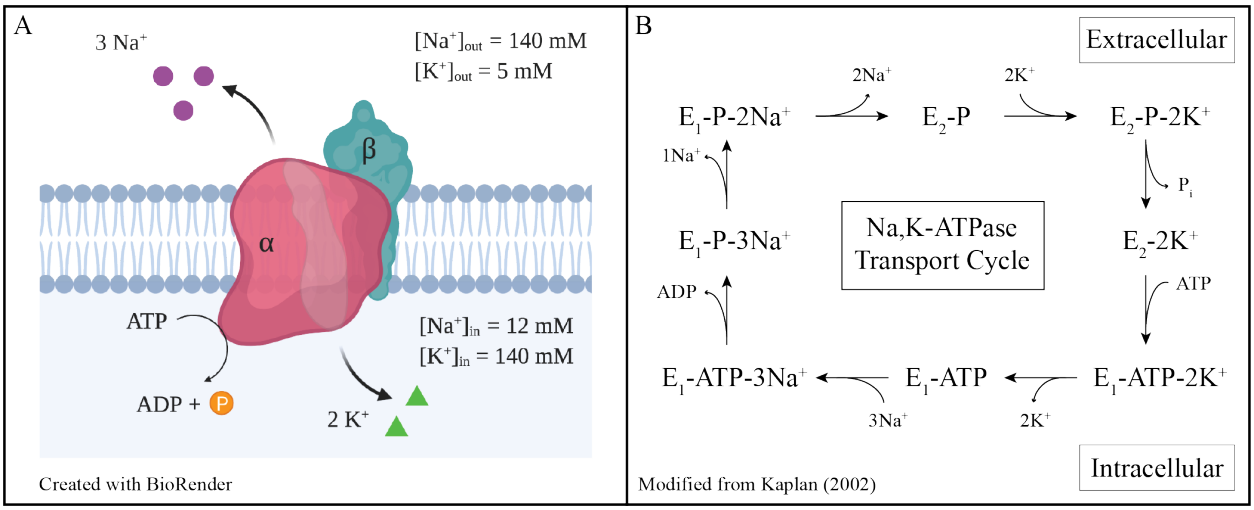

Figure 1.1: Na,K-ATPase Ion Transport and the Post-Albers Cycle. The NKA pump functions to actively transport three sodium ions into the extracellular space while returning two potassium ions (A). This imbalance in charged ion transport along with membrane permeability characteristics establish a negative resting membrane potential and maintain ionic gradients necessary for biological viability and proper cellular function. The NKA-α subunit (red) hydrolyzes one molecule of ATP per full transport cycle to bind and shuttle ions via internal transmembrane domains. The associated β-subunit (blue) is necessary for proper membrane localization and functional fine-tuning of catalytic rate and ion affinities, but does not play a direct role in ion transport. The complete Post-Albers Cycle for P-type ATPases (B) describes a process during which intracellular sodium binds to three sites within the NKA-α subunit. This occurs as the "E1" conformation prefers to bind sodium, while the "E2" conformation facilitates potassium ion binding. Phosphorylation and sodium release occur with the ATP catalysis, also requiring the presence of one Mg^{2+} ion. With ensuring conformational changes, an initial Na^+ ion is released followed quickly by the evacuation of the remaining two Na^+ ions to the extracellular space. Two K^+ ions enter the vacated ion binding pockets and subsequent dephosphorylation of a cytoplasmic aspartate residue results in structural occlusion of the K^+ binding sites. Association of one intracellular ATP molecule causes further conformational changes and releases K^+ ions into the cytoplasmic space allowing a reestablishment of the E_1-ATP state initiating the start of another transport cycle. This cycle of gate transitions has been likened to that of space shuttle airlocks (Clausen et al., 2017; Kaplan, 2002; Poulsen et al., 2010a).

The NKA-α subunit is the catalytically active portion of the NKA pump complex, involved in binding and transporting sodium and potassium ions across the plasma membrane. It is comprised of 10 transmembrane domains (M1-M10) with large intracellular protein domains and small extracellular loops connecting membrane-spanning regions. The initial publication of a high-resolution structure of the closely related P-type ATPase SERCA in 2000 showed three conserved intracellular domains that underly subunit functionality. The actuator (A) domain is responsible for the transmission of energy to the transmembrane domains resulting from movement in the nucleotide binding (N) and phosphorylation (P) domains following the molecular events described in Figure 1.1B (Kaplan, 2002; Toyoshima et al., 2000). More recent publications have described in more granular detail Na,K-ATPase structure and domain motion that is outside of the scope of this document (Holm et al., 2016; Toyoshima et al., 2011). The NKA-β subunit is a smaller protein with a single transmembrane domain that interacts with several transmembrane domains of the NKA-α subunit. Expression of the β-subunit is obligatory for proper pump function, as it serves as a molecular chaperone necessary for proper insertion in the plasma membrane after assembly and folding in the endoplasmic reticulum (Clausen et al., 2017; Geering, 2001).

Four isoforms (isozymes) of the NKA-α protein subunit exist – α1, α2, α3, and α4 – often exhibiting striking specificity in tissue expression patterns. α1, α2, and α3 are strongly conserved proteins, showing a high degree of identity (87%) in amino acid sequence upon protein alignment. While α4 is less

conserved, it is still 78% identical to the α1 subunit. The greatest regions of similarity across these proteins includes the hydrophobic transmembrane domains involved in ion binding as well as the cytoplasmic ATP binding site and phosphorylation sites (Blanco and Mercer, 1998). There are three isoforms of the NKA-β subunit (β1, β2, and β3), all of which are expressed in neurons. All three of the β-subunit isoforms can partner with any of the four α-subunit isoforms, although over time it has become clear that certain combinations are preferred and observed over others, including heteromers $\alpha_1\beta_1$, $\alpha_2\beta_2$, and $\alpha_3\beta_1$ (Arystarkhova et al., 2019; Holm et al., 2016; Tokhtaeva et al., 2012). Although functional NKA pump units are mainly composed of αβ dimers, there is evidence in the field of dimer oligomerization into larger structures through studies of optimal enzyme kinetics, structural analysis of interaction sites, and biochemical assays of associated protein subunits (Ivanov et al., 2002; Laughery et al., 2004; Taniguchi et al., 2001).

The *ATP1A1* gene encodes the NKA-α1 protein subunit that is ubiquitous across all cell types and serves as the prototypical subunit in the field. Many studies involving NKA structural crystallography have taken advantage of massive quantities of $\alpha_1\beta_1$ dimers expressed in the kidney involved in renal sodium concentration (Laursen et al., 2015; Shinoda et al., 2009). Other studies have investigated the role of the NKA-α1 subunit in heart failure. Cardiotonic steroids including digitalis (digoxin) bind to the extracellular and transmembrane portions of NKA-α subunits with varying affinities and block forward cycling, preventing ion transport. A resultant increase in intracellular sodium inhibits the Na^+/Ca^{2+} exchanger, thus increasing intracellular calcium concentrations, lowering heart rates, and increasing cardiac muscle contractility. NKA-α1 protein and related subunits are downregulated as left ventricular failure progressively worsens, likely increasing baseline intracellular Na^+ concentration and explaining the increased sensitivity of cardiotonic steroids in failing hearts (Clausen et al., 2017; Schwinger et al., 2003; Shamraj et al., 1993; Virgadamo et al., 2015). Other cardiotonic steroids including the toxin ouabain can inhibit NKA-α subunits with varying affinities for each isoform. Rodent studies have described ouabain binding to α2 and α3 with higher affinity (low nM range) compared α1, while studies in human tissue have shown similar affinities for all three major isoforms (Lingrel, 2010; Urayama and Sweadner, 1988; Wang et al., 2001). New research in the *ATP1A1* field focuses on the genetics of hypertension, where it is known that specific NKA-α1 variants can lead to excessive aldosterone-producing tissue in adrenal glands (Nishimoto et al., 2015). Studies have elucidated that gain-of-function mutations in the transmembrane region of the NKA-α1 can turn the normal pump into a cation channel, severely impacting normal ionic balance (Kopec et al., 2014). Other mutations in *ATP1A1* have been associated with axonal Charcot-Marie-Tooth disease and a condition known as HOMGSMR2 – hypomagnesemia, seizures, and mental retardation 2 (Lassuthova et al., 2018; Schlingmann et al., 2018).

The NKA-α2 subunit, encoded by *ATP1A2*, is expressed in a much more tissue-specific pattern. α2 has been identified in skeletal and cardiac muscle tissue and in astrocytes and other glial cells in the brain. Mutations in *ATP1A2* are associated with phenotypes similar to AHC including autosomal dominant familial hemiplegic migraine (FHM) (Bottger et al., 2012; Clausen et al., 2017; Spiller and Friedrich, 2014). With a decreased affinity for K^+ ions, the role of the NKA-α2 subunit appears to be the rapid clearance of extracellular potassium into supportive cells like glia following neuronal and muscular activity (Crambert et al., 2000).

The NKA-α3 subunit is encoded by *ATP1A3* and associated with diseases previously mentioned including AHC, RDP, and CAPOS, among others (Heinzen et al., 2014). NKA-α3 subunits are highly expressed in neuronal tissue where they localize to both neuronal projections and dendritic spines, but can be expressed in skeletal and cardiac muscle tissue as well (Blom et al., 2011; Bottger et al., 2011; Sweadner et al., 1994). This critical subunit is finely tuned for neuronal firing via a decreased sodium affinity

compared to other α isoforms, allowing rapid sodium expulsion from the cytoplasm following neuronal activity (Azarias et al., 2013).

ATP1A4 encodes the even more tissue-specific NKA-α4 subunit that is only expressed in spermatozoa and less well-studied than other α-isoforms (Clausen et al., 2017; McDermott et al., 2012). The α4 subunit possesses decreased responsiveness to variations in the cellular environment such as membrane voltage, temperature, and ion concentrations. This allows for enzyme activity across a diverse range of conditions experienced during the process of fertilization (Clausen et al., 2016). Variants in the α4 subunit can result in male infertility in mouse models, although human mutations in *ATP1A4* have not been thoroughly investigated (Jimenez et al., 2011a; Jimenez et al., 2011b). Of note, although many studies describe tissue-specific expression patterns of NKA-α subunits, multiple isoforms are often expressed within a given cell and tissue type (Benarroch, 2011; Clausen et al., 2017; Dobretsov and Stimers, 2005).

The three known NKA-β subunits are encoded by the genes *ATP1B1*, *ATP1B2*, and *ATP1B3*. These subunits are much more evolutionarily distinct than the NKA-α subunits, all sharing between than 36% and 47% sequence identity. NKA-β subunits are single transmembrane domain proteins that associate with α–subunits at a 1:1 ratio and functionally impact function by allowing proper intracellular trafficking and fine-tuning ion affinity. Three crucial and conserved disulfide bonds in the extracellular region of β–subunits are needed for pump stability, and each has a unique glycosylation profile that may contribute to tissue specific function (Noguchi et al., 1994). While these subunits are much more promiscuous in expression profiles compared to their α–subunit partners, some patterns have emerged. NKA–β1 seems to be the most widely expressed of the subunits including in the brain, while NKA-β2 may be more specific to glial cells. NKA-β3 is less well studied but can be found in testes, retina, liver, brain, kidney, and lung, among other potential locations (Clausen et al., 2017; Martin-Vasallo et al., 1989; Tokhtaeva et al., 2010). NKA-β subunits are also known to play a role in cell-to-cell adhesion and have been found to be downregulated during the process of epithelial-to-mesenchymal transition during tumor cell infiltration of normal tissue, although the impacts of this function on NKA pump activity is less clear (Lee et al., 2015; Selvakumar et al., 2014). While genetic disease associations with NKA-β are sparse in the literature, there is a clear association of risk variants in hypertension that have been discovered in large genetic screening studies (Chang et al., 2007; Faruque et al., 2011; Xiao et al., 2009).

The FXYD subunit (γ–subunit) of the NKA pump is a nonessential modifying protein with a single transmembrane span that can be present in many different tissue types. These small proteins normally function to modulate NKA-pump activity, alter ion binding affinity, or stabilize the protein against environmental insults, and represent another relatively understudied component in the field (Mishra et al., 2011; Sweadner and Rael, 2000). Seven different FXYD proteins exist and are often expressed in tissue specific manners. Muscle and brain tissue express FXYD1, FXYD6, and FXYD7. Kidney tissue is positive for FXYD2 and FXYD4. Expression patterns of FXYD3 and FXYD5 are either nonspecific or unknown (Geering, 2006). No disease associations for the NKA-γ subunit are characterized, and mammalian knockout models generally show only subtle phenotypes (Clausen et al., 2017).

The NKA-α subunit also plays roles in intracellular signaling and synaptic scaffolding. In developing cortical neurons, low dose ouabain treatment is known to trigger dendritic growth and related transcriptional programs via CREB-mediated signal pathways, calcium oscillations, and regulation of Src kinase mediated phosphorylation patterns (Aperia et al., 2016; Desfrere et al., 2009; Haas et al., 2002). These signaling mechanisms may provide information to neurons and other cells regarding distant energetic requirements, serving as a feedback loop between the NKA pump and mitochondrial ATP production. As α1 and α3 are both necessarily expressed in most neurons, the contribution of each subunit isoform to these signaling pathways remains unclear. In neurons, the NKA-α3 subunit often localizes synaptically,

sometimes directly within macromolecular groups forming functional synapses (Doi and Iwasaki, 2008; Rose et al., 2009). Intracellular interaction sites with synaptic proteins including with PSD-95, ankyrin B, and caveolin-1 have been reported across multiple studies (Illarionova et al., 2010; Junghans et al., 2017; Reinhard et al., 2013). Links have been made between NKA pump activity or synaptic localization with cholinergic, glutamatergic, dopaminergic, serotoninergic, and GABAergic synapses (Pivovarov et al., 2018). Altogether, it is clear that NKA-α subunits are responsible for more than simple ion transport across cell membrane, with the NKA-α3 subunit playing a particularly important role in synaptic function and signaling in neurons.

Pathophysiological Insights from *ATP1A3*-Mutant Disease Modeling

Much of the field of AHC research has focused on discovering the impacts of *ATP1A3* mutations and related NKA-α3 protein variants in model systems, ranging from *in silico* structural discovery to pharmacological testing in mammals. Structural modeling has described that almost all disease-causing mutations in *ATP1A3*, particularly for AHC, cluster in the transmembrane regions responsible for sodium and potassium ion binding (Heinzen et al., 2014; Heinzen et al., 2012; Rosewich et al., 2012). These heterozygous missense mutations generally insert of a variant residue into ion binding regions or the shift adjacent residues causing steric blockade of crucial regions (Sweadner et al., 2019; Toyoshima et al., 2011). The lack of sequential ion binding makes forward cycling impossible and prevents proper ion transfer across the membrane. Recent *in silico* experiments have shown that pump function can be theoretically rescued with secondary mutations in structurally connected domains that relieve the steric pressure caused by AHC variants. These findings were bolstered by functional rescue in biological follow-up studies, providing intriguing possibilities for therapeutics options (Holm et al., 2015; Holm et al., 2016). While AHC mutations may impact both sodium and potassium binding, there is new structural and electrophysiological evidence that the E815K mutation creates an additional disruption of an inward proton route within the NKA pump that may explain the heightened disease severity seen in human patients harboring this mutation (Li et al., 2015; Vedovato and Gadsby, 2014).

Heterologous expression models have been utilized across multiple *in vitro* studies to provide evidence of NKA pump dysfunction in the presence of AHC mutations as well. Crucial electrophysiological studies in *Xenopus* oocytes identified that all of the major AHC mutations (D801N, E815K, G947R) have loss-of-function outcomes, often resulting in complete pump failure (Koenderink et al., 2003; Weigand et al., 2014). Further studies using luminescent kinase assays suggest that while ion transporting function may be impaired, AHC mutations do not cause any NKA subunit trafficking abnormalities and the αβ pump complex is properly inserted into the plasma membrane. This evidence suggests that any neuronal dysfunction seen in AHC is likely due to pump inactivation and ensuing consequences. While this is true for all AHC mutations studied, some *ATP1A3* mutations in RDP and related diseases have been shown to cause misfolding or imbalanced NKA subunit competition (Arystarkhova et al., 2019; Heinzen et al., 2012). Advanced *in vitro* models using human neurons have also been introduced to the field recently. Neuroblastoma-based differentiation models employing fluorescent indicators of intracellular sodium concentration are being used to rapidly screen potential therapeutic compounds, including flunarizine (Tiziano, 2019). An induced pluripotent stem cell (iPSC)-derived neuronal model of the G947R mutation described a general depolarization of resting membrane potential and altered electrophysiologic properties in mutant cells (Simmons et al., 2018). Along with the systems introduced in later chapters, these models serve as crucial platforms for experimentation, directly connecting discovery in the laboratory to the care of human patients with AHC.

Rodent models of disease have become prevalent in the field of *ATP1A3*-related disease. One of the first studies into the pathogenesis of *ATP1A3* mutations investigated the impact of ouabain as an NKA

pump inhibitor in rat hippocampus (Vaillend et al., 2002). Although the gene was not yet linked to AHC in the literature, this study showed that bath application of ouabain resulted in network hyperactivity caused by reduced GABAergic inhibitory potential, among other drivers. In 2009, researchers identified that a strain known as the "*Myshkin"* mouse displayed seizures and hippocampal hyperexcitablility. Genetic and functional analysis revealed an $Atp1a3^{+/I810N}$ genotype resulting in a 42% reduction in overall NKA activity and tissue hyperexcitability that was rescued by wildtype transgenesis (Clapcote et al., 2009). A subsequent study outlined the similarities in structural impacts between the mouse I810N mutation and common human AHC variants while describing behavioral deficits in frontal cortex function, mirroring what is seen in human patients (Kirshenbaum et al., 2013). A D801N mutation model ("*Mashlool"* mouse) was then created and assessed for phenotypes, revealing a predisposition to seizures, increased hippocampal excitability, abnormal motor coordination, behavioral deficits, hemiplegic events, and increased rates of sudden death (Hunanyan et al., 2015). The creation of an E815K mutant mouse ("*Matoub*") followed several years later and showed similar phenotypes of spontaneous seizures, triggered hemiplegic attacks, and decreased survival (Capuano et al., 2020; Helseth et al., 2018). These E815K mice showed minor symptomatic improvement following flunarizine administration without decompensation following drug withdrawal. Any literature regarding a mouse model of the third most common AHC mutation in humans, G947R, has yet to be published.

In mouse models of *ATP1A3* disease, complete gene knockout and homozygous mutant genotypes result in perinatal lethality. While phenotypes are well described in mice carrying heterozygous missense mutations in *Atp1a3*, the phenotypes of heterozygous knockout animals ($Atp1a3^{+/-}$) are often less severe than previously described AHC models. Two different knockout mouse variants have been created and analyzed, both showing perinatal death with homozygosity and only subtle phenotypes with heterozygous knockout genotypes (Ikeda et al., 2013; Moseley et al., 2007). In addition to the lack of evidence of heterozygous knockout *ATP1A3* mutations amongst human patients, this has led some to speculate regarding a dominant-negative mechanism of disease. While some evidence suggests the possibility of oligomerization as possible explanation for such a mechanism, this topic remains understudied (Heinzen et al., 2014; Holm and Lykke-Hartmann, 2016).

Symptomatic triggers in humans with AHC are numerous, complex, and often quite patient-specific: exposure to heat, acute changes in temperature, physical exertion, specific foods, infections, fever, etc. These triggers bring about episodes of hemiplegia in addition to seizures or painful dystonic events (Brashear et al., 2018; Heinzen et al., 2014; Kansagra et al., 2013). It is clear that stressful situations and environmental triggers play a large role in symptoms manifestations amongst animal models as well. Mouse models of *ATP1A3* disease with heterozygous disease-related missense mutations display more frequent and severe hemiplegic spells, dystonic events, and seizures under stressful conditions such as forced swim, vestibular stimulation by tailspin, or hypothermia (Clapcote et al., 2009; Heinzen et al., 2014; Helseth et al., 2018; Isaksen et al., 2017). Stressors such as chronic restraint in heterozygous knockout models has revealed triggered symptoms including motor skill deterioration that were not apparent at baseline (DeAndrade et al., 2011; Sugimoto et al., 2014). Even *Drosophila* models of NKA-α subunit mutations have revealed heat-induced paralysis in the absence of baseline phenotypes (Palladino et al., 2003). Regardless of the model system or patient profile, it has become obvious that stressful triggers play an important role in symptomatic expression and may provide insights into disease etiology and progression. While animal modeling provides one route to etiologic discovery, complex diseases such as AHC often require a multitude of modeling approaches and even human-specific studies to progress toward better therapies for patients and families.

Harnessing the Power of Stem Cells in Disease Models

Studying human disease in the laboratory is difficult. The goal of almost all translational research is to simplify study designs and model systems of human conditions so that targeted hypotheses about disease origins or therapeutic mechanisms can be studied in reductionist disease models. In this manner, many researchers study immortalized human lines such as HEK293 or HeLA cells using perpetual cell culture conditions and forced expression of proteins of interest. As a different approach, many scientists turn towards animal modeling using organisms with tractable genetics including worms (*C. elegans*), flies (*Drosophila*), and mice. These model systems are extremely valuable and have provided the scientific and medical communities with massive amounts of knowledge and understanding of biology and pathophysiology over the past century. However, as experimentation and data collection methods become increasingly complicated, it has become clear that many of these models fall short at properly mimicking human disease and results can be overinterpreted (Jucker, 2010; Onos et al., 2016; Perel et al., 2007; Perrin, 2014; Seok et al., 2013). This is particularly true in the fields of neurodevelopmental and neurodegenerative conditions where primary tissue samples from patients are difficult if not impossible to obtain, and brain structure, connectivity, and complexity differ greatly between species (Benam et al., 2015). The lack of tissue availability changed forever at the turn of the millennium as the field of stem cell research exploded.

Stem cells can be described as totipotent, pluripotent, multipotent, oligopotent, or unipotent. Totipotent cells within the zygote and morula stages immediately following fertilization can generate all the tissues in a developing organism plus the placental tissue necessary for fetal nourishment. Pluripotent cells composing the inner cell mass of the blastocyst stage can differentiate into all three germline tissue subtypes (endoderm, mesoderm, and ectoderm) necessary to build an organism, but cannot compose extra-embryonic tissues like the placenta. Multipotent, oligopotent, and finally unipotent cells have decreasing differentiation potential within this continuum (Stadtfeld and Hochedlinger, 2010). A groundbreaking paper published in 1998 described the isolation of cell lines from human blastocysts that could maintain their pluripotent status for months in culture, form derivatives of all three germ layers, and eventually develop into mature postmitotic cells (Thomson et al., 1998). These cells were labeled human embryonic stem cells (hESCs) and built upon decades of research in mouse ES cells where early editing technologies made genetic manipulation possible (Ben-David et al., 2012). While expanding the possibilities of research and discovery, many found this work controversial as it requires the destruction of early human embryos. This led to a federal moratorium on funding for ES cell generation in 2001, although researchers were still allowed to use previously created lines. While these restrictions were reduced in 2009, significant barriers to hESC research and considerable ethical concerns created an impetus to identify other possible sources of pluripotent tissue for human disease modeling (Lo and Parham, 2009; Williams, 2009).

Researchers in Japan led by Shinya Yamanaka spent years isolating the factors necessary to convert postmitotic mouse fibroblasts into pluripotent stem cells. After screening 24 genes for their hypothesized ability to induce or maintain pluripotency, a sufficient set of 4 genes was identified that could generate "ES-like" colonies in culture: *Oct4*, *Sox2*, *Klf4*, and *c-Myc*. These cells were later labeled induced pluripotent stem cells, or iPSCs (Takahashi and Yamanaka, 2006). A shocking scientific revelation at the time, these experimental successes were first presented at a 2006 conference. Less than a year later, these findings were repeated with hiPSC generation across multiple international laboratories, ushering in more than a decade of research and discovery using human iPSCs and derivative tissues for patient-specific "disease-in-a-dish" modeling (Maherali et al., 2007; Okita et al., 2007; Shi et al., 2017; Wernig et al., 2007). Dr. Yamanaka would go on to share the 2012 Nobel Prize in Medicine for the discovery of hiPSC technology with Sir John Gurdon for his earlier contributions to the field of stem cell research that paved the road towards iPSCs (Lensch and Mummery, 2013; Scudellari, 2016).

Although the classical approach to hiPSC generation involves a minimally invasive punch skin biopsy and fibroblast outgrowth prior to transduction, iPSC generation from numerous other cell types has

been optimized in recent years. Hair follicle keratinocytes, peripheral blood cells, and urine epithelial cells are other commonly used origin sources that provide less invasive approaches (Aasen et al., 2008; Staerk et al., 2010; Zhou et al., 2012). The initial approach to iPSC transduction utilized lentiviral-based insertion of the Yamanaka factor genes into human fibroblasts, resulting in the integration of the genes into the host genome. To avoid the potential genetic alterations inherent when delivering genes with lentivirus, newer methods of non-integrative transduction have been created that are even more efficient at iPSC generation, commonly including the use of episomal DNA (Okita et al., 2011), recombinant proteins (Kim et al., 2009), mRNA (Warren et al., 2010), and Sendai virus (Fusaki et al., 2009). While the epigenetic landscape and gene expression of hiPSCs is similar to that of hESCs, it has been shown that some epigenetic memory is retained from the cell of origin which can potentially impact the differentiation potential of these cells (Kim et al., 2011; Ohi et al., 2011). This fact is reflected in the status of most hiPSC colonies as "primed" to differentiate towards specific lineages rather than the "naïve" iPSC state seen in mouse ESCs and iPSCs, adding a potential source of variability to scientific outcomes. Regardless, many studies show alignment of data using both hESCs and hiPSCs, adding validity to the model system (Hough et al., 2014; Narsinh et al., 2011).

A major benefit of *in vitro* disease modeling using iPSCs in cell culture is the ability to perform genome editing and mutation screening in clonal cell populations. Genome editing techniques such as ZFN (zinc finger nucleases) and TALEN (transcription activator-like effector nucleases) have been used for years, but the introduction of CRISPR (clustered regularly interspaced short palindromic repeats) and associated nucleases like Cas9 (CRISPR associated protein 9) greatly increased the flexibility and specificity of genome editing in human cells. The realization that CRISPR could be utilized to edit the human genome and the intensive research that followed was another massive innovation in the field of *in vitro* disease modeling, generating countless popular science articles and earning shared accolades for researchers around the globe (Cong et al., 2013; Gasiunas et al., 2012; Jinek et al., 2012). A major barrier in interpreting results within the field of iPSC research involves potential variation between stem cell lines generated from different individuals, for instance between unaffected control volunteers and patient donors. With CRISPR/Cas9, researchers can relatively easily knockout specific genes via double stranded breaks and non-homologous end-joining or create single nucleotide resolution modifications leveraging donor DNA strands and homologous recombination. The CRISPR toolbox is continually expanding with numerous enzyme modifications and associated proteins that yield even greater experimental flexibility and specificity (Ben Jehuda et al., 2018). While CRISPR/Cas9 technology also provides avenues for cell replacement and direct genomic therapy in human patients (Hirakawa et al., 2020; Ormond et al., 2019; Sheridan, 2017), a discussion of the rationale, development, and ethics of those applications is outside the scope of this document.

The process of disease modeling using iPSCs has been streamlined into a paradigm that is generally followed amongst stem cell scientists (**Figure 1.2).** The model begins with the identification of patient donors and control volunteers from whom fibroblast or other tissues are collected. iPSCs are then generated using one of the methods described above, taking around a month from induction to clonal isolation. These iPSCs are validated using a well-described toolbox of methods including staining for protein markers of pluripotency, karyotyping or sequencing for unintended genetic alterations, and undirected differentiation into aggregates (embryoid bodies) to ensure uniformity in differentiation potential. From this point, genome editing techniques are often used for gene knockout or isogenic line creation. While some scientists choose to start from patient lines and correct mutations, an alternative approach is to create disease-associated mutations in iPSCs from unaffected individuals. Some research groups utilize iPSCs as a renewable source of cell populations for the study of stemness maintenance and pluripotency, while others differentiate iPSCs toward cells of interest, for example cardiomyocytes, motor neurons, or hepatocytes. These cells are then studied as patient-specific disease models, used for drug discovery, or can even be collected for cell replacement therapy (Avior et al., 2016; Colman and Dreesen, 2009; Diecke et al., 2014; Doss and Sachinidis, 2019; Shi et al., 2017).

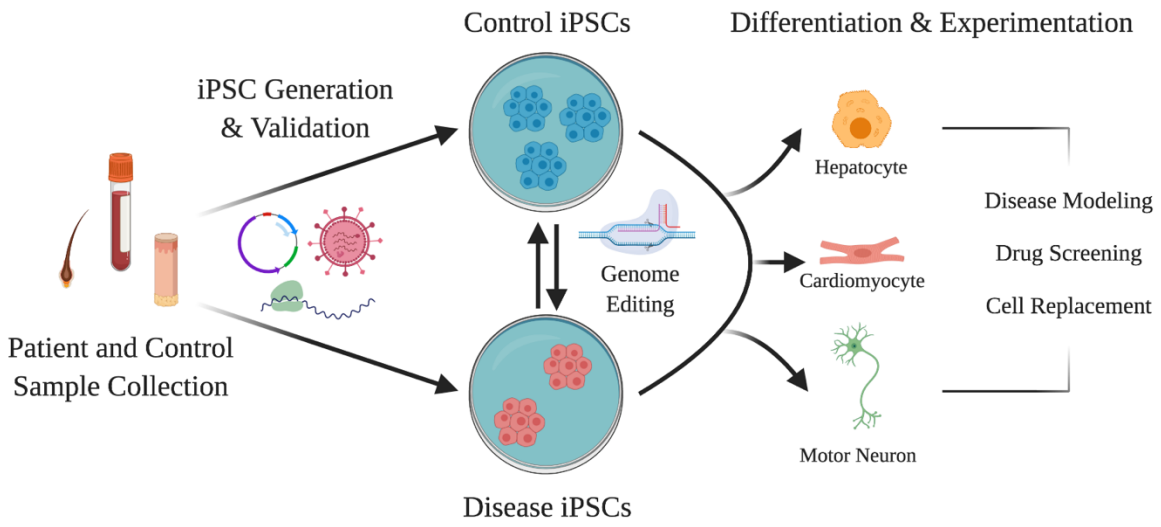

Figure 1.2: General Paradigm of iPSC Disease Modeling: Many groups performing iPSC-based disease modeling use a pipeline similar to the workflow described above. While this paradigm is quite streamlined, multiple avenues for potential variation exist at almost every step of the process. Figure modified from Diecke et al., 2014 and created using BioRender.

Many challenges exist that create barriers to success within the field of iPSC derivative disease modeling. For the most efficient groups, creation and validation of a single iPSC line can cost $10,000 - $25,000, without even considering the expenses associated with isogenic editing, continued maintenance, and years of extended differentiation and experimentation (Huang et al., 2019). iPSC-derived systems exist as another reductionist model, as generation of a single cell type or differentiation lineage do not accurately approximate the diversity and complexity of human organ systems (Saha and Jaenisch, 2009). Along with advances in bioengineering, a push for more accurate tissue heterogeneity and system complexity has begun with the spread of more complicated 3D model systems including organoids, "organ-on-a-chip" setups, and connected multi-organ systems derived from iPSCs (Lancaster and Knoblich, 2014; Liu et al., 2018; Ramme et al., 2019; Vatine et al., 2019). Unfortunately, limiting factors of cost and complexity often decrease the number of iPSC lines reasonable for experimental comparison. Nonetheless, iterative improvements in iPSC-derived disease modeling efficiency and reproducibility will ensure that these techniques continue to provide pathophysiological insights and treatment approaches for years to come.

iPSC-Derived Modeling of the Developing Cerebral Cortex

Multiple brain regions including the cerebral cortex, deep brain structures, and cerebellum have been implicated in the pathogenesis of AHC (Bottger et al., 2011; Chu et al., 2009; Helseth et al., 2018; Moseley et al., 2007; Severino et al., 2020). Given the symptomatic profile of AHC and our specific hypotheses, iPSC-derived neurons generated in our model system are created to represent human neurons of cortical origin. Before describing the iPSC-derived cortical neuron model of disease used in the research presented in Chapter II and beyond, it is important to review the process of normal mammalian corticogenesis.

The human brain has up to 100 billion neurons and perhaps even more supportive cells. Great complexity is achieved when this number is combined with genetic, molecular, and synaptic characteristics unique to human neurons. The cerebral cortex takes up more than half of the entire brain volume, being

overdeveloped compared to those of other mammals. Activity of neurons within this cortex is responsible for generating and processing perception, thought, language, memory, attention, and voluntary control, among other complex human behaviors (Herculano-Houzel, 2012). Much of what is known about the developing cortex in humans has been built upon knowledge from genetic manipulations and anatomical investigations in chicken, zebrafish, amphibian, and mouse embryos. During embryonic development, morphogenic signals from a dorsal region of the mesoderm called the notochord cause overlying ectoderm to undergo neural induction, forming the neural plate. After groove formation and folding, a neural tube is created that defines the early components of the nervous system. Further regionalization and expansion of the developing nervous system includes forebrain (prosencephalon) development and the production of early neural precursor cells (NPCs) that form an expanding pool of progenitors in the ventricular zone (VZ) (Florio and Huttner, 2014; Wilson and Houart, 2004).

As reviewed by Molnar et al. (2019), the complexity of mammalian cortical neurogenesis can be simplified into discrete stages. Neural progenitor cells within the VZ eventually divide into ventricular radial glia (vRG) that extend a process outward towards the pial surface. Asymmetric divisions of vRG cells produce intermediate precursor cells and early neurons along with more vRG cells. Newborn neurons begin climbing up vRG fibers and in this manner the cortical plate is built via classical "inside-out" lamination: layer 6 neurons are deposited first followed by layers 5, 4, 3, and 2. Closest to the pial surface, the marginal zone (layer 1) is developed earlier following initial neurogenesis. Some vRG daughter cells migrate into the subventricular zone to become outer radial glial (oRG) cells, continuing neurogenesis and construction of upper cortical layers. Evolutionary expansion of this oRG population is unique to primate and human neocortical development, creating large amounts of expanded brain volume and resulting in significant pial folding. vRG cells that remain in the ventricular zone eventually detach from the ventricular surface to become gliogenic cells, creating astrocytes, oligodendrocytes, and ependymal cells. Throughout this process, interneurons born in the ganglionic eminences migrate tangentially to their final positions in developing cortex (Gilmore and Herrup, 1997; Molnar et al., 2019; Myers et al., 2020; Zirra et al., 2016). In mice, the formation of the entire cortical plate and peak neurogenesis occurs between 11-17 days after conception, with normal gestational duration being around 20-21 days (Finlay and Darlington, 1995). In humans, initial neural expansion and cortical lamination take place between weeks 4-20 of gestation, along with neural migration and subsequent development. Synaptogenesis and apoptosis, or neural pruning, continue in the neonatal period and infancy while myelination of axons occurs throughout development into early adulthood (Tau and Peterson, 2010).

Understanding the intricacies of complex cortical development in humans is incomplete and mimicking this process in a cell culture dish is not a simple task. Following the publication of iPSC technology in 2006, research groups around the world began defining protocols to turn these stem cells into differentiated tissues. While many of these differentiation techniques existed in the hESC research field, the newfound availability, consistency, and flexibility of iPSCs opened the proverbial floodgates. In 2009, a reproducible method for neural conversion of hESCs and hiPSCs was published using two small molecules that mimic notochord signaling in the developing embryo (Chambers et al., 2009). This protocol calls for the application of molecules that synergistically inhibit SMAD signaling within the TGF-β pathway, resulting in neuroectoderm formation. Continued optimization of this approach has increased the efficiency and reproducibility of dual-SMAD inhibition-based neural induction from iPSCs (Kim et al., 2010; Muratore et al., 2014; Neely et al., 2012; Qi et al., 2017). After expansion and passage of neuroectoderm tissue, neural rosettes mimicking neural precursor formation appear within two weeks of induction. Early born neurons derived from these centers of production can be expanded and further specified into cortical neurons by application of morphogenic factor FGF2 (Shi et al., 2012a). The timing of cortical neuron birth and layer-specific generation *in vitro* is strikingly similar to what is seen *in vivo*: initial expansion mimics precursor development in the VZ followed by cortical plate construction, rosettes stain positive for markers of progenitor and outer radial glia cells, cortical layers are generated on the classic "inside-out" timeline, and functionally active glutamatergic projection neurons are formed before gliogenic

populations arise (Shi et al., 2012b). Tweaks to the recipe of small molecules, concentration of morphogens, timing of treatment, and duration of differentiation can be implemented to generate a wide variety of neuronal and glial lineages, including but not limited to: forebrain glutamatergic neurons (Shi et al., 2012a), cortical GABAergic interneurons (Maroof et al., 2013), midbrain dopaminergic neurons (Kriks et al., 2011), cholinergic motor neurons (Sances et al., 2016), and astrocytes and oligodendrocytes (Douvaras et al., 2014; Li et al., 2018b). Furthermore, the timing and concentration of morphogen administration in specific protocols can pattern lineage subtypes into iPSC-derived neurons representing very specific brain regions (Bitar and Barry, 2020; Li et al., 2018a).

Although *in vitro* iPSC-derived neural development closely mirrors the same process *in vivo*, it is important to experimentally correlate the age of cells being studied to human growth and development (van den Ameele et al., 2014). In general, the "resetting" of a somatic cell to pluripotency erases many of the hallmarks of aged cells, in the process extending telomeric length and dramatically decreasing markers of senescence. In a broad sense, it is agreed that for the differentiation methods described above, the age of the tissue donor from which iPSCs are created is not highly relevant (Mahmoudi and Brunet, 2012; Studer et al., 2015; Tang et al., 2017). Investigations have shown that in current dual-SMAD based differentiation protocols, post-mitotic neurons that are produced are expectedly more representative of early fetal neurons rather than mature adult cells (Cornacchia and Studer, 2017; Handel et al., 2016). While these iPSC-derived neurons are undoubtedly functional and develop synaptic networks over time, they are generally better for studying severe neurodevelopmental conditions rather than subtle neurologic phenotypes or diseases of neurodegeneration. Much work in recent years has focused on ways to better differentiate iPSCs into mature neurons that would have greater validity across human aging timelines (Mertens et al., 2018; Vera et al., 2016). Other methods of optimizing iPSC-derived neuronal differentiation involve completely different approaches.

One of the limitations of dual-SMAD inhibition driven neural differentiation is a lack of cell population purity. By mimicking neural development, a heterogenous population of cells is produced that lacks the specificity needed for many disease models where neural subtype purity is a benefit. One way to shortcut the extended timeline of human neurobiology is to directly induce differentiation by viral insertion of genes encoding transcription factors that cause iPSCs to directly differentiate to the neuron subtype of interest. These protocols are highly specialized but allow for simultaneous insertion of other important tools such as fluorescent tags or reporter molecules like GFP or GCaMP, gene control mechanisms like the TetOn system, or antibiotic resistance genes for downstream purification. While these tools are still being developed and optimized, they serve as an important step forward in the reproducibility and control of iPSC-derived neuronal protocols (Yang et al., 2017; Zhang et al., 2013b). Recently, the combination of developmental patterning using dual-SMAD inhibition for neural induction along with viral transduction of expedited differentiation factors has become common in the field (Nehme et al., 2018; Simmons et al., 2018). Importantly, these viral induction methods are being continually refined and updated for the generation of many different neural subtypes and even non-neural cell populations found in the brain including astrocytes (Caiazzo et al., 2015; Sauter et al., 2019).

The protocols for neural differentiation above were developed with either two-dimensional (2D) iPSC culture or floating aggregates of iPSCs as a starting point. While 2D differentiation models offer relative simplicity and reproducibility, a lack of complexity fails to replicate many aspects of *in vivo* neurodevelopment leading to a push for more relevant *in vitro* culture models. Protocols for the generation of three-dimensional (3D) neuronal models have been generated over the past several years, with aggregates referred to as cerebral organoids or spheroids. Production of organoids can be guided with the morphogens and factors described above, but organoids can also form with unguided or minimally guided differentiation. 3D protocols require intensive culture methods to allow nutrient diffusion for continued neuronal survival and development, but result in incredible models that biochemically, transcriptionally, and structurally resemble the developing human cortex better than 2D differentiation methods. For these

reasons, brain organoid culture and experimentation models are being adapted at a high rate by the iPSC-derived neuron research community (Amiri et al., 2018; Centeno et al., 2018; Pasca et al., 2019; Qian et al., 2019). No model system is perfect, and new publications show that even the most complicated of 3D iPSC-derived neuronal systems must be carefully interpreted compared to the complexity of the human brain (Bhaduri et al., 2020; Hong and Do, 2019). From the variety of differentiation methods to the complexity of cell culture paradigms, there has been a push in the field to develop standards of best practice when modeling disease with iPSC-derived neurons (Engle et al., 2018). Adherence to best practices and sharing of cell lines via tissue repositories will lead to more efficient, reproducible, and translatable research.

Summary

Alternating hemiplegia of childhood is a devastating neurodevelopmental condition described by early onset of ocular abnormalities, alternating hemiplegic events, seizures, and dystonia. Developmental delay, intellectual disability, and neuropsychiatric disorders persist as patients reach adolescence. Unfortunately, no empirically proven treatments exist for patients with AHC, although the sodium and calcium channel antagonist flunarizine is commonly prescribed. AHC is caused by heterozygous missense mutations in *ATP1A3*, the gene encoding a neural specific α3 subunit of the Na,K-ATPase transporter (NKA-α3). Mutations in this gene cause a spectrum of neurological disease that includes AHC, RDP, and CAPOS, along with an expanding number of disease associations.

The NKA pump complex includes a catalytic α subunit responsible for sodium and potassium transport across the cell membrane, a smaller β subunit necessary for proper intracellular trafficking of the pump and resultant membrane expression, and a dispensable γ subunit which fine tunes enzyme activity. Common AHC mutations D801N, E815K, and G947R disrupt sodium and potassium ion binding pockets within the transmembrane regions of the NKA-α3 subunit. Insights into disease pathogenesis have been provided by structural analysis, *in vitro* disease modeling, and genetically engineered mouse models in recent years. In many different model systems and human patients, stressful triggers often reveal or exacerbate disease phenotypes and AHC symptoms. While animal modeling provides one route to etiologic discovery, complex diseases such as AHC often require a multitude of modeling approaches and even human-specific studies to progress toward better therapies for patients and families.

The model system that we have chosen as an experimental model for AHC involves the creation of patient specific iPSC-derived cortical neurons. iPSC technology was introduced in 2006 and has revolutionized the way human models are created in the laboratory setting. Utilizing new methods of genome editing including CRISPR/Cas9 technology, elegant study designs involving isogenic iPSCs and their derivatives are now feasible. To create neurons from iPSCs, researchers have learned to harness morphogens and transcription factors to replicate the complex process of mammalian corticogenesis. iPSC-derived cortical neurons can be generated in a dish with a timeline similar to *in vivo* development, and protocols have been created to generate large variety of neurons and non-neuronal subtypes. New protocols allow for the generation of 3D brain organoids that better replicate corticogenesis but require more intensive culture techniques. Chapter II will explore the creation an iPSC-derived cortical neuron model of AHC, while Chapters III and IV will detail our experimental findings in this model system.

CHAPTER II

CREATION OF A NOVEL iPSC-DERIVED NEURONAL MODEL OF AHC

Parts of this work are published in *Neurobiology of Disease* by Elsevier entitled "Neuronal Modeling of Alternating Hemiplegia of Childhood Reveals Transcriptional Compensation and Replicates a Trigger-Induced Phenotype" (Snow, Westlake, Klofas, Jeon, Armstrong, Swoboda, George, and Ess; 2020)
DOI: 10.1016/j.nbd.2020.104881

Abstract

Alternating hemiplegia of childhood (AHC) is a rare neurodevelopmental disease caused by heterozygous de novo missense mutations in the *ATP1A3* gene that encodes the neuronal specific α3 subunit of the Na,K-ATPase (NKA) pump. Mechanisms underlying patient episodes including environmental triggers remain poorly understood, and there are no empirically proven treatments for AHC. Multiple regions of the brain, particularly neuronal lineages within the cerebral cortex, have been postulated as major contributors to the disease pathogenesis and symptom evolution. *To better study disease mechanisms in AHC, we generated a patient-specific induced pluripotent stem cell (iPSC) derived neuronal disease model including isogenic controls for the* ATP1A3$^{+/E815K}$ *genotype associated with the most phenotypically severe form of disease.* Separate cortical differentiation protocols were adopted and optimized to generate (1) mixed cortical populations comprised mainly of early born glutamatergic neurons and (2) cultures shifted toward cortical GABAergic interneuron populations. These cultures have been validated for neuronal properties and lineage specificity by immunoblotting, immunostaining, and RNA sequencing. iPSC-derived neurons generated in our synchronized paired differentiation protocols display electrical activity on microelectrode array (MEA) analysis consistent with synaptic formation and continued maturation over time. This model system is outlined and validated here to provide a platform for further studies in this document and as a possible tool for other researchers in disease modeling and drug screening.

Introduction

A revolution in the field of disease modeling was initiated with the publication of iPSC technology in 2006 (Scudellari, 2016; Takahashi and Yamanaka, 2006). For the first time, scientists could collect samples from patients and convert somatic cells into pluripotent stem cells available to then generate any tissue for *in vitro* study. These techniques have been particularly important for the fields of neuroscience, where already fragile primary tissue samples are often impossible, dangerous, and unethical to collect from patients. Quickly, new protocols for differentiating iPSCs into various neuronal lineages were published for disease modeling and drug screening and rapidly adopted by researchers in neurodevelopment, neuropsychiatry, and neurodegeneration (Chailangkarn et al., 2012; Fink and Levine, 2018). iPSCs and derivative neurons have become frequently applied in developmental diseases similar to AHC, where early symptom onset is combined with strong genotype-to-phenotype correlations. Scientists can leverage the flexibility of patient-specific iPSCs and techniques of evolving genome editing technology like CRISPR to ask specific questions that before were only approachable via animal modeling (Bassett, 2017; Ran et al., 2013). For these reasons, we pursued the creation of an iPSC-derived neuronal model system for mechanistic discovery in AHC. We have decided to focus our efforts on iPSC-derived neurons harboring the E815K mutation in *ATP1A3*, as this is consistently described as the most phenotypically severe mutation in human AHC patients (Ishii et al., 2013; Sasaki et al., 2014; Viollet et al., 2015). The generation of

isogenic controls for this variant serve in combination with unrelated controls to increase the power and impact of our findings.

Multiple brain regions and different subtypes of neurons therein have been hypothesized or demonstrated to contribute to the pathogenesis and unique symptom profile of AHC, including cortical neurons, deep brain structures, and cerebellar regions. Review of the literature and communications with experts in the field have led us to investigate both glutamatergic and GABAergic cortical neurons as potential contributors to disease etiology (Bottger et al., 2011; Clapcote et al., 2009; Helseth et al., 2018; Hunanyan et al., 2015; Ikeda et al., 2013; Murata et al., 2020; Richards et al., 2007; Simmons et al., 2018). To create iPSC-derived neuronal cultures, two protocols have been optimized for use within the Ess Laboratory. The Shi protocol (Shi et al., 2012a) creates a "mixed cortical" population of neurons that mimics cortical plate formation with cultures primarily composed of glutamatergic neurons and later born populations of GABAergic and glial cells. The Maroof protocol uses similar small molecule techniques to drive neural induction, but includes the use of morphogens to drive a ventral forebrain fate resulting in a much larger proportion of GABAergic interneurons in early cultures (Maroof et al., 2013). These neural induction methods have been slightly modified in the Ess Laboratory for synchrony of passage dates and induction density, such that only the small molecules are modulating changes in culture conditions, lineage decisions, and neuronal yields between protocols. Both culture methods create expandable cultures of iPSC-derived neurons producing a large amount of tissue for study and have been shown to generate electrically active neuronal populations by both whole cell patch clamping and microelectrode array analysis. Immunoblotting and immunofluorescent staining of these cultures for neuronal and specific lineage markers have recapitulated data from the original authors and allowed for the production of reproducible cell populations. Chapter II serves as an overview of the creation, optimization, and validation of this disease model, which will be used to test our hypotheses about the pathophysiology of AHC and can serve as a platform for therapeutic screening and discovery in the future.

Results

Generation of E815K patient-specific iPSCs and isogenic wildtype controls

We employed episomal plasmid reprogramming methods to generate iPSC lines from fibroblasts of an AHC patient harboring a heterozygous missense mutation in exon 18 of *ATP1A3* (c.2443G>A, p.E815K; AHC *ATP1A3*$^{+/E815K}$; lines AHC-20 and AHC-24). While the original goal of the disease model was to incorporate lines representing all three common AHC mutations, prioritization of resources for reproducible neural differentiation and inclusion of isogenic controls required a focusing of the project onto a single mutation of interest. Validated iPSCs from patients with D801N and G947R mutations (and other less common variants) are also available and banked by the Ess Laboratory but are not included in this study. Clones from two unrelated individuals were used as wildtype controls (unrelated *ATP1A3*$^{+/+}$*;* lines UC1 and UC2). iPSC genotypes were reconfirmed after reprogramming, and clone pluripotency was assessed by immunostaining for common pluripotency markers, successful germline marker identification in trilineage differentiation assays, and the presence of a normal karyotype (**Figure 2.1**). PCR assays (not shown) were performed to ensure that episomal plasmids used in reprogramming had not integrated into the host genome.

Initial attempts at CRISPR/Cas9 genome editing utilized a cell line stably incorporated with doxycycline-inducible Cas9 nuclease (Mandegar et al., 2016), with the goal of inserting a heterozygous E815K mutation into a wildtype line. While editing was successful in producing a high number of *ATP1A3*$^{+/E815K}$ colonies confirmed by restriction enzyme screening and sequencing, results were confounded by lack of clonal purity after puromycin selection and persistent Y-chromosome loss in a subset of host and edited iPSCs upon karyotyping. To circumvent this problem, we altered our approach to instead

correct heterozygous mutations in AHC lines to wildtype using episomal transduction methods (Ran et al., 2013). This protocol was rapidly successful and resulted in verified isogenic iPSC wildtype clones (isogenic *ATP1A3*$^{+/+}$; lines IC1 and IC2). Extended chromatographs included along with standard pluripotency validation data show the lack of genetic alterations surrounding the cut sites (**Figure 2.2**). The full sequences for CRISPR guide RNAs and template ssODNs are included in the Appendix (**Supplemental Figure 2.1**). Further validation of isogenic controls included PCR amplification with more distant primers and whole exome sequencing of line IC2 to confirm the homozygous status of the PAM site alteration observed on initial sequencing.

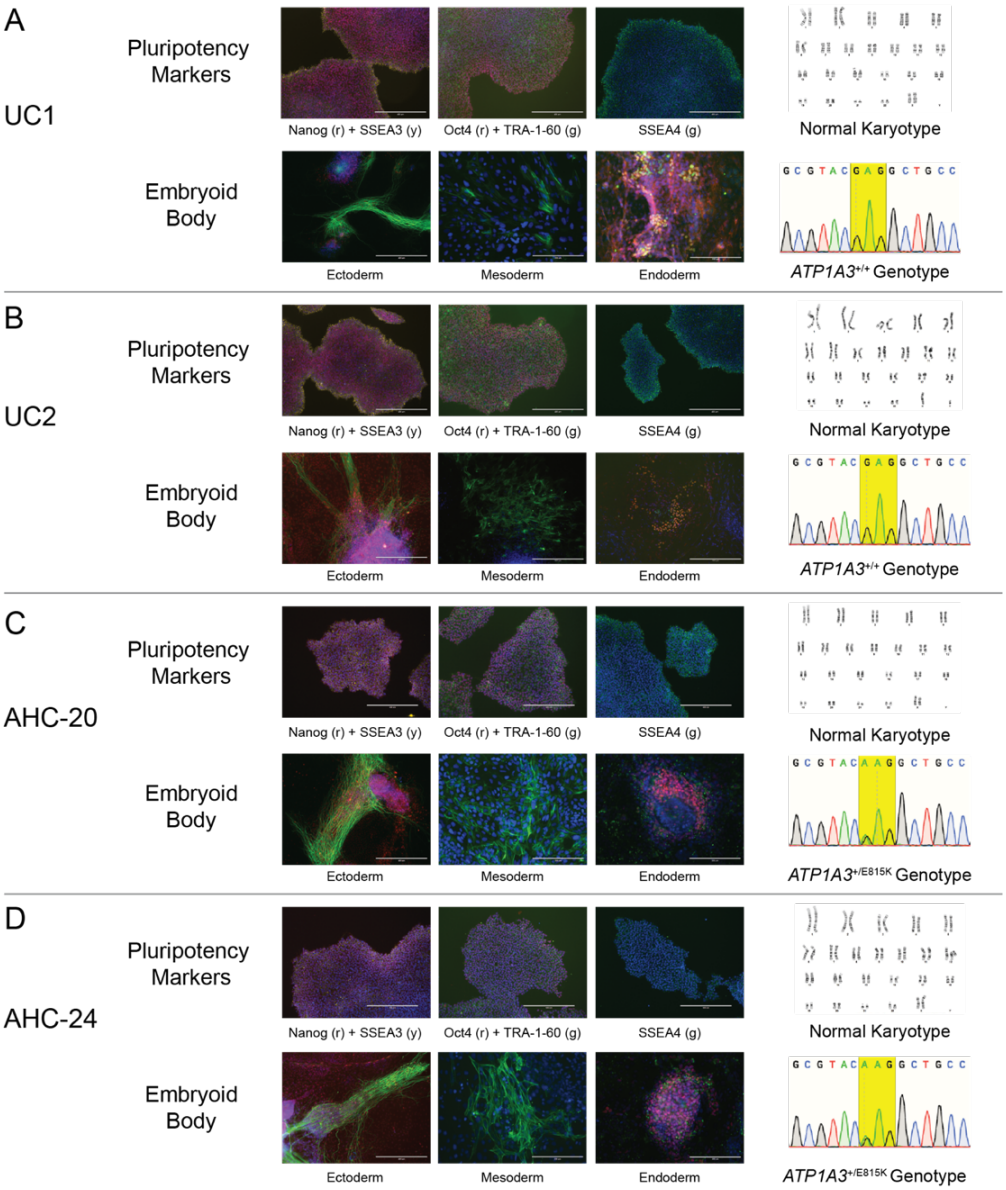

Figure 2.1: Generation and validation of iPSCs from an AHC patient and unrelated control volunteers. Genotyping and validation for the original clones used in this study (A) UC1 [CC3], (B) UC2 [CX3], (C) AHC-20 [91759-20], and (D) AHC-24 [91759-24]. Pluripotency validation of iPSC clones for all lines included immunostaining for markers of pluripotency (Nanog, Oct4, SSEA4, SSEA3, and TRA-1-60). Teratoma-like embryoid bodies were generated using unguided aggregate differentiation and immunostained for characteristic markers of all

three germline lineages: ectoderm (β-III-Tubulin [green] and Sox1 [red]), mesoderm (smooth muscle actin [green]), and endoderm (GATA4 [red], Sox17 [green]). Scale bars = 200 or 400 μm. DAPI nuclear stain shown in blue across all images. Metaphase spreads were performed (Genetic Associates, Nashville, TN) on all clones to ensure a normal karyotype. PCR analysis demonstrated the expected wildtype (UC1, UC2) genotype in unrelated controls and the heterozygous c.2443G>A *ATP1A3*$^{+/E815K}$ genotype in AHC patient-derived lines. All clones underwent further PCR analysis to determine that the episomal pluripotency transduction plasmids had not been incorporated into the host genome (not shown).

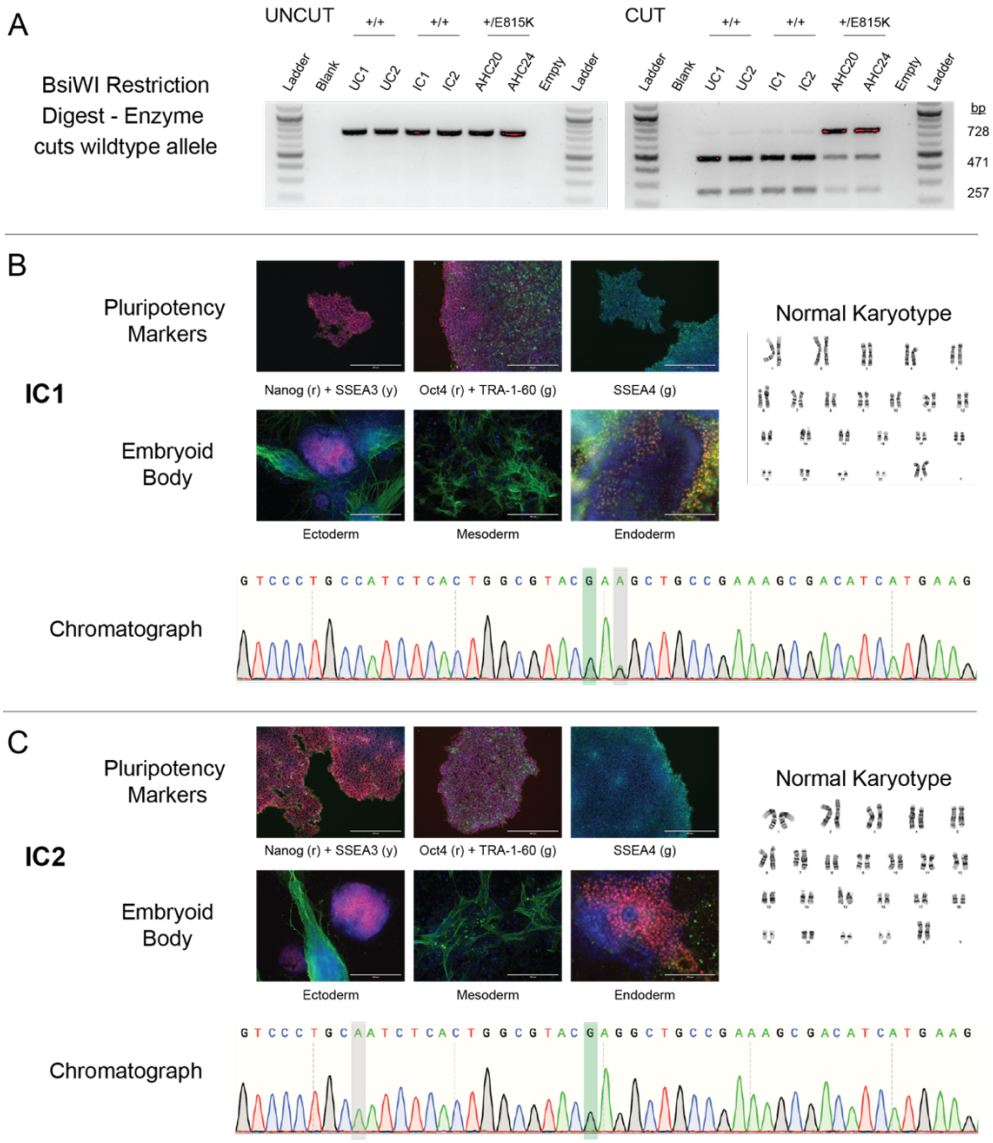

Figure 2.2: Creation and validation of isogenic wildtype controls from AHC E815K patient iPSCs. CRISPR/Cas9 episomal transduction strategies were used to generate isogenic iPSC clones. Sequences of guide RNA and template ssODN molecules along with further validation data are provided in the Appendix (Supplemental Figure 2.1). (A) Following puromycin selection, surviving clones were screened using restriction enzyme BsiWI. The cut site for this enzyme is rescued with the corrected change, resulting the disappearance of a larger uncut PCR product seen in heterozygous E815K clones when the restriction enzyme is active. Multiple rounds of restriction enzyme screening occurred during cell culture to ensure the correct genotypes were used prior to neural differentiations. Sequencing of PCR products confirmed the sequence surrounding the cut site was unchanged outside of the intended alterations. Pluripotency validation was performed for isogenic corrected iPSC lines IC1 (C) and IC2 (D). For chromatographs,

outlined green bases notate correction to wildtype. Synonymous PAM-site mutations intended to limit repetitive cutting events are highlighted in gray.

Implementation and optimization of a paired neural differentiation scheme

Two clones of each genotype (unrelated *ATP1A3*$^{+/+}$, isogenic *ATP1A3*$^{+/+}$, AHC *ATP1A3*$^{+/E815K}$) were used to generate an iPSC-derived neuronal model of disease to discover and analyze *in vitro* phenotypes caused by the AHC E815K mutation (**Figure 2.3A**). Two related protocols were synchronized to generate unique neuronal populations representing early born glutamatergic neurons (Shi "mixed cortical" protocol, **Figure 2.3B**) or cortical interneurons (Maroof "GABAergic" protocol, **Figure 2.3C**). As broad expression patterns in brain tissue suggest that multiple neuronal lineages contribute to AHC pathogenesis, an approach of paired differentiation allowed us to expand the scope of our studies to neural populations in the developing brain without narrowing on a specific group. Both of these protocols employ 2D plating of iPSCs at high density followed by application of dual-SMAD pathway inhibitors (SB-431542 and LDN-193189) to neuralize a confluent sheet of iPSCs. The Shi protocol includes FGF2 treatment and withdrawal while neural rosettes are expanding. Early Wnt-antagonism (XAV-939), and later dual-SHH agonism (rhSHH, purmorphamine) specify cells in the Maroof protocol to ventralize towards interneuron precursors generated in the ganglionic eminences during brain development. Both protocols exit morphogen treatment windows and are treated with maturation factors including BDNF and GDNF from day 20 onward. By d32, singularization of cultures and eventual plating on destination wells allows for flexibility in maintenance and experimentation. This experimental approach introduces slight modifications to the original protocols to include standardized passage dates and morphogen treatment windows, allowing for more reproducible data collection timepoints throughout differentiation.

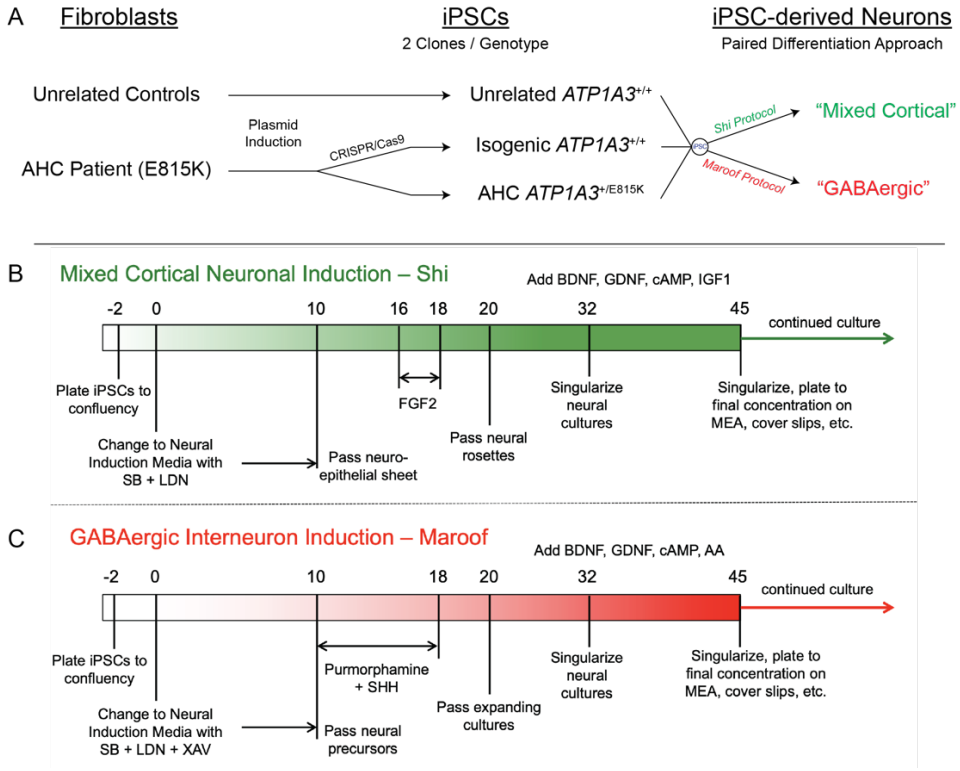

Figure 2.3: Paired differentiation model and protocol schematics for investigation of iPSC-derived neurons. (A) Fibroblasts were collected by punch skin biopsy from two unrelated control volunteers (*ATP1A3*$^{+/+}$) and from a

patient with AHC harboring the *ATP1A3*$^{+/E815K}$ genotype. Cultured fibroblasts were induced to pluripotency using episomal transduction methods. Isogenic wildtype clones (*ATP1A3*$^{+/+}$) were generated from a patient line to be used as an additional control group. Two clones of each genotype (unrelated, isogenic, AHC) were differentiated to mixed cortical (Shi protocol) or GABAergic shifted (Maroof protocol) neuronal cultures. Schematic descriptions of modified Shi (B) and Maroof (C) protocols are shown.

Control and AHC iPSCs successfully differentiate into neurons unique to each protocol

Immunoblotting of iPSC derived neurons from both mixed cortical and GABAergic protocols at d32 show the loss of pluripotency master regulator Oct4 and the acquisition of neural marker β-III-Tubulin. Overall expression of the NKA-α1 subunit decreased to around half of iPSC levels by d32 of both cultures systems, while NKA-α3 subunit protein was significantly elevated in neurons of both unrelated control and AHC genotypes. Maroof protocol iPSC-derived GABAergic cultures demonstrate elevated levels of inhibitory cortical interneuron markers Nkx2.1 and GAD67 compared to samples from mixed cortical cultures (**Figure 2.4; Supplemental Figure 2.2**). On immunostaining, iPSC-derived neurons from both protocols remain robustly positive at d60 for neural markers β-III-Tubulin and MAP2 (**Figure 2.5**). Mixed cortical cultures from neuronal populations include small subsets of GABAergic neurons at this age, while substantial numbers of glial cells are not generated until after the time periods analyzed in these studies (d80+). Maroof protocol cultures show elevated numbers of cells that stain positive for GABA. While the true proportion was never quantified in our hands, GABAergic marker immunostaining aligns with the original publication suggesting the production of iPSC-derived neurons most similar to medial ganglionic eminence-born cortical interneurons. Immunostaining for NKA-α3 subunits confirms general expression in neurons that is better shown tracking along membrane surfaces and neural projections at high resolution (**Supplemental Figure 2.3**). No significant difference in NKA subunit protein expression was appreciated between genotypes on quantification, as described in Chapter III.

Bulk tissue RNA sequencing was performed on unrelated control and AHC samples prior to the generation of isogenic controls. As expected, assessment of variance contribution by principal component analysis demonstrates the creation of unique cultures (**Figure 2.6A-B**). Gene ontology pathway analysis also supports the existence of unique glutamatergic and GABAergic neurons within these populations (**Figure 2.6C**). Differential expression analysis performed on bulk RNA from mixed cortical population of neurons at d32 was performed, highlighting genes that may be impacted in disease state versus control neurons (**Supplemental Figure 2.4**). Of the differentially expressed genes, one finding of particular interest included a significant downregulation of *FXYD2* in AHC neurons, a gene encoding an accessory Na,K-ATPase γ-subunit. As preliminary results, these must be further validated with more replicates and isogenic clones before conclusions are made. Similar analysis of GABAergic differentiation protocol samples at d60 did not replicate this finding.

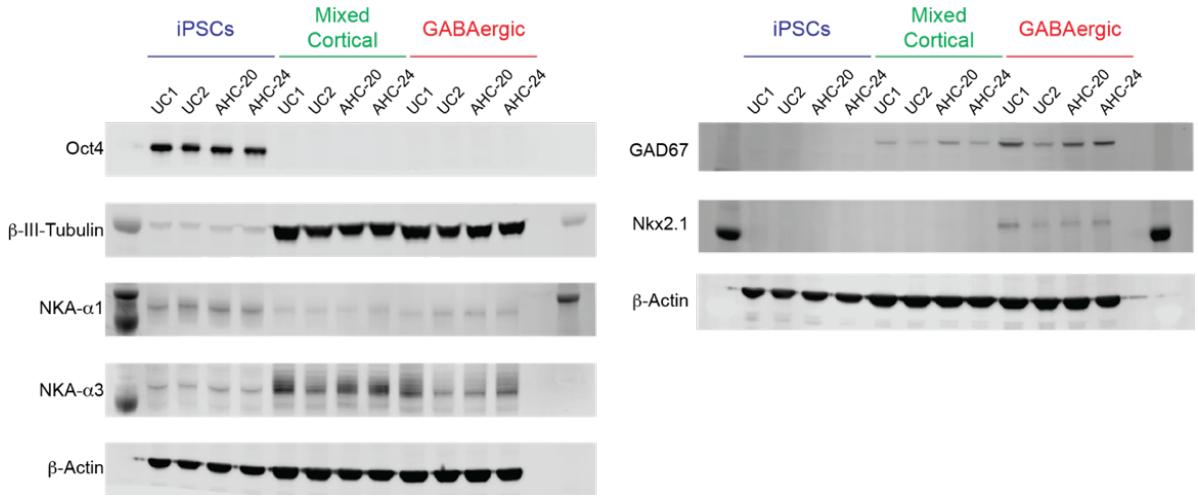

Figure 2.4: Lineage-specific neural differentiation is confirmed by immunoblotting for common markers. Immunoblotting of protein samples collected from unrelated control or AHC lines (before generation of isogenic lines) after 32 days of differentiation show successful neuralization by loss of pluripotent maker Oct4 and acquisition of robust β-III-Tubulin positivity. Expression of the NKA-α1 subunit decreases during in this early stage of neural differentiation as NKA-α3 subunit protein begins being expressed in large amounts, particularly in mixed cortical cultures (left). Maroof protocol samples show higher intensity for markers GAD67 and Nkx2.1, suggesting greater yield of GABAergic populations compared to mixed cortical cultures (right). β-actin shown as loading control for simultaneously produced gels; true normalization performed with total protein stains shown for each gel in the Appendix.

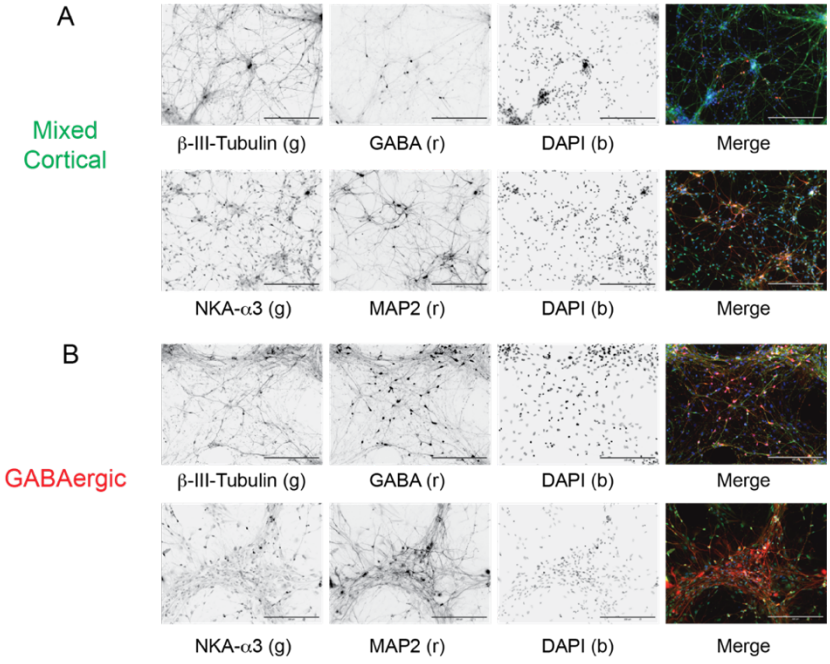

Figure 2.5: Paired differentiation immunostaining supports neural identity and NKA-α3 expression. (A) Immunostaining of mixed cortical AHC cultures fixed at d60 shows the expression of neural markers including β-III-Tubulin and MAP2. Shi protocol cultures at this stage generate small populations of GABAergic neurons in addition to the dominant glutamatergic populations described in the original publication. Neurons generated in these cultures stain positive for the NKA-α3 subunit, with no obvious differences between genotypes or intracellular aggregations observed. Higher resolution images of NKA-α3 are shown in the Appendix to support this finding. (B) Neurons derived from a GABAergic shifted protocol express standard neural markers including β-III-Tubulin and MAP2 when fixed at d60. GABAergic staining shows increased amounts of GABA-positive cells compared to mixed cortical cultures that also stain positive for the NKA-α3 subunit. DAPI shown as a nuclear stain; scale bars = 200 μm

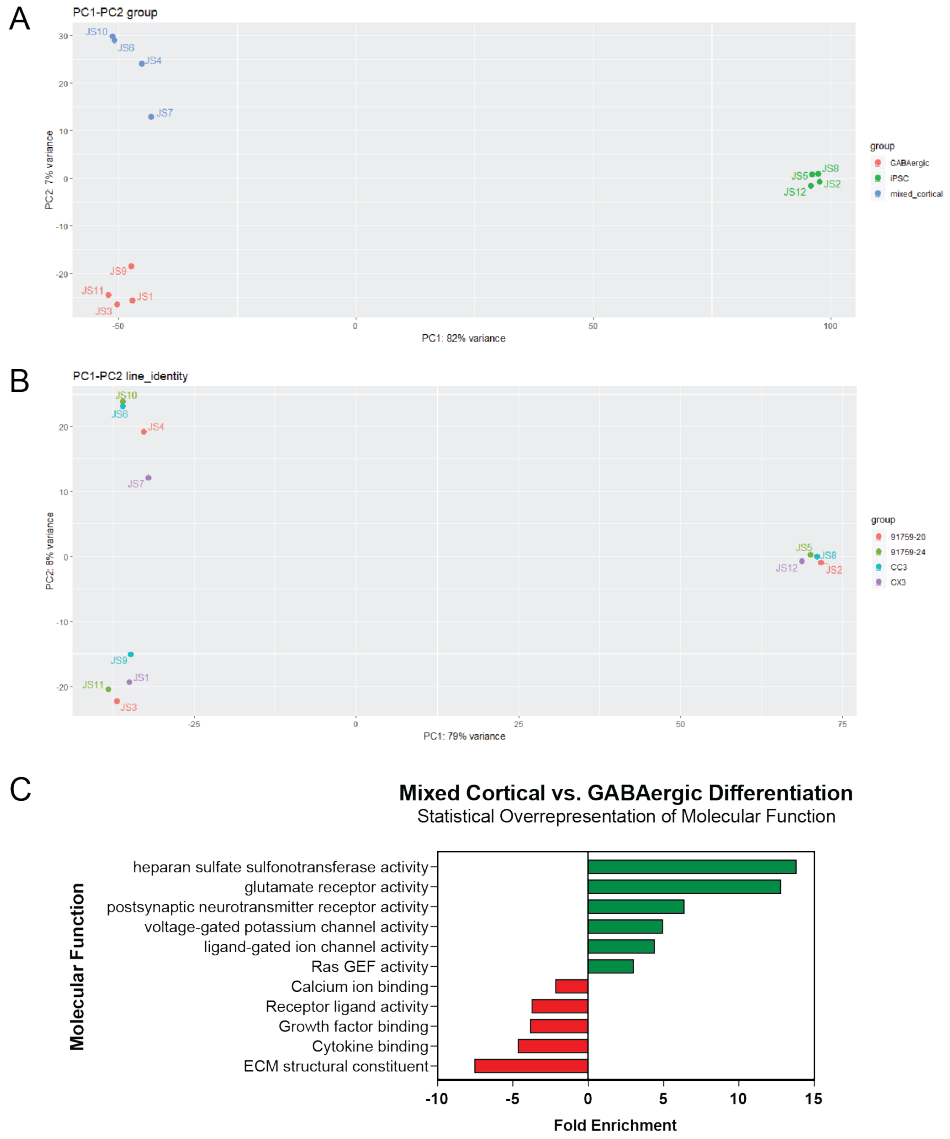

Figure 2.6: Bulk tissue RNA-sequencing demonstrates creation of unique neural populations. (A) Principal component analysis of purified mRNA collected from d0 iPSC (green), d32 mixed cortical (blue), and d32 GABAergic (red) cultures shows three unique groupings clearly separated by differentiation protocol. The majority of the variance lies on the PC1 axis between the iPSCs and the neural groups, while the separation described by PC2 more clearly defines neural lineage subgroupings. (B) No clear pattern of difference along these principal components exists between AHC or control genotypes: CC3 (UC1, aqua), CX3 (UC2, purple), 91759-20 (AHC-20, red), and 91759-24 (AHC-24, green). Isogenic wildtype lines were not yet created at the time of this experiment. (C) Gene ontology overrepresentation analysis shows significant differences between mixed cortical and GABAergic cultures as a proof-of-principle analysis for differentiation protocols. Molecular functions including glutamate receptor activity and postsynaptic neurotransmitter receptor activity were elevated in mixed cortical combined groups, while the inverse enhancement of calcium ion binding molecules correlates to known expression of parvalbumin, calbindin, and somatostatin in inhibitory interneurons. No patterns of specific pathways or molecular functions were noted in AHC vs. control analyses.

Control and AHC iPSC-derived neurons display electrical activity

iPSC-derived neurons generated in these protocols have been shown in multiple publications to have activity on whole-cell patch clamping. Unfortunately, this technique for electrophysiological measurement and manipulation was very irreproducible in our hands. Although we were able to measure some action potentials, very few iPSC-derived neurons of both control and AHC genotypes survived the technical process of clamping to provide sufficient data. Whether due to biological characteristics of fetal-like neurons or technical issues, we instead sought to study population level activity using microelectrode array (MEA) technology. MEAs allow for field potential acquisition and assessment of neural activity at local and network levels and are very amenable to manipulation with techniques approachable to scientists experienced in cell culture. After failing for multiple years with an experimental 3Brain MEA system, the lab acquired an Axion Maestro Pro MEA system that has been very reliable. Neurons are plated onto a 48-well MEA plate, with each well containing a 16-electrode system for field potential acquisition of plated neurons (**Figure 2.7A-B**). Neurons generated by the mixed cortical protocol are more active on this system, as further described in Chapter III, but both Shi and Maroof protocols produce reproducibly active neuronal populations by d60 of differentiation. iPSC-derived neurons are inhibited in a dose-depended manner by application of the voltage-gated sodium channel blocker tetrodotoxin (**Figure 2.7C**), suggesting that the acquisition settings used are truly measuring neural spike patterns. Flunarizine, a sodium and calcium channel antagonist commonly used to treat AHC patients, also inhibits the activity of mixed cortical neurons in a dose-dependent inhibition of activity after 24-hours of treatment (**Figure 2.7D**). These results suggest that MEA measurement of iPSC-derived neural activity may be a valuable and reproducible method for testing hypotheses regarding the pathogenesis of AHC.

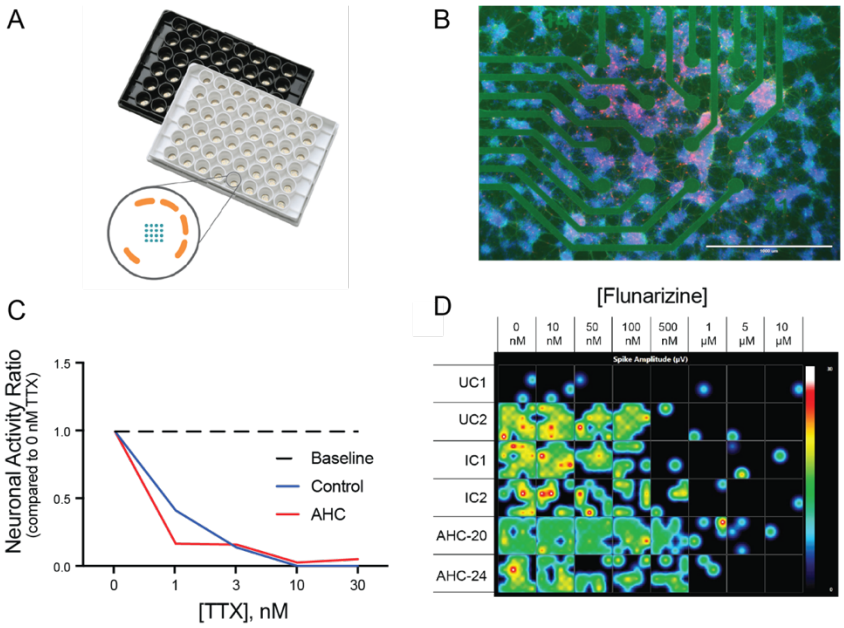

Figure 2.7: iPSC-derived neurons display electrical activity with neural signatures on MEA analysis. (A) Plate schematic shows 16-electrode array schematic in a 48-well plate with the MEA system (Axion Biosystems). (B) Post-analysis fixation and immunostaining of iPSC-derived neurons from a mixed cortical differentiation show neuronal markers (β-III-Tubulin [green], GABA [red]) and the relationship of neurons to the recording electrodes. (C) Initial validation of acquisition settings and plating methods shows that spontaneous electrical activity is eliminated in a dose-responsive fashion following application of voltage-gated sodium channel blocker TTX. (D) Field potential amplitude heat map over a 10-minute recording demonstrates that flunarizine, a sodium and calcium channel antagonist commonly used to treat AHC patients, inhibits mixed cortical culture activity in a dose-dependent manner.

Discussion

Human iPSCs and derivative tissues have allowed researchers to study disease phenotypes specific to human neurons in the laboratory setting (Ben Jehuda et al., 2018; Okita et al., 2011). While hiPSC-based model systems are not meant to replace genetically engineered mouse models, they serve as an additional system and may better replicate some mechanisms of complex human diseases (Jucker, 2010; Maussion et al., 2019). This is particularly true when considering early onset neurodevelopmental syndromes and conditions with strong genotype-to-phenotype correlations like alternating hemiplegia of childhood (Chailangkarn et al., 2012; Fink and Levine, 2018). In order to better study the neuronal manifestations and pathophysiology of AHC, we sought to create an hiPSC-derived cortical neuronal disease model. The synchronization of two dual-SMAD inhibition based neural differentiation protocols (Maroof et al., 2013; Shi et al., 2012a) allowed us to study separate cultures of early born glutamatergic neurons and GABAergic interneurons in simultaneous timeframes without prematurely narrowing our hypotheses. This system creates significant improvements in the reproducibility of data and culture conditions in our hands when compared to temporally separated differentiation runs that start from disparate iPSC populations. Standardized morphogen treatment windows and passage dates create more clarity in often opaque protocol language allowing for greater reproducibility between scientists and laboratories.

Neurons generated from the modified Shi and Maroof differentiation protocols replicated the findings of the original publications. iPSC-derived neurons were positive on immunoblotting and immunostaining for common neuronal markers, and the ventralized (Maroof) cultures express higher levels of inhibitory interneuron markers including GABA, GAD67, and Nkx2.1. Importantly, these neurons express the NKA-α3 subunit of interest in AHC by d32 of neural differentiation, making the system amenable to rapid *in vitro* study designs using expandable neuronal cultures. iPSC-derived neurons segregate independently from each other and are grossly different from iPSCs on principal component analysis of mRNA transcript expression. Differential expression also suggests that transcript levels of *FXYD2*, an NKA-associated subunit that is known to be expressed in different neuronal subtypes (Venteo et al., 2012), may be downregulated in diseased neurons and could be of interest in follow up studies.

Spontaneous electrical activity on microelectrode array analysis is present even in the absence of astrocyte coculture and is silenced by TTX treatment, supporting data from the original publications regarding synaptic maturation immunostaining and whole cell patch clamp electrophysiological data. While glial co-culture associated improvements in electrical maturation have been reported across multiple studies, neural activity in these protocols can proceed without the presence of exogenous glial populations (Gunhanlar et al., 2018; Kuijlaars et al., 2016; Odawara et al., 2016; Schutte et al., 2018; Xie et al., 2018). MEA analysis also confirms that flunarizine, a drug commonly used to prevent AHC episodes, has an inhibitory effect on iPSC-derived neuron electrical activity at nanomolar concentrations. Initial data has not revealed any striking differences in neural viability or lineage preference between AHC and control genotypes within each differentiation protocol, suggesting that future data generated can be analyzed for phenotypes without reservation.

The optimization of a synchronized paired differentiation protocol included initial attempts at generating GABAergic cultures via multiple other dual-SMAD inhibition-based culture methods, including the use of floating aggregate culture systems and different morphogen recipes (Kim et al., 2014; Liu et al., 2013). In the end, the Maroof protocol was the most reproducible and generated the largest tissue volume, resulting in cell populations with very similar dynamics and expansion rates to Shi protocol mixed cortical cultures. Newer differentiation protocols including lentivirus transduction of transcription factors to drive glutamatergic (Zhang et al., 2013b) and GABAergic (Yang et al., 2017) neural lineage specification are now available for use in the field and will be explored in later chapters but did not reach levels of production necessary for the experiments described in Chapter III.

Using the phenotypically severe *ATP1A3*$^{+/E815K}$ genotype as the starting point in our model system, we generated novel isogenic wildtype lines to be studied in parallel with unrelated control lines. Two iPSC clones per genotype (AHC E815K, isogenic control, and unrelated control) will be used throughout the remainder of this document when possible, after the establishment of this consistent model system. Isogenic lines have gone through thorough validation efforts including initial screening restriction enzyme digests and confirmation with PCR product sequencing that was repeated multiple times to ensure line identity prior to the beginning of differentiations. Extended primer site PCR was performed to ensure that no major indels exists near initial primer binding sites that would cause false positives during screening and sequencing of isogenic clone DNA. Whole exome sequencing was performed on clone IC2 and successfully verified wildtype status and homozygosity of an intended PAM site silent mutation. The inclusion of isogenic lines has become expected in the field of iPSC research and greatly increases the power and reproducibility of study results (Bassett, 2017). Further studies in this document will utilize this defined model system to identify phenotypes in human neurons derived from AHC patient iPSCs, and we hope that this model system is of use to other researchers in the field of iPSC derivative disease modeling.

Materials and Methods

Study subjects

Cell lines from a subject diagnosed with AHC were generated for this study. AHC patient 91759 is female and was diagnosed with AHC at 2 years of age. She first displayed symptoms at 4 weeks of age including tonic arm extension and abnormal ocular movements. Spells of alternating hemiplegia lasting 1-2 days began at 5 months of age, with quadriplegic episodes starting at 10 months. Genetic testing subsequently revealed a heterozygous c.2443G>A (p.E815K) missense mutation in the *ATP1A3* gene. The patient had subsequent disease progression including developmental delay, intellectual disability, and behavioral issues. Two iPSC clones generated from this patient line were used in this study (AHC-20, AHC-24). Isogenic wildtype controls (IC1, IC2) were then created from CRISPR/Cas9 editing of patient clone AHC-24 as described below. Unaffected female (UC1, 18 years old) and male (UC2, 25 years old) unrelated controls were also used in this study and previously reported as valid iPSC clones (Armstrong et al., 2017; Kumar et al., 2014).

Generation and validation of iPSCs

Fibroblasts were isolated by 3 mm punch skin biopsy from unrelated control volunteers or the described AHC patient following informed consent of volunteer or parent/guardian (study approved by the Vanderbilt Institutional Review Board). Isolated fibroblasts were cultured in DMEM (Gibco) with 10% FBS, 1% non-essential amino acids, and 1% penicillin-streptomycin. To reprogram fibroblasts to pluripotency, dividing cells were electroporated using the Neon System (Invitrogen) with plasmids expressing *OCT4, SOX2, KLF4, L-MYC, and LIN28* (Addgene plasmids #27077, #27078, and #27080) using previously published protocols (Armstrong et al., 2017; Okita et al., 2011). Two days following transfection, culture media was changed to TeSR-E7 (StemCell Technologies). Defined iPSC-like colonies were manually isolated 3-4 weeks post-transfection and expanded on Matrigel (Corning) in mTeSR1 (StemCell Technologies). Validation was performed through: pluripotency marker validation (Nanog, Oct4, SSEA3, SSEA4, and TRA-1-60); embryoid body differentiation and immunostaining with trilineage tissue markers defining ectoderm (Sox1, β-III-Tubulin), mesoderm (smooth muscle actin), and endoderm (GATA4, Sox17); and karyotype analysis of iPSC clones (Genetic Associates Inc, Nashville, TN). See supplementary reagents table for additional information on antibodies, dilutions, and applications. Validated iPSCs were cultured on Matrigel-coated plates, fed daily with mTeSR1, and passed weekly at a ratio of 1:10-50 dependent on colony confluency using ReLeSR (StemCell Technologies).

Creation of isogenic wildtype lines and genotyping

Genome editing was performed following previously published methods (Ran et al., 2013). CRISPR guide RNAs were designed to target the region containing the AHC-causing *ATP1A3* c.2443G>A mutation in exon 18 using an online tool (ChopChop). Single-stranded DNA oligos were designed to flank the targeted cut site by 60-80 bps on each side and contained both the intended wildtype correction along with synonymous PAM-site mutations to limit repetitive cutting events (Paquet et al., 2016). sgRNA oligos (IDT) were phosphorylated, annealed, and ligated into plasmid DNA containing the Cas9 enzyme and a puromycin resistance cassette (PX459, Addgene) followed by exonuclease treatment. Ligated plasmids were transformed into DH5-alpha competent *E. coli*. Plasmid DNA was sequence verified using a primer for the U6 promoter. iPSCs were dispersed to single cells with Accutase (StemCell) and suspended to a concentration of 10^6 cells per 100 µL. Plasmid constructs were delivered to suspended solutions of iPSCs containing the AHC patient genotype $ATP1A3^{+/E815K}$ by electroporation (Neon System, settings: 1200 V, 20 ms, 2 pulses) and plated at low density in mTeSR1 with 10 µM ROCK-inhibitor Y-27632 (StemCell). Thirty-six hours after plasmid delivery, selection for plasmid expression in iPSCs was performed by a 48-hour treatment of 0.5 µg/mL puromycin. mTeSR1 media was subsequently changed every other day for the following two weeks. Surviving colonies were picked and expanded for genotyping and continued culture. PCR amplification was performed using primers described in the supplemental methods. Restriction digest with BsiWI-HF (NEB, R3553) followed by confirmatory sequencing of products (GenHunter) identified corrected clones. Confirmed isogenic wildtype iPSC clones were validated for pluripotency with methods described above. Deep sequencing (100x) of line IC2 (isogenic corrected) was also performed using the VANTAGE Core at Vanderbilt to validate wildtype homozygosity. The synonymous PAM-site change (115 variant reads, 0 reference reads) was found in addition to the absence of original AHC mutation, without indels that would impair primer site binding and allele amplification during PCR.

Neural differentiation from iPSCs: Shi mixed cortical protocol

iPSCs were differentiated toward a cortical glutamatergic fate as described previously (Neely et al., 2012; Shi et al., 2012a; Telias et al., 2014) with minor modifications. iPSCs were maintained on Matrigel in mTeSR1 and incubated at 37°C in the presence of 5% CO_2 until they reached approximately 70-80% confluency. iPSC colonies were passaged with Accutase and plated at high density ($25x10^4$ cells / cm^2) in mTeSR1 with ROCK-inhibitor onto Matrigel-coated 12-well plates (day -2). The cells were fed mTeSR1 the following day (day -1), reached confluency, and switched to neural induction media (Shi NIM: Neural maintenance media [NMM] supplemented with 10 µM SB-431542 and 100 nM LDN-193189) on day 0. Cultures were refed with Shi NIM daily from d1-d9. Neuroepithelial sheets were passaged using Dispase on day 10 at a ratio of 1:1 into NIM-containing Matrigel-coated 6-well plates. The following day (day 11), cultures were fed NMM. Upon the appearance of rosettes (around day 16), NMM was supplemented with 20 ng/mL FGF2 for 3 days before being withdrawn. Cells were passaged at day 20 with Dispase at a ratio of 1:2-3 onto Matrigel-coated 6-well plates and expanded until day 32 in mixed cortical neural differentiation media (Mixed Cortical NDM supplemented with 10 ng/mL BDNF, 10 ng/mL GDNF, 10 ng/mL IGF-1, and 1 µM dibutyryl cAMP). At day 32, iPSC-derived neurons were dispersed to single cells with Accutase and plated onto destination or maintenance plates for further analysis and culture. Half media changes were performed every 2-3 days as determined by media usage. Neural media recipes and full reagent list are included in the appendix.

Neural differentiation from iPSCs: Maroof GABAergic protocol

iPSCs were differentiated toward a GABAergic cortical interneuron fate as described previously (Maroof et al., 2013) with slight modifications. iPSCs were plated to confluency in a 12-well plate as described above. At d0, media was switched to Maroof NIM (KSR media supplemented with 10 μM SB-431542, 100 nM LDN-193189, and 2 μM XAV939). A titration of the base media from KSR to NMM occurred during days 5-7 of differentiation, with small molecules present until passage at day 10. Differentiating cultures were passaged using Dispase on day 10 at a ratio of 1:1 into Matrigel-coated 6-well plates into NMM containing 50 ng/mL sonic hedgehog (SHH) and 1 μM purmorphamine (NMM+PurSHH). Cultures were fed daily with NMM+PurSHH until day 18. Cells were passaged at day 20 with Dispase at a ratio of 1:2-3 onto Matrigel-coated 6-well plates and expanded until day 32 in GABAergic neural differentiation media (GABAergic NDM supplemented with 10 ng/mL BDNF, 10 ng/mL GDNF, 200 μM ascorbic acid, and 200 μM dibutyryl cAMP). At day 32, iPSC-derived neurons were dispersed to single cells with Accutase and plated onto destination plates. Half media changes of were performed every 2-3 days as determined by media usage.

Immunoblotting

Protein was collected from iPSCs at d0 and from neurons at d32 of differentiation using ice-cold RIPA buffer containing protease and phosphatase inhibitors. Ten micrograms of total protein mixed with 4x Laemmli loading buffer (BioRad) per lane were run on NuPAGE Bis-Tris 4-12% polyacrylamide gels and separated in MOPS buffer at 200V for 60 minutes. Protein was transferred to PVDF membranes at 95V for 60 minutes. Membranes were washed with TBS three times before being stained for total protein with REVERT (Li-Cor). The protein stain was removed, blots were washed three times with TBS, and the membranes were blocked with Odyssey Blocking Buffer for 60 minutes at room temperature. Primary antibodies were applied overnight at 4°C in an antibody incubation solution of TBS + 0.1% Tween-20 (TBST) with 5% BSA. See supplementary antibody table for more information on antibody usage and dilutions. Blots were washed five times with TBST the following day, and secondary antibodies (IRDye, Li-Cor) were applied for two hours at room temperature in antibody incubation solution. Membranes were washed five times with TBST prior to image capture on an Odyssey Scanner. Intensity data was collected using Image Studio Lite. β-Actin bands are shown as a visual aid for gels that were loaded with the same samples and run simultaneously. Total protein stein for individual membranes are shown in the Appendix (Supplemental Figure 2.2)

Immunostaining

For pluripotency validation in iPSCs and for immunostaining of embryoid body aggregates, cells were washed with PBS and fixed with 4% PFA for 20 minutes at room temperature. Samples were permeabilized with 0.1% TritonX-100 in PBS (PBST) for 5 minutes and blocked with a solution of 2.5% normal goat serum (NGS) in PBST for 1 hour at room temperature. This protocol was modified for staining iPSC-derived neurons to preserve cellular architecture, with neurons fixed in 2% PFA and the blocking solution including 5% NGS. Primary antibodies were applied in the blocking solution overnight at 4°C followed by three PBS washes. Secondary antibodies were applied in blocking solution for two hours at room temperature followed by another PBS wash before nuclear staining with DAPI and mounting on coverslips or plate storage at 4C, if necessary. Low magnification (4-20x) images were collected using an EVOS fluorescent microscope. High magnification (60x) images were acquired using an Andor DU-897 EMCCD camera mounted on a Nikon spinning disk microscope. Confocal images are shown for qualitative

assessment of membrane expression of NKA-α3 subunits. Software used for image acquisition and reconstruction included NIS-Elements Viewer (Nikon) and ImageJ (FIJI).

Bulk Tissue RNAseq

RNAeasy Mini Kits (Qiagen) were used to isolate total RNA from iPSCs or iPSC-derived neuronal cultures of unrelated control or AHC *ATP1A3*$^{+/E815K}$ patient lines at d0 (iPSC) and d32 using either the Shi (mixed cortical) or Maroof (GABAergic shifted) differentiation protocols. Collection included on-column DNase treatment to further purify RNA. Samples were stored at -80C until sent to the Vanderbilt Technologies for Advanced Genomics (VANTAGE) Core for further processing. VANTAGE performed quality control (QC) prior to sample analysis, and all samples passed QC standards by RNA integrity measures and sample yield. mRNA enrichment and cDNA library preparation was performed utilizing a stranded mRNA (polyA-selected) sample prep kit. Sequencing was performed at Paired-End 150 bp on an Illumina NovaSeq6000. Initial data analysis was performed in collaboration with VANTAGE. Data was trimmed using FastQC and aligned to HG38 using RSEM and count data was analyzed using edgeR. Delivered results included demultiplexed FASTQ files containing the PF reads, targeting a mean of ~30M reads/sample, aligned BAM files, and a differential expression table. Principal component analysis (PCA) graphs and further RNA data processing were completed in R with the assistance of Kevin Yang. Gene ontology charts were created using differentially expressed gene lists imported into GO Enrichment Analysis powered by PANTHER.

MEA Plating and Dose Curves

Axion Cytoview 48-well MEA plates were pretreated with a 0.1% polyethyleneimine (Sigma, P3143) in borate buffer solution for one hour, washed thoroughly with water, and dried overnight the day prior to plating. Neurons from mixed cortical protocol cultures were dispersed with Accutase at d45-50 of differentiation and plated at a concentration of $3x10^5$ cells/well into MEA plates in 50 µL of culture media containing 10 µg/mL laminin (Sigma, 11243217001). One hour after plating, the well was gently flooded with 300 µL culture media. After approximately two weeks on the MEA surface, baseline recordings were taken for a period of 10 minutes prior to drug application. For TTX (Abcam, ab120055) dose curve, concentrated solutions in culture media were added directly to ambient media and therefore diluted to the necessary final concentration. The plate was read immediately after drug additions for another 10-minute period to calculate activity ratios compared to baseline. For flunarizine (Enzo, ALX-550-268) dose curve, a full media change was performed 24 hours before the recording period with flunarizine at the labeled dosage or with DMSO vehicle. Data were analyzed using AxIS 2.0 Software (Axion Biosystems) by replaying recordings in offline neural spontaneous mode.

CHAPTER III

TRANSCRIPTIONAL COMPENSATION AND TRIGGERED PHENOTYPES IN AHC IPSC-DERIVED NEURONS

Parts of this work are published in *Neurobiology of Disease* by Elsevier entitled "Neuronal Modeling of Alternating Hemiplegia of Childhood Reveals Transcriptional Compensation and Replicates a Trigger-Induced Phenotype" (Snow, Westlake, Klofas, Jeon, Armstrong, Swoboda, George, and Ess; 2020)
DOI: 10.1016/j.nbd.2020.104881

Abstract

An *in vitro* iPSC-derived neuron disease model was created to search for phenotypes in human cell lines that may provide clues towards disease pathogenesis or improved therapeutic routes. *We hypothesized that diseased neurons from our paired differentiation protocols would not show changes in NKA subunit protein or mRNA expression but may display abnormal development and hyperactive neural activity on microelectrode array analysis that would be exacerbated in the presence of a heat stress trigger.* In both mixed cortical and GABAergic iPSC-derived neuronal cultures, we found elevated levels of *ATP1A3* mRNA in AHC lines compared to controls without significant perturbations in protein expression. MEA analyses demonstrated that in mixed cortical neuronal cultures, *ATP1A3*$^{+/E815K}$ iPSC-derived neurons displayed less overall activity than neurons differentiated from isogenic and unrelated control cell lines. However, induction of cellular stress by elevated temperature revealed a hyperactivity phenotype following heat stress in diseased neurons compared to controls. While weighted mean firing rate was not different between genotypes, AHC neuron firing patterns failed to develop signatures of local bursting. Treatment with flunarizine, a drug commonly prescribed to prevent AHC episodes, did not impact these phenotypes. These are the first reports of human iPSC-derived neuronal hyperactivity and abnormal population level electrical maturation in AHC. These findings support the use of iPSC-derived neuronal cultures for studying complex neurodevelopmental conditions such as AHC and provide a potential route toward future mechanistic discovery.

Introduction

Alternating hemiplegia of childhood (AHC) is a rare and devastating neurodevelopmental disorder caused by heterozygous missense mutations in *ATP1A3*, the gene encoding the α3 subunit of the Na,K-ATPase (NKA) ion transporter (Heinzen et al., 2012). As described in Chapter I, the NKA complex is responsible for exchanging three cytoplasmic sodium ions for two extracellular potassium ions, thus establishing electrochemical gradients essential for crucial cellular functions and membrane potential (Benarroch, 2011; Clausen et al., 2017; Dobretsov and Stimers, 2005). Patients with AHC present early in life with a constellation of symptoms including abnormal eye movements, seizures, dystonia, and characteristic spells of alternating hemiplegia or full quadriplegia (Bourgeois et al., 1993; Heinzen et al., 2014). Episodes in AHC are often triggered by external stimulation including temperature changes, physical exertion, or exposure to certain foods, among other triggers (Kansagra et al., 2013; Sweney et al., 2009). Over time, AHC patients manifest developmental delay and acquire intellectual disabilities. 60% of patients worldwide diagnosed clinically as AHC have one of three unique *ATP1A3* missense mutations, leading to amino acid changes D801N, E815K, or G947R (Viollet et al., 2015). Only symptomatic treatment options exist for patients diagnosed with AHC, including benzodiazepines and other antiepileptic drugs. A non-specific sodium and calcium channel blocker, flunarizine, has been anecdotally used to treat many patients

for the past several decades (Casaer, 1987; Heinzen et al., 2012). Flunarizine has been reported in several recent studies to reduce the severity, duration, or frequency of hemiplegic spells in some patients with AHC, although not all individuals respond to treatment (Delorme et al., 2017; Kansagra et al., 2013; Pisciotta et al., 2017). Conclusions from these studies are limited by small numbers of patients and lack of randomized control groups.

While the NKA-α1 subunit is ubiquitously expressed across cell types, expression of the NKA-α3 subunit is generally restricted to neurons (Clausen et al., 2017; Richards et al., 2007). A critical component of neuronal functionality, the α3 subunit has lower affinity for sodium ions allowing the rapid expulsion of positive ions following neuronal activity and depolarization, particularly in dendrites (Azarias et al., 2013; Blom et al., 2011; Kim et al., 2007). Common AHC-causing mutations in the NKA-α3 subunit result in impaired ion transporting ability without impacting protein trafficking to the plasma membrane (Heinzen et al., 2014; Koenderink et al., 2003; Li et al., 2015). A recent study demonstrated lower pump current and depolarized resting membrane potential in AHC-mutant iPSC-derived excitatory neurons (Simmons et al., 2018). *Drosophila* and mouse models of *Atp1a3* mutations associated with human disease often replicate trigger-induced symptoms or exacerbation (DeAndrade et al., 2011; Helseth et al., 2018; Holm and Lykke-Hartmann, 2016; Isaksen et al., 2017; Palladino et al., 2003; Sugimoto et al., 2014).

Chapter II described a patient-specific iPSC-derived neuronal model was that focuses on the most phenotypically severe mutation in AHC, E815K. In Chapter III, we sought to test if this mutation results in transcriptional or protein level NKA subunit compensation for impaired pump function in patient-specific human iPSC-derived neurons. Using both unrelated and isogenic corrected *ATP1A3*$^{+/+}$ controls, we measured transcript levels of multiple NKA-α and NKA-β subunits. We found elevation of *ATP1A3* mRNA during neuronal differentiation of iPSCs, while differences in NKA-α3 protein expression did not reach statistical significance. We then studied heat stress within this model by employing microelectrode array (MEA) analyses to determine if a trigger-induced phenotype was replicated in this system. We found that rapid temperature increase resulted in diminished neuronal firing in both control and AHC patient neurons. However, neurons derived from AHC patient lines revealed an exaggerated rebound of activity and ultimately became hyperactive compared to controls. Intriguingly, while mean firing rate was variable but similar between genotypes, AHC lines failed to develop local bursting patterns characteristic of maturing networks (Cotterill et al., 2016). Treatment with flunarizine, a non-FDA approved drug used anecdotally to prevent AHC patient episodes, had minimal impact on neuronal firing and temperature-triggered rebound hyperactivity phenotypes. Our findings importantly suggest that elevated expression of *ATP1A3* mRNA may be both a feature of AHC pathogenesis and a possible biomarker for future *in vitro* studies. Additionally, modeling complex symptoms such as trigger-induced episodes is possible in iPSC-derived neuronal models, providing a potential route for screening of future treatments including both small molecules and gene replacement or genome editing therapies.

Results

Experimental design for analysis of AHC phenotypes in iPSC-derived neurons

With the establishment of standardized and reproducible protocols for neural differentiation of iPSCs into mixed cortical (Shi et al., 2012a) and GABAergic (Maroof et al., 2013) lineages, we sought to create an equally standardized experimental design for data collection (**Figure 3.1**). After plating iPSCs at high density onto plates at day -2, differentiations began at d0 with morphogen treatment and subsequent expansion passages until d32 as previously described. MEA plating at d45 allowed for a week of maturation prior to the initiation of a heat stress recording protocol at d52 that is described later and was repeated every 4 days. Flunarizine or DMSO treatment began at d60 and continued until the conclusion of the experiment

at d80. Protein and RNA was collected at d0, d32, and d60 for analysis. To eliminate variability inherent in human iPSC and derivative experiments, five separate runs of paired differentiations were generated and completed using this paradigm, each with two clones per genotype (unrelated control [UC], isogenic control [IC], AHC E815K [AHC]). The initial figures in this chapter describe our findings in mixed cortical cultures which will then be complemented by data from GABAergic cultures. They are presented as such to simplify the results and due to accumulating culture impurities in GABAergic protocol products by d60-d80 which will be described later.

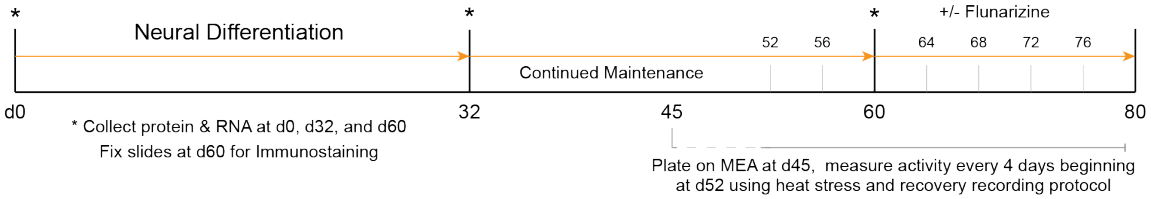

Figure 3.1 – Experimental design for phenotype analysis in an iPSC-derived neuronal model of AHC. Experimental design included three collection timepoints for protein and RNA (*; d0, d32, d60) from iPSCs and derivative neurons using both mixed cortical and GABAergic shifted differentiation protocols. iPSC-derived neurons were plated onto microelectrode array (MEA) plates at d45 and recordings began at d52 through d80 at 4-day intervals using a heat-stress and recovery protocol to mimic triggers experienced by AHC patients. From d60-d80, 100 nM flunarizine or vehicle (DMSO) were added to the MEA feeding media.

iPSC-derived neurons express NKA-α3 subunit protein early during in vitro neurodevelopment

Evidence from heterologous overexpression studies suggest that while some *ATP1A3* mutations have the potential to cause trafficking abnormalities, no known AHC causing mutations result in altered membrane expression of the NKA-α3 subunit (de Carvalho Aguiar et al., 2004; Heinzen et al., 2014). We hypothesized that our *in vitro* human stem cell derived model would not show changes in NKA-α3 protein expression and localization. Indeed, previously described immunostaining for NKA-α3 did not reveal any obvious localization differences or intracellular aggregation between AHC and control iPSC-derived neurons (Figure 2.5, Supplemental Figure 2.3). Recent studies have explored the possibility of competitive relationships between NKA-α1 and NKA-α3 in phenotypic expression of disease variants (Arystarkhova et al., 2019), highlighting the importance of expression characteristics in our disease model. We therefore performed immunoblotting to analyze NKA-α1 and NKA-α3 expression relationships in control and disease lines throughout the course of *in vitro* neural differentiation (**Figure 3.2A, Supplemental Figure 3.1**). No significant differences in differentiation toward a neuronal fate by β-III-Tubulin expression were noted between controls and disease at d32 or d60 (**Figure 3.2B**). NKA-α1 expression dropped during early neural development at d32 then rebounded by d60 of differentiation, with no differences between control lines and AHC patient lines (**Figure 3.2C**). The neuronal specific NKA-α3 subunit was absent in iPSCs before rising substantially during neural differentiation, as expected. No differences in NKA-α3 subunit expression existed at d32 between disease and control neurons, while at d60 α3 expression was significantly elevated in *ATP1A3*$^{+/E815K}$ mixed cortical cultures compared to unrelated controls ($p = 0.0047$). However, no significant difference was noted compared to isogenic controls ($p = 0.7257$) at d60, highlighting the importance of incorporating isogenic lines in experimental disease modeling when possible (**Figure 3.2D**). Overall, data trends support nonsignificant changes in neural differentiation outcomes and NKA-α subunit protein expression in *ATP1A3*$^{+/E815K}$ disease lines compared to control lines.

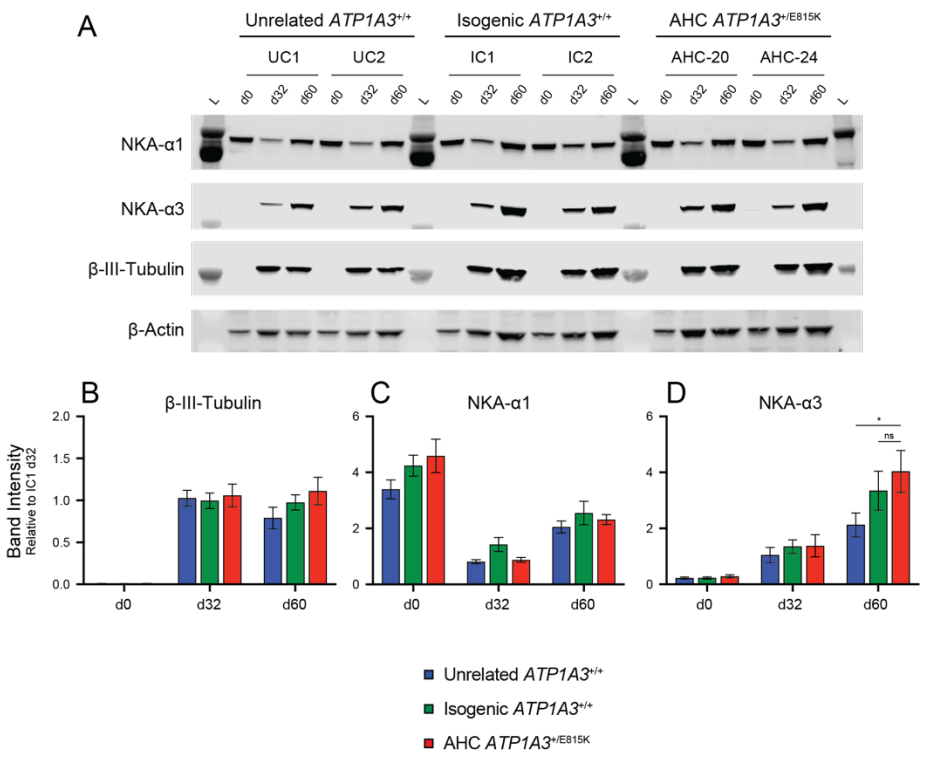

Figure 3.2 - AHC and control iPSC-derived neurons express similar levels of NKA-α3 subunit protein. (A) Representative immunoblot of protein collected from mixed cortical neuronal cultures and probed for NKA-α1, NKA-α3, and β-III-Tubulin. While β-Actin is shown as a visual guide for protein loading, intensity data was normalized to total protein by REVERT staining show in the Appendix. (B) β-III-Tubulin expression increases as expected during iPSC-derived neuronal induction. No significant differences in induction efficiency by this measure are noted on immunoblot between genotypes. (C) NKA-α1 expression dropped during early neurodevelopment at d32 then increased by d60 in a consistent pattern with no significant differences between genotypes. (D) NKA-α3 expression was very low to nondetectable in iPSCs and increased drastically by d32 and d60 of differentiation. AHC lines expressed significantly more NKA-α3 by immunoblot compared to unrelated control lines ($p = 0.0047$) at d60, while this difference was not observed in isogenic corrected and AHC lines ($p = 0.7257$). Graphs display quantified intensity data relative to clone IC1 d32 intensity. n = 10 per data point (5 differentiations, 2 clones per genotype). 2-way ANOVA with Bonferroni's multiple comparisons test; significant findings notated by *, $p < 0.005$; ns = not significant ($p > 0.005$).

AHC neurons display increased NKA-α3 subunit transcripts

While no statistically significant differences were noted for NKA-α1 and NKA-α3 subunit protein expression between isogenic control and AHC lines during neural differentiation, this does not rule out differences in transcriptional regulation of these or other related NKA subunits. To assess whether transcriptional compensation of these subunits existed in our disease model, we profiled NKA-subunit transcription of iPSC-derived neurons at d0, d32, and d60 of differentiation. *ATP1A4* transcript levels were not assessed as this gene product has been shown to be expressed only in a testes-specific pattern, with no transcript expression observed in our model during preliminary studies. iPSCs expressed predominantly *ATP1A1* and *ATP1B3* transcripts (**Figure 3.3A**), with some expression of *ATP1A2* and other β-subunit transcripts. These patterns in iPSCs were consistent between genotypes. While there was a significant elevation in unrelated control cells of *ATP1A2* mRNA compared to the disease and isogenic control groups, there were no differences in any other transcripts. The NKA-subunit expression profile shifts toward an

ATP1A3 and *ATP1B1* dominant pattern in iPSC-derived neurons. Intriguingly, there was a significantly greater level of *ATP1A3* transcript expression in disease neurons compared with control groups at both neural collection timepoints (AHC-to-isogenic: d32 p = 0.0015; d60 p = 0.0005). These patterns remain consistent whether comparing AHC transcript levels to unrelated or isogenic control data (**Figure 3.3B-C**). Later significant elevation of *ATP1B1* transcripts was also noted, suggesting the possibility of a lagging compensation of this interacting subunit. These data suggest the existence of a feedback mechanism in iPSC-derived neural cultures resulting in elevated expression of neural specific NKA-subunit transcripts in the presence of a disease causing AHC mutation and associated cellular abnormalities.

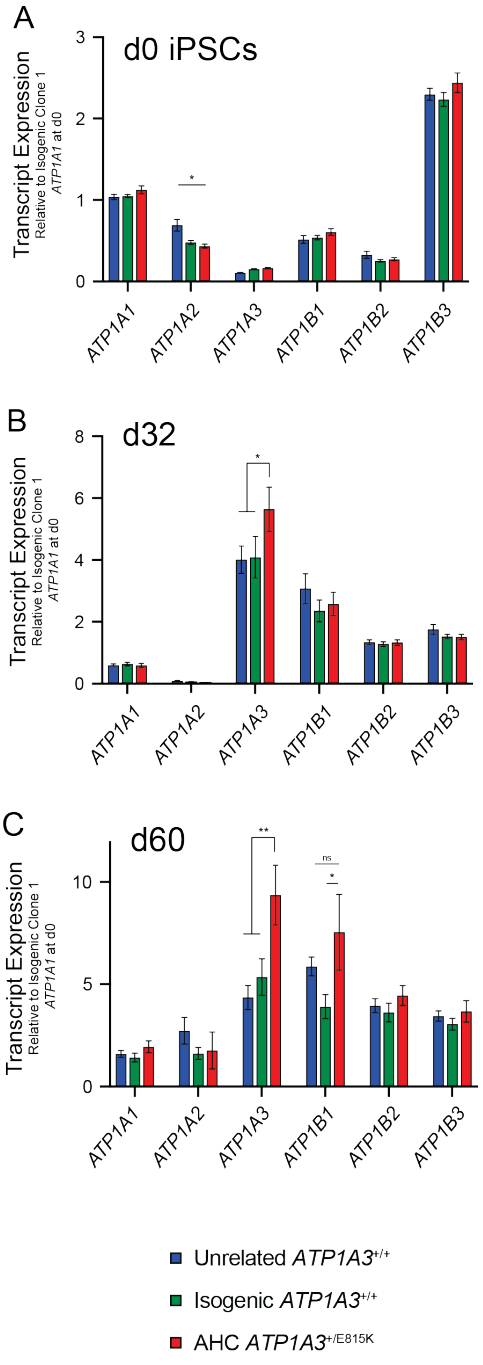

Figure 3.3 - The transcriptional profile of NKA-subunits is altered in AHC patient iPSC-derived neurons. (A) The NKA transcriptional profile of iPSCs is dominated by *ATP1A1* and *ATP1B3* expression. While *ATP1A2* transcripts are elevated in unrelated *ATP1A3*$^{+/+}$ iPSCs compared to AHC lines (p = 0.0010), there is no difference noted between AHC and isogenic corrected iPSCs (p > 0.9999). (B) By d32 of *in vitro* neuronal differentiation, the NKA-subunit transcription pattern shifts toward *ATP1A3* and *ATP1B1* expression. There was a significant elevation at this timepoint in *ATP1A3* transcript levels between AHC and both isogenic (p = 0.0015) and unrelated (p = 0.0008) control neurons. (C) At d60, elevated production of *ATP1A3* mRNA was maintained (AHC-to-isogenic p = 0.0005; AHC-to-unrelated p < 0.0001), and a lagging elevation of *ATP1B1* mRNA was noted in AHC groups compared to isogenic corrected neurons (p = 0.0018). Graphs display transcript expression relative to clone IC1 *ATP1A1* transcripts at d0. Statistical conclusions are maintained if normalizing to *ATP1A1* expression values for each individual clone at d0. n = 10 (5 differentiations, 2 clones per genotype). 2-way ANOVA with Bonferroni's multiple comparisons test; significant findings notated by: * p < 0.005, ** p < 0.001; ns = not significant (p > 0.005).

iPSC-derived neurons are electrically active on MEA analysis

To assess if AHC patient derived neurons manifest differences in neural activity on a population level, we interrogated iPSC-derived neurons using microelectrode array (MEA) recordings. Activity was first recorded at d52 and continued every 4 days until cultures were terminated at d80. Coculture with glial cells was not performed in an attempt to isolate changes specific to this differentiation protocol. MEA plates were visually observed several days after plating to ensure coverage of the recording area (**Supplemental Figure 3.2**). Neurons from this mixed cortical differentiation protocol were active on MEA analysis, and neural activity of iPSC-derived cultures continued to increase over the course of the d52-to-d80 recording window (**Figure 3.4A**). AHC lines consistently trended towards lower activity compared to both control groups at most timepoints, although no statistically significant phenotypes were noted. Chronic treatment with flunarizine was performed to identify any impact in disease versus control lines (**Figure 3.4B**). A dose of 100 nM was chosen based on an initial dose-response

experiment where concentrations at or above 500 nM caused significant loss of neuronal activity in all genotypes (Figure 2.7). This concentration is consistent with the limited literature available regarding *in vitro* treatment of cortical cultures (Ye et al., 2011). Flunarizine-treated groups displayed similar dynamics to vehicle-treated groups, although flunarizine generally prevented the time-dependent activity increase in neuronal cultures without significant differences between control and E815K mutant groups. While flunarizine treatment decreased neural activity maturation in both isogenic control and AHC disease lines over time, unrelated control groups did not experience a large activity change in the presence of this drug, further stressing the importance of including isogenic cells in study designs (**Figure 3.4C**).

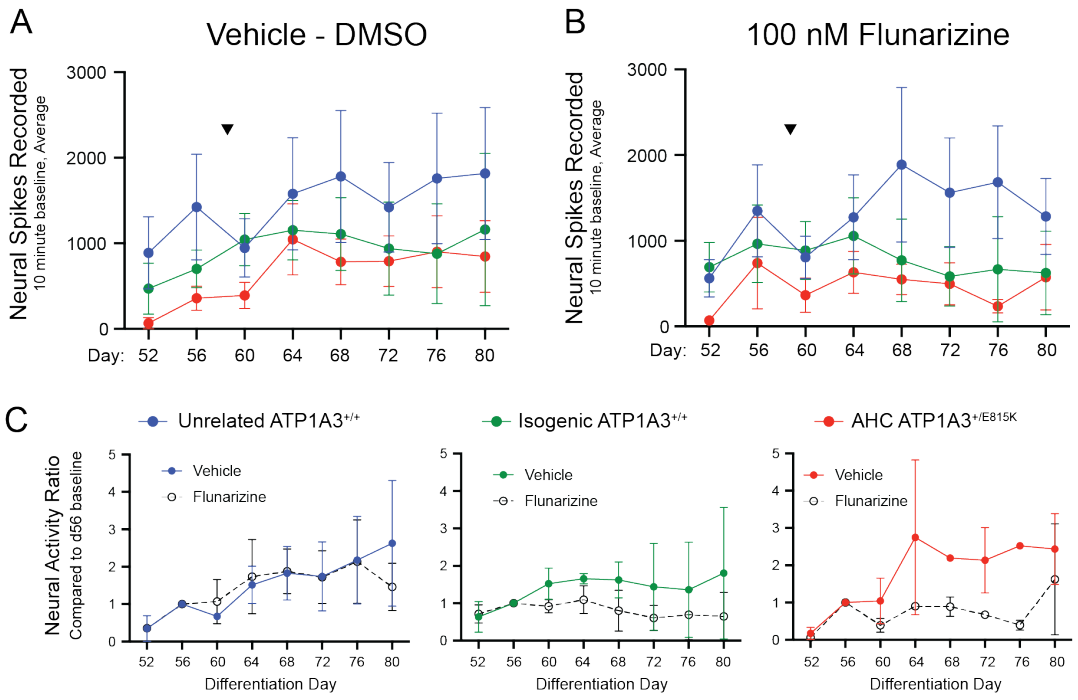

Figure 3.4 - iPSC-derived neurons electrically mature over time and are generally inhibited by flunarizine. Mixed cortical neuronal cultures were chronically treated beginning at d59 (arrowheads) with either DMSO (A) or 100 nM flunarizine (B). Regardless of treatment, baseline recordings of spontaneous neural activity show electrical activity and maturation over the course of the 28-day recording window. While unrelated wildtype and isogenic corrected neurons trend toward increased overall activity compared to AHC neurons, particularly at the beginning of the recording period, variability in spontaneous activity is too high to allow for statistically significant conclusions. n = 10 (5 differentiations, 2 clones per genotype) for each recording day. (C) Flunarizine resulted in a loss of activity maturation and thus decreased overall activity over time in isogenic corrected and AHC cultures, but not in unrelated control neurons. Data represents mean activity for each clone summed across all baseline recording periods (n=2 for each data point), normalized to activity levels at d56 for each condition prior to treatment with vehicle or flunarizine. Error bars represent SEM. Data collected on Axion Maestro Pro using spontaneous neural activity acquisition settings.

Trigger-induced neural hyperactivity in AHC cultures

Trigger-induced hemiplegic spells are a pathognomonic aspect of AHC and thus a possible insight into mechanistic underpinnings of the disease and related disorders. Described triggers range from fever to water exposure, ingestion of specific foods, and infection, among others. Animal models of disease have replicated stress-induced phenotype exacerbation, including vestibular stimulation or chronic restraint induced hemiplegia and dystonia in mouse models and heat-induced paralysis in *Drosophila* models of

ATP1A3 disease (Helseth et al., 2018; Holm and Lykke-Hartmann, 2016; Isaksen et al., 2017; Palladino et al., 2003; Sugimoto et al., 2014). To model triggered phenotypes in an iPSC-derived neuronal system, a novel temperature-based stress model was created (**Figure 3.5A**). Cultures on MEA plates were exposed to a heat stress protocol involving separate 10-minute recordings at baseline temperature (37°C), with heat stress (40°C), and during a recovery period (37°C) in the presence (**Figure 3.5B**) or absence (**Figure 3.5C**) of chronic flunarizine treatment. When normalizing to baseline activity for each clone per recording session, heat stress resulted in a slight reduction of activity that was insignificantly different between genotypes. However, a robust rebound hyperactivity phenotype was observed in AHC neurons compared to both the unrelated and isogenic control lines ($p < 0.0001$ for both comparisons). Chronic flunarizine treatment did not affect this phenotype compared to isogenic controls (AHC-to-isogenic $p < 0.0001$; AHC-to-unrelated $p = 0.0119$). However, when analyzed by individual recording day, vehicle treated cultures had more days with significant differences (4/6 days, **Figure 3.5D**) compared to flunarizine treatment (2/6 days, **Figure 3.5E**).

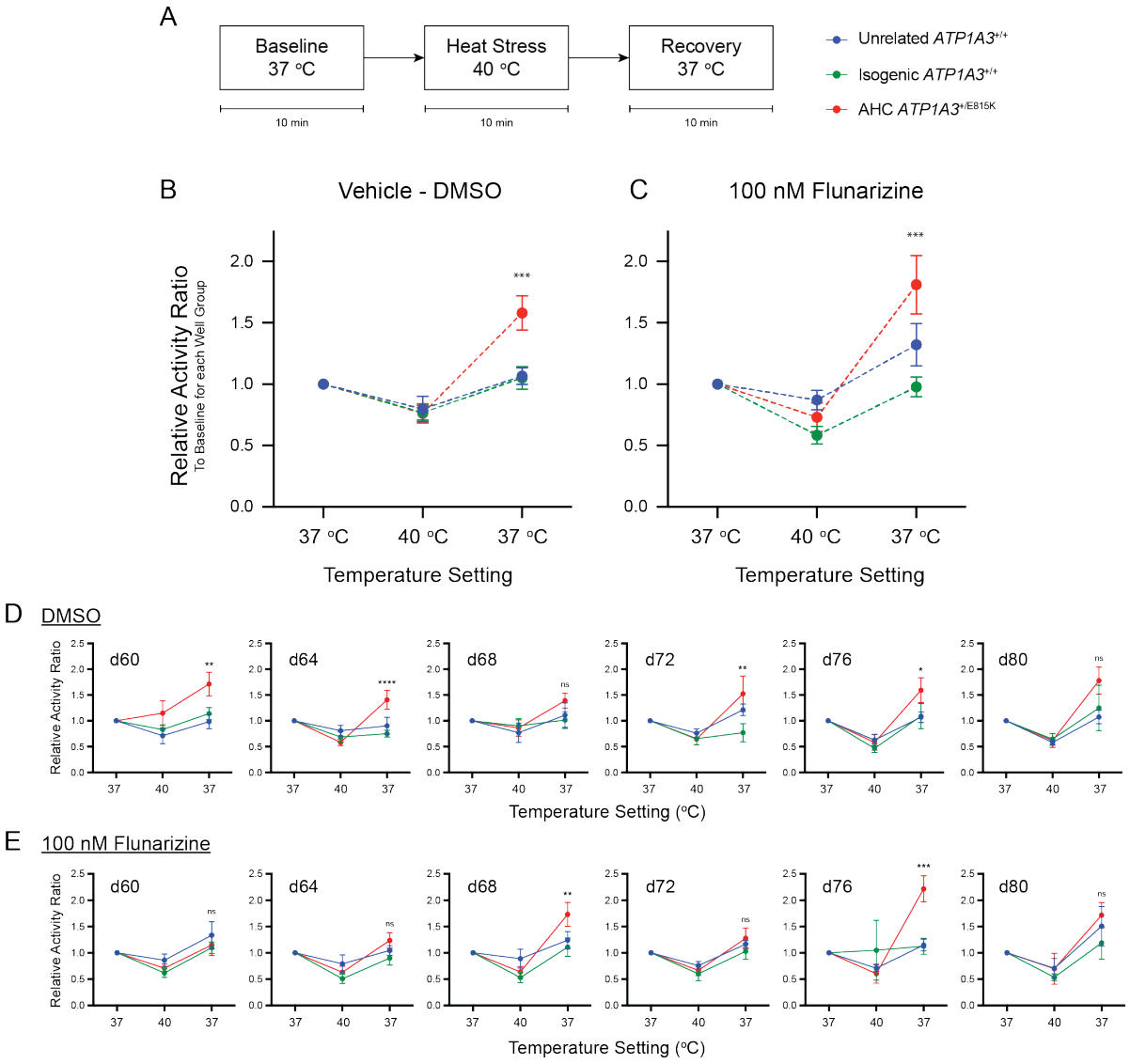

Figure 3.5 - AHC neurons display a stressed-induced hyperactivity phenotype following heat exposure. A paradigm of increased temperature and recovery (A) was designed for use on the MEA recording device to mirror stressors like fever experienced by AHC patients. Activity of well groups for each clone and treatment condition were normalized to the baseline period for each recording day to eliminate inherent variability in activity across different recording days and differentiations. (B) In the presence of elevated temperature, spontaneous neural activity dropped to approximately 75-85% of baseline activity across all genotypes. During the 10-minute recovery period, a relative hyperactivity phenotype was noted in the AHC neurons compared both unrelated wildtype and isogenic corrected control neurons (recovery period AHC-to-isogenic $p < 0.0001$; AHC-to-unrelated $p = 0.0001$). (C) Recovery phase hyperactivity in AHC neurons is unchanged following chronic 100 nM flunarizine treatment. (recovery period AHC-to-isogenic $p < 0.0001$; AHC-to-unrelated $p = 0.0119$) Heat stress protocol was repeated across all treatment recording days (d60, d64, d68, d72, d76, and d80), with each subsequent recording being treated as a technical replicate for that differentiation. n = 10 (5 differentiations, 2 clones per genotype). 2-way ANOVA with Bonferroni's multiple comparisons test; significant findings notated by: *** AHC-to-isogenic $p < 0.0001$. Neural spike activity ratios during heat stress protocol for each recording day are shown in the presence of vehicle (D) or chronic flunarizine (E) treatment. Supplemental Table 3.1 describes the sample size along with significance values and notations for each data point. Significance notations represent AHC-to-isogenic comparisons in the recovery period (37C). 2-way ANOVA with Bonferroni's multiple comparisons test, significance notated for D and E at $p < 0.05$ (*), $p > 0.01$ (**), $p<0.001$ (***), and $p<0.0001$ (****); ns $p > 0.05$. Error bars represent SEM.

AHC neurons fail to develop bursting characteristics over recording period

MEA data readouts are able to generate more sophisticated data than spike counts, although generally much of the data is derivative of overall activity (Amin et al., 2016; Cotterill et al., 2016). Weighted mean firing rate (wMFR) is a metric showing activity normalized over all active electrodes, yielding a standardized metric of neural activity. While high variability prevented conclusions generated from statistical analysis, it is clear that the wMFR rates are comparable between genotypes. Hyperactivity of AHC lines during the recovery phase compared to their own baseline is subtle but noticeable in this data set. Bursting metrics are another commonly utilized data point in MEA analysis. Bursting can occur locally over one electrode, or in more mature cultures can occur at a network level where full well bursting becomes synchronous. Unfortunately, consistent network bursting never occurred in this model system across any genotype. Interestingly, a clear phenotype emerged when analyzing local bursting over time. Both isogenic controls and unrelated controls begin experiencing significant bursting patterns towards the end of the recording window in mixed cortical cultures. This was not true in AHC E815K neurons, where little to no bursting occurred (**Figure 3.6**). However, when bursts did occur, they were generally of the same duration compared to both control groups, albeit showing substantial variance by recording day (**Supplemental Figure 3.4**). While more experimentation is needed to elucidate the mechanisms underlying this phenotype and the clinical correlates in AHC patients, it is possible that a lack of bursting is related to NKA-α3 dysfunction either via indirect developmental etiologies or direct electrophysiological impacts (Azarias et al., 2013; Hunanyan et al., 2018; Simmons et al., 2018; Zhang et al., 2009).

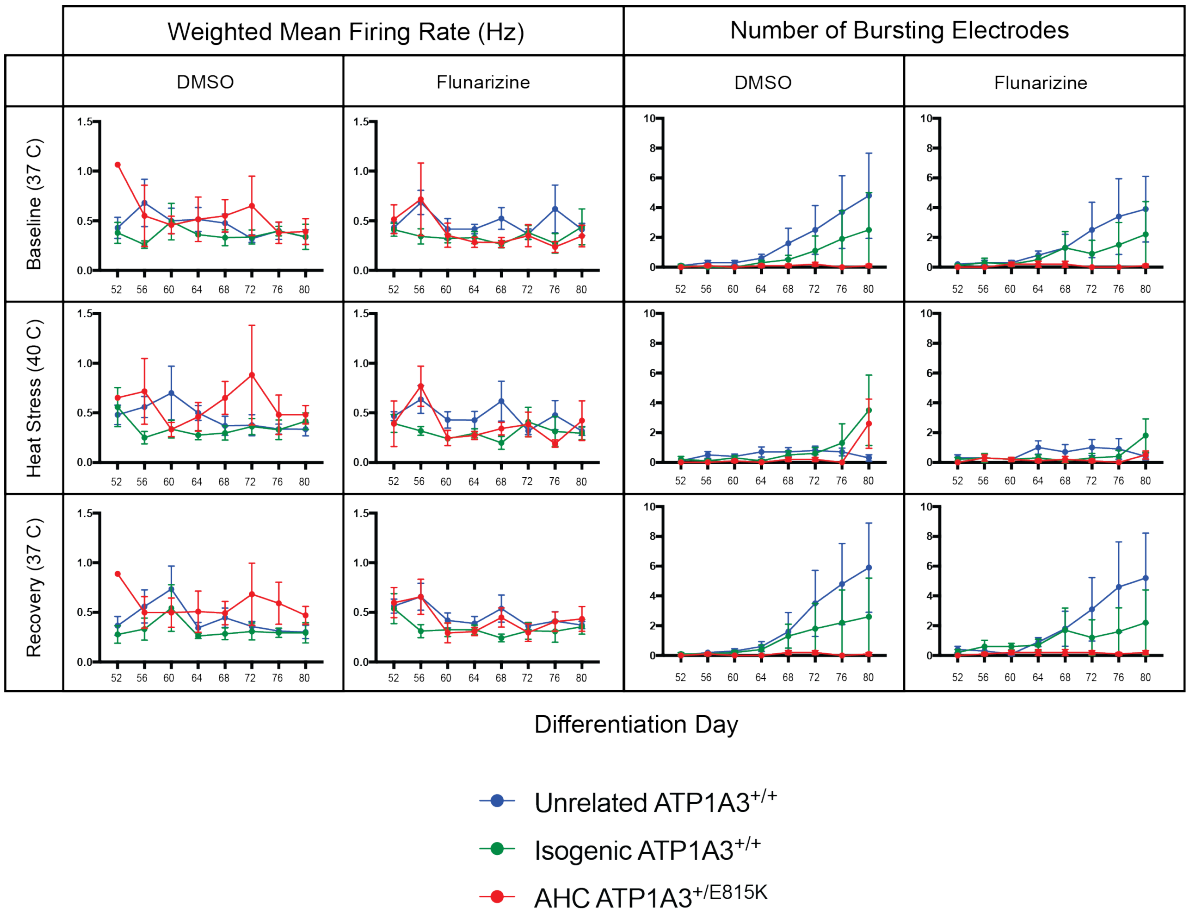

Figure 3.6 – Weighted MFR and bursting metrics further characterize iPSC-derived neuronal populations. Weighted mean firing rate (wMFR) is a metric normalizing mean firing rate over the active electrodes in a given well group to yield a more standardized rate value. While high variance exists between differentiations, it is clear that no major trends exist over time between genotypes. While MFRs did not show disease-specific trends, bursting metrics did reveal a difference. Both unrelated and isogenic control neurons developing local bursting patterns over time while AHC E815K neurons did not mature to noticeable levels using this metric. Exposure to elevated temperature silenced most bursting in the controls, which returned during the recovery phase of the experimental paradigm.

Findings are broadly replicated using a GABAergic differentiation protocol

A distinct protocol that drives iPSCs toward cortical GABAergic interneuron fates was simultaneously used to assess if our findings were specific to the glutamatergic predominant mixed cortical protocol or representative of a more generalized feature of AHC patient iPSC-derived neurons. While early neural cultures at d32 were consistently pure using this protocol (at the timepoint when previous RNAseq samples was collected) contaminating non-neuronal populations became obvious by d60 as demonstrated by loss of β-III-Tubulin staining on immunoblotting (**Figure 3.7A**). At d32, similar nonsignificant profiles of NKA-α1 and NKA-α3 protein expression existed compared to the mixed cortical differentiation protocol (**Figure 3.7B-C**). Importantly, a significant elevation of *ATP1A3* transcript expression in disease over control groups was again noted at d32 that deteriorated with loss of culture purity by d60 (**Figure 3.7D-E**). Transcriptional differences were consistent when comparing AHC transcript levels to either unrelated or isogenic controls at d32. Due to culture impurity at d60+, MEA recordings were unable to record sufficient levels of activity for relevant analysis of GABAergic neuronal cultures (**Supplemental Figure 3.4**).

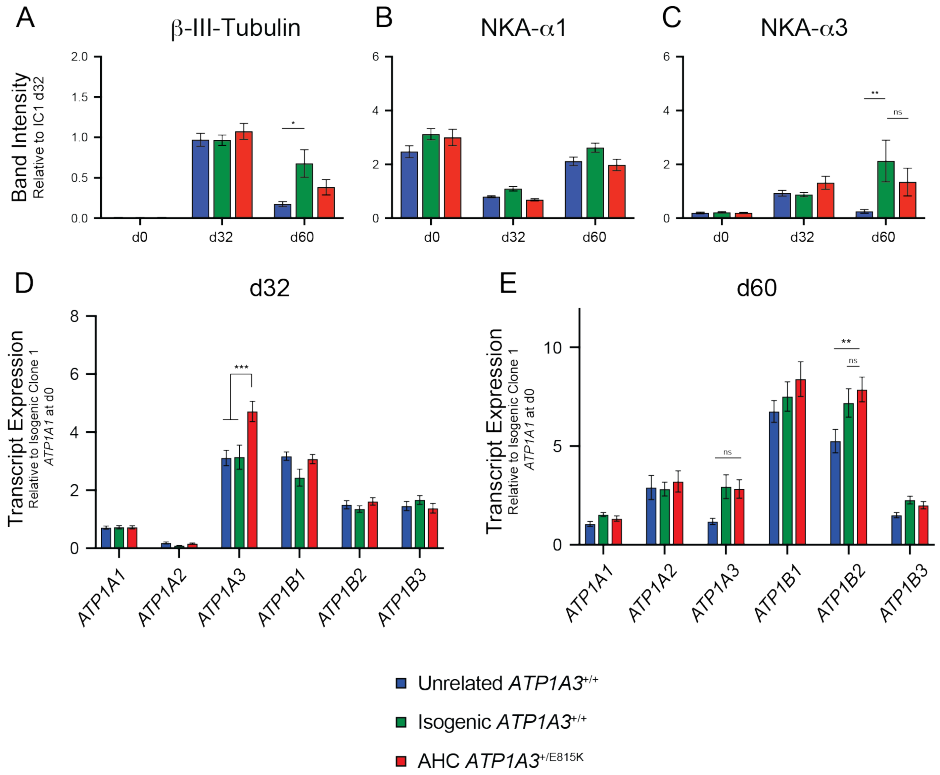

Figure 3.7: GABAergic shifted cultures display similar expression trends to mixed cortical populations. (A) Immunoblotting data shows an increase in β-III-Tubulin expression at d32 that is nonsignificant between genotypes. Due to the presence of contaminating cell types in this protocol by d60 of differentiation, β-III-Tubulin and other neural markers become less consistently expressed resulting in spurious differences (d60 isogenic-to-unrelated $p = 0.0001$). (B) Expression of the NKA-α1 subunit follows a very similar pattern to mixed cortical differentiation with nonsignificant differences at individual timepoints between genotypes. (C) No significant differences in NKA-α3 subunit protein expression were noted between isogenic corrected and AHC lines across GABAergic shifted differentiation. (D) RTqPCR analysis showed a significant elevation of *ATP1A3* transcripts at d32 ($p < 0.0001$) in AHC iPSC-derived neurons compared to both control groups. (E) By d60, deterioration of neural purity resulted in a relative loss of *ATP1A3* transcript levels compared to d32 with nonsignificant differences between isogenic control and AHC cultures. $n = 10$ (5 differentiations with 2 clones per genotype). 2-way ANOVA with Bonferroni's multiple comparisons test; significant findings notated by: * $p < 0.005$, ** $p < 0.001$, *** $p < 0.0001$; ns = not significant ($p > 0.01$).

Discussion

Alternating hemiplegia of childhood is the prototypical member of an expanding spectrum of disorders attributable to mutations in *ATP1A3* (Brashear et al., 2018; Rosewich et al., 2012; Sweney et al., 2015; Yano et al., 2017). *ATP1A3* spectrum disorders are almost exclusively caused by heterozygous *de novo* missense mutations in this essential gene that encodes the neuronal-specific catalytic subunit of the Na,K-ATPase ion transporter. Distinct diseases within this spectrum share symptomatic profiles but have unique diagnostic criteria and strong genotype-to-phenotype correlations (Heinzen et al., 2014; Rosewich et al., 2014b). While a singular molecular mechanism is unlikely to be responsible for all of these phenotypes, uncovering the biological basis of AHC may yield important information about the others.

The majority of AHC patients harbor one of three unique heterozygous missense mutations: D801N, E815K, or G947R (Ishii et al., 2013; Viollet et al., 2015). These mutations cluster around ion binding pockets within the transmembrane core and result in decreased pump function (Koenderink et al., 2003; Sweadner et al., 2019; Weigand et al., 2014). Heterologous expression studies demonstrated that AHC mutations result in impaired ion transport including loss of proton transport availability particularly in the case of E815K mutations (Li et al., 2015; Weigand et al., 2014). Mouse models of *ATP1A3* disease often recapitulate some symptoms experienced by AHC patients, especially following stress. For instance, a previously published E815K mouse model demonstrated increased hemiplegic spells following vestibular stimulation-induced stress compared to control animals (Helseth et al., 2018). Electrophysiological recordings in mouse hippocampal slices in D801N and I810N variant models of AHC have also shown hyperexcitable responses to electrical stimulation or seizures (Clapcote et al., 2009; Hunanyan et al., 2015; Hunanyan et al., 2018). Investigations have also reported neural hyperexcitability in the presence of pharmacologically inhibited NKA ion transport (Vaillend et al., 2002). Other studies in the field have demonstrated that these electrophysiological aberrations may be related to intracellular increases in sodium concentration in both the presence of AHC causing mutations and with ion transport inhibition after treatment with pump antagonists (Pivovarov et al., 2018; Tiziano, 2019; Toustrup-Jensen et al., 2014). In collaboration, we recently used iPSC-derived neurons with the G947R mutation to investigate fundamental cellular defects and observed impaired ion pump activity and depolarized resting membrane potentials in AHC mutant neurons (Simmons et al., 2018).

In this study, we chose to study the E815K mutation as this common AHC variant is often associated with the most severe patient phenotype (Panagiotakaki et al., 2015; Sasaki et al., 2014). Using patient-specific iPSCs along with isogenic and unrelated controls, we created an iPSC-derived neuronal model of AHC to investigate possible mechanisms underlying disease pathogenesis. We found elevated expression of *ATP1A3* transcripts in AHC lines compared to controls without significant changes in protein expression. Previous studies have shown that the complex transcriptional regulation of NKA-subunits includes pump inhibition-induced increases in NKA-subunit transcripts across various cell types (Li and Langhans, 2015). Interestingly, reports have implicated elevated intracellular sodium and low intracellular potassium concentrations as transcriptional regulators of NKA-subunit expression patterns (Johar et al., 2014; Vinciguerra et al., 2003; Wang et al., 2007). Our findings identify alterations in transcriptional control as a new phenomenon in *ATP1A3* variant disease. No significant difference in NKA-subunit protein expression was consistently seen across *in vitro* neurodevelopment in this study, as may be expected. This may be due to insensitivity of the available antibodies to detect such changes with immunoblotting or may reflect lower stability of the mutant protein. Higher resolution immunostaining studies may result in more detailed conclusions about protein expression, stability, and subcellular localization in AHC disease models. Others have described an increase in NKA-α3 protein expression in cortex following acute NKA inhibition with ouabain, suggesting that abnormalities may exist with chronic inhibition in disease as well (Bersier et al., 2011). While transcript levels and protein expression are related, they are not necessarily correlative for all NKA subunits (Clifford and Kaplan, 2009; Devarajan et al., 1992). This is the first report of compensatory transcription of NKA-subunit mRNA in AHC, which has implications for the experimental design and early implementation of genomic therapies targeting mutant or wildtype transcripts, even in the absence of protein-level aberrations. Other AHC-causing *ATP1A3* mutations should be analyzed to validate this observation.

Microelectrode array analyses demonstrated that in iPSC-derived neuronal cultures, $ATP1A3^{+/E815K}$ cells trended towards less overall activity than their wildtype equivalents early in the recording period, with stabilization comparable to isogenic control levels over time. This protocol did not yield activity levels representing synchronous network bursting, limiting our ability to perform more complex MEA analysis. However, our approach allowed us to isolate genotype-specific changes including the lack of local bursting in AHC lines activity without necessitating further modifications to already prolonged differentiation protocols. The novel induction of cellular stress by elevated temperature revealed a clear hyperactivity

phenotype following heat stress in *ATP1A3*$^{+/E815K}$ neurons compared to controls. At this time, we do not know if these phenotypes are related to pathological neurodevelopment or altered electrophysiological properties associated with a mutant NKA-α3 subunit. Furthermore, the correlation of this phenotype with epilepsy or non-epileptic symptoms of AHC was not determined. The phenomenon of stress-induced triggers is a shared phenotype of AHC with other *ATP1A3* mutant diseases, and has been recapitulated in other disease models including heat stress induced paralysis in a *Drosophila* model (Helseth et al., 2018; Holm and Lykke-Hartmann, 2016; Isaksen et al., 2017; Palladino et al., 2003; Sugimoto et al., 2014). Intriguingly, another study has identified a temperature-sensitive ion leakage phenomenon in a closely related Type II P-Type ATPase family member, after identifying an uncoordination phenotype in *Drosophila* harboring mutations in SERCA (Kaneko et al., 2014). Moving forward, it will be of great interest to test outcomes of stress modeling using newer lentivirally-induced neuron protocols that can generate more consistent network activity (Yang et al., 2017; Zhang et al., 2013b).

Flunarizine is one of the most commonly used drugs in AHC to prevent triggered episodes, although patients do not consistently respond to treatment (Panagiotakaki et al., 2015; Pisciotta et al., 2017; Sasaki et al., 2001). Chronic *in vitro* treatment with flunarizine did not have an impact on stress-triggered hyperactivity or local bursting behaviors in our study. However, flunarizine may be exerting an influence on other neuronal lineages that we have not addressed. Previous studies have implicated altered GABAergic inhibition as a possible pathological driver of disease (Bottger et al., 2011; Ikeda et al., 2013; Murata et al., 2020). We did not observe pathological differences between early glutamatergic and GABAergic neural differentiation protocols, although the failure of GABAergic cultures to maintain neuronal purity and electrical activity on MEA recording limited our analysis. While NKA signaling has been shown to be important for dendritic growth along with synaptic coordination and maturation, the potential impact on cellular signaling resulting from pump inhibition relative to AHC mutations in human iPSC-derived neurons remains understudied (Aperia et al., 2016; Desfrere et al., 2009; Reinhard et al., 2013). Structural modeling has shown similarities between common AHC mutation impacts on ion binding and passage within the Na,K-ATPase catalytic subunit, suggesting a potential broader validity of our findings (Sweadner et al., 2019).

The inclusion of isogenic wildtype controls and the replication of findings in two separate differentiation protocols in this study certainly increased our confidence in the robustness of our findings of both transcriptional changes and heat induced hyperactivity (Germain and Testa, 2017). Our model system can be used in the future to test important questions existing in the *ATP1A3* field regarding disease pathogenesis arising from either haploinsufficiency or dominant negative mechanisms. Furthermore, researchers in the field working on potential new therapeutics, whether small molecule or genetic therapies, can use these findings, model system, and assay techniques to test various future hypotheses on treatment efficacy. In summary, our iPSC-derived model of AHC demonstrated that neurons from the most phenotypically severe AHC mutation show elevated expression of *ATP1A3* transcripts during *in vitro* neurodevelopment compared to both isogenic corrected and unrelated wildtype controls. Neurons derived from these AHC patient iPSCs form electrically active populations upon MEA analysis similar to controls and display hyperexcitability following exposure to a trigger of elevated temperature. The commonly used medication flunarizine did not rescue this phenotype or improve the absence of local bursting activity in AHC neuronal cultures. Our results provide new evidence for phenotypes in AHC neurons harboring the *ATP1A3*$^{+/E815K}$ genotype and describe a platform for future mechanistic discovery and possibly therapeutic screening.

Materials and Methods

Cell culture and neural differentiation

See Chapter II Materials and Methods for detailed explanations of Shi (mixed cortical) and Maroof (GABAergic interneuron) differentiation protocols. Media recipes and reagent lists are supplied in the Appendix.

Immunoblotting

Protein was collected from iPSCs at d0 and from neurons at d32 and d60 of differentiation using ice-cold RIPA buffer containing protease and phosphatase inhibitors. Protein was not boiled prior to electrophoresis to avoid aggregation of NKA-α3, a membrane associated protein. Ten micrograms of total protein mixed with 4x Laemmli loading buffer (BioRad) per lane were run on Criterion XT Bis-Tris 4-12% polyacrylamide gels and separated in MOPS buffer at 200V for 60 minutes. Protein was transferred to PVDF membranes at 95V for 65 minutes. Membranes were washed with TBS three times before being stained for total protein with REVERT (Li-Cor). The protein stain was removed, blots were washed three times with TBS, and the membranes were blocked with Odyssey Blocking Buffer for 60 minutes at room temperature. Primary antibodies were applied overnight at 4°C in an antibody incubation solution of TBS + 0.1% Tween-20 (TBST) with 5% BSA. See supplementary antibody Table for more information on usage and dilutions. Blots were washed five times with TBST the following day, and secondary antibodies were applied for two hours at room temperature in antibody incubation solution. Membranes were washed five times with TBST prior to image capture on an Odyssey Scanner. Intensity data was collected using Image Studio Lite. Data was normalized to total protein with β-Actin shown as a visual aid.

RTqPCR

RNA was collected from iPSCs at d0 and iPSC-derived neurons at d32 and d60 of differentiation (Qiagen RNeasy Kit, QIAshredder) and processed with on-column DNase treatment to remove genomic DNA, followed by long-term storage at -80C. cDNA was generated using the High Capacity cDNA RT Kit (Applied Biosystems, 4368814) and stored at -20°C until further processing. Custom formatted qPCR plates were ordered from Applied Biosystems to profile for relevant NKA subunits with primers and TaqMan probes described in the Appendix. cDNA samples were prepared using TaqMan PCR Master Mix (Applied Biosystems, 4304437), and data was collected on a QuantStudio 3 qPCR machine. Analysis was performed using averages of technical duplicates for each sample. Calculations were performed using the $2^{(-\Delta\Delta C_t)}$ method, normalizing to GAPDH and then comparing results to expression of *ATP1A1* mRNA in clone IC1 at d0 to assess NKA subunit transcript expression across differentiation timepoints.

MEA culture and flunarizine treatment

For Shi protocol cortical cultures, Axion Cytoview 48-well MEA plates were pretreated with a 0.1% polyethyleneimine (Sigma, P3143) in borate buffer solution for one hour, washed thoroughly with water, and dried overnight the day prior to plating. For Maroof Protocol GABAergic cultures, a thin coat of Matrigel was used instead of PEI as this significantly enhanced adhesion to the electrode recording surface during extended culture periods. Neurons were dispersed with Accutase at d45 of differentiation and plated at a concentration of $3x10^5$ cells/well into MEA plates in 50 µL of culture media containing 10 µg/mL laminin (Sigma, 11243217001). One hour after plating, the well was gently flooded with 300 µL culture

media (NDM). From MEA plating onward, culture media included B27 Plus (Gibco) instead of standard B27 to promote neuronal activity. MEA cultures were fed on d48 with a half-media change and visualized under light microscope to ensure coverage of the electrode surface. At and after d51, half-media changes with media including 1 μg/mL laminin were performed every other day, including 24 hours before recording sessions. From d59 onward, media included 0.1% DMSO vehicle or 100 nM flunarizine (Sigma, F8257) for treatment groups.

MEA recordings and heat stress modeling of trigger-induced phenotypes

MEA recordings were performed every 4 days beginning at d52 on an Axion Maestro Pro MEA system. The recording chamber was preheated to 37°C with CO_2 concentration set to 5%. Spontaneous neural activity was recorded with a sampling frequency of 12.5 kHz and a digital bandpass filter from 200 Hz to 3 kHz. Plates were pre-incubated for 10 minutes within the MEA system before a 10-minute baseline recording was initiated. At the end of this recording period, the temperature was rapidly increased to 40°C and a new 10-minute "heat stress" recording period started once the temperature reached 39.5°C. When this recording period concluded, the temperature was reset to 37°C and a 10-minute "recovery" period began when the chamber temperature fell to 37.5°C. Data were analyzed using AxIS 2.0 Software (Axion Biosystems) by replaying recordings in offline neural spontaneous mode. A burst was defined by trains of at least 5 spikes with a maximum interspike interval of 100 ms at one electrode. For each individual recording, activity metrics from four wells of the same clone and treatment condition were summed to control for internal variation between wells and days. Pooled values of less than 50 total spikes (5 spikes/minute) in a baseline period resulted in the exclusion all three heat conditions (baseline, heat stress, and recovery) for that recording session in ratiometric analyses. One set of heat stress recording data was excluded from a single differentiation and day for clone UC1 given abnormally high heat stress and recovery period activity ratios, as determined by Grubbs' test for outliers.

Data analysis

Statistical analysis was performed using Prism 8 (GraphPad). Two iPSC clones for each genotype (unrelated *ATP1A3*$^{+/+}$, isogenic *ATP1A3*$^{+/+}$, AHC *ATP1A3*$^{+/E815K}$) over 5 differentiation runs are reported for all iPSC-derived neuron data sets. For analysis of multiple comparisons where n=10, a Bonferroni-corrected threshold p-value of < 0.005 was considered statistically significant. Data are presented as mean ± SEM. Relevant statistical tests and sample sizes are indicated in figure legends.

CHAPTER IV

INVESTIGATION OF AHC PHENOTYPES AND POTENTIAL THERAPEUTICS USING EVOLVING DISEASE MODELS

Abstract

iPSC-derived neuronal model systems provide tremendous flexibility for studying human cells in culture. AHC phenotypes of transcriptional *ATP1A3* compensation, heat-triggered hyperexcitability, and local bursting deficiencies have been described in our model system. *Next, we sought to expand our knowledge of* in vitro *AHC pathophysiology, phenotypes, and treatment options in iPSC-derived mixed cortical neurons.* First, we utilized our knowledge of AHC iPSC-derived neurons and *in vitro* disease modeling to study the biological rationale and treatment impacts of the increasingly popular therapeutic compound cannabidiol. We found that the CB1 receptor of the endocannabinoid system was highly expressed in iPSC-derived neurons. Cannabidiol treatment enacted strong but reversible inhibition on iPSC-derived neuronal activity that was not different between control and AHC genotypes. A search was initiated for other hypothesized neuronal phenotypes related to NKA-a3 subunit dysfunction. These included potential metabolic abnormalities associated with energetic requirements along with proposed ionic dysregulation of sodium, potassium, and calcium. While no consistent phenotypes in these domains were reported, these data provide a strong foundation for future experiments. Finally, new protocols were adopted, optimized, and characterized for rapid directed differentiation of iPSC-derived neurons using lentivirally transduced transcription factors. These protocols generate neurons that more rapidly reach electrical maturation and recapitulate previously described *in vitro* phenotypes of AHC. In total, these experiments and optimization endeavors will serve as the basis for the next generation of iPSC-derived neuronal disease modeling in AHC.

Introduction

Chapters II and III described the creation of an iPSC-derived neuronal disease model and explored phenotypes including transcriptional abnormalities and heat triggered hyperexcitability in AHC neurons. While these findings reflect a productive step towards understanding disease pathophysiology, the resources invested in generating this model system, the flexibility of iPSC-derived neuronal protocols and analysis techniques, and the potential of essentially unlimited *in vitro* human tissue supply provide the impetus for further model utilization. Recent interactions with patients, families, and clinicians has highlighted the need for more extensive and inclusive testing of therapeutics in AHC patients. As outlined in Chapter I, flunarizine is the most commonly used drug in AHC along with antiepileptics. While at times promising and apparently effective in some individuals, neither of these approaches has shown consistent success across the varied spectrum of AHC patients. Small clinic trials and individual case studies of other drugs have reached the same conclusion (Ju et al., 2016; Kansagra et al., 2013; Pisciotta et al., 2017). Some patient families and pediatric neurologists have begun looking into cannabidiol (CBD) as a potential therapeutic route, given its success in reducing symptoms associated with other neurodevelopmental and neurodegenerative conditions (Devinsky et al., 2017; Kaplan et al., 2017; Karl et al., 2017; Szaflarski and Bebin, 2014). While likely not a curative solution, we were interested in understanding the biological rationale for CBD treatment in AHC in support of a future clinical trial.

CBD has shown substantial efficacy in treating seizures, neuropsychiatric conditions, motor disorders, and depression, and has recently gained FDA approval for the treatment of rare forms of epilepsy (Campos et al., 2016; Gaston and Szaflarski, 2018; Leo et al., 2016; Peres et al., 2018). These are all

neurological domains impacted by *ATP1A3* mutations and experienced by AHC patients, not to mention the potential that anxiolytic effects may reduce triggered symptoms and improve behavioral disorders. Recently, several neurodevelopmental and neuropsychiatric conditions have been associated with perturbations in the endocannabinoid (eCB) signaling pathways commonly associated with both direct and indirect mechanisms of CBD action in the central nervous system (Basavarajappa et al., 2017; Busquets-Garcia et al., 2013; Cassano et al., 2020; Chakrabarti et al., 2015; Mechoulam and Parker, 2013). Unfortunately, the pharmacologic properties and targets of CBD are opaque, and the compound is often listed as polypharmacological in the literature. Somewhat confusingly, CBD does not show good cannabinoidergic activity against canonical eCB receptors compared to more potent endogenous compounds like AEA (arachindonylethanolamide) and 2-AG (2-arachindonyl glycerol) (Ligresti et al., 2009). The eCB signaling pathway is heterogenous in nature but mainly associated with fine tuning synaptic control via local communication at both excitatory and inhibitory synapses. Known eCB receptors are an ever-expanding group of proteins, including CB1, CB2, GPR55, and TRPV1, with each possessing unique expression patterns (Gorzkiewicz and Szemraj, 2018; Zou and Kumar, 2018). In this chapter, we will detail our findings on eCB receptor expression in iPSC-derived neurons and the effect of cannabidiol treatment on neuronal activity *in vitro*. Although CBD may act both directly and indirectly on the eCB system, it is our goal that these studies can serve as a foundation for future interrogation into potential alterations of these pathways in AHC and provide data to support a future clinical trial with CBD in a patient population.

One of the most striking characteristics of AHC is the appearance of hemiplegic episodes after defined triggers and the temporary resolution of symptoms during sleep (Sweney et al., 2015). The differential diagnosis for AHC appropriately includes genetic disorders of metabolic dysfunction or energetic production defects including pyruvate dehydrogenase deficiency and MELAS. The NKA-α3 subunit must by definition utilize energy in its function as an ATPase enzyme, in the process consuming over half of available neuronal ATP (Howarth et al., 2012). A dysfunctional pump resulting from AHC mutations may cause ionic dysregulation requiring even greater ATP usage by wildtype NKA pumps. These aggregated factors have led scientists and clinicians to look for phenotypes and biomarkers associated with metabolic abnormalities in AHC. Generally, these have resulted in few consistent observations regarding metabolic or mitochondrial changes, but hint at possible dysfunction in a general sense (Fons et al., 2012; Kemp et al., 1995; Nevsimalova et al., 1994; Sasaki et al., 2009). We took advantage of our *in vitro* culture system and recent new technology in the form of mitochondrial stress assays to test model specific questions. Using these tools, we tested our iPSC-derived mixed cortical neurons at baseline or after heat stress, and in the presence or absence of flunarizine. While we initially hypothesized that AHC neurons may exhibit higher basal respiration than isogenic neurons to compensate for pump failure, the opposite was in fact true. Treatment with flunarizine had little impact on neuronal metabolic activity, but heat stress trended toward having a greater impact on AHC lines compared to controls when comparing to their own baseline OCR. More studies are needed to further assess this phenotype, but this may provide rationale for novel routes to therapeutic approaches in the future.

Heterologous expression studies in HEK cells and *Xenopus* oocytes have consistently demonstrated that the common AHC mutations (D801N, E815K, and G947R) result in decreased pump activity. This lack of ion transport likely underlies disease pathophysiology and may result in further dysregulation of sodium, potassium, and calcium ion concentration in neurons. Studies have shown that neurons harboring *ATP1A3* mutations have a depolarized resting membrane potential (Simmons et al., 2018), display elevated intracellular sodium concentrations (Tiziano, 2019), and display drastically altered sodium homeostasis in dendrites (Fritz N, 2015). Alterations in intracellular concentrations of sodium, potassium, and calcium likely exist in our iPSC-derived neuronal model of AHC as well. We set out to study these with fluorescent indicator assays including CoroNa green (sodium indicator), thallium flux assays (potassium indicator), and GCaMP6f transfection (calcium indicator). These assays were often low throughput and difficult to consistently repeat given evolving model system design. While our conclusions are limited, the data we

collected during initial thallium flux assays point to possible phenotypes that can be followed up in future studies.

While the iPSC-derived neurons created in our well described paired differentiation scheme provide large amounts of human neuronal tissue for study, there are significant limitations. First, these neurons tend to stall in a developmental stage similar to that of early fetal brains. Dual-SMAD inhibition generated iPSC-derived neurons tend to be more fragile and less electrically mature than optimal for constant manipulation like MEA recording and whole cell patch clamping. These factors and age correlations prevent study of diseases that involve later onset of symptoms or neurodegeneration (Cornacchia and Studer, 2017; Handel et al., 2016). As discussed in Chapter I, the field is rapidly moving towards the adoption of neural induction by inducible transcription factor expression. Often packaged and delivered in non-infectious lentiviral particles, these factors allow researchers immense flexibility in developmental control. Neurons derived in this more direct manner are often referred to as induced neurons, or "iNeurons". With recent protocol optimizations, iNeurons can reach electrical maturation in weeks rather than months and are more similar to neurons seen during mid-to-late fetal development (Nehme et al., 2018). We have adopted two directed differentiation methods to more finely study neural lineages differences in contribution to AHC (Yang et al., 2017; Zhang et al., 2013b). Excitatory neurons were created by transduction with Ngn2 (iNgn2), while inhibitory interneurons were generated by transduction of Ascl1 and Dlx2 (iGABA). Here, we present the protocols we have optimized to this point for iNgn2 production, importantly incorporating an earlier lentiviral transduction timepoint than previously published to increase the reproducibility, expandability, and rapidity of induction. This iNgn2 protocol generates cells morphological similar to month-old mixed cortical neurons within 3-4 days of induction. Importantly, AHC iNgn2 cells display similar metabolic and hyperactivity phenotypes to previously studied excitatory neuron differentiation protocols. iGABA cells have been more difficult to produce in numbers amenable to experimental manipulation but show promise for lineage specificity. These iNeuron protocols will be indispensable to AHC and iPSC-derived neuron research in the future, allowing for more efficient, cost-effective, and reproducible data generation and resource sharing.

Results

CB1 is the dominant endocannabinoid receptor expressed in iPSC-derived neurons

Endocannabinoids and related synaptic signaling mechanisms have been implicated in neurodevelopmental diseases including Fragile X syndrome and autism, and may play an indirect role in the pathogenesis of chronic symptoms in AHC shared with these disorders (Busquets-Garcia et al., 2013; Chakrabarti et al., 2015). To assess the profile of eCB receptors in our paired differentiation disease model, we looked back to RNAseq data generated previously in our laboratory. Based on a review of the available literature regarding common and orphan eCB receptors expressed in the central nervous system, we looked at 5 candidates: *CNR1*, *CNR2*, *GPR18*, *GPR55*, and *GPR119* (Gorzkiewicz and Szemraj, 2018; Irving et al., 2017). Of these, only *CNR1* (CB1) was expressed to notable levels in both mixed cortical and GABAergic populations of iPSC-derived neurons (**Figure 4.1A**). *CNR2*, *GPR18*, and *GPR119* showed no expression, while transcripts of *GPR55* were only measurable in GABAergic shifted cultures. Not shown on this graph, the known eCB receptor *TRPV1* was also negligibly expressed in iPSCs and derivative neurons. Representative brightfield images of iPSC-derived neurons for each clone at d32 can be seen in the Appendix (**Supplementary Figure 4.1**), representing the tissue samples collected for this RNAseq dataset in mixed cortical populations. By d32, cells have taken the general appearance of neurons and are not grossly different in appearance than at future points in culture.

To study these patterns in more detail, we performed RTqPCR on samples from iPSCs (**Figure 4.1B**) and mixed cortical cultures (**Figure 4.1C**) to profile *CNR1*, *CNR2*, and *GPR55* expression along with

AHC-related gene *ATP1A3*, neuronal marker *MAP2*, and synaptic marker *DLG4* (encoding PSD-95). Data confirmed that *CNR1* transcripts are most highly expressed in neurons, and its expression was not different between AHC *ATP1A3*$^{+/E815K}$ and control genotypes. This data also supports our finding of elevated *ATP1A3* transcripts in AHC, although a smaller sample size precluded a conclusion of significance when comparing to isogenic controls (p = .0843). While *MAP2* was significantly elevated in AHC E815K neurons compared to isogenic (p = .0420) and unrelated (p = .0018) controls, *DLG4* did not show this pattern. We did not appreciate a significant difference in earlier RTqPCR data assessing β-III-Tubulin transcript expression between genotypes (see Chapter III). An initial immunoblot confirmed elevated expression of CB1 receptor protein in iPSC-derived neurons compared to control (**Figure 4.1D**), although concerns remain regarding antibody specificity (**Supplemental Figure 4.2**). Follow-up immunostaining and confocal microscopy of iPSC-derived mixed cortical neurons revealed positivity for CB1 receptor protein on neuron cell bodies and extensions, with puncta highlighting synapses on neurites as tracked with β-III-Tubulin co-expression (**Figure 4.1E**).

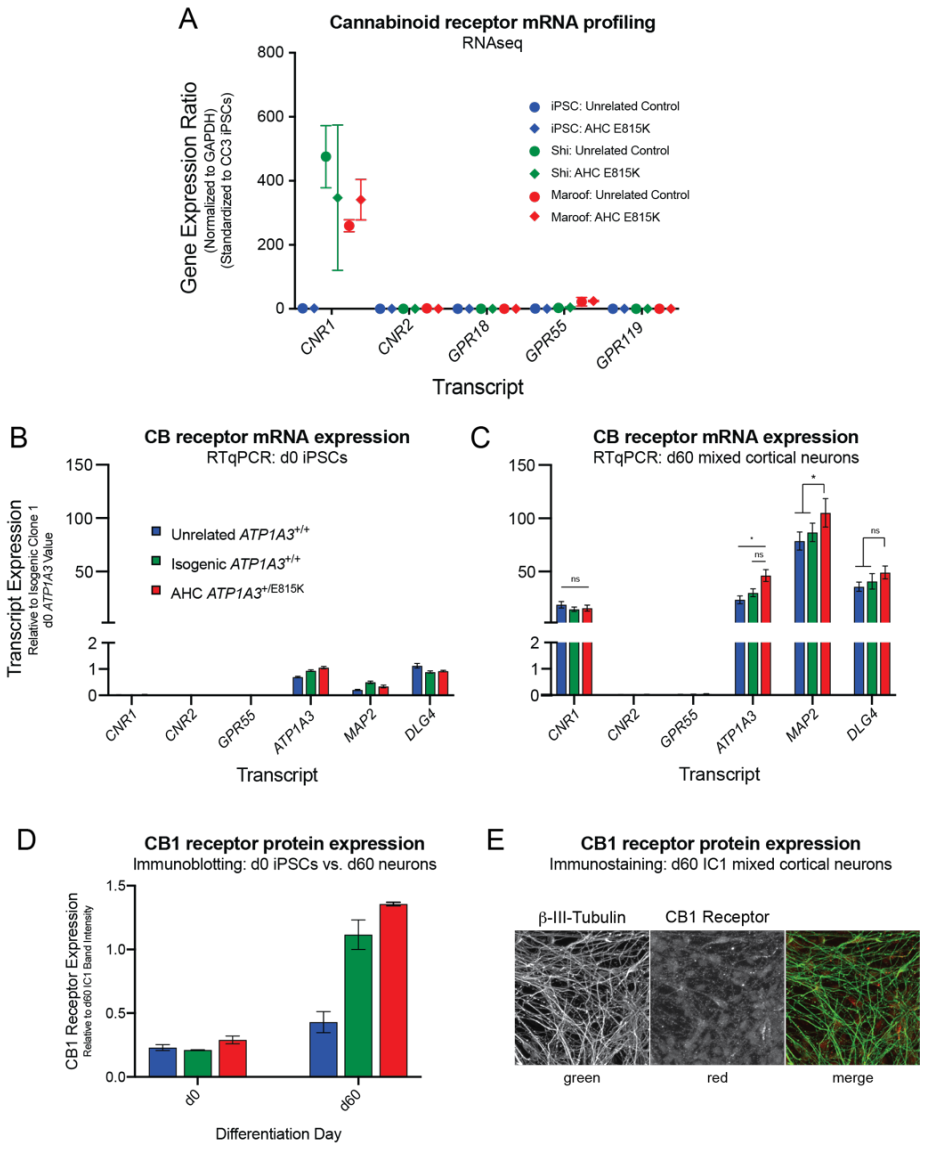

Figure 4.1: The cannabinoid receptor CB1 is highly expressed in iPSC-derived neurons. (A) Data analysis of previously performed bulk tissue RNA-sequencing of iPSCs, Shi protocol mixed cortical neurons, and Maroof protocol GABAergic neurons shows transcript expression of endocannabinoid-associated receptors *CNR1* (CB1), *CNR2* (CB2), *GPR18*, *GPR55*, and *GPR119*. *CNR1* is the only transcript expressed at significant levels, although some *GPR55* expression is seen particularly in GABAergic shifted cultures (Data points represent two clones per genotype from one differentiation). RTqPCR follow up analysis of top cannabinoid receptors, *ATP1A3* (NKA-α3), *MAP2* (neural marker), and *DLG4* (PSD-95, synaptic marker) confirmed limited expression of *CNR1* and other neural markers in iPSCs (B) that is significantly upregulated in mixed cortical cultures at d60 (C). No difference in *CNR1* expression was found between genotypes. *ATP1A3* trended upwards in AHC cultures (AHC-to-isogenic p = .0843; AHC-to-unrelated p = .0084) as previously seen. *MAP2* was elevated in AHC lines (AHC-to-isogenic p = .0420; AHC-to-unrelated p = .0018), although *DLG4* was not significantly different (AHC-to-isogenic p = .5042; AHC-to-unrelated p = .1784). For RTqPCR analysis, n = 4 differentiations with 2 clones per genotype; data normalized to *GAPDH* and displayed relative to *ATP1A3* expression for clone IC1 at d0; statistics represent 2-way ANOVA with Bonferonni multiple comparison test. Significance notated a (*) $p < 0.05$. Protein expression assessment confirms that CB1 protein is elevated by d60 of differentiation (D) and not strikingly different between AHC and isogenic controls (n = 2 clones per genotype over one differentiation). Immunostaining for CB1 protein (E) shows localization to cell membrane tracking closely with β-III-tubulin staining of neurite extensions in high magnification (60x) images. Error bars represent SEM across all data sets.

Cannabidiol treatment reversibly inhibits population level neuronal activity

Although CBD and related drugs have recently been popularized by the media and patients as a kind of "cure-all" drug, there are scientifically founded benefits across multiple neurological disorders that have been previously mentioned. To assess the impact of CBD on our model system, we performed MEA analysis of population level activity in d75+ mixed cortical neurons in the presence of vehicle or drug (**Figure 4.2**). Time is presented as days post-plating to allow for better data integration in this non-standardized approach. An initial dose of 5 μM on d11 post-plating was decided upon based on literature review (Bisogno et al., 2001; Ghovanloo et al., 2018; Scott et al., 2017), with initial plans to increase the concentration to 10 μM over the ensuing recording sessions. Although the DMSO and CBD conditions displayed similar baseline activity levels based on spike counts on d8 before drug addition, CBD rapidly silenced neuronal activity at both 5 μM on d12 and 7.5 μM in the ensuing planned recording session on d16. To see if this activity would recover, a relatively rapid dilution was performed over the next 4 days with activity recorded on d18 at 1.0 μM and d20 at 0.125 μM. A clear recovery of activity tracking with CBD concentration dilutions ensued, suggesting that doses in future experiments should lie in the 100 nM – 1 μM range or below. This return of activity following CBD dilution was reflected in heat stress and recovery periods (not shown) using the protocol described in Chapter III, although those results are too limited to draw any phenotypic conclusions. Similar patterns are reported in the recovery of activity for both isogenic controls and AHC E815K lines.

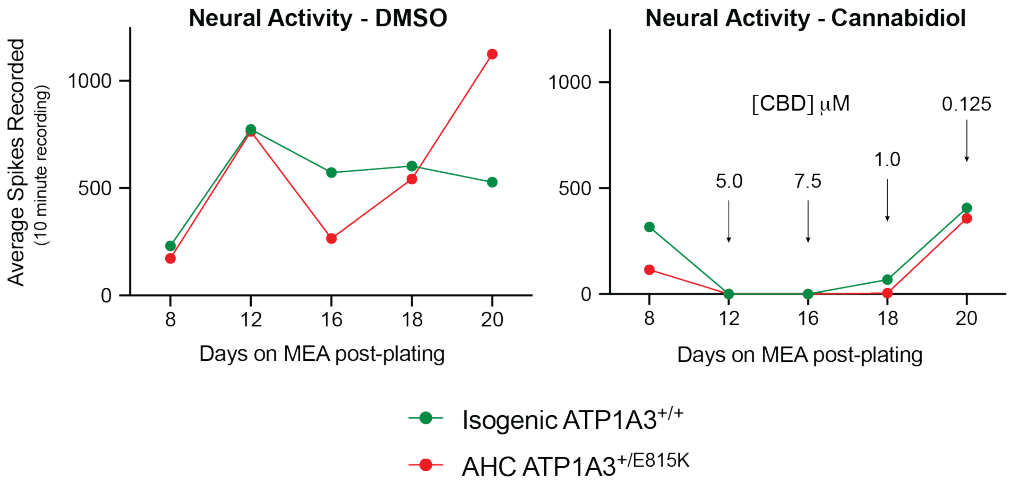

Figure 4.2: Cannabidiol treatment reversibly inhibits iPSC-derived neuronal activity on MEA analysis. Recording of d75+ iPSC-derived mixed cortical neurons (Shi) protocol shows maturation of spike counts over time in the presence of DMSO (left) in both AHC and isogenic control neurons. x-axis is labeled as days-post plating to simplify future incorporation of repeat experiments with non-standardized plating dates. Application of cannabidiol at a concentration of 5 μM (right, treatment beginning at d11) causes complete loss of neural activity in cultures after 24 hours of treatment. Silencing of activity continued at 7.5 μM CBD but then recovered to greater than baseline levels after CBD was diluted out of culture media to a concentration of less than 1.0 μM by d12. Data represent averages of two clones per genotype over a single differentiation.

AHC neurons trend toward decreased overall metabolic rate and may have a heightened sensitivity to heat stress compared to isogenic controls

Researchers have been searching for metabolic phenotypes or biomarkers in AHC patients and animal models of disease for decades, given the disease's unique presentation and etiology. To assess our iPSC-derived mixed cortical neurons for metabolic phenotypes, we turned to a metabolic stress test that employs fluorescent readout of oxygen consumption to measure mitochondrial respiration of plated cells (Agostini et al., 2016; Jaber et al., 2020). Our hypothesis was that AHC neurons would require greater baseline energy production to facilitate normal neuronal function, and that preincubation in elevated temperatures would exacerbate this metabolic phenotype. In fact, we found that both AHC iPSCs and neurons consistently tracked lower in OCR (oxygen consumption rate) than isogenic controls throughout the duration of the experiment (**Figure 4.3A, 4.3C**), regardless of mitochondrial transport chain manipulation. This is best reflected in the shifting of AHC lines toward more quiescent metabolic phenotypes when plotting OCR (mitochondrial respiration) against extracellular acidification rate (ECAR), a marker of glycolysis (**Supplemental Figure 4.3**). Heat stress generally decreased metabolic rates across all curve points in both iPSCs and neurons (**Figure 4.3B, 4.3D**). While these trends are not significant due to low sample size, a clear trend exists across two differentiations. As this data is not normalized to total protein levels or terminal cell counts, data comparisons between iPSC and neuronal OCR and energetic phenotypes would be premature. The presence of altered basal respiration in iPSCs complicates interpretation, as this suggests the results may be an unfortunate but general feature of iPSC clonal variation instead of a phenotype specific to NKA-α3 expression in neurons. To simplify interpretation, we looked at respiration in the various conditions between genotypes while normalizing to baseline OCR for each clone. These conditions included baseline, flunarizine, heat stress, and flunarizine plus heat stress. We found that while iPSCs showed similar sensitivities to these factors between genotypes, AHC neurons appeared more sensitive to heat stress induced decreases in OCR, particularly when combined with the presence of

flunarizine. While this is only a trend (p = 0.283) given the small sample size of a pilot experiment, it remains worthy of further characterization.

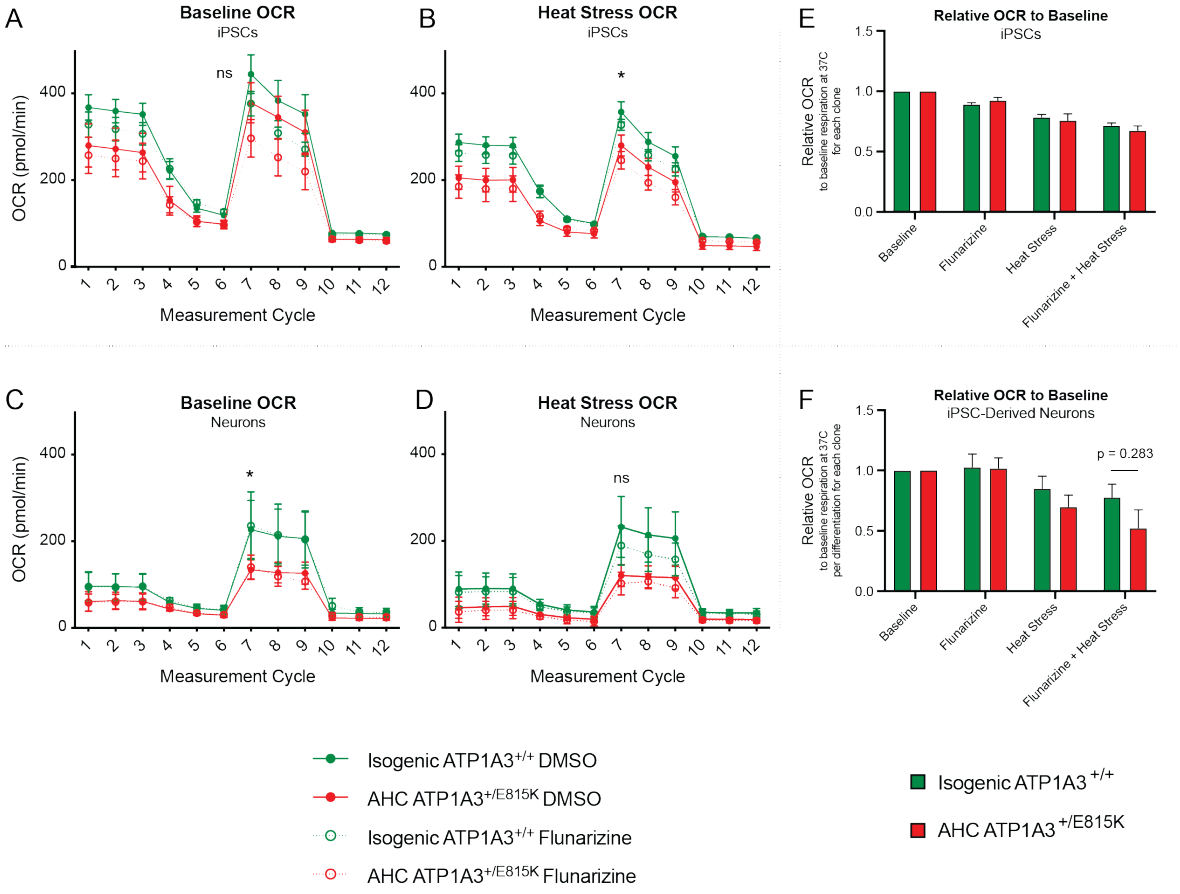

Figure 4.3: Mitochondrial respiration rates in AHC and isogenic iPSC-derived neurons. Seahorse Cell Mito Stress Test results depict oxygen consumption rate (OCR, pmol/min) across 12 measurement cycles. After an initial baseline recording period, addition of electron transport chain component inhibitors oligomycin, FCCP, and rotenone/antimycin A after cycles 3, 6, and 9 respectively reveals a well described curve in OCR. iPSCs (A) and mixed cortical neurons (C) display similar metabolic properties comparing between AHC (red) or isogenic control (green) genotypes in the presence of DMSO (closed circles) or 100 nM flunarizine (open circles). OCR was reduced following a 15-minute preincubation period at 40C instead of baseline 37C preincubation. The only significant difference amongst data points in the same measurement cycle group existed between Isogenic DMSO and AHC flunarizine conditions during maximal uncoupling after FCCP addition, when noted above (*, $p < 0.05$). The maximum baseline OCR standardized to each clone's baseline is quantified on the right in these various conditions. No difference was noted between iPSCs (E) and neurons (F) in respect to baseline OCR. Flunarizine had minimal effect on basal respiration, although heat stress decreased baseline OCR to ~75% of standard conditions. A trend toward heat stress exerting a greater impact on AHC neurons compared isogenic controls was noted, although this did not reach significance and was not improved by flunarizine. Data represent 2 clones per genotype across 2 differentiations, statistical significance determined by a 2-way ANOVA with Bonferonni multiple comparison test; error bars represent SEM across all data sets.

Intracellular ion concentration measurements reveal abnormalities in AHC iPSC-derived neurons

Our initial approach to investigate the potential phenotypes of iPSC-derived neurons involved the assessment of intracellular sodium, potassium, and calcium ion concentrations. Our hypothesis suggested that due to NKA dysfunction, intracellular sodium would be elevated along with a decrease in potassium concentration. Due to subsequent impacts on the sodium-calcium exchanger, intracellular calcium would also increase as is seen with digoxin treatment and NKA inhibition. This proposed approach included thallium flux assays to measure potassium concentration (Beacham et al., 2010; Weaver et al., 2004), CoroNa green assays to measure sodium concentration (Meier et al., 2006), and Fura2-AM (Barreto-Chang and Dolmetsch, 2009) and eventually GCaMP6f assays (Chen et al., 2013) to measure intracellular calcium and neural activity dynamics. Perpetual optimization, reinterpretation of preliminary studies, variability in results, and constantly evolving neural differentiation protocols created a low throughput environment that limited significant conclusions. For completed experiments, some promising results were achieved. Previous data from the Ess Laboratory suggested that all three common AHC mutants resulted in decreased intracellular potassium concentrations by thallium flux assay. Unfortunately, these results were later questioned when it was realized that a protein tag caused mutant NKA subunit accumulation and resultant trafficking defects. However, experimental results in a preliminary study with AHC G947R neurons showed very similar profiles of thallium flux curves by genotype.

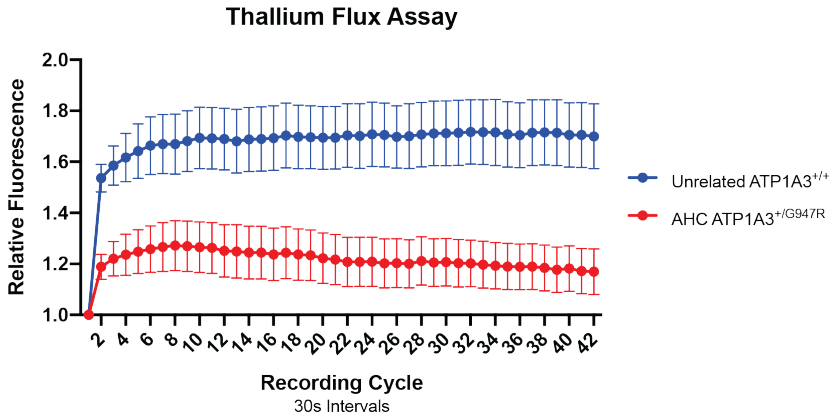

Figure 4.4: Thallium flux assay suggests ionic dysregulation in AHC iPSC-derived neurons. Preliminary data shows the results of a thallium flux assay carried out on an AHC line harboring the G947R mutation in *ATP1A3* compared to an unrelated control line. AHC mixed cortical neurons display less fluorescence over time, suggesting decreased potassium entry and lower intracellular concentration, consistent with previous studies using heterologous expression of NKA-α3 subunits in HEK cells. These data represent only one clone per genotype over a single mixed cortical differentiation, with averages of 21 cells analyzed at d100+; error bars represent SEM.

Lentiviral transduction of iNgn2 neurons replicates AHC phenotypes discovered in mixed cortical cultures

More rapid and customized differentiation protocols are being published weekly across the field of iPSC disease modeling, and lentiviral-based neuronal differentiation using transcription factors has become increasingly popular amongst neurobiology laboratories. Protocols developed by Zhang et al. (2013b) and further optimized by Nehme et al. (2018) and others have revolutionized the way researchers approach iPSC-derived neuron experimental design. This updated protocol for producing iNeurons combines previous knowledge about differentiation pathways and developmental morphogens with specific cortical neuronal transcription factors (e.g., mouse Ngn2), systems for sophisticated gene control (e.g., TetOn), and

antibiotic resistance cassettes for the generation of pure neuronal cultures (e.g., puromycin). These methods were updated for use in our laboratory to simplify the lentiviral transduction process by temporally separating it from the differentiation pipeline (**Figure 4.5A**). iPSCs are transduced with the necessary transcription factors before being expanded and frozen across multiple (10+) cryotubes at known densities. These samples can then be thawed for immediate differentiation in a consistent and reproducible manner without constantly repeating the lentivirus transduction process. iNeurons, or excitatory iNgn2 cells, generated in this manner display neuronal morphologies within days of induction as opposed to weeks in previously discussed protocols (**Figure 4.5B**). In our series of unrelated control, isogenic wildtype, and AHC E815K iPSCs, consistent high-density neuronal cultures are visible after puromycin selection by day 4 of differentiation that are then available for co-culture with astrocytes (**Figure 4.5C**) before analysis.

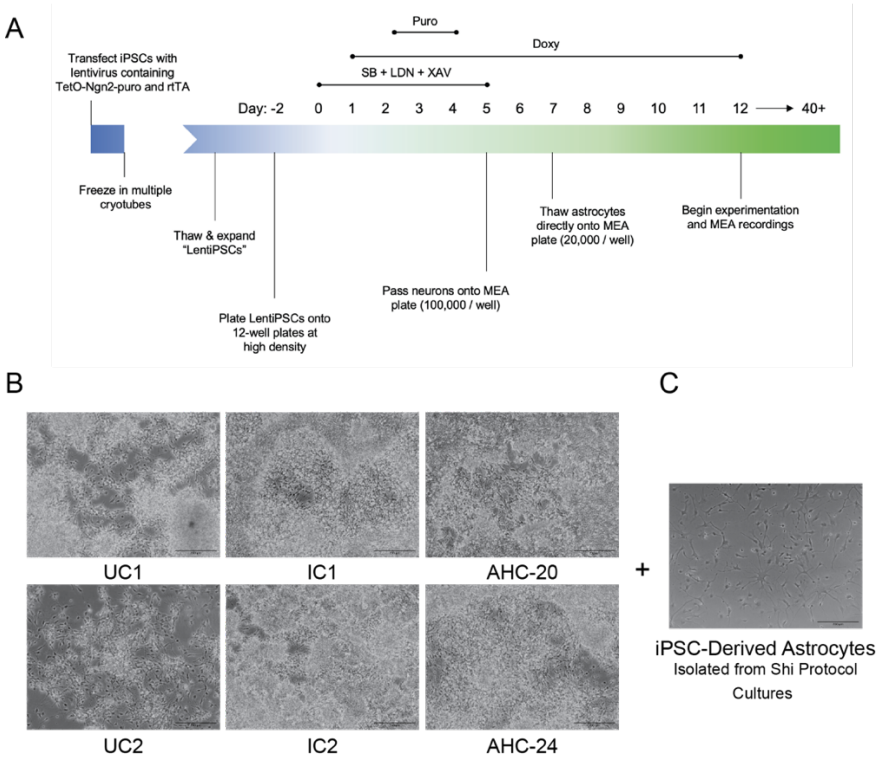

Figure 4.5: Optimized protocol for directed differentiation of iNgn2 excitatory neurons from iPSCs. Following literature review and discussions with collaborators, we optimized a protocol for lentiviral based directed differentiation of iPSCs to excitatory neurons using the transcription factor Ngn2 (iNgn2 neurons). This is a modified version synthesized from previously published differentiation protocols (Nehme et al., 2018; Simmons et al., 2018; Zhang et al., 2013b), importantly incorporating a step to separate lentiviral transduction from iPSC plating. This allows for increased reproducibility as dozens of identical stock tubes can be created from a single transduction run. With co-culture of astrocytes, this protocol allows for the rapid culture of iPSC-derived neurons that display electrical activity within two weeks of generation. Phase images of iNgn2 neurons (B) demonstrate high density populations of purified neurons across unrelated control, isogenic control, and AHC E815K cultures with clear neurite outgrowth by d4 of the protocol. For initial studies, glial populations added to this culture system were mitomycin C treated astrocytes from isogenic control mixed cortical cultures that were collected and purified after gliogenesis has occurred (d120+).

As proof-of-principle testing, these iNgn2 neurons underwent testing with the Mito Stress Test and the heat stress MEA protocol to assess if phenotypes described in dual-SMAD inhibition-based induction samples were repeated. iNgn2 cells show a very similar pattern on OCR analysis (**Figure 4.6A**), with AHC

neurons displaying slightly decreased mitochondrial respiration than their isogenic wildtype counterparts. On MEA analysis, activity is apparent between 12-16 days post-induction, a large improvement in experimental duration from the 45+ days required to generate activity in mixed cortical cultures. Again, isogenic lines trended towards greater activity levels than AHC lines and flunarizine had little overall effect on the recordings (**Figure 4.6B-C**). In the heat stress paradigm, AHC iNgn2 cells show hyperactivity in the recovery phase again, while also displaying hyperactivity in the heat stress stage that was not fundamentally impacted by flunarizine (**Figure 4.6D-E**). More testing will have to be done to determine if this direct hyperactivity during heat stress is a novel component of the phenotype in iNgn2 neurons or unique to this single differentiation run.

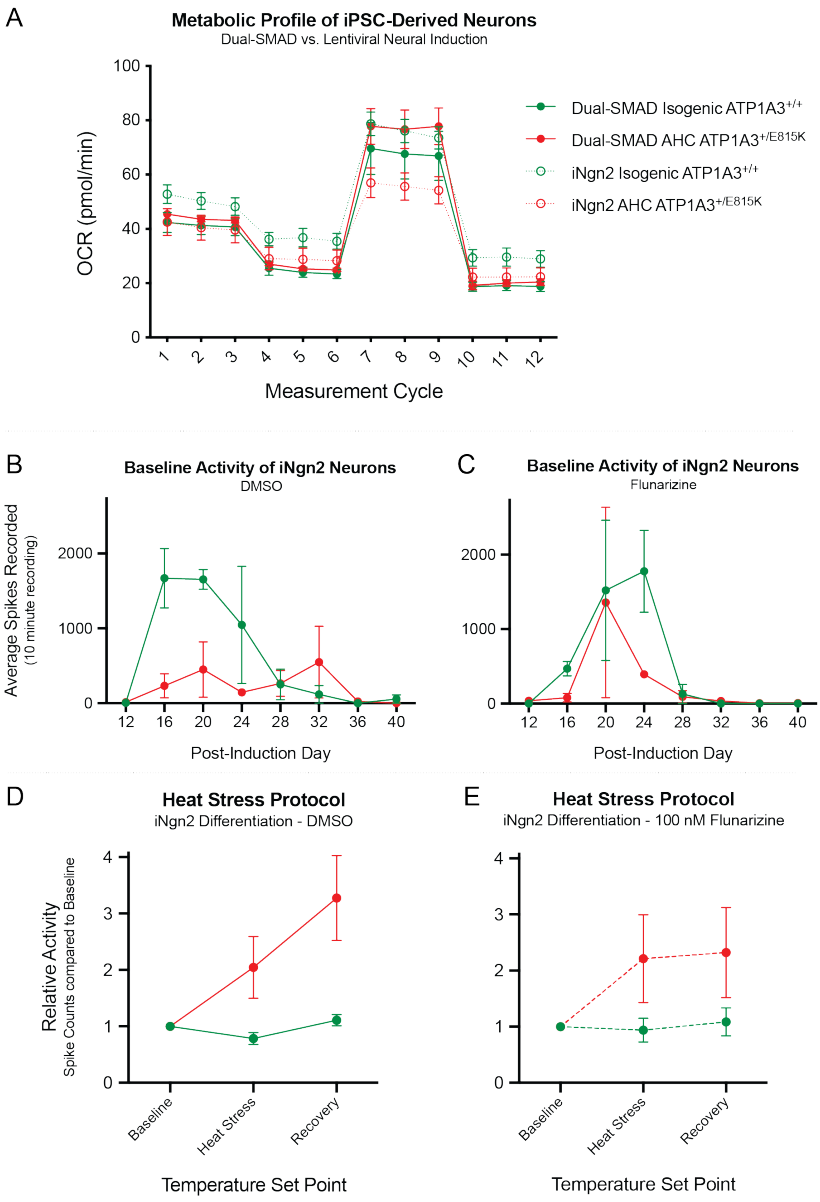

Figure 4.6: iNgn2 and dual-SMAD protocols result in similar energetic profiles and AHC activity phenotypes. (A) iNgn2 neurons (open circles) display similar metabolic rates to mixed cortical neurons (closed circles) within the same Mito Stress Test experiment run. AHC E815K neuronal OCR trends lower than isogenic controls in iNgn2 cultures, similar to previously shown data. Seahorse data represent two clones for each genotype across one

differentiation for each respective protocol. Baseline neural spiking activity in iNgn2 cultures demonstrates activity is generated within 12-16 days of induction, much faster than with dual-SMAD based culture systems. DMSO treated cultures (B) and flunarizine treated cultures (C) show similar dynamics to previously presented data, where AHC lines trend toward decreased overall activity. iNgn2 neurons of AHC origin also experience hyperexcitability in the recovery phase of a heat stress protocol with vehicle treatment (D) that is nonresponsive to flunarizine (E). Interestingly, AHC iNgn2 neurons also show hyperexcitability compared to baseline in the immediate heat stress period. MEA baseline data represent two clones per genotype across one iNgn2 differentiation run. MEA heat stress data was calculated using repeated heat stress protocol runs every 4 days in iNgn2 cultures from d20 to d40, resulting in a max n = 12 per data point. Wells were pooled into groups of four to limit variability, and the entire data set for a recording day was excluded if baseline activity was < 5 spikes / minute. For D-E after data exclusion: isogenic DMSO n = 7; AHC DMSO n = 8; Isogenic flunarizine n = 5; AHC flunarizine n = 6. Error bars represent SEM.

GABAergic neurons remain difficult to create even after iGABA protocol optimization

Newer innovations in the field of transcription factor based neuronal differentiation have continued with the publication of cortical GABAergic interneuron specific protocols (Yang et al., 2017). With the combination of excitatory iNgn2 and inhibitory iGABA neurons, pointed questions can be posed about the contribution of each of these cell types to AHC pathogenesis in a new "paired differentiation" scheme. GABAergic differentiation of iPSCs has generally proven difficult in the laboratory compared to excitatory neuron differentiation with its better elucidated developmental pathways. A larger milieu of transcription factors including *Ascl1*, *Dlx2*, and *Myt1l* along with a double purification step including puromycin and hygromycin complicates this approach (**Figure 4.7A**) compared to the production of iNgn2 neurons. Initial attempts of differentiation in the Ess Laboratory involved producing and packaging lentivirus with these transcription factor plasmids. After further optimization, successful iGABA factor transduction was achieved, but at low efficiency (**Figure 4.7B**). Success in producing limited amounts of iGABA neurons ensued, marked with a co-transduced GFP molecule (**Figure 4.7C**). While this method remains complicated and produces a low yield of neurons, work with collaborators continues on protocol optimizations to increase production to the point where MEA electrophysiological measurements are feasible.

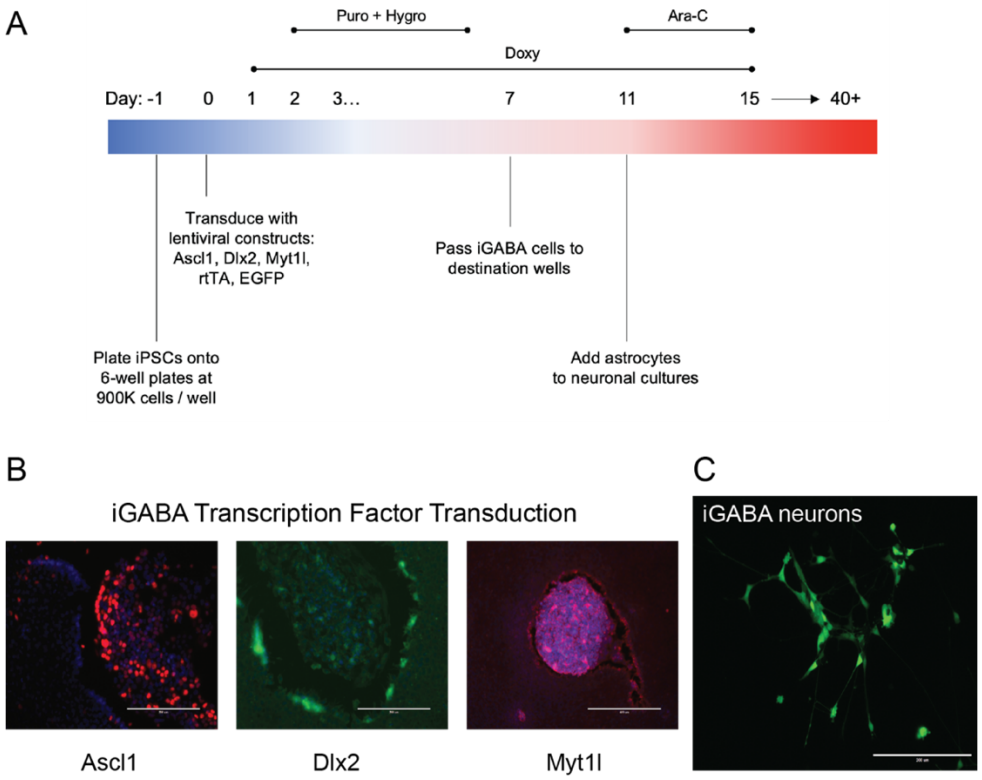

Figure 4.7: iGABA differentiation protocol adoption and optimization. A protocol for lentiviral transduction of iPSCs using a previously published cocktail of inducible transcription factors (Yang et al., 2017) was optimized with collaborators (BCH) to rapidly generate GABAergic interneurons. Initial packaging and production of lentivirus particles occurred in the Ess Laboratory, where transduction efficiencies and immunostaining confirmation (B) were described for Ascl1 (red), Dlx2 (green), and Myt1l (magenta). GFP-positive iGABA neurons were created (C) that demonstrated neurite outgrowth by 20 days following induction, but yield was too low for true experimentation. Lentiviral production has since been assigned to an outside core (University of Iowa) although iGABA production remains a challenge in the laboratory compared to iNgn2 cells.

Discussion

In this chapter, we set out to utilize our iPSC-derived neuronal model of AHC to investigate potential phenotypes and treatment options, while also adopting and analyzing updated differentiation methods to generate better data and disease models. First, we assessed the foundations of endocannabinoid (eCB) signaling in iPSC-derived neurons by profiling receptor expression. We expected and found that CB1 (*CNR1*) is the main eCB receptor expressed in the iPSC-derived neurons using multiple testing modalities including RNAseq, RTqPCR, immunoblotting, and immunostaining. We also report negligible expression of *CNR2* (CB2), *GPR55*, *GPR18*, and *GPR119* that are also involved in nervous system eCB signaling. eCB abnormalities in synaptic regulation and signaling have been reported across multiple other neurodevelopmental conditions. For example, *GPR55* transcripts have been shown to be downregulated in frontal cortex in rat models of autism, while hippocampal tissue demonstrated abnormal eCB signal molecule concentrations (Kerr et al., 2013). In the *Fmr1*$^{-/-}$ mouse model of Fragile X Syndrome, inhibition of CB1 and CB2 receptors through both pharmacologic and genetic approaches rescued disease associated deficits including cognitive impairment, seizure susceptibility, and anxiety-related behaviors (Busquets-Garcia et al., 2013). These neurological deficits are shared features with AHC, warranting further study of eCB physiology in *ATP1A3* mutant disease models.

One compound that has been suggested to modulate the eCB system is cannabidiol (CBD). While this drug has been shown to act as an negative allosteric modulator of CB1, it also has broader impacts exerting influence on other cellular signaling pathways and proteins (Gaston and Friedman, 2017; Ibeas Bih et al., 2015; Laprairie et al., 2015; Ryan et al., 2009; Thomas et al., 2007). Regardless of mechanism of action, clinicians and patient families are requesting more investigations of CBD's potential efficacy in the treatment of AHC symptoms. In our iPSC-derived mixed cortical neuronal cultures, CBD application above 5 μM caused complete loss of neuronal activity. However, neural spiking patterns did return once the compound was diluted out of culture media to a point below 1 μM. In this pilot experiment, no difference was noted between AHC neurons and isogenic controls. These studies reveal as expected that CBD concentration in the μM range inhibits neuronal activity but give little more information about potential efficacy or rationale for treatment in AHC. The recent approval of CBD therapeutics by the FDA for rare forms of epilepsy and the widespread availability of CBD containing compounds opens the door to potential large translational and clinical studies in AHC (Levinsohn and Hill, 2020).

As discussed in the introduction, researchers have previously investigated possible metabolic consequences of AHC related mutations while searching for improved diagnostic biomarkers, etiologic understanding, and possible treatment routes (Sweney et al., 2015). While a study of 157 European AHC patients showed no common metabolic abnormalities (Fons et al., 2012), previous investigations have reported mitochondrial abnormalities in skeletal muscle (Kemp et al., 1995) or changes in cerebral glucose metabolism between hemiplegic spells (Sasaki et al., 2009). Our studies using oxygen consumption rate (OCR) as an indicator of mitochondrial respiration suggested that AHC neurons are less metabolically active than isogenic controls. This trend was unexpectedly also found in iPSCs that do not express the neuronal specific protein associated with mutations in AHC, clouding interpretation of results. AHC E815K neurons were more sensitive to heat stress than isogenic control neurons, while this difference was not observed in iPSCs. While these data are limited in scope, results do align well with reports of decreased cerebral metabolic rate reported in frontal lobes of AHC patients (Sasaki et al., 2009; Sweney et al., 2009).

Our initial methodology for phenotypic discovery in this disease model involved the assessment of ionic dysregulation in AHC iPSC-derived neurons. While this approach was stymied by low throughput methods and variability in results and differentiation protocols, thallium flux assays measured decreased potassium influx in AHC neurons and recapitulated previous internal results attained using heterologous expression systems. These thallium flux results were unfortunately difficult to interpret over the long course of acquisition, as most publications study this method to screen for modulations in extremely rapid potassium entry via ion channels (Weaver et al., 2004). Conference presentations, publications, and known disease mechanisms of NKA-pump dysfunction suggest alterations in sodium and calcium dynamics likely exist as well (Fritz N, 2015; Simmons et al., 2018; Tiziano, 2019; Xiao et al., 2002), although our attempts at measuring these ion dynamics failed to culminate in reportable data. It is likely that refined studies addressing these research questions will result in positive data yielding knowledge about this disease model. However, it is important to note that some fluorescent ionic indicators themselves might alter ion status or even directly inhibit NKA pump function and confound experimental results (Smith et al., 2018).

New approaches to neural differentiation of iPSCs allow for rapid generation of more mature neurons compared to previous methods. These methods of directed reprogramming utilize the viral insertion of controllable transcription factors that directly reset cell identity rather than the slower process of manipulating neurodevelopmental signaling pathways. iNgn2 and iGABA neurons have been generated in our laboratory and when optimized will serve as the next system for AHC disease modeling (Nehme et al., 2018; Yang et al., 2017; Zhang et al., 2013b). Indeed, some labs have already switched to these methods within the field of AHC research (Simmons et al., 2018). In our pilot differentiations, AHC iNgn2 neurons recapitulated phenotypes seen using morphogen-based cortical differentiation protocols, including heat stress induced neural hyperactivity. One important avenue for research now available with these protocols

includes the generation, analysis, and mixing of pure glutamatergic and GABAergic populations to determine lineage contribution to disease burden. These differentiation systems will continue to drive the adoption of *in vitro* model systems that more closely mimic human physiology with quicker timelines and more cost-effective studies in mind.

Materials and Methods

See Chapter II for details on RNAseq, TaqMan RTqPCR, immunoblotting, immunostaining, Shi protocol mixed cortical differentiation, and Maroof protocol GABAergic differentiation methods. Primers, probes, and antibodies are listed in reagent tables found in the Appendix. See Chapter III for MEA plating methods and MEA heat stress recording protocol details.

Cannabidiol treatment and recording of iPSC-derived mixed cortical neurons

iPSC-derived neurons were cultured using the Shi protocol for mixed cortical differentiation as previously described. d67 neurons were plated onto the MEA plates coated with PEI in mcNDM+ with ROCK-inhibitor (10 μM) and laminin (10 μg/mL) at 100,000 cells per well using the drop method to plate cells directly on the electrode surface. A baseline recording was performed at d8 post-plating before cannabidiol (Cayman Chemical, 90080) or vehicle (DMSO) treatment began at d11. Although the heat stress and recovery protocol previously described occurred on recording days 12+, only the baseline 10-minute recording period is reported here due to limited overall activity. As cannabidiol treatment eliminated neural activity at initial concentrations of 5.0 and 7.5 μM, media dilutions without CBD were performed and recording frequency was increased to assess possible recovery of function. MEA data recorded on a Maestro Pro MEA (Axion) in spontaneous neural mode and processed using AxIS 2.0 software.

Seahorse Cell Mito Stress Test Kit

Between post-induction d60-d70 of mixed cortical differentiation, neurons were singularized using Accutase and passed through a 40-μM cell strainer before plating on 96-well Matrigel-coated Seahorse assay plates at a concentration of 150,000 cells / well in mcNDM+ with ROCK-inhibitor (10 μM). iPSCs were similarly passaged to plated but at an initial concentration of 10,000 cells per well in mTeSR + ROCK-inhibitor. The day after passage, 100 μL of appropriate culture media (without ROCK-inhibitor) was added to each well. 2 days after plating, a full media change was performed including DMSO (1:1000) or 100 nM flunarizine. 4 days after plating the assay cartridges were hydrated in preparation for running the assay. On d5 post plating, the Seahorse Cell Mito Stress Test Kit (Agilent) was performed according to user guide instructions on a Seahorse XFe96 Analyzer (Agilent). Briefly, assay media (Seahorse XF DMDM with 1 mM pyruvate, 2 mM glutamine, and 10 mM glucose) was added to the culture plates one hour before the assay began. The cultures were then incubated at 37C in an atmospheric incubator for 60 minutes. For heat stress conditions, the final 15 minutes of this period was performed at 40C. Drugs were prepared and loaded onto the guide plate to be used at the following final concentrations: Oligomycin (1.5 μM), FCCP (1.5 μM), and Rotenone/Antimycin A (0.5 μM). Plates were loaded into the analyzer and run according to preformatted assay guidelines, with 12 measurement cycles occurring at approximately 6-minute intervals. Assays were performed with the assistance of Megan Rasmussen. Two mixed cortical differentiations and parallel iPSC cultures and were analyzed in this protocol using two clones per genotype. Assays comparing iNgn2 neurons followed the same assay protocol, but with only one differentiation available for comparison.

Thallium flux assay for the assessment of intracellular potassium

iPSC-derived mixed cortical neurons were thoroughly washed with 1x Assay Buffer (see below) then incubated for 1 hour with Thallos Dye (1:1000) in Assay Buffer. After another wash, cells were preincubated for 10-minutes with bumetanide (1 μM) in Assay Buffer to block Na-K-Cl cotransport and better isolate NKA activity. Thallium Stimulus Buffer (5x: 12 mM thallium sulfate (Honeywell Fluka, 88290), 125 mM sodium gluconate, 1 mM magnesium sulfate, 1.8 mM calcium gluconate, 5 mM glucose, 10 mM HEPES) was directly applied to this solution using a premanufactured guide. Thallium rapidly enters the cell in similar routes to potassium ions, and binding to the preloaded dye results in increased fluorescence. Fluorescent images were captured from preset beacon sites every 30 seconds for 20 minutes on an EVOS FL microscope and individual cells were analyzed manually using ImageJ software. Protocols were adapted for use with iPSC-derived neurons from Weaver et al. (2004).

Thallium flux assay buffer (100 mL)

Start with 50 mL water
Add 2.759 mL 5 M NaCl (to 137.93 mM)
Add 2.52 mL 50 mM CaCl2 (to 1.26 mM)
Add 98 μL 0.5 M MgCl2 (to 0.49 mM)
Add 2.0 mL 20 mM MgSO4 (to 0.4 mM)
Add 220.5 μL 0.2 M NaH2PO4 (to 0.441 mM)
Add 2.085 mL 200 mM NaHCO3 (to 4.17 mM)
Add 3.0 mL 0.5 M D-Glucose (to 15 mM)
Add 5 mL 400 mM HEPES (to 20 mM)
Add 71.34 mg (FW = 285.36) Probenecid powder (to 2.5 mM)
Complete with 32.317 mL water.

iNgn2 differentiation

This protocol is a slightly modified version of that from Simmons et al. (2018), which adapted protocols from Zhang et al. (2013b) that were further optimized by Nehme et al. (2018). Lentivirus particles packaged with TetO-Ngn2-puro and rtTA plasmids were generated by The University of Iowa Viral Vector Core after validation of plasmids acquired from Addgene (see Appendix). iPSCs were transduced with these vectors at an MOIs of 8.3 (rtTA) and 3.4 (TetO-Ngn2-puro) with the addition of polybrene (8 μg/mL), followed by expansion of transduced "LentiPSCs" before freezing cells down. When ready for a differentiation run, LentiPSCs were thawed onto 6-well plates in mTeSR1 and expanded for one week. On d-2 of the differentiation protocol, LentiPSCs were plated at high density (1,000,000 cells / well) on 12-well plates in mTeSR + ROCK-inhibitor (10 μM). Cells were fed fresh mTeSR the following day (d-1), then neural induction media (NIM) [NMM + 10 μM SB + 100 nM LDN + 2 μM XAV] on d0, with daily NIM feeds through d5. Doxycycline was added at 2 μg/mL the following day (d1) and continued throughout the duration of the experiment. Progressive selection with puromycin occurred using 1 μg/mL (d2) then 2 μg/mL (d3). On d5, iNgn2 cells were passaged using Accutase onto a 48-well MEA plate at a concentration of 100,000 cells per well using the central drop method and PEI/laminin plating as previously described in NIM + ROCK-inhibitor. Media was changed to mcNDM+ with maturation factors GDNF, BDNF, cAMP, and IGF-1 the following day (d6). Mitomycin-C treated iPSC-derived astrocytes manually purified from

previous Shi protocol cultures (isogenic line IC1) were thawed from frozen directly onto wells at 20,000 cells / well on d7, although they can also be added before neural MEA plating. Cultures were fed with half media changes of mcNDM+ +doxy every two days for the duration of the experiment. Flunarizine or DMSO treatment began at d19. Seahorse assays were performed on d18 iNgn2 neurons; MEA recordings of iNgn2 neurons took place between d12-d40 post-induction.

iGABA differentiation and optimization

Lentiviral based iGABA differentiation protocols were followed according to the original publication (Yang et al., 2017) and with optimization performed in collaboration with the Sahin Lab and Human Neuron Core at Boston Children's Hospital. Briefly, iGABA plasmids containing tetracycline driven transcription factors including *Ascl1, Dlx2*, and *Myt1l* were acquired from Addgene (see Reagents Table in Appendix), expanded, purified, and verified. Vectors were packaged in lentivirus using the Takara Single Shot system in Lenti-X HEK Cells. Purified lentiviral particles were collected from supernatants and isolated by ultracentrifugation. Viral titer was estimated using Lenti-X GoStix and the associated mobile app, then concentrated virus was aliquoted and frozen at -80C. On d0 of iGABA differentiation, virus was introduced to iPSCs, followed by antibiotic selection to isolate transduced cells according to original protocols. While MOI's would have optimally been around 5, true values in the differentiation for the images shown were closer to 0.5-1 given low viral titer production. TetO-EGFP was also included in iGABA runs to evaluate transduction and differentiation efficiency. Given consistent low viral titers and time-consuming protocols for lentiviral generation, viral production has since been outsourced to The University of Iowa Viral Vector Core where more consistent and validated resources can be produced.

CHAPTER V

GENERATION OF AN NKA-α3 ANTIBODY

Abstract

Alternating hemiplegia of childhood is caused by mutations in the NKA-α3 subunit that disrupt ion transporting ability and result in neuronal dysfunction. To answer important questions about the pathophysiology of this neurodevelopmental disease, a sensitive and specific antibody is required. This research tool is particularly important for *in vitro* disease models of AHC, including in iPSC-derived neurons. The similarity of NKA-α isoforms creates challenges to the creation of specific antibodies given high percentages of identical amino acid residues across all regions of these proteins. While commercially produced antibodies exist, their availability has been inconsistent and significant concerns regarding specificity across multiple applications such as immunoblotting and immunostaining have arisen. *For these reasons, we set out to create and validate a new monoclonal mouse antibody against NKA-α3 with the goal of making better reagents available to the field*. In collaboration with internal and external cores, subclonal supernatants have been achieved that are available for further production and screening. This Chapter will briefly outline our antibody production rationale, pipeline, and reagents allowing future scientists to profile specific characteristics of these antibodies for the study of AHC and other *ATP1A3*-related disorders.

Introduction

AHC is a complex neurodevelopmental disease both in patient presentation and hypothesized disease mechanisms (Arystarkhova et al., 2019; Heinzen et al., 2014; Kansagra et al., 2013). While it is known that this rare disease is caused by heterozygous missense mutations in *ATP1A3* that result in NKA-α3 dysfunction, the fine details of how ion dysregulation in neurons leads to complex symptoms remains mysterious. Our previous studies in an iPSC-derived cortical neuron model of disease have revealed phenotypes including altered *ATP1A3* transcript expression and population level electrophysiological abnormalities. In these studies, we utilized separate anti-NKA-α3 antibodies for immunoblotting and immunostaining. Significant optimization of our protocols including protein preparation and gentle fixation techniques allowed us to reach conclusions about protein expression and general localization, although published methods of protein analysis had initially failed. In parallel with these studies, we set forth the process of creating a novel and more specific NKA-α3 antibody to be shared with the research community.

Initial assessment of commercially available antibodies revealed that several commonly used reagents failed to specifically stain NKA-α3 over closely related α subunit isoforms and did not result in linear banding patterns with increasing protein concentrations on immunoblotting. Unfortunately, production was discontinued for a commercial antibody that showed positive results (Santa Cruz, S19-R). Many commercial NKA-α3 antibodies are monoclonal versions derived from clone XVIF9-G10, as sold by Thermo Fisher (MA3-915), that resulted from a thorough study conducted over 20 years ago in skeletal muscle tissue (Arystarkhova and Sweadner, 1996). While this antibody has been used in the field of NKA research for years and particularly for immunostaining experiments, it has not tested well in our lab for immunoblotting specificity. NKA-α3 and α1 subunits are over 96% identical in amino acid sequence, thus posing significant problems for the design of specific antibodies (Blanco and Mercer, 1998; Sweadner et al., 2019). This chapter will outline our attempts to create a new antibody that binds to a unique sequence within an NKA-α3 intracellular loop, while other antibody generation attempts have focused on N-terminal

epitopes that are known to be frequently altered by post-translational modifications (Benallal and Anner, 1994; Pedemonte and Kaplan, 1992; Pedemonte et al., 1990; Sweadner et al., 1994).

Important questions remain regarding the expression of NKA-α3 in response to dysfunctional pump activity in AHC. Although we previously described that immunoblotting data demonstrated no significant difference between disease and control iPSC-derived neurons in subunit expression, it is possible that antibody assays were not sensitive enough show subtle changes in protein levels. Although much is known about the overall expression of the NKA-α3 in neurons, very few studies have been performed to address if these characteristics are altered in human *ATP1A3* mutant neurons (Arystarkhova et al., 2019; Bersier et al., 2011; Blom et al., 2011; Bottger et al., 2011). Better experiments and reagents are needed to address possible changes of NKA-α3 subunit subcellular distribution within diseased neurons, the impact of AHC mutations on protein stability and turnover within synapses, and oligomerization characteristics of NKA subunits in control and AHC neurons.

The process of generating a unique antibody that would be useful in approaching these questions began with the identification of a unique region for the target epitope within the large intracellular loop connecting transmembrane domains M4 and M5, a region unaffected by common AHC mutations. A protein fragment containing this target was cloned into plasmids, verified, and submitted to the Vanderbilt Antibody and Protein Resource (VAPR) Core for expansion. This core produced and validated the protein then purified natively folded fragments to ensure proper epitope recognition. Mice were immunized with the protein antigen after which serial serum collections were performed. Initial rounds of immunoblots were executed to select samples for further processing. Splenic tissue was then sent for hybridoma formation and monoclonal antibody production in collaboration with the Fred Hutchinson Antibody Technology Resource. Two rounds of subclonal purification ensued using multiple screening techniques that yielded a clone with positive results on immunoblotting. Further details of this process and resultant data are presented in this chapter for subsequent scientists to continue screening and production of a more specific NKA-α3 antibody.

Results

Epitope for NKA-a3 specific region identified for protein fragment generation

A region within a large intracellular domain of the NKA-α3 protein was selected as a unique target epitope amongst other NKA-α subunits (**Figure 5.1**). This region including residues 484-493 shares few identical amino acids with other isoforms expressed in neurons (NKA-α1, 0/10 identical) or glia (NKA-α2, 3/10 identical). Given that these three proteins are over 87% identical to each other, this represents a region of significant dissimilarity and a suitable target for antibody generation (Blanco and Mercer, 1998; Sweadner et al., 2019). To begin the process of antibody generation, a larger segment of *ATP1A3* cDNA encompassing protein residues 329 – 762 was cloned into a plasmid and sequence verified before bacterial protein production. Large flanking regions adjacent to the target sequence were included to increase the probability of native secondary and tertiary protein structures forming during protein fragment production. In collaboration with the VAPR core, this protein was produced in large quantities, verified by mass spectrometry, and prepared for mouse immunization.

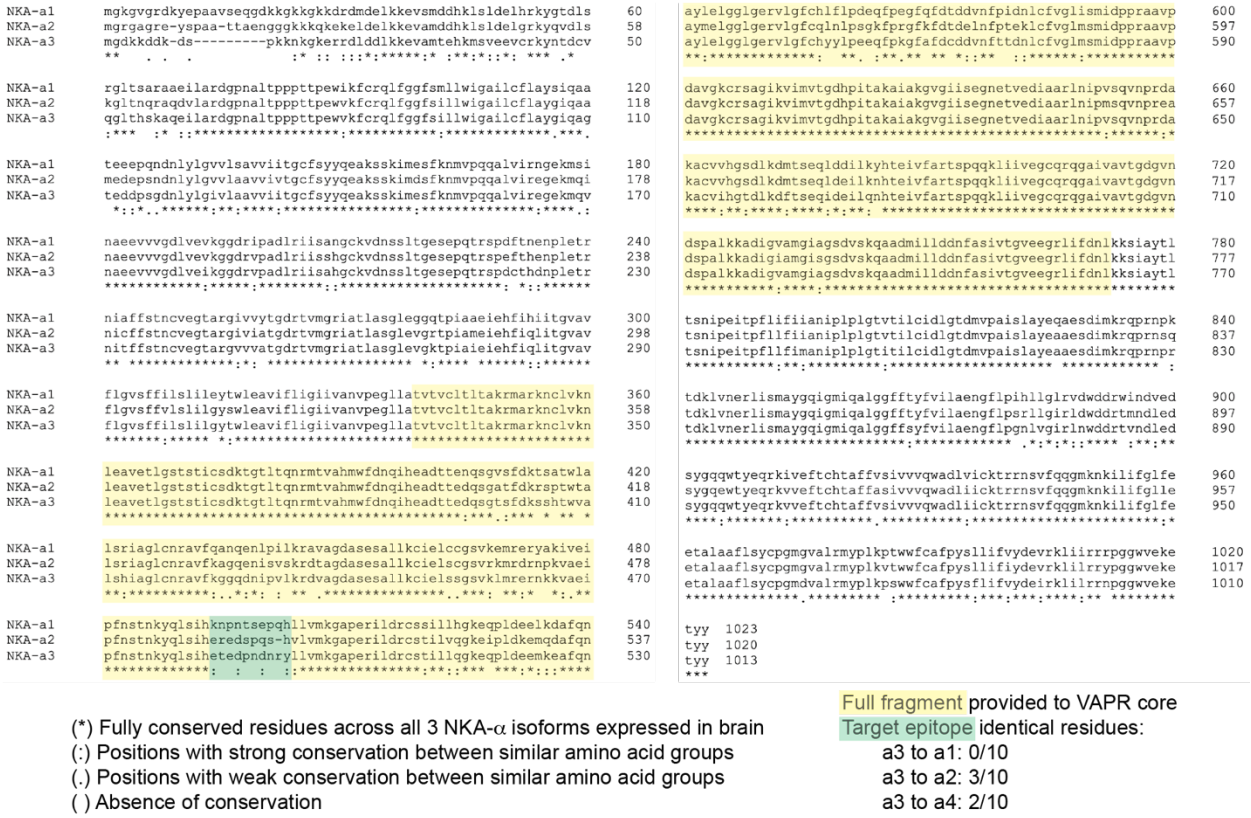

Figure 5.1: NKA-α subunit isoform alignment reveals unique cytoplasmic epitope region. Full sequence multiple sequence alignment (Clustal Omega) of NKA subunits α1 (NP_000692.2), α2 (NP_000693.1), and α3 (NP_689509.1) highlights identical residues (*), strongly conserved residues (:), weakly conserved residues (.), or the absence of conservation (_) between all three major subunit sequences. A region of 10 residues completely unique to α3 compared to α1 exists in a large intracellular loop connecting transmembrane domains M4 and M5 (highlighted green). This amino acid sequence is also relatively specific to α3 when comparing to α2 (3/10 identical) or α4 (2/10 identical [not shown]). As the initial step in antibody production, a larger fragment containing this specific sequence (NKA-α3 protein residues 329 – 762, highlighted yellow) was cloned into a plasmid for protein generation and purification in bacteria.

Vanderbilt Antibody and Protein Resource production pipeline and initial screening

Once protein preparations were ready for injection, the VAPR antibody production pipeline began (**Figure 5.2**). Four mice were selected for immunization, and blood samples were collected for baseline comparison. Protein fragment antigen and adjuvant were injected subdermally and intramuscularly. Four weeks after initial immunization, the mice received boost injections with the same protein. Bleed #1 samples were collected two weeks later, and a subsequent round of boosting and collection was repeated for Bleed #2. The VAPR core performed custom ELISA quantification to assess the initial sensitivity of serum samples for the protein fragment and to monitor proportions of IgG and IgM production. In parallel, we performed immunoblotting for antibody sensitivity against protein lysates from NKA-α1-expressing HEK cells and previously generated ORWT-α3 HEK cells that express a ouabain resistant version of wildtype NKA-α3 in addition to endogenous NKA-α1 (**Figure 5.3A**) (de Carvalho Aguiar et al., 2004; Price et al., 1990). These data were used in combination to select two out of four immunized mice for splenic dissection, based on sensitivity to the protein fragment immunogen and native NKA-α3 by immunoblotting (**Figure 5.3B**).

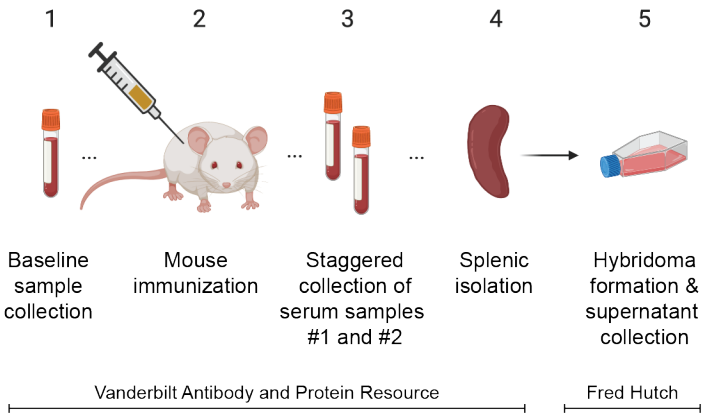

Figure 5.2: NKA-α3 antibody production and collaboration schematic. Once the protein fragment containing our epitope of interest was fully validated and folded to a native state, the antibody production pipeline in mice began. (1) A pre-immunization blood sample was collected from four mice, which were then injected (2) with an antigen-adjuvant combination by the Vanderbilt Antibody and Protein Resource (VAPR) Core. (3) Blood and serum samples resulting from these immunizations and subsequent boosts were returned to our lab for processing after ELISA assays confirmed IgG amplification. (4) Two mice were selected for further processing after initial analysis. (5) Isolated spleens were sent to Fred Hutchinson for hybridoma formation, production of polyclonal and monoclonal supernatants, and clone banking. Figure generated using BioRender.

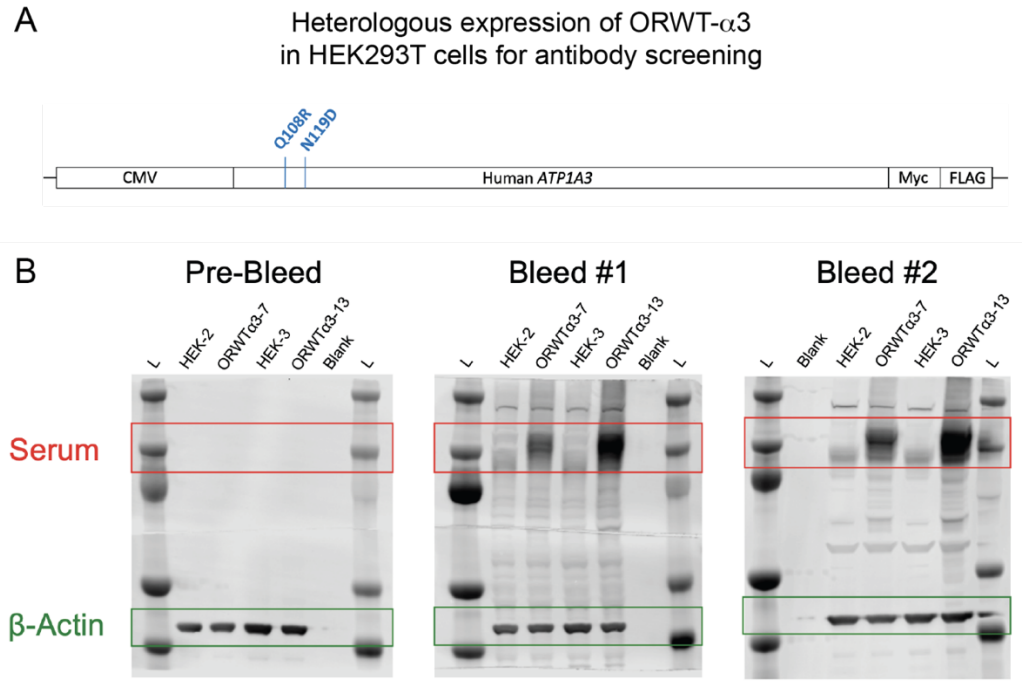

Figure 5.3: Immunoblotting reveals samples suitable for processing to monoclonality. (A) Schematic of ouabain-resistant wild type NKA-α3 (ORWT-α3) used in previous heterologous expression studies in HEK293T cells. This tagged protein was a readily available reagent utilized for antibody sample screening in combination with untransfected HEK293T cells that only express NKA-α1. (B) Initial immunoblots from serum samples of a single mouse yield positive results. While the pre-immunization bleed sample shows no banding patterns, the 110-115 kDA range containing NKA-α subunits is highlighted by samples from Bleed #1 (1:500) and Bleed #2 (1:1000), particularly in the NKA-α3 expressing ORWT cells.

Monoclonal antibody clones show promise in sensitivity and specificity testing

Spleens were sent to the Fred Hutchinson Antibody Technology Resource where hybridoma lines were produced via traditional methods. Polyclonal culture supernatants were returned to the Ess Laboratory for parallel processing. These samples underwent initial screening using a fluorescent bead assay (Fred Hutchinson) using the target immunogen fragment and in cell Westerns (Ess Lab) using ORWTα3 heterologous expression cell lines (**Figure 5.4**). In both cases, higher antibody-epitope binding results in increased fluorescence on analysis. Simultaneously, dot blotting was performed to show specificity of these antibody supernatants for NKA-α3 over NKA-α1. Representative images show that many clones display specificity for α3 (**Figure 5.5**), although significant cross reactivity with α1 exists in some, as expected given the size of the initial antigen fragment and similarity between isoforms. Notably, this dot blot highlights concerns with the commonly used anti-NKA-α3 clone XVIF9-G10. While the antibodies used for previous characterization of NKA subunit expression (Chapter III: A6F [anti-α1]; EPR [anti-α3]) show strong specificity for their respective targets, XVIF9-G10 shows intense positivity for both α1 and α3. Supernatants identified between these assays as containing sensitive and specific anti-NKA-α3 IgG antibodies were selected for further processing to monoclonality.

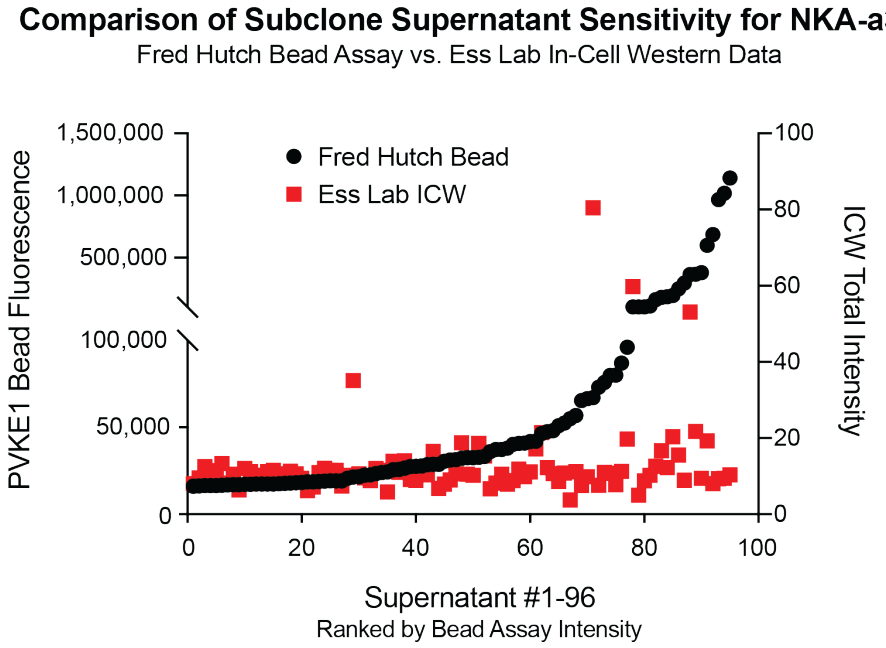

Figure 5.4: Bead assays and in-cell Western blots describe sensitivity and align for clonal selection. The fragment used in antibody production was coupled in an external bead assay (PVKE1) at Fred Hutchinson, where increased antibody binding results in heightened fluorescent signal (left y-axis). For simplification, these samples are ranked by bead assay intensity and plotted in a curve (black circles). In-cell Westerns were performed with the same supernatant samples, resulting in total intensity values (right y-axis) collected using an Odyssey Imaging System (red squares). With guidance of antibody production experts at Fred Hutchinson, the double-positive hits across these assays along with some other top clonal candidates were selected for further subcloning.

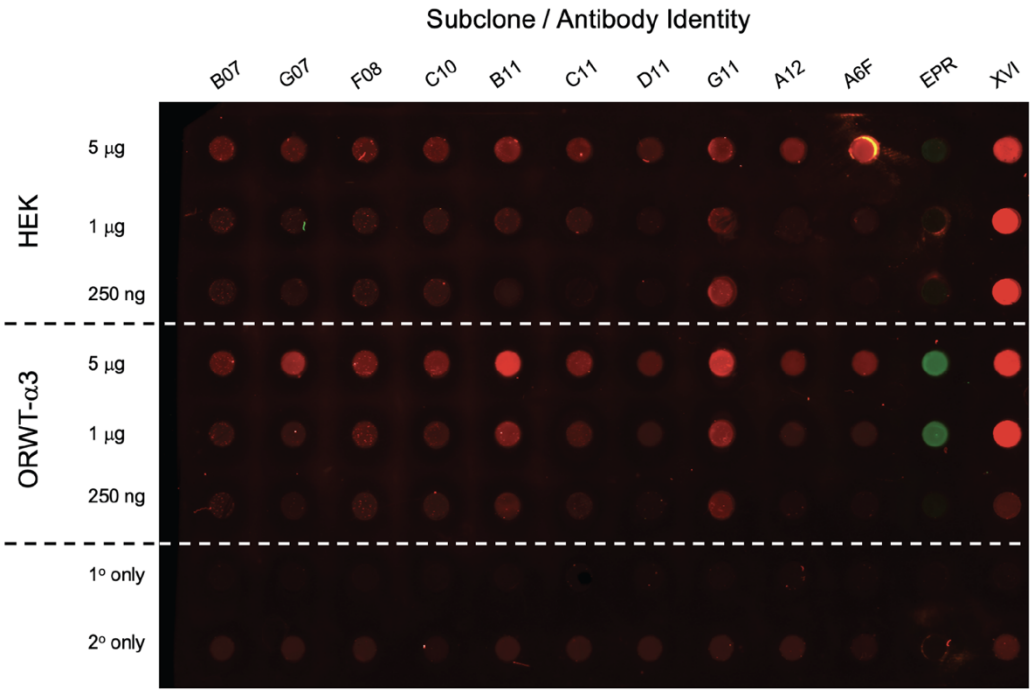

Figure 5.5: Specificity screening via dot blotting identifies hybridoma clones for further processing. Representative dot blot assays show the specificity of many subclonal supernatants for NKA-α3 over NKA-α1. Increasing concentrations of total HEK cell protein containing NKA-α1 fill the first three rows of the membrane, while NKA-α3 and NKA-α1 expressing ORWTα3 cell lysates fill the middle rows. Primary and secondary only controls compose the bottom two rows. Subclonal supernatants as primary antibody are highlighted in red by an anti-mouse IgG secondary. Commercial antibodies A6F (mouse anti-α1), EPR14137 (rabbit anti-α3, green), and XVIF-G10 (mouse anti-α3) are shown for comparison. While A6F and EPR antibodies are quite specific to their intended targets, this dot blot highlights a continued concern with the specificity of XVIF-G10 for the NKA-α3 subunit using these probing methods. Based on this data, multiple subclones were selected for further monoclonal processing and testing via classical immunoblotting.

Pooled subclone immunoblotting narrows the focus for future optimization

Hybridomas were processed to monoclonality and supernatants collected from these cultures were processed via immunoblotting for antibody binding characteristics. Of the clones tested, only pooled monoclonal supernatants from clone B4 showed efficacy on immunoblotting (**Figure 5.6**). This clone highlighted NKA-α3 expressing samples (ORWT-α3 and UC1 d32 iPSC-derived neurons) stronger than isolated NKA-α1 lysates (HEK293T cells and UC1 d0 iPSCs). Unfortunately, banding patterns would suggest that this clone is not greatly specific for α3 over α1. Recent immunoblots with non-boiled protein samples enhanced the resolution of this banding pattern but did not change the ineffectiveness of other pooled monoclonal supernatants for NKA subunit detection on immunoblotting (not shown). While a neutral result in a low throughput screening method, the success of antibody production highlights the possibility that further screening and optimization will describe a more specific anti-NKA-α3 clone.

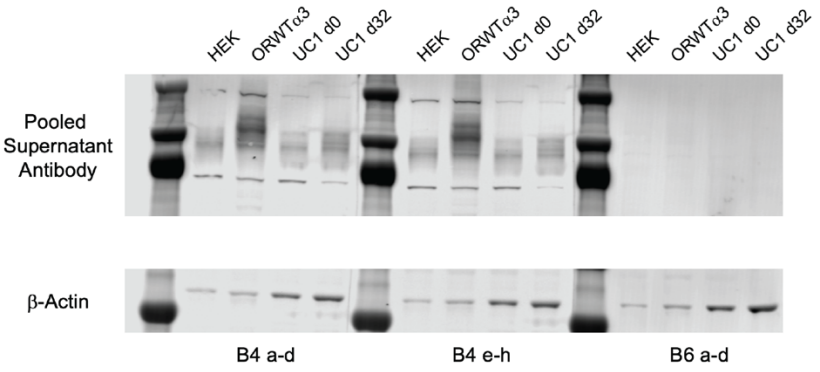

Figure 5.6: Pooled subclone screening via Western blot identifies supernatants with possible specificity. After secondary subcloning, selected subclones were divided into eight groups for supernatant collection and further screening. Of the ten pooled supernatants tested, only two (B4 a-d and B4 e-h) showed banding patterns on immunoblotting in the 110-115 kDa range suggestive of possible utility as an NKA-α3 antibody in immunoblotting. β-Actin shown as visual loading control.

Discussion

Commercially available NKA-α3 antibodies have been successful in discrete experimental domains but remain applied for methods in which isoform cross-reactivity has been demonstrated in our lab. For this reason, deliberate efforts were made to generate a more specific antibody against a unique cytoplasmic region of NKA-α3 subunit. Monoclonal mouse antibodies have been generated in collaboration with internal cores and external agencies. Multiple screening modalities narrowed the focus of our antibody search to promising subclones, and these antibody-producing hybridomas have been banked for future expansion and application. However, further isolation, screening, epitope identification, and protocol optimization are needed to produce a useful experimental reagent following best practice guidelines for antibody development (Bordeaux et al., 2010; Uhlen et al., 2016). While this chapter does not describe definitive production of purified antibody, it is our hope that the data presented serve as a transparent and significant step in that direction.

Important considerations regarding epitope target selection included isolating a region unaffected by both common AHC mutations and post-translational modification events. Phosphorylation and other methods of reversible modifications can impact the affinity of an antibody for its target epitope (Sternberger and Sternberger, 1983). The "key" aspartate residue in the DKTGT motif is Asp366 in NKA-α3, which is phosphorylated during the transfer of the ATP γ-phosphate during the ion transport cycle (Capuano et al., 2020; Paciorkowski et al., 2015). The Na,K-ATPase α subunit family is negatively modulated by PKA-mediated phosphorylation of Ser943 in α1 (Ser933 in α3), while more variable N-terminal PKC phosphorylation sites increase enzyme recruitment to the plasma membrane (e.g., Ser16 in α1) (Beguin et al., 1994; Cheng et al., 1999; Fisone et al., 1994; Mordasini et al., 2005; Oliveira et al., 2009; Ridge et al., 2002). Other possible NKA-α1 modifications include insulin-induced ERK1/2 phosphorylation of Tyr10 and Thr86 and subsequent increases in pump activity, with other possible ERK activity at Thr85, Thr226, Ser228, Thr282, and Thr788 residues (Al-Khalili et al., 2004; Feraille et al., 1999). While many of these modifications have been studied for the NKA-α1 isoform, their impact on NKA-α3 pumps is less well known although involved residues and flanking regions show high similarity between isoforms (Poulsen et al., 2010b). Regardless, most of these post-translational modification sites do not lie within the antigen fragment or the central epitope target region. This design may lead to the production of a better suite of

antibody reagents that will give researchers greater flexibility in study design and allow for improvements in experiment reproducibility.

Materials and Methods

Target epitope fragment preparation and validation

A cDNA fragment of *ATP1A3* encoding NKA-α3 residues 329 - 762 was cloned into a core plasmid (pN6HSIIb) using BamHI and NotI and verified by sequencing. Fragment design and cloning was performed by postdoctoral researcher Mark Grier. The Vanderbilt Antibody and Protein resource (VAPR) produced purified protein in *E. coli*, validated fragment characteristics by mass spectrometry, and ensured the presence of natively folded structures prior to mouse immunization.

Antibody generation in mice

Antibodies were generated by VAPR under the coordination of Erin Gribben using general mouse immunization, sample collection methods and timelines, and ELISA screening for appropriate immune response as described previously (Akingbade et al., 2012; Markham et al., 2012). For these studies, four mice were immunized and tagged for identification as R, L, RL, and O. Blood and serum samples were returned to the Ess Laboratory representing the pre-immunization bleed and two collection timepoints following immunization and subsequent boosts. Following initial screening via immunoblot, two spleens were selected for monoclonal antibody production.

Hybridoma Formation and PVKE Bead Assays

Spleens were shipped to the Fred Hutchinson Antibody Technology Resource (Seattle, WA) for hybridoma formation and processing to monoclonality. An external assay for antibody binding sensitivity was performed at Fred Hutchinson with monoclonal hybridoma culture supernatants under the guidance of Ben Hoffstrom. Specific antibody binding to bead-coupled protein targets resulted in increased measurement of fluorescence at the end of the assay in many of the clones. Purified protein fragments produced for immunization as described above and used to detect antibody sensitivity for NKA-α3. Specificity assays were performed against full length human NKA-α1 and NKA-α2 acquired as HEK-cell overexpression lysates together with negative controls from Novus Biological (NBL1-07807 and NBL1-07808).

In-cell Western (ICW) assays

ICW assays were performed on an Odyssey Imaging platform using NKA-α3 expressing HEK cells (ORWTα3) generated in the Ess Laboratory by Christine Simmons. In-cell Western blotting was performed using general protocols from Cell Signaling Technology. Cells were passed with trypsin and plated on polyethyleneimine coated 96-well plates at 20,000 cells per well and fed fresh media after two days (DMEM [Gibco, 11996-065] with 10% FBS and 1% penicillin-streptomycin). ORWTα3 cells reached confluence after 3 days and were fixed with 2% PFA for 20 minutes at room temperature, washed 3 times with PBS, and permeabilized with 0.1% PBST for 1 minute. Blocking step was performed with 0.1% PBST + 2.5% normal goat serum overnight at 4C. Primary antibodies were applied in blocking solution and included 96 mouse monoclonal anti-NKA-α3 candidate supernatants from Fred Hutchinson (1:20). Primary solutions

were incubated overnight at 4C. After several PBS washes, secondary antibodies (1:1000) were applied in blocking solution for 2 hours at room temperature. Prior to imaging, the plate was inverted and blotted dry with a paper towel to remove residual liquid.

Dot Blotting

Dot blotting was performed using Bio-Dot Microfiltration Apparatus (BioRad) and associated protocols with the assistance of Brittany Parker. Briefly, a nitrocellulose membrane was prepared and pre-washed with TBS prior to addition of protein. Sample lysates collected in RIPA buffer from HEK cells expressing α1 or ORWT cells expressing both endogenous α1 and exogenous α3 were quantified by Bradford Assay, diluted in TBS, denatured at 80C for 10 minutes, and loaded at increasing concentrations (250 ng, 1.0 μg, 5.0 μg) to the membrane using vacuum pressure. The membrane was then blocked with 1% BSA in TBS using gravity filtration followed by washes with 0.05% TBST. Antibodies were diluted in 1% BSA in 0.05% TBST at the following concentrations: monoclonal supernatants (1:10), DHSB A6F mouse anti-α1 (1:500), Abcam EPR14137 rabbit anti-α3 (1:1000), ThermoFisher XVIF9-G10 mouse anti-α3 (1:1000). Primary incubation was conducted via gravity filtration followed by 2 TBST washes. Secondary antibodies were applied in the same manner before the membrane was imaged on an Odyssey scanner.

Western Blotting

Immunoblotting (Western) was performed using techniques previously described on PVDF membranes. For antibody screening, some samples were screened both denatured (boiled in SDS buffer at 80C prior to gel loading) and non-denatured (not boiled). The immunoblots shown described denatured samples. Optimization of antibody probing with non-boiled protein samples was performed and resulted in significantly improved band resolution for the positive clone B4 (a-h), although did not improve the negative results for other clones tested. For initial screening, mouse bleeds from VAPR were used as primary antibodies at 1:500 (bleed #1) or 1:1000 (bleed #2). For downstream screening, secondary subclonal supernatants from Fred Hutchinson were pooled into groups of 4 (e.g., B4a-d) and used as primary antibodies at 1:5-1:10 dilution.

CHAPTER VI

SUMMARY AND FUTURE DIRECTIONS

AHC is a neurodevelopmental disorder characterized by early onset of hemiplegia or quadriplegia, autonomic disturbances, painful dystonia, seizures, and developmental delay. This disease was found to be associated with mutations in *ATP1A3* in 2012 and has since been placed amongst an expanding spectrum of related disorders including RDP and CAPOS, which share common features including triggered symptoms. Unfortunately, there are no curative or widely beneficial treatment for AHC patients or related *ATP1A3* diseases. While model systems using genetically engineered mice or cell culture techniques have yielded significant information regarding disease mechanisms and pathophysiology, many gaps in knowledge remain in the field. This chapter will summarize our findings in an iPSC-derived cortical neuronal disease modal and place them in a larger context for patients, clinicians, and scientists alike. Considerations for future directions in AHC disease modeling will be discussed that may help answer important questions regarding disease pathophysiology and treatment.

Review of Findings in the Context of *ATP1A3*-Related Disease Research

The three most common heterozygous missense mutations in *ATP1A3*, causing D801N, E815K, and G947R variants of the neuronal specific NKA-α3 subunit, represent over half of the AHC patient population (Capuano et al., 2020; Viollet et al., 2015). AHC mutations result in the loss of sodium and potassium transport by preventing the binding of these ions to pockets within transmembrane domains of the protein (Koenderink et al., 2003; Sweadner et al., 2019; Weigand et al., 2014). We decided to focus our efforts on studying a cortical neuronal disease model using *ATP1A3*$^{+/E815K}$ iPSC-derived neurons. The E815K genotype in AHC has been consistently associated with the most severe disease phenotype, and may lead to more rapid phenotype identification in cultured neurons (Panagiotakaki et al., 2015; Sasaki et al., 2014). Significant energy and resources were spent creating isogenic wildtype lines from patient iPSCs to increase the power of our studies and the confidence in our results. This model system allowed us to perform well-controlled studies and describe novel disease phenotypes in human neurons that share features with observations in mouse models of disease and with symptoms in human patients.

We report that AHC iPSC-derived neurons have increased *ATP1A3* transcript expression compared to isogenic and unrelated controls. Compensatory transcript elevation may be a response to ion dysregulation, as intracellular sodium and potassium concentrations are known to regulate NKA-α1 subunit expression in renal tissue (Johar et al., 2014; Vinciguerra et al., 2003; Wang et al., 2007). Elevated *ATP1A3* transcript expression was contrasted by the observation of comparable NKA-α3 protein expression levels across genotypes. While a trend towards protein elevation existed by d60 of mixed cortical differentiation, this data point never reached statistical significance. It will be important for future experiments to better clarify this discrepancy, although a difference in mRNA and protein expression may have true biological basis in the case of decreased mutant protein stability. This was the first report of altered *ATP1A3* transcript expression in AHC, although previous reports have shown increased protein expression in response to acute pharmacologic inhibition of neuronal NKA pumps (Bersier et al., 2011). Little information has been published about expression patterns in mouse models of disease, particularly regarding possible transcriptional compensation for pump failure. Future studies may look to brain biopsy samples to profile RNA and protein expression in AHC patient neurons to correlate our findings to human patient data. The presence of increased mutant protein expression or elevated RNA transcripts would have significant impact on the design and dosing of future genomic therapies that may specifically target these components (Lykken et al., 2018), with overall *ATP1A3* transcript elevation a possible feature of diseased neurons at baseline.

iPSC-derived neurons from AHC patients consistently demonstrated generally decreased firing rates and bursting metrics on MEA analysis, which is consistent with conclusions made by Simmons et al. (2018) when measuring stimulated activity in iNgn2 ATP1A3$^{+/G947R}$ neurons. More experiments should be conducted to determine if this phenotype is related to altered synaptic development, changes in NKA-α3 subcellular localization, or abnormal neuronal morphology in AHC neurons. While baseline recordings did not yield significant phenotypes given high variability of MEA measurements in iPSC-derived neurons, neural hyperactivity in AHC lines was revealed by a heat stress recording paradigm and standardization to baseline activity metrics. Mouse models of AHC mutations have also shown neuronal hyperexcitability and heightened seizure sensitivity (Clapcote et al., 2009; Hunanyan et al., 2015). The biological relevance of these findings has yet to be determined, but they undoubtedly have sound origins related to disease pathophysiology when reconciling repeated findings of neuronal hyperactivity over multiple model systems. Symptomatic development or exacerbation upon insults such as elevated temperature are common in *ATP1A3*-related diseases and laboratory models (Helseth et al., 2018; Holm and Lykke-Hartmann, 2016; Isaksen et al., 2017; Kansagra et al., 2013; Palladino et al., 2003; Sugimoto et al., 2014). The presence of stress-induced phenotypes is a challenge for disease modeling but also offers clues regarding pathophysiology and opportunities for context dependent investigation.

Flunarizine has been posited to prevent or reduce the frequence of triggered episodes in AHC. While it has been studied across multiple clinical and laboratory investigations, patients and disease models do not consistently respond positively to treatment (Helseth et al., 2018; Panagiotakaki et al., 2015; Pisciotta et al., 2017; Sasaki et al., 2001). In our studies, *in vitro* treatment with flunarizine did not have an impact on stress-triggered hyperactivity or local bursting neural activity. It is possible that flunarizine may be exerting an influence on other neuronal lineages that we have not addressed and that are not generated in our model system. While we do not conclude that flunarizine is ineffective in AHC patients, we found that 100 nM treatment of iPSC-derived neurons had limited impact on model phenotypes. Low throughput iPSC-derivative studies limited our ability to investigate other drugs such as topiramate or antiepileptics that may have impacted *in vitro* phenotypes. Future experiments harnessing more rapid iPSC neural differentiation protocols should consider expanding pharmacological screening to more compounds. In this vein, recent pilot experiments in our hands have described key aspects of endocannabinoid signaling in iPSC-derived neurons and the impact of cannabidiol treatment on AHC and control neurons.

Brief explorations of metabolic dysfunction highlighted that *ATP1A3* mutant iPSC-derived neurons may be more susceptible to heat stress alterations in mitochondrial respiratory rate compared to isogenic controls. While this finding has few direct correlates in patients, researchers and clinicians have long been searching for metabolic phenotypes in AHC with little consistent success (Fons et al., 2012; Kemp et al., 1995; Nevsimalova et al., 1994; Sasaki et al., 2009). Metabolic abnormalities resulting from altered ionic control at the cortical neuron level may reconcile clinical and neuroimaging similarities between AHC and other migraine conditions, including cerebral hyperexcitability and cortical spreading depression susceptibility (Ferrari et al., 2015). These findings may also partially explain the efficacy of migraine-targeted therapeutics in some AHC patients. While ionic dysregulation was briefly studied in the Ess Laboratory, the specific impact of NKA-a3 mutations on intracellular sodium, potassium, and calcium dynamics remains an understudied area of the field (Fritz N, 2015; Tiziano, 2019; Xiao et al., 2002).

Previous studies have implicated altered inhibitory tone as a possible pathological driver of AHC, given findings of increased NKA-α3 expression overall and relative to NKA-α1 in GABAergic neurons (Bottger et al., 2011; Ikeda et al., 2013; Murata et al., 2020). In our iPSC-derived neuronal model of disease, we did not find increased NKA-α3 in GABAergic neurons and did not observe pathological differences between early excitatory and inhibitory neural differentiation protocols. Unfortunately, the failure of GABAergic cultures to maintain neuronal purity and electrical activity on MEA recording limited our analysis. The introduction of optimized iNgn2 and iGABA protocols that replicate many phenotypic

findings of morphogen-based differentiation strategies will allow greater culture purity and experimental design flexibility that can help address targeted hypotheses in an *in vitro* disease model (Nehme et al., 2018; Simmons et al., 2018; Yang et al., 2017; Zhang et al., 2013a). Progress made toward the production of a more specific NKA-α3 antibody will also help address these etiologic questions.

Due to the high costs and time requirements of iPSC clone generation and neural differentiation, we were only able to study one AHC mutation for the majority of the experiments presented in this document. The creation of isogenic controls was a necessary step in creating a reproducible data set and has become standard in the field of iPSC derived neuronal research (Ben Jehuda et al., 2018; Ran et al., 2013). Given unlimited time and resources, these experiments would have been performed across all three major AHC mutations with greater patient inclusion and larger clone numbers of disease and isogenic controls. Sharing of patient tissue samples and isogenic iPSC line series will be of critical importance to make these goals a reality as the *ATP1A3*-related disease community continues into the next decade of iPSC-derived neuronal research.

Future Directions for Disease Modeling in AHC

While providing novel information to the field regarding *in vitro* phenotypes in human neurons derived from iPSCs harboring a common AHC mutation, many questions have also been generated by our studies. We showed elevation of *ATP1A3* transcripts in diseased neurons but it remains unknown if wildtype and mutant alleles are expressed at the same ratio. Although we do not anticipate allele-specific transcriptional regulation, this information may be just as important as total allele expression in regard to genomic therapy generation. Likewise, are there changes to the stability of mutant NKA-α3 protein that explain a discrepancy between RNA and protein expression, particularly following exposure to heat stress? Transient changes in protein stability or synaptic localization related to trigger exposure resulting in exacerbated ion dysregulation may underly unique aspects of alternating hemiplegia symptoms. Initial stability studies can be performed *in silico* using structural analysis techniques and then translated to *in vitro* experimentation methods in mutant iPSC-derived neurons.

The trigger profile of AHC patients is both expansive and unique to individual cases (Heinzen et al., 2014; Kansagra et al., 2013). When a higher throughput screening method is established with iNgn2 and iGABA neurons, other insults could be included for phenotype testing such as nutrient withdrawal, cold exposure, and ATP depravation. Technologies like MEA recording are very amenable to these experimental modifications and can be used in tandem with whole cell patch clamp electrophysiology for increased confidence and better mechanistic understanding. The integration of the methods described in this document with mouse models of *ATP1A3* disease would provide significant insights into shared phenotypes between mouse and human AHC neurons. Cortical neuronal cultures from mice show rapid and robust networking within two weeks of plating compared to the months of culture necessary for human mixed cortical iPSC-derived neurons to show network-level bursting. Studies describing phenotypes in mouse and human neurons under trigger stressors and pharmacologic treatment would be of high impact and would bolster both model systems.

The signaling mechanisms of the NKA-α3 subunit have been explored in the field but remain understudied in AHC disease models. Inhibition of NKA activity by ouabain treatment triggers dendritic growth and related transcriptional programs, but the impact of AHC mutations remains unknown (Aperia et al., 2016; Desfrere et al., 2009; Haas et al., 2002). While most patients do not show abnormalities on brain imaging, a minority have significant abnormalities that indicate the presence of broader neurodevelopmental defects. Knowledge of the impact of AHC mutations on NKA subunit signaling

mechanisms would provide novel information to the field and may suggest alternative routes to treatment that are not yet recognized as possibilities.

Perhaps the most important knowledge gap in the field regards the etiology of AHC as driven by haploinsufficiency or dominant negativity. While it is accepted that common AHC mutations result in decreased NKA turnover and ion transport defects, it is still unknown if mutant subunit dysfunction can also impact wildtype NKA-α3 protein cycling. A hypothesis of dominant negativity (**Figure 6.1**) is supported by animal models of *ATP1A3* disease, in which *Atp1a3*$^{+/-}$ mice (DeAndrade et al., 2011; Ikeda et al., 2013) often have little or no phenotype compared to the sometimes-striking phenotypes of *Atp1a3*$^{+/AHC}$ mice (Clapcote et al., 2009; Heinzen et al., 2014; Helseth et al., 2018; Hunanyan et al., 2015). Additionally, reports of human patients with *ATP1A3*-spectrum diseases due to *ATP1A3*$^{+/-}$ genotypes are lacking, with *ATP1A3*-related diseases isolated from frameshift and early termination nonsense mutations. An isogenic series of *ATP1A3*-edited iPSCs composed of wildtype, heterozygous knockout, heterozygous AHC, and complete knockout genotypes would be of great use to answer these questions. In even more complicated but elegant study designs, new genetic editing techniques would also allow the generation of iPSC lines and derivative neurons capable of genotype switching using inducible knockout constructs (Chen et al., 2015). Should these techniques fail, improved tools for CRISPR-based transcriptional inhibition could be used to study knockdown models of haploinsufficiency (Tian et al., 2019).

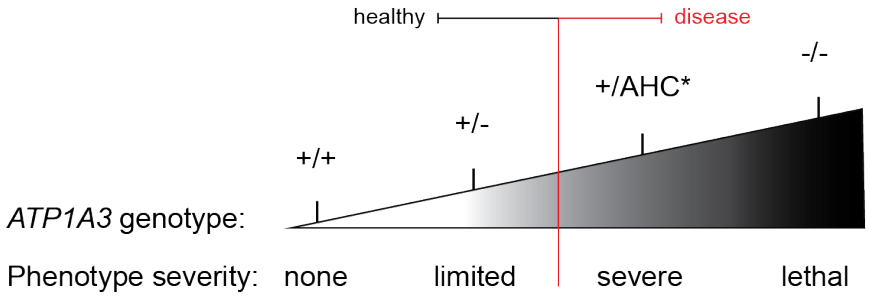

Figure 6.1: Graphical hypothesis for dominant negativity in AHC. Heightened disease severity occurs with common AHC* mutations (*ATP1A3*$^{+/AHC}$; D801N, E815K, G947R) compared to mouse models and human individuals with heterozygous knockout (*ATP1A3*$^{+/-}$) genotypes that often display no noticeable neurological abnormalities at baseline. These features suggest that AHC mutations result in dominant negative (or gain of function) disease mechanisms instead of simple loss-of-function impacts. Homozygous knockout or AHC mutation homozygosity (*ATP1A3*$^{-/-}$) leads to perinatal death in animal models. Wildtype represented by *ATP1A3*$^{+/+}$ shows no phenotype.

Another large knowledge gap in the field exists regarding *ATP1A3* mutation negative AHC cases. If 82% of AHC cases are attributable to *ATP1A3* mutations (Viollet et al., 2015), what explains the other 18%? Identifying the etiology of these atypical cases may represent an important step in mechanistic understanding, as shared dysfunction may be common amongst the causative insults. Studies in relatively large atypical AHC cohorts are underway to determine if patterns emerge that could generate new ideas for the treatment of AHC or the mechanisms underlying patient symptoms.

In summary, the power of iPSC-based disease modeling allowed us to gain significant insight into the *in vitro* phenotypes of human AHC neurons. Optimized differentiation protocols, treatment methods, and novel trigger induction paradigms are available to the AHC research field for further study. While our results provide new evidence for phenotypes in iPSC-derived neurons harboring the *ATP1A3*$^{+/E815K}$ genotype, it is our hope that the methods and data described in this document provide a general platform for future mechanistic discovery and therapeutic screening with the ultimate goal of improving treatment options for patients with *ATP1A3*-related diseases.

APPENDIX

CHAPTER II SUPPLEMENT

Clone IC1	gRNA 1: TGCCATCTCACTGGCGTACA(***AGG***) ssODN Template-Induced Changes: c.2443A>G - K815E correction to wildtype c.2445G>A - E815E PAM-site synonymous	ssODN (1) CTCCCCTCTCCGGCTCACCCGGCCTCCTCCGCCTAGGT CCCTGCCATCTCACTGGCGTAC***G******A******G***CTGCCGAAAGCG ACATCATGAAGAGACAGCCCAGGAACCCGCGGACGGAC AAATTGGTC
Clone IC2	gRNA 2: AGCCTTGTACGCCAGTGAGA(***TGG***) Template-Induced Changes: c.2443A>G - K815E correction to wildtype c.2427C>A - A809A PAM-site synonymous	ssODN (2) CCAGGAGGGTGGAGTCCTCCCCTCTCCGGCTCACCCGG CCTCCTCCGCCTAGGTCCCTG***C******A******A***TCTCACTGGCGTAC***G*** AGGCTGCCGAAAGCGACATCATGAAGAGACAGCCCAGG AACCCGCGGACGGACAAATTGG

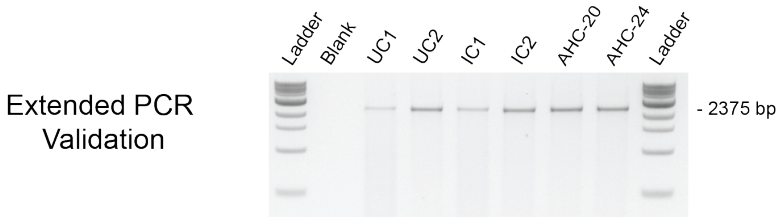

Supplemental Figure 2.1: CRISPR guide and template sequences and further validation for isogenic clone generation. (A) Separate sgRNAs were designed to generate unique clones of isogenic corrected *ATP1A3*$^{+/+}$ lines from AHC patient line AHC-24. ssODN templates unique to each sgRNA included the intended c.2443A<G correction of the AHC mutation (green), along with synonymous changes to the PAM-site (red) to prevent repetitive cutting events by the Cas9 nuclease. Extended PCR validation with primers located over 1kb from the intended cut site show a single band suggesting no large insertions or deletions that would result in the inability of PCR primers to anneal properly during initial screening attempts. The faintness of bands UC1 and IC1 is due to limited DNA availability at the time of analysis. Whole exome sequencing on line IC2 (not shown) further confirmed that the PAM-site silent mutation seen on initial screening (c.2427C>A) was indeed homozygous and not the result of potential imbalanced allelic amplification.

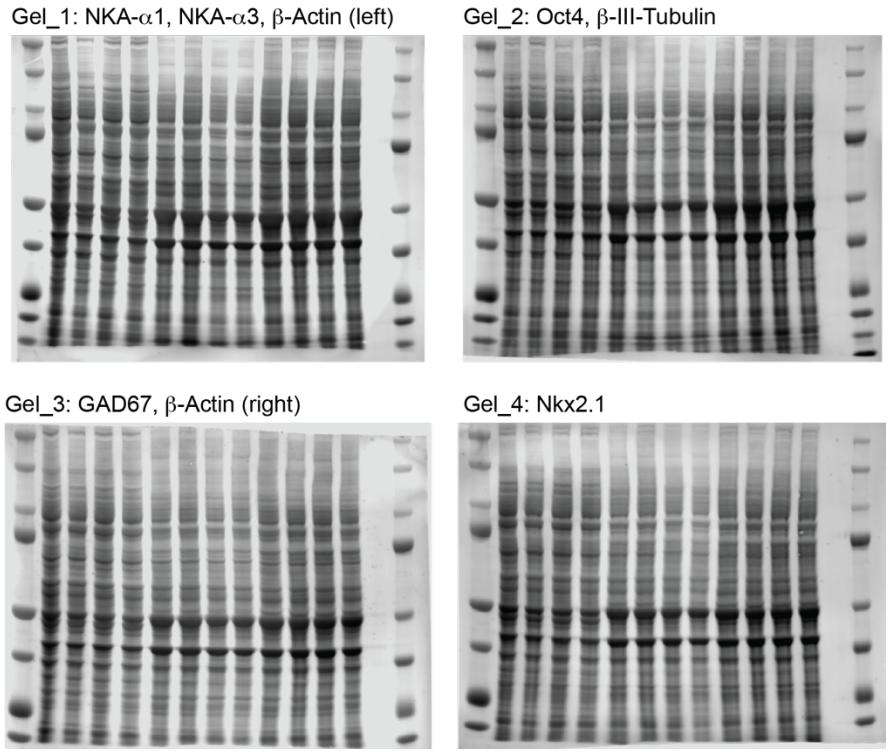

Supplemental Figure 2.2 –Total protein stains for paired differentiation marker immunoblots. To profile outcomes of initial paired differentiation runs and confirm protocol techniques, multiple blots were created and probed simultaneously. B-Actin bands shown for Figure 2.4 were designed to represent simplified blots that were loaded on the same days with the same samples and volumes as a visual guide for protein loading; i.e., blots 1-2 and blots 3-4 above. True total protein stains that would be used for normalization and data visualization are shown here for complete transparency. Left and right designations for b-Actin is in reference to the placement of blots within Figure 2.4.

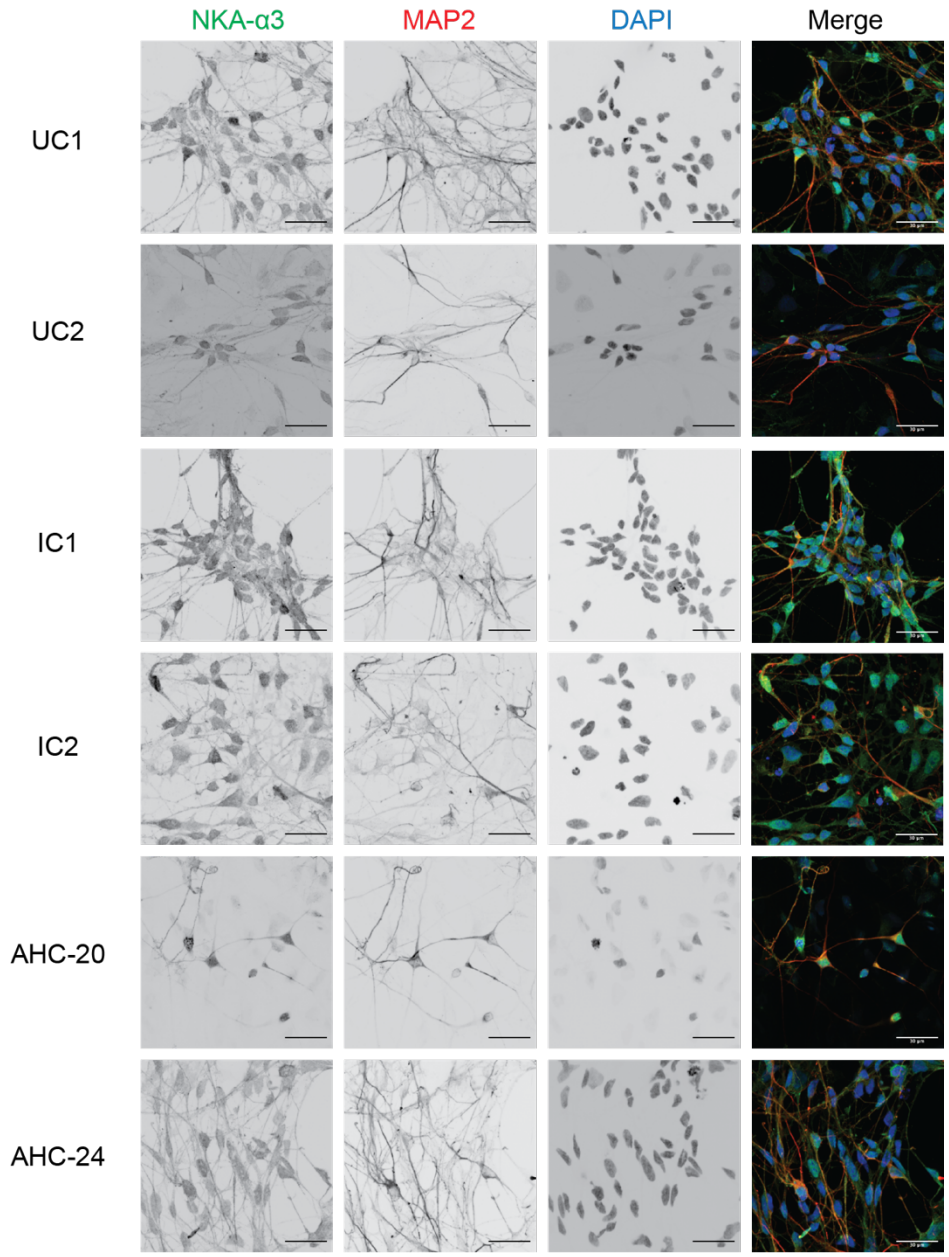

Supplemental Figure 2.3: High resolution images of NKA-α3 expression in iPSC-derived mixed cortical neurons. Confocal microscopy shows 60x magnification of NKA-α3 subunit (green) expression in MAP2 positive neurons (red) resulting from the Shi protocol at d60 of differentiation. DAPI shows nuclei (blue). No obvious differences in localization or expression patterns were noted across genotypes or differentiation by qualitative observation. Scale bar = 30 μm.

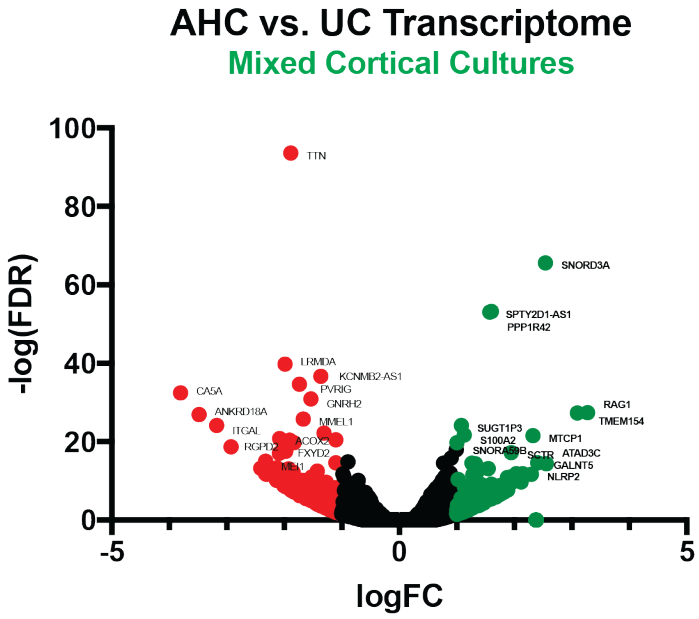

Downregulated Genes

Gene Name	logFC	logFDR
CA5A	-3.804	32.466
ANKRD18A	-3.478	26.914
ITGAL	-3.173	24.172
RGPD2	-2.927	18.670
MEI1	-2.326	15.000
FXYD2	-2.086	17.058
ACOX2	-2.082	20.812
LRMDA	-1.987	39.804
TTN	-1.888	93.627
PVRIG	-1.737	34.652
MMEL1	-1.668	25.740
GNRH2	-1.538	30.889
KCNMB2-AS1	-1.364	36.693

Upregulated Genes

Gene Name	logFC	logFDR
RAG1	3.275	27.421
TMEM154	3.099	27.326
ATAD3C	2.556	14.398
SNORD3A	2.543	65.559
GALNT5	2.409	14.656
MTCP1	2.325	21.539
NLRP2	2.296	11.706
SCTR	1.945	17.257
PPP1R42	1.604	53.182
SPTY2D1-AS1	1.572	53.038
S100A2	1.133	21.682
SUGT1P3	1.082	24.119
SNORA59B	1.001	19.750

Supplemental Figure 2.4: Bulk tissue RNAseq highlights potential transcriptional differences in mixed cortical cultures. Differential expression plots of (logFC) vs. –log(FDR) display genes that are upregulated (green) and downregulated (red) in AHC clones compared to unrelated controls (UC) at post-induction d32 in mixed cortical cultures. In this pilot study (2 samples of each genotype), it was intriguingly noted that mRNA transcripts for *FXYD2*, a gene encoding an accessory Na,K-ATPase γ-subunit, may be downregulated in AHC lines compared to controls. GABAergic protocol sample analysis (not shown) did not pull out this same association, and more replicates and validation need to be performed before conclusions are made. FC = fold change; FDR = false discovery rate.

CHAPTER III SUPPLEMENT

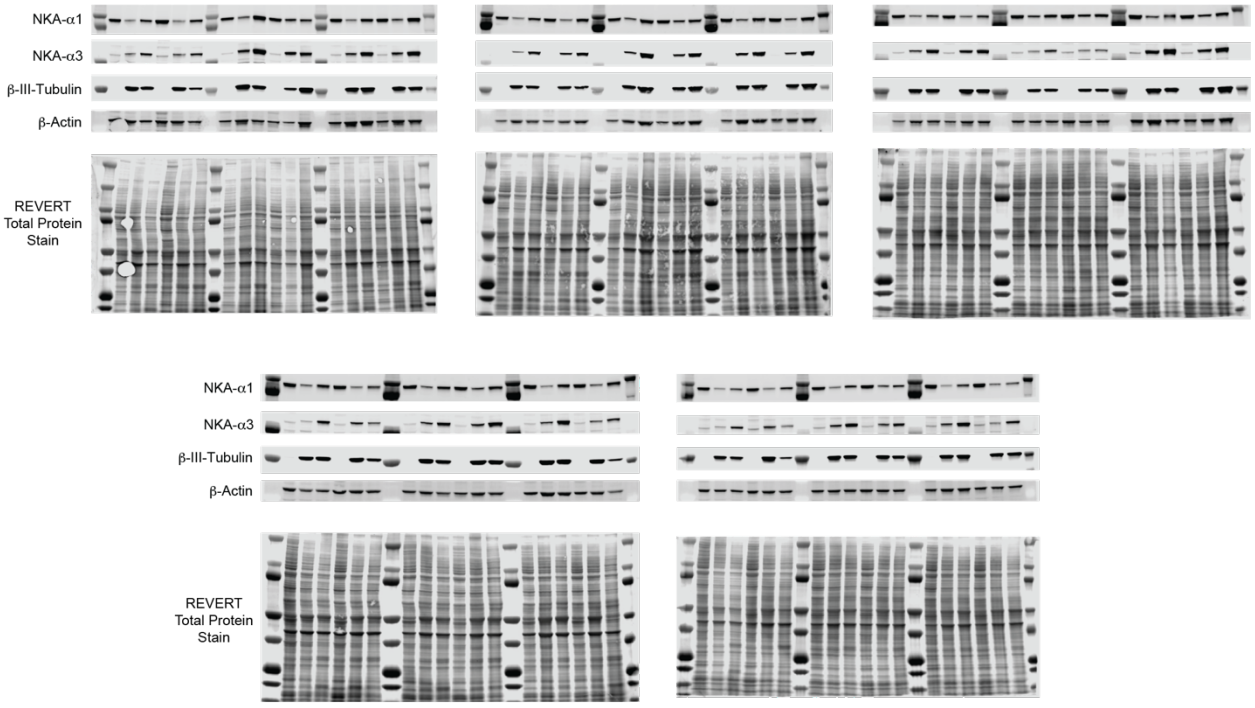

Supplemental Figure 3.1 – Full immunoblots and total protein stains for neuralization data and NKA-subunit profiling. Blots were cut to size and probed for NKA-α1, NKA-α3, β-III-Tubulin, and β-Actin. β-Actin is shown as a visual guide for protein loading while intensity data was normalized to total protein shown here for each lane. Lysates from six clones of a given differentiation at three timepoints (d0, d32, d60) were run on the same gel, loaded as outlined in Figure 3.2.

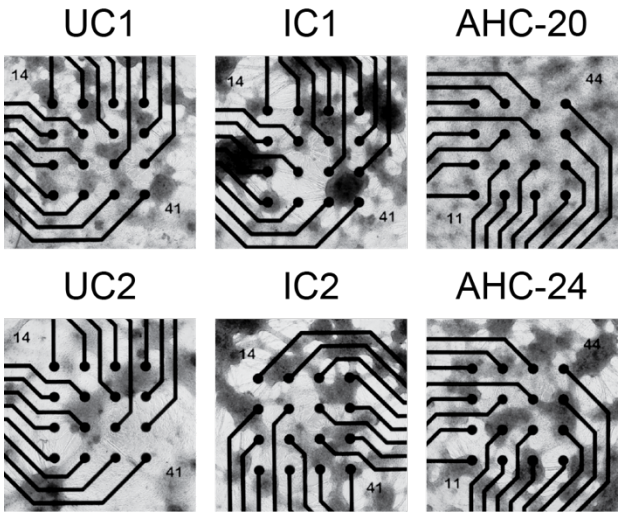

Supplemental Figure 3.2 – Images of mixed cortical neurons show plating density and aggregation on MEA electrodes. Representative brightfield images of MEA plates at d80 shows clusters of neurons in relation to the 16 electrodes on each plate (black circles) at the end of the recording period. Following dispersion and plating at d45 of differentiation, neurons begin to cluster as seen in these photos. No obvious patterns of survival differences or overall network structures were noted between genotypes either at plating after experimental collection timepoints concluded.

	Sample Size (n)				Significance (p-value)				Significance (notation)			
DMSO	Day	UC-to-IC	AHC-to-UC	AHC-to-IC	Day	UC-to-IC	AHC-to-UC	AHC-to-IC	Day	UC-to-IC	AHC-to-UC	AHC-to-IC
	d60	7	9	7	d60	>0.9999	0.0013	0.0088	d60	ns	**	**
	d64	8	8	8	d64	0.8382	0.0020	<0.0001	d64	ns	**	****
	d68	8	9	10	d68	>0.9999	0.4820	0.1647	d68	ns	ns	ns
	d72	8	7	9	d72	0.1708	0.4601	0.0037	d72	ns	ns	**
	d76	9	6	7	d76	>0.9999	0.0135	0.0379	d76	ns	*	*
	d80	7	5	7	d80	>0.9999	0.0092	0.1112	d80	ns	**	ns
	Sample Size (n)				Significance (p-value)				Significance (notation)			
100 nM Flunarizine	Day	UC-to-IC	AHC-to-UC	AHC-to-IC	Day	UC-to-IC	AHC-to-UC	AHC-to-IC	Day	UC-to-IC	AHC-to-UC	AHC-to-IC
	d60	7	7	6	d60	0.5491	0.9586	>0.9999	d60	ns	ns	ns
	d64	7	8	7	d64	0.9455	0.6337	0.0720	d64	ns	ns	ns
	d68	8	7	8	d68	>0.9999	0.0352	0.0068	d68	ns	*	**
	d72	8	7	8	d72	>0.9999	>0.9999	0.3016	d72	ns	ns	ns
	d76	8	4	8	d76	>0.9999	<0.0001	0.0007	d76	ns	****	***
	d80	8	4	5	d80	>0.9999	>0.9999	0.5459	d80	ns	ns	ns

Table S3.1 – MEA heat stress recording protocol statistical breakdown by recording day. Sample sizes, significance values, and notations for each data point in Figure 3.5D and 3.5E. Data points represent values across 5 differentiations with 2 clones per genotype. Significance notations represent AHC-to-isogenic comparisons in the recovery period (37C). Significance calculated using 2-way ANOVA with Bonferroni's multiple comparisons test; significance noted as $p < 0.05$ (*), $p > 0.01$ (**), $p < 0.001$ (***), and $p < 0.0001$ (****); $p > 0.05$ (ns). Error bars represent SEM.

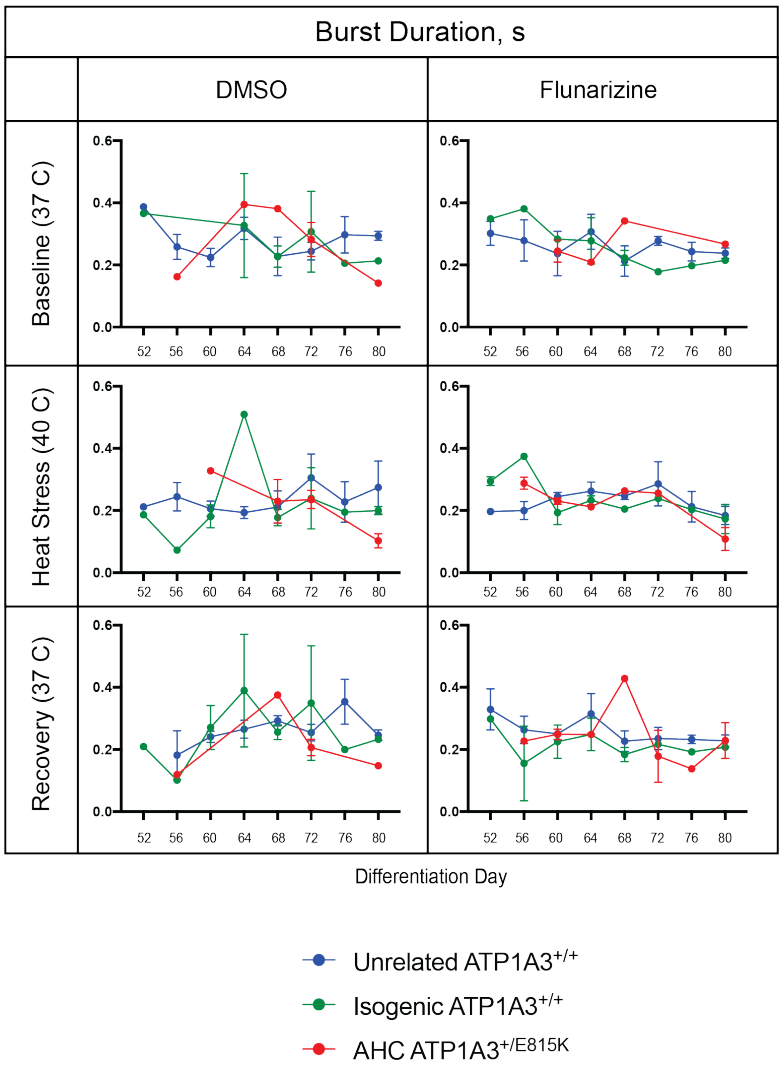

Supplemental Figure 3.3 – Burst duration is variable but similar across genotypes and recording conditions. Burst duration represents the time between the first and last spikes in a particular local burst, which is defined by AxIS software settings as a minimum spike count of 5 in a defined time window with maximum interspike interval of 100 ms occurring at a single electrode. The burst duration in seconds shown above trended similarly between unrelated controls (blue), isogenic controls (green), and AHC E815K neurons (red). Although AHC neurons did not experience as many bursting events as controls, the burst durations were similar between genotypes. High variance and limited data limits statistical testing of this dataset, but trends toward similarly are apparent.

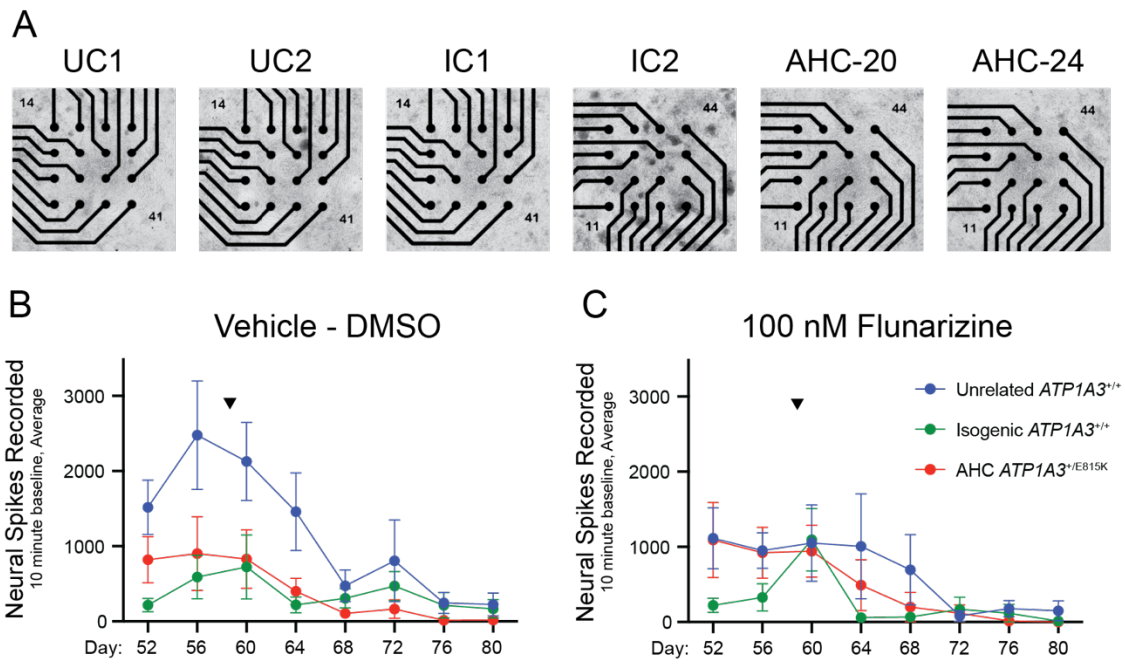

Supplemental Figure 3.4 – GABAergic shifted cultures do not sustain sufficient MEA measurements for detailed analysis. As appreciated in MEA wells (A), while Maroof protocol cultures survived as a consistent monolayer during the duration of the recording window, they never aggregated into neuronal clusters over time as seen in the Shi protocol cultures. Neural activity extinguished over time in both vehicle (B) and flunarizine (C) treatment conditions, disallowing any analysis of MEA metrics. It is unknown whether this is related to inherent properties of the neurons or networks differentiated using this protocol, possible overgrowth of contaminating cell populations, or another incompatibility between this protocol and data collection techniques.

CHAPTER IV SUPPLEMENT

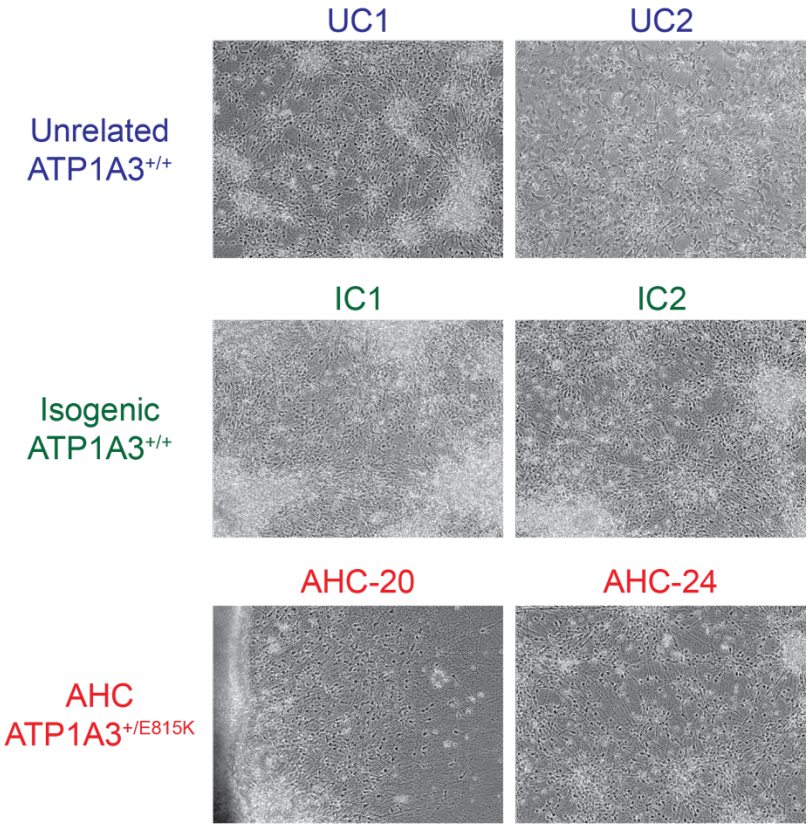

Supplemental Figure 4.1: Representative brightfield images of d32 neurons generated with the mixed cortical protocol. Images show mixed cortical neurons generated from the Shi Protocol at d32, demonstrating even survival between genotypes and relatively consistent yield. These neurons are similar to those that were used for RNAseq (d32) and do not change greatly in morphological appearance between d32 and d60, when samples were collected for RTqPCR assessment of CB receptors in Figure 4.1.

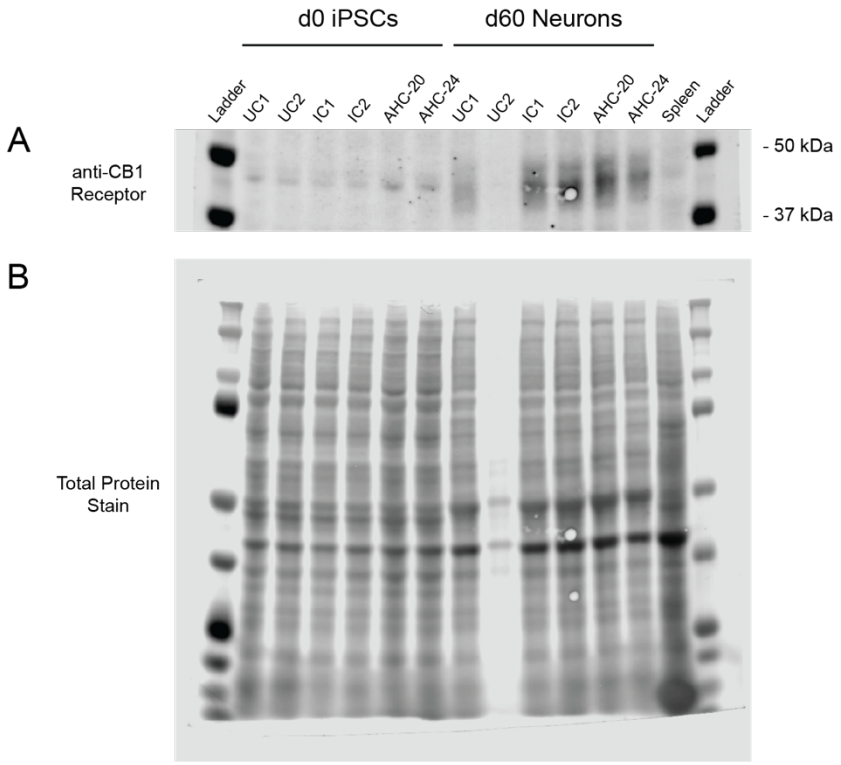

Supplemental Figure 4.2: Blots and total protein stain for CB1 expression assessment. (A) Blots show a clear banding pattern at the approximate weight expected for CB1 and common isoforms (49-53 kDa), with proteins often running lower than expected in this gel setup. (B) Total protein stain shown for normalization related to Figure 4.1. Sample UC2 for d60 neurons did not get quantified or loaded properly although normalized intensity values for clone UC2 (0.35) are similar to clone UC1 (0.51) for CB1 expression when normalizing to IC1 expression.

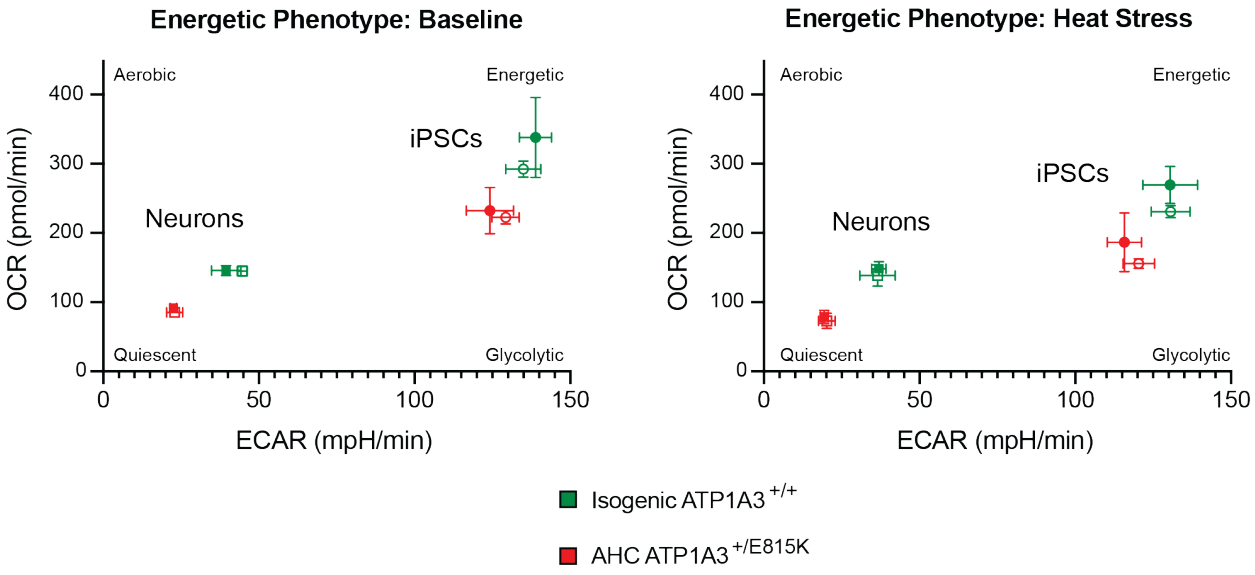

Supplemental Figure 4.3: iPSCs and derivative AHC neurons display distinct energetic phenotypes. Both OCR (oxygen consumption rate), and ECAR (extracellular acidification rate) are readouts of the Seahorse Cell Mito Stress Kit. OCR can be seen as a measure of mitochondrial respiration, while ECAR is interpreted as an indicator of glycolysis. Four points can therefore be drawn on an energetic phenotype plot representing cells that are aerobic, energetic, glycolytic, or quiescent. As data are not normalized to total protein levels or terminal cell counts, different cell types should not be directly compared although iPSCs and neurons are plotted together for simplification. In both iPSCs and derivative neurons, AHC lines (red) slide toward a less energetic phenotype than their isogenic control counterparts (green). This feature is not significantly changed by the application of 100 nM flunarizine (open data points). The energetic phenotypes remain consistent even after preincubation at 40C as a heat stress insult. Data represent two clones per genotype from one mixed cortical differentiation; error bars represent SEM.

REAGENT TABLES AND MEDIA RECIPES

Plasmids for Pluripotency Induction

Plasmid Description	Addgene Identifier
pCXLE-hOCT3/4-shp53-F	27077
pCXLE-hSK	27078
pCXLE-hUL	27080

Primers for Genotyping and Validation (Integrated DNA Technologies)

Primer Name	Primer Sequence
ATP1A3 Exon 18 PCR Forward Primer	CGCCTGATCTTCGACAACCT
ATP1A3 Exon 18 PCR Reverse Primer	TAACCTGGAGCCCCTCTCTC
ATP1A3 Exon 18 PCR Nested Forward Primer	TACACCCTGACCAGCAATATC
PX459 U6P Primer for Ligation Validation	GGACTATCATATGCTTACCG

Primers and Probes for qPCR (Applied Biosystems)

Transcript	Assay Identifier
GAPDH	Hs99999905_m1
ATP1A1	Hs00167556_m1
ATP1A2	Hs00265131_m1
ATP1A3	Hs00958036_m1
ATP1B1	Hs00426868_g1
ATP1B2	Hs01020302_g1
ATP1B3	Hs00740857_mH
CNR1	Hs01038522_s1
CNR2	Hs05019229_s1
GPR55	Hs00271662_s1
MAP2	Hs00258900_m1
DLG4	Hs01555373_m1

Antibodies for Immunostaining and Immunoblotting

Antibody Target	Application	Host	Dilution	Provider	Catalog #
Nanog	ICC	Rabbit	1:250	Cell Signaling	4903
Oct4	ICC / WB	Rabbit	1:250 / 1:1000	Cell Signaling	2750
TRA-1-60	ICC	Mouse	1:250	EMD Millipore	MAB4360
SSEA3	ICC	Rat	1:250	EMD Millipore	MAB4303
SSEA4	ICC	Mouse	1:250	EMD Millipore	MAB4304
β-III-Tubulin	ICC / WB	Mouse	1:250 / 1:2000	EMD Millipore	MAB1637
Sox1	ICC	Rabbit	1:100	Genetex	gtx62974
Smooth Muscle Actin	ICC	Mouse	1:200	Abcam	ab5694
GATA4	ICC	Rabbit	1:200	Abcam	ab84593

Sox17	ICC	Mouse	1:100	Abcam	ab84990
GABA	ICC	Rabbit	1:500	Sigma	a2052
NKA-α3	ICC	Mouse	1:200	Thermo Fisher	MA3-915
NKA-α3	WB	Rabbit	1:1000	Abcam	ab182572
NKA-α1	WB	Mouse	1:250	Iowa DSHB	A6F
β-Actin	WB	Rabbit	1:2000	Cell Signaling	4967S
GAD67	WB	Mouse	1:500	Abcam	ab26116
Nkx2.1	WB	Mouse	1:100	Santa Cruz	sc-53136
CB1	ICC	Rabbit	1:1000	Immunogenes	-
CB1	WB	Rabbit	1:200	Abcam	ab23703
Ascl1	ICC	Rabbit	1:100	Abcam	ab211327
Dlx2	ICC	Mouse	1:100	Abcam	ab117546
Myt1l	ICC	Rabbit	1:50	Abcam	ab139732

iPSC Culture and Maintenance

Reagent / Product	Provider	Catalog #
mTeSR1 Complete Kit	Stemcell Technologies	85875
Matrigel Matrix	Corning	356234
ReLeSR	Stemcell Technologies	05872

Neural Differentiation and Maintenance Reagents

Reagent / Product	Provider	Catalog #
Accutase	Innovative Cell Technologies	AT-104
Ascorbic Acid	Sigma	A4403
B27 Supplement	Gibco	17504044
B27 Plus Supplement	Gibco	A3582801
BDNF	Peprotech	450-02
BME	Sigma	M6250
Dibutyryl cAMP	Sigma	D0627
Dispase	Stemcell Technologies	07923
DMEM	Gibco	11995-065
DMEM/F12 + Glutamax	Gibco	10565-018
Doxycycline	Sigma	D9891
FGF2	Peprotech	100-18B
GDNF	Peprotech	450-10
Glutamax	Gibco	35050061
Hygromycin	Sigma	H3274
IGF-1	Peprotech	100-11
Insulin	Life Technologies	12585014
KnockOut Serum Replacement	Gibco	10828028
LDN-189193	Tocris	6053
N2 Supplement	Gibco	17502048
Neurobasal Medium	Gibco	21103049
Non-essential amino acids	Sigma	M7145
Penicillin-Streptomycin	Gibco	15140122

Purmorphamine	EMD Millipore	540220
Puromycin	Sigma	P8833
rhSHH (C24II)	R&D Systems	1845-SH
SB-431542	Cayman Chemical	13031
XAV939	Cayman Chemical	13596
Y-27632 (ROCK-i)	Cayman Chemical	10005583

Plasmids for Directed Differentiation of iNgn2 and iGABA Neurons

Plasmid Description	Addgene Identifier
Tet-O-FUW-Ngn2-puro	52047
Tet-O-FUW-Myt1l	27152
Tet-O-FUW-Ascl1-puro	97329
Tet-O-FUW-DLX2-hygro	97330
FUW-M2rtTA	20342
Tet-O-FUW-EGFP	30130

Neural Differentiation: Base Media Recipes

Neural Maintenance Media (NMM, 500 mL)

- 242 mL Neurobasal
- 242 mL DMEM/F12 + Glutamax
- 2.5 mL Non-Essential Amino Acids
- 3.75 mL 100x Glutamax
- 5.0 mL Penicillin-Streptomycin
- 2.5 mL 100x N2 Supplement
- 5.0 mL 50x B27 Supplement
- 312.5 µL Insulin (2.5 µg/mL)
- 1.75 µL BME (50 µM)

Knockout Serum Replacement Media (KSR, 300 mL)

- 252 mL DMEM
- 45 mL KSR
- 3 mL Penicillin-Streptomycin
- 1.05 µL BME (50 µM)

Mixed Cortical Neural Differentiation Media (mcNDM, 500 mL)

- 475 mL Neurobasal
- 10 mL 50x B27 Supplement
- 5 mL 100x N2 Supplement
- 5 mL Non-Essential Amino Acids
- 5 mL Pen-Strep
- Supplemented day of feeding with:
    - 10 ng/mL BDNF
    - 10 ng/mL GDNF
    - 10 ng/mL IGF-1
    - 1 µM Dibutyryl cAMP

GABAergic Neural Differentiation Media (gNDM, 500 mL)

- 475 mL Neurobasal
- 10 mL 50x B27 Supplement
- 5 mL 100x Glutamax
- 5 mL Non-Essential Amino Acids
- 5 mL Pen-Strep
- Supplemented day of feeding with:
    - 10 ng/mL BDNF
    - 10 ng/mL GDNF
    - 200 μM Ascorbic Acid
    - 200 μM Dibutyryl cAMP

REFERENCES

Aasen, T., Raya, A., Barrero, M.J., Garreta, E., Consiglio, A., Gonzalez, F., Vassena, R., Bilic, J., Pekarik, V., Tiscornia, G.*, et al.* (2008). Efficient and rapid generation of induced pluripotent stem cells from human keratinocytes. Nat Biotechnol *26*, 1276-1284.

Agostini, M., Romeo, F., Inoue, S., Niklison-Chirou, M.V., Elia, A.J., Dinsdale, D., Morone, N., Knight, R.A., Mak, T.W., and Melino, G. (2016). Metabolic reprogramming during neuronal differentiation. Cell Death Differ *23*, 1502-1514.

Aishworiya, R., Low, P.S., and Tay, S.K. (2011). Alternating hemiplegia of childhood: successful treatment with topiramate and flunarizine, a case report. Ann Trop Paediatr *31*, 149-152.

Akingbade, D., Kingsley, P.J., Shuck, S.C., Cooper, T., Carnahan, R., Szekely, J., and Marnett, L.J. (2012). Selection of monoclonal antibodies against 6-oxo-M(1)dG and their use in an LC-MS/MS assay for the presence of 6-oxo-M(1)dG in vivo. Chem Res Toxicol *25*, 454-461.

Al-Khalili, L., Kotova, O., Tsuchida, H., Ehren, I., Feraille, E., Krook, A., and Chibalin, A.V. (2004). ERK1/2 mediates insulin stimulation of Na(+),K(+)-ATPase by phosphorylation of the alpha-subunit in human skeletal muscle cells. J Biol Chem *279*, 25211-25218.

Albers, R.W. (1967). Biochemical aspects of active transport. Annu Rev Biochem *36*, 727-756.

Amin, H., Maccione, A., Marinaro, F., Zordan, S., Nieus, T., and Berdondini, L. (2016). Electrical Responses and Spontaneous Activity of Human iPS-Derived Neuronal Networks Characterized for 3-month Culture with 4096-Electrode Arrays. Front Neurosci *10*, 121.

Amiri, A., Coppola, G., Scuderi, S., Wu, F., Roychowdhury, T., Liu, F., Pochareddy, S., Shin, Y., Safi, A., Song, L.*, et al.* (2018). Transcriptome and epigenome landscape of human cortical development modeled in organoids. Science *362*.

Aperia, A., Akkuratov, E.E., Fontana, J.M., and Brismar, H. (2016). Na+-K+-ATPase, a new class of plasma membrane receptors. Am J Physiol Cell Physiol *310*, C491-495.

Armstrong, L.C., Westlake, G., Snow, J.P., Cawthon, B., Armour, E., Bowman, A.B., and Ess, K.C. (2017). Heterozygous loss of TSC2 alters p53 signaling and human stem cell reprogramming. HumMol Genet *26*, 4629-4641.

Arystarkhova, E., Haq, I.U., Luebbert, T., Mochel, F., Saunders-Pullman, R., Bressman, S.B., Feschenko, P., Salazar, C., Cook, J.F., Demarest, S.*, et al.* (2019). Factors in the disease severity of ATP1A3 mutations: Impairment, misfolding, and allele competition. Neurobiol Dis *132*, 104577.

Arystarkhova, E., and Sweadner, K.J. (1996). Isoform-specific monoclonal antibodies to Na,K-ATPase alpha subunits. Evidence for a tissue-specific post-translational modification of the alpha subunit. J Biol Chem *271*, 23407-23417.

Attwell, D., and Laughlin, S.B. (2001). An energy budget for signaling in the grey matter of the brain. J Cereb Blood Flow Metab *21*, 1133-1145.

Avior, Y., Sagi, I., and Benvenisty, N. (2016). Pluripotent stem cells in disease modelling and drug discovery. Nat Rev Mol Cell Biol *17*, 170-182.

Azarias, G., Kruusmagi, M., Connor, S., Akkuratov, E.E., Liu, X.L., Lyons, D., Brismar, H., Broberger, C., and Aperia, A. (2013). A specific and essential role for Na,K-ATPase alpha3 in neurons co-expressing alpha1 and alpha3. J Biol Chem *288*, 2734-2743.

Barreto-Chang, O.L., and Dolmetsch, R.E. (2009). Calcium imaging of cortical neurons using Fura-2 AM. J Vis Exp.

Basavarajappa, B.S., Shivakumar, M., Joshi, V., and Subbanna, S. (2017). Endocannabinoid system in neurodegenerative disorders. J Neurochem *142*, 624-648.

Bassett, A.R. (2017). Editing the genome of hiPSC with CRISPR/Cas9: disease models. Mamm Genome *28*, 348-364.

Beacham, D.W., Blackmer, T., M, O.G., and Hanson, G.T. (2010). Cell-based potassium ion channel screening using the FluxOR assay. J Biomol Screen *15*, 441-446.

Beguin, P., Beggah, A.T., Chibalin, A.V., Burgener-Kairuz, P., Jaisser, F., Mathews, P.M., Rossier, B.C., Cotecchia, S., and Geering, K. (1994). Phosphorylation of the Na,K-ATPase alpha-subunit by protein kinase A and C in vitro and in intact cells. Identification of a novel motif for PKC-mediated phosphorylation. J Biol Chem *269*, 24437-24445.

Ben Jehuda, R., Shemer, Y., and Binah, O. (2018). Genome Editing in Induced Pluripotent Stem Cells using CRISPR/Cas9. Stem Cell Rev Rep *14*, 323-336.

Ben-David, U., Kopper, O., and Benvenisty, N. (2012). Expanding the boundaries of embryonic stem cells. Cell Stem Cell *10*, 666-677.

Benallal, M., and Anner, B.M. (1994). Identification of organ-specific glycosylation of a membrane protein in two tissues using lectins. Experientia *50*, 664-668.

Benam, K.H., Dauth, S., Hassell, B., Herland, A., Jain, A., Jang, K.J., Karalis, K., Kim, H.J., MacQueen, L., Mahmoodian, R.*, et al.* (2015). Engineered in vitro disease models. Annu Rev Pathol *10*, 195-262.

Benarroch, E.E. (2011). Na+, K+-ATPase: functions in the nervous system and involvement in neurologic disease. Neurology *76*, 287-293.

Bersier, M.G., Pena, C., and Arnaiz, G.R. (2011). Changes in Na+, K+-ATPase activity and alpha 3 subunit expression in CNS after administration of Na+, K+-ATPase inhibitors. Neurochem Res *36*, 297-303.

Bhaduri, A., Andrews, M.G., Mancia Leon, W., Jung, D., Shin, D., Allen, D., Jung, D., Schmunk, G., Haeussler, M., Salma, J.*, et al.* (2020). Cell stress in cortical organoids impairs molecular subtype specification. Nature *578*, 142-148.

Bisogno, T., Hanus, L., De Petrocellis, L., Tchilibon, S., Ponde, D.E., Brandi, I., Moriello, A.S., Davis, J.B., Mechoulam, R., and Di Marzo, V. (2001). Molecular targets for cannabidiol and its synthetic analogues: effect on vanilloid VR1 receptors and on the cellular uptake and enzymatic hydrolysis of anandamide. Br J Pharmacol *134*, 845-852.

Bitar, M., and Barry, G. (2020). Building a Human Brain for Research. Front Mol Neurosci *13*, 22.

Blanco, G., and Mercer, R.W. (1998). Isozymes of the Na-K-ATPase: heterogeneity in structure, diversity in function. Am J Physiol *275*, F633-650.

Blom, H., Ronnlund, D., Scott, L., Spicarova, Z., Widengren, J., Bondar, A., Aperia, A., and Brismar, H. (2011). Spatial distribution of Na+-K+-ATPase in dendritic spines dissected by nanoscale superresolution STED microscopy. BMC Neurosci *12*, 16.

Bordeaux, J., Welsh, A., Agarwal, S., Killiam, E., Baquero, M., Hanna, J., Anagnostou, V., and Rimm, D. (2010). Antibody validation. Biotechniques *48*, 197-209.

Bottger, P., Doganli, C., and Lykke-Hartmann, K. (2012). Migraine- and dystonia-related disease-mutations of Na+/K+-ATPases: relevance of behavioral studies in mice to disease symptoms and neurological manifestations in humans. Neurosci Biobehav Rev *36*, 855-871.

Bottger, P., Tracz, Z., Heuck, A., Nissen, P., Romero-Ramos, M., and Lykke-Hartmann, K. (2011). Distribution of Na/K-ATPase alpha 3 isoform, a sodium-potassium P-type pump associated with rapid-onset of dystonia parkinsonism (RDP) in the adult mouse brain. J Comp Neurol *519*, 376-404.

Bourgeois, M., Aicardi, J., and Goutieres, F. (1993). Alternating hemiplegia of childhood. J Pediatr *122*, 673-679.

Brashear, A., Sweadner, K.J., Cook, J.F., Swoboda, K.J., and Ozelius, L. (2018). ATP1A3-Related Neurologic Disorders. In GeneReviews((R)), M.P. Adam, H.H. Ardinger, R.A. Pagon, S.E. Wallace, L.J.H. Bean, K. Stephens, and A. Amemiya, eds. (Seattle (WA)).

Busquets-Garcia, A., Gomis-Gonzalez, M., Guegan, T., Agustin-Pavon, C., Pastor, A., Mato, S., Perez-Samartin, A., Matute, C., de la Torre, R., Dierssen, M*., et al.* (2013). Targeting the endocannabinoid system in the treatment of fragile X syndrome. Nat Med *19*, 603-607.

Caiazzo, M., Giannelli, S., Valente, P., Lignani, G., Carissimo, A., Sessa, A., Colasante, G., Bartolomeo, R., Massimino, L., Ferroni, S*., et al.* (2015). Direct conversion of fibroblasts into functional astrocytes by defined transcription factors. Stem Cell Reports *4*, 25-36.

Campos, A.C., Fogaca, M.V., Sonego, A.B., and Guimaraes, F.S. (2016). Cannabidiol, neuroprotection and neuropsychiatric disorders. Pharmacol Res *112*, 119-127.

Capuano, A., Garone, G., Tiralongo, G., and Graziola, F. (2020). Alternating Hemiplegia of Childhood: Understanding the Genotype-Phenotype Relationship of ATP1A3 Variations. Appl Clin Genet *13*, 71-81.

Casaer, P. (1987). Flunarizine in alternating hemiplegia in childhood. An international study in 12 children. Neuropediatrics *18*, 191-195.

Cassano, T., Villani, R., Pace, L., Carbone, A., Bukke, V.N., Orkisz, S., Avolio, C., and Serviddio, G. (2020). From Cannabis sativa to Cannabidiol: Promising Therapeutic Candidate for the Treatment of Neurodegenerative Diseases. Front Pharmacol *11*, 124.

Centeno, E.G.Z., Cimarosti, H., and Bithell, A. (2018). 2D versus 3D human induced pluripotent stem cell-derived cultures for neurodegenerative disease modelling. Mol Neurodegener *13*, 27.

Chailangkarn, T., Acab, A., and Muotri, A.R. (2012). Modeling neurodevelopmental disorders using human neurons. Curr Opin Neurobiol *22*, 785-790.

Chakrabarti, B., Persico, A., Battista, N., and Maccarrone, M. (2015). Endocannabinoid Signaling in Autism. Neurotherapeutics *12*, 837-847.

Chambers, S.M., Fasano, C.A., Papapetrou, E.P., Tomishima, M., Sadelain, M., and Studer, L. (2009). Highly efficient neural conversion of human ES and iPS cells by dual inhibition of SMAD signaling. Nat Biotechnol *27*, 275-280.

Chang, Y.P., Liu, X., Kim, J.D., Ikeda, M.A., Layton, M.R., Weder, A.B., Cooper, R.S., Kardia, S.L., Rao, D.C., Hunt, S.C.*, et al.* (2007). Multiple genes for essential-hypertension susceptibility on chromosome 1q. Am J Hum Genet *80*, 253-264.

Chaumette, B., Ferrafiat, V., Ambalavanan, A., Goldenberg, A., onne-Laporte, A., Spiegelman, D., Dion, P.A., Gerardin, P., Laurent, C., Cohen, D.*, et al.* (2018). Missense variants in ATP1A3 and FXYD gene family are associated with childhood-onset schizophrenia. Mol Psychiatry.

Chen, T.W., Wardill, T.J., Sun, Y., Pulver, S.R., Renninger, S.L., Baohan, A., Schreiter, E.R., Kerr, R.A., Orger, M.B., Jayaraman, V.*, et al.* (2013). Ultrasensitive fluorescent proteins for imaging neuronal activity. Nature *499*, 295-300.

Chen, Y., Cao, J., Xiong, M., Petersen, A.J., Dong, Y., Tao, Y., Huang, C.T., Du, Z., and Zhang, S.C. (2015). Engineering Human Stem Cell Lines with Inducible Gene Knockout using CRISPR/Cas9. Cell Stem Cell *17*, 233-244.

Cheng, S.X., Aizman, O., Nairn, A.C., Greengard, P., and Aperia, A. (1999). [Ca2+]i determines the effects of protein kinases A and C on activity of rat renal Na+,K+-ATPase. J Physiol *518*, 37-46.

Chu, Y., Parada, I., and Prince, D.A. (2009). Temporal and topographic alterations in expression of the alpha3 isoform of Na+, K(+)-ATPase in the rat freeze lesion model of microgyria and epileptogenesis. Neuroscience *162*, 339-348.

Clapcote, S.J., Duffy, S., Xie, G., Kirshenbaum, G., Bechard, A.R., Rodacker Schack, V., Petersen, J., Sinai, L., Saab, B.J., Lerch, J.P.*, et al.* (2009). Mutation I810N in the alpha3 isoform of Na+,K+-ATPase causes impairments in the sodium pump and hyperexcitability in the CNS. Proc Natl Acad Sci U S A *106*, 14085-14090.

Clausen, M.V., Hilbers, F., and Poulsen, H. (2017). The Structure and Function of the Na,K-ATPase Isoforms in Health and Disease. Front Physiol *8*, 371.

Clausen, M.V., Nissen, P., and Poulsen, H. (2016). The alpha4 isoform of the Na(+),K(+)-ATPase is tuned for changing extracellular environments. FEBS J *283*, 282-293.

Clausen, T., and Persson, A.E. (1998). Jens Christian Skou awarded the Nobel prize in chemistry for the identification of the Na+, K(+)-pump. Acta Physiol Scand *163*, 1-2.

Clifford, R.J., and Kaplan, J.H. (2009). Regulation of Na,K-ATPase subunit abundance by translational repression. J Biol Chem *284*, 22905-22915.

Colman, A., and Dreesen, O. (2009). Pluripotent stem cells and disease modeling. Cell Stem Cell *5*, 244-247.

Cong, L., Ran, F.A., Cox, D., Lin, S., Barretto, R., Habib, N., Hsu, P.D., Wu, X., Jiang, W., Marraffini, L.A.*, et al.* (2013). Multiplex genome engineering using CRISPR/Cas systems. Science *339*, 819-823.

Cornacchia, D., and Studer, L. (2017). Back and forth in time: Directing age in iPSC-derived lineages. Brain Res *1656*, 14-26.

Cotterill, E., Hall, D., Wallace, K., Mundy, W.R., Eglen, S.J., and Shafer, T.J. (2016). Characterization of Early Cortical Neural Network Development in Multiwell Microelectrode Array Plates. J Biomol Screen *21*, 510-519.

Crambert, G., Hasler, U., Beggah, A.T., Yu, C., Modyanov, N.N., Horisberger, J.D., Lelievre, L., and Geering, K. (2000). Transport and pharmacological properties of nine different human Na, K-ATPase isozymes. J Biol Chem *275*, 1976-1986.

Dard, R., Mignot, C., Durr, A., Lesca, G., Sanlaville, D., Roze, E., and Mochel, F. (2015). Relapsing encephalopathy with cerebellar ataxia related to an ATP1A3 mutation. Dev Med Child Neurol *57*, 1183-1186.

de Carvalho Aguiar, P., Sweadner, K.J., Penniston, J.T., Zaremba, J., Liu, L., Caton, M., Linazasoro, G., Borg, M., Tijssen, M.A., Bressman, S.B.*, et al.* (2004). Mutations in the Na+/K+ -ATPase alpha3 gene ATP1A3 are associated with rapid-onset dystonia parkinsonism. Neuron *43*, 169-175.

de Vries, B., Stam, A.H., Beker, F., van den Maagdenberg, A.M., Vanmolkot, K.R., Laan, L., Ginjaar, I.B., Frants, R.R., Lauffer, H., Haan, J.*, et al.* (2008). CACNA1A mutation linking hemiplegic migraine and alternating hemiplegia of childhood. Cephalalgia *28*, 887-891.

DeAndrade, M.P., Yokoi, F., van Groen, T., Lingrel, J.B., and Li, Y. (2011). Characterization of Atp1a3 mutant mice as a model of rapid-onset dystonia with parkinsonism. Behav Brain Res *216*, 659-665.

Delorme, C., Hainque, E., and Roze, E. (2017). Alternating Upper Limb Monoplegia due to ATP1A3 Mutation. Pediatr Neurol *68*, 79-80.

Demos, M.K., van Karnebeek, C.D., Ross, C.J., Adam, S., Shen, Y., Zhan, S.H., Shyr, C., Horvath, G., Suri, M., Fryer, A.*, et al.* (2014). A novel recurrent mutation in ATP1A3 causes CAPOS syndrome. Orphanet J Rare Dis *9*, 15.

Desfrere, L., Karlsson, M., Hiyoshi, H., Malmersjo, S., Nanou, E., Estrada, M., Miyakawa, A., Lagercrantz, H., El Manira, A., Lal, M.*, et al.* (2009). Na,K-ATPase signal transduction triggers CREB activation and dendritic growth. Proc Natl Acad Sci U S A *106*, 2212-2217.

Devarajan, P., Gilmore-Hebert, M., and Benz, E.J., Jr. (1992). Differential translation of the Na,K-ATPase subunit mRNAs. J Biol Chem *267*, 22435-22439.

Devinsky, O., Cross, J.H., and Wright, S. (2017). Trial of Cannabidiol for Drug-Resistant Seizures in the Dravet Syndrome. N Engl J Med *377*, 699-700.

Diecke, S., Jung, S.M., Lee, J., and Ju, J.H. (2014). Recent technological updates and clinical applications of induced pluripotent stem cells. Korean J Intern Med *29*, 547-557.

Dobretsov, M., and Stimers, J.R. (2005). Neuronal function and alpha3 isoform of the Na/K-ATPase. Front Biosci *10*, 2373-2396.

Doi, M., and Iwasaki, K. (2008). Na+/K+ ATPase regulates the expression and localization of acetylcholine receptors in a pump activity-independent manner. Mol Cell Neurosci *38*, 548-558.

Doss, M.X., and Sachinidis, A. (2019). Current Challenges of iPSC-Based Disease Modeling and Therapeutic Implications. Cells *8*.

Douvaras, P., Wang, J., Zimmer, M., Hanchuk, S., O'Bara, M.A., Sadiq, S., Sim, F.J., Goldman, J., and Fossati, V. (2014). Efficient generation of myelinating oligodendrocytes from primary progressive multiple sclerosis patients by induced pluripotent stem cells. Stem Cell Reports *3*, 250-259.

Engle, S.J., Blaha, L., and Kleiman, R.J. (2018). Best Practices for Translational Disease Modeling Using Human iPSC-Derived Neurons. Neuron *100*, 783-797.

Faruque, M.U., Chen, G., Doumatey, A., Huang, H., Zhou, J., Dunston, G.M., Rotimi, C.N., and Adeyemo, A.A. (2011). Association of ATP1B1, RGS5 and SELE polymorphisms with hypertension and blood pressure in African-Americans. J Hypertens *29*, 1906-1912.

Feraille, E., Carranza, M.L., Gonin, S., Beguin, P., Pedemonte, C., Rousselot, M., Caverzasio, J., Geering, K., Martin, P.Y., and Favre, H. (1999). Insulin-induced stimulation of Na+,K(+)-ATPase activity in kidney proximal tubule cells depends on phosphorylation of the alpha-subunit at Tyr-10. Mol Biol Cell *10*, 2847-2859.

Ferrari, M.D., Klever, R.R., Terwindt, G.M., Ayata, C., and van den Maagdenberg, A.M. (2015). Migraine pathophysiology: lessons from mouse models and human genetics. Lancet Neurol *14*, 65-80.

Fink, J.J., and Levine, E.S. (2018). Uncovering True Cellular Phenotypes: Using Induced Pluripotent Stem Cell-Derived Neurons to Study Early Insults in Neurodevelopmental Disorders. Front Neurol *9*, 237.

Finlay, B.L., and Darlington, R.B. (1995). Linked regularities in the development and evolution of mammalian brains. Science *268*, 1578-1584.

Fisone, G., Cheng, S.X., Nairn, A.C., Czernik, A.J., Hemmings, H.C., Jr., Hoog, J.O., Bertorello, A.M., Kaiser, R., Bergman, T., Jornvall, H.*, et al.* (1994). Identification of the phosphorylation site for cAMP-dependent protein kinase on Na+,K(+)-ATPase and effects of site-directed mutagenesis. J Biol Chem *269*, 9368-9373.

Florio, M., and Huttner, W.B. (2014). Neural progenitors, neurogenesis and the evolution of the neocortex. Development *141*, 2182-2194.

Fons, C., Campistol, J., Panagiotakaki, E., Giannotta, M., Arzimanoglou, A., Gobbi, G., Neville, B., Ebinger, F., Nevsimalova, S., Laan, L.*, et al.* (2012). Alternating hemiplegia of childhood: metabolic studies in the largest European series of patients. Eur J Paediatr Neurol *16*, 10-14.

Fritz N, A.E., Liebmann T, Lindskog M, Brismar H, and Aperia A (2015). Functional consequences of the disease-causing T613M mutation of NKAalpha3 for hippocampal neurons. FASEB Abstract 84529.

Fusaki, N., Ban, H., Nishiyama, A., Saeki, K., and Hasegawa, M. (2009). Efficient induction of transgene-free human pluripotent stem cells using a vector based on Sendai virus, an RNA virus that does not integrate into the host genome. Proc Jpn Acad Ser B Phys Biol Sci *85*, 348-362.

Gasiunas, G., Barrangou, R., Horvath, P., and Siksnys, V. (2012). Cas9-crRNA ribonucleoprotein complex mediates specific DNA cleavage for adaptive immunity in bacteria. Proc Natl Acad Sci U S A *109*, E2579-2586.

Gaston, T.E., and Friedman, D. (2017). Pharmacology of cannabinoids in the treatment of epilepsy. Epilepsy Behav *70*, 313-318.

Gaston, T.E., and Szaflarski, J.P. (2018). Cannabis for the Treatment of Epilepsy: an Update. Curr Neurol Neurosci Rep *18*, 73.

Geering, K. (2001). The functional role of beta subunits in oligomeric P-type ATPases. J Bioenerg Biomembr *33*, 425-438.

Geering, K. (2006). FXYD proteins: new regulators of Na-K-ATPase. Am J Physiol Renal Physiol *290*, F241-250.

Germain, P.L., and Testa, G. (2017). Taming Human Genetic Variability: Transcriptomic Meta-Analysis Guides the Experimental Design and Interpretation of iPSC-Based Disease Modeling. Stem Cell Reports *8*, 1784-1796.

Ghovanloo, M.R., Shuart, N.G., Mezeyova, J., Dean, R.A., Ruben, P.C., and Goodchild, S.J. (2018). Inhibitory effects of cannabidiol on voltage-dependent sodium currents. J Biol Chem *293*, 16546-16558.

Ghusayni, R., Richardson, J.P., Uchitel, J., Abdelnour, E., McLean, M., Prange, L., Abrahamsen, T., Song, A., Petrella, J.R., and Mikati, M.A. (2020). Magnetic resonance imaging volumetric analysis in patients with Alternating hemiplegia of childhood: A pilot study. Eur J Paediatr Neurol.

Gilmore, E.C., and Herrup, K. (1997). Cortical development: layers of complexity. Curr Biol *7*, R231-234.

Golden, G.S., and French, J.H. (1975). Basilar artery migraine in young children. Pediatrics *56*, 722-726.

Gorzkiewicz, A., and Szemraj, J. (2018). Brain endocannabinoid signaling exhibits remarkable complexity. Brain Res Bull *142*, 33-46.

Gunhanlar, N., Shpak, G., van der Kroeg, M., Gouty-Colomer, L.A., Munshi, S.T., Lendemeijer, B., Ghazvini, M., Dupont, C., Hoogendijk, W.J.G., Gribnau, J.*, et al.* (2018). A simplified protocol for differentiation of electrophysiologically mature neuronal networks from human induced pluripotent stem cells. Mol Psychiatry *23*, 1336-1344.

Haas, M., Wang, H., Tian, J., and Xie, Z. (2002). Src-mediated inter-receptor cross-talk between the Na+/K+-ATPase and the epidermal growth factor receptor relays the signal from ouabain to mitogen-activated protein kinases. J Biol Chem *277*, 18694-18702.

Handel, A.E., Chintawar, S., Lalic, T., Whiteley, E., Vowles, J., Giustacchini, A., Argoud, K., Sopp, P., Nakanishi, M., Bowden, R.*, et al.* (2016). Assessing similarity to primary tissue and cortical layer identity

in induced pluripotent stem cell-derived cortical neurons through single-cell transcriptomics. Hum Mol Genet *25*, 989-1000.

Heinzen, E.L., Arzimanoglou, A., Brashear, A., Clapcote, S.J., Gurrieri, F., Goldstein, D.B., Jóhannesson, S.H., Mikati, M.A., Neville, B., Nicole, S.*, et al.* (2014). Distinct neurological disorders with ATP1A3 mutations. The Lancet Neurology *13*, 503-514.

Heinzen, E.L., Swoboda, K.J., Hitomi, Y., Gurrieri, F., Nicole, S., de Vries, B., Tiziano, F.D., Fontaine, B., Walley, N.M., Heavin, S.*, et al.* (2012). De novo mutations in ATP1A3 cause alternating hemiplegia of childhood. Nat Genet *44*, 1030-1034.

Helseth, A.R., Hunanyan, A.S., Adil, S., Linabarger, M., Sachdev, M., Abdelnour, E., Arehart, E., Szabo, M., Richardson, J., Wetsel, W.C.*, et al.* (2018). Novel E815K knock-in mouse model of alternating hemiplegia of childhood. Neurobiol Dis *119*, 100-112.

Herculano-Houzel, S. (2012). The remarkable, yet not extraordinary, human brain as a scaled-up primate brain and its associated cost. Proc Natl Acad Sci U S A *109 Suppl 1*, 10661-10668.

Hirakawa, M.P., Krishnakumar, R., Timlin, J.A., Carney, J.P., and Butler, K.S. (2020). Gene editing and CRISPR in the clinic: current and future perspectives. Biosci Rep.

Hockaday, J.M. (1979). Basilar migraine in childhood. Dev Med Child Neurol *21*, 455-463.

Holm, R., Einholm, A.P., Andersen, J.P., and Vilsen, B. (2015). Rescue of Na+ affinity in aspartate 928 mutants of Na+,K+-ATPase by secondary mutation of glutamate 314. J Biol Chem *290*, 9801-9811.

Holm, R., Toustrup-Jensen, M.S., Einholm, A.P., Schack, V.R., Andersen, J.P., and Vilsen, B. (2016). Neurological disease mutations of alpha3 Na(+),K(+)-ATPase: Structural and functional perspectives and rescue of compromised function. Biochim Biophys Acta *1857*, 1807-1828.

Holm, T.H., and Lykke-Hartmann, K. (2016). Insights into the Pathology of the alpha3 Na(+)/K(+)-ATPase Ion Pump in Neurological Disorders; Lessons from Animal Models. Front Physiol *7*, 209.

Hong, Y.J., and Do, J.T. (2019). Neural Lineage Differentiation From Pluripotent Stem Cells to Mimic Human Brain Tissues. Front Bioeng Biotechnol *7*, 400.

Hosking, G.P., Cavanagh, N.P., and Wilson, J. (1978). Alternating hemiplegia: complicated migraine of infancy. Arch Dis Child *53*, 656-659.

Hough, S.R., Thornton, M., Mason, E., Mar, J.C., Wells, C.A., and Pera, M.F. (2014). Single-cell gene expression profiles define self-renewing, pluripotent, and lineage primed states of human pluripotent stem cells. Stem Cell Reports *2*, 881-895.

Howarth, C., Gleeson, P., and Attwell, D. (2012). Updated energy budgets for neural computation in the neocortex and cerebellum. J Cereb Blood Flow Metab *32*, 1222-1232.

Huang, C.Y., Liu, C.L., Ting, C.Y., Chiu, Y.T., Cheng, Y.C., Nicholson, M.W., and Hsieh, P.C.H. (2019). Human iPSC banking: barriers and opportunities. J Biomed Sci *26*, 87.

Hunanyan, A.S., Fainberg, N.A., Linabarger, M., Arehart, E., Leonard, A.S., Adil, S.M., Helseth, A.R., Swearingen, A.K., Forbes, S.L., Rodriguiz, R.M*., et al.* (2015). Knock-in mouse model of alternating hemiplegia of childhood: behavioral and electrophysiologic characterization. Epilepsia *56*, 82-93.

Hunanyan, A.S., Helseth, A.R., Abdelnour, E., Kherallah, B., Sachdev, M., Chung, L., Masoud, M., Richardson, J., Li, Q., Nadler, J.V*., et al.* (2018). Mechanisms of increased hippocampal excitability in the Mashl(+/-) mouse model of Na(+) /K(+) -ATPase dysfunction. Epilepsia *59*, 1455-1468.

Ibeas Bih, C., Chen, T., Nunn, A.V., Bazelot, M., Dallas, M., and Whalley, B.J. (2015). Molecular Targets of Cannabidiol in Neurological Disorders. Neurotherapeutics *12*, 699-730.

Ikeda, K., Satake, S., Onaka, T., Sugimoto, H., Takeda, N., Imoto, K., and Kawakami, K. (2013). Enhanced inhibitory neurotransmission in the cerebellar cortex of Atp1a3-deficient heterozygous mice. J Physiol *591*, 3433-3449.

Illarionova, N.B., Gunnarson, E., Li, Y., Brismar, H., Bondar, A., Zelenin, S., and Aperia, A. (2010). Functional and molecular interactions between aquaporins and Na,K-ATPase. Neuroscience *168*, 915-925.

Irving, A., Abdulrazzaq, G., Chan, S.L.F., Penman, J., Harvey, J., and Alexander, S.P.H. (2017). Cannabinoid Receptor-Related Orphan G Protein-Coupled Receptors. Adv Pharmacol *80*, 223-247.

Isaksen, T.J., Kros, L., Vedovato, N., Holm, T.H., Vitenzon, A., Gadsby, D.C., Khodakhah, K., and Lykke-Hartmann, K. (2017). Hypothermia-induced dystonia and abnormal cerebellar activity in a mouse model with a single disease-mutation in the sodium-potassium pump. PLoS Genet *13*, e1006763.

Ishii, A., Saito, Y., Mitsui, J., Ishiura, H., Yoshimura, J., Arai, H., Yamashita, S., Kimura, S., Oguni, H., Morishita, S*., et al.* (2013). Identification of ATP1A3 mutations by exome sequencing as the cause of alternating hemiplegia of childhood in Japanese patients. PLoSONE *8*, e56120.

Ivanov, A.V., Modyanov, N.N., and Askari, A. (2002). Role of the self-association of beta subunits in the oligomeric structure of Na+/K+-ATPase. Biochem J *364*, 293-299.

Jaber, S.M., Yadava, N., and Polster, B.M. (2020). Mapping mitochondrial respiratory chain deficiencies by respirometry: Beyond the Mito Stress Test. Exp Neurol *328*, 113282.

Jen, J.C., Wan, J., Palos, T.P., Howard, B.D., and Baloh, R.W. (2005). Mutation in the glutamate transporter EAAT1 causes episodic ataxia, hemiplegia, and seizures. Neurology *65*, 529-534.

Jiang, W., Chi, Z., Ma, L., Du, B., Shang, W., Guo, H., and Wu, W. (2006). Topiramate: a new agent for patients with alternating hemiplegia of childhood. Neuropediatrics *37*, 229-233.

Jimenez, T., McDermott, J.P., Sanchez, G., and Blanco, G. (2011a). Na,K-ATPase alpha4 isoform is essential for sperm fertility. Proc Natl Acad Sci U S A *108*, 644-649.

Jimenez, T., Sanchez, G., McDermott, J.P., Nguyen, A.N., Kumar, T.R., and Blanco, G. (2011b). Increased expression of the Na,K-ATPase alpha4 isoform enhances sperm motility in transgenic mice. Biol Reprod *84*, 153-161.

Jinek, M., Chylinski, K., Fonfara, I., Hauer, M., Doudna, J.A., and Charpentier, E. (2012). A programmable dual-RNA-guided DNA endonuclease in adaptive bacterial immunity. Science *337*, 816-821.

Johar, K., Priya, A., and Wong-Riley, M.T. (2014). Regulation of Na(+)/K(+)-ATPase by neuron-specific transcription factor Sp4: implication in the tight coupling of energy production, neuronal activity and energy consumption in neurons. Eur J Neurosci *39*, 566-578.

Ju, J., Hirose, S., Shi, X.Y., Ishii, A., Hu, L.Y., and Zou, L.P. (2016). Treatment with Oral ATP decreases alternating hemiplegia of childhood with de novo ATP1A3 Mutation. Orphanet J Rare Dis *11*, 55.

Jucker, M. (2010). The benefits and limitations of animal models for translational research in neurodegenerative diseases. Nat Med *16*, 1210-1214.

Junghans, C., Vukojevic, V., Tavraz, N.N., Maksimov, E.G., Zuschratter, W., Schmitt, F.J., and Friedrich, T. (2017). Disruption of Ankyrin B and Caveolin-1 Interaction Sites Alters Na(+),K(+)-ATPase Membrane Diffusion. Biophys J *113*, 2249-2260.

Kaneko, M., Desai, B.S., and Cook, B. (2014). Ionic leakage underlies a gain-of-function effect of dominant disease mutations affecting diverse P-type ATPases. Nat Genet *46*, 144-151.

Kansagra, S., Mikati, M.A., and Vigevano, F. (2013). Alternating hemiplegia of childhood. Handb Clin Neurol *112*, 821-826.

Kaplan, J.H. (2002). Biochemistry of Na,K-ATPase. Annu Rev Biochem *71*, 511-535.

Kaplan, J.S., Stella, N., Catterall, W.A., and Westenbroek, R.E. (2017). Cannabidiol attenuates seizures and social deficits in a mouse model of Dravet syndrome. Proc Natl Acad Sci U S A *114*, 11229-11234.

Karl, T., Garner, B., and Cheng, D. (2017). The therapeutic potential of the phytocannabinoid cannabidiol for Alzheimer's disease. Behav Pharmacol *28*, 142-160.

Kasinathan, A., Sharawat, I.K., Sahu, J.K., and Sankhyan, N. (2017). Topiramate Therapy in Alternating Hemiplegia of Childhood. Indian J Pediatr *84*, 957-958.

Kemp, G.J., Taylor, D.J., Barnes, P.R., Wilson, J., and Radda, G.K. (1995). Skeletal muscle mitochondrial dysfunction in alternating hemiplegia of childhood. Ann Neurol *38*, 681-684.

Kerr, D.M., Downey, L., Conboy, M., Finn, D.P., and Roche, M. (2013). Alterations in the endocannabinoid system in the rat valproic acid model of autism. Behav Brain Res *249*, 124-132.

Kim, D., Kim, C.H., Moon, J.I., Chung, Y.G., Chang, M.Y., Han, B.S., Ko, S., Yang, E., Cha, K.Y., Lanza, R.*, et al.* (2009). Generation of human induced pluripotent stem cells by direct delivery of reprogramming proteins. Cell Stem Cell *4*, 472-476.

Kim, D.S., Lee, J.S., Leem, J.W., Huh, Y.J., Kim, J.Y., Kim, H.S., Park, I.H., Daley, G.Q., Hwang, D.Y., and Kim, D.W. (2010). Robust enhancement of neural differentiation from human ES and iPS cells regardless of their innate difference in differentiation propensity. Stem Cell Rev Rep *6*, 270-281.

Kim, J.H., Sizov, I., Dobretsov, M., and von Gersdorff, H. (2007). Presynaptic Ca2+ buffers control the strength of a fast post-tetanic hyperpolarization mediated by the alpha3 Na(+)/K(+)-ATPase. Nat Neurosci *10*, 196-205.

Kim, K., Zhao, R., Doi, A., Ng, K., Unternaehrer, J., Cahan, P., Huo, H., Loh, Y.H., Aryee, M.J., Lensch, M.W.*, et al.* (2011). Donor cell type can influence the epigenome and differentiation potential of human induced pluripotent stem cells. Nat Biotechnol *29*, 1117-1119.

Kim, T.G., Yao, R., Monnell, T., Cho, J.H., Vasudevan, A., Koh, A., Peeyush, K.T., Moon, M., Datta, D., Bolshakov, V.Y.*, et al.* (2014). Efficient specification of interneurons from human pluripotent stem cells by dorsoventral and rostrocaudal modulation. Stem Cells *32*, 1789-1804.

Kirshenbaum, G.S., Dawson, N., Mullins, J.G., Johnston, T.H., Drinkhill, M.J., Edwards, I.J., Fox, S.H., Pratt, J.A., Brotchie, J.M., Roder, J.C.*, et al.* (2013). Alternating hemiplegia of childhood-related neural and behavioural phenotypes in Na+,K+-ATPase alpha3 missense mutant mice. PLoS One *8*, e60141.

Koenderink, J.B., Geibel, S., Grabsch, E., De Pont, J.J., Bamberg, E., and Friedrich, T. (2003). Electrophysiological analysis of the mutated Na,K-ATPase cation binding pocket. J Biol Chem *278*, 51213-51222.

Kopec, W., Loubet, B., Poulsen, H., and Khandelia, H. (2014). Molecular mechanism of Na(+),K(+)-ATPase malfunction in mutations characteristic of adrenal hypertension. Biochemistry *53*, 746-754.

Krageloh, I., and Aicardi, J. (1980). Alternating hemiplegia in infants: report of five cases. DevMedChild Neurol *22*, 784-791.

Kriks, S., Shim, J.W., Piao, J., Ganat, Y.M., Wakeman, D.R., Xie, Z., Carrillo-Reid, L., Auyeung, G., Antonacci, C., Buch, A.*, et al.* (2011). Dopamine neurons derived from human ES cells efficiently engraft in animal models of Parkinson's disease. Nature *480*, 547-551.

Kuijlaars, J., Oyelami, T., Diels, A., Rohrbacher, J., Versweyveld, S., Meneghello, G., Tuefferd, M., Verstraelen, P., Detrez, J.R., Verschuuren, M.*, et al.* (2016). Sustained synchronized neuronal network activity in a human astrocyte co-culture system. Sci Rep *6*, 36529.

Kumar, K.K., Lowe, E.W., Jr., Aboud, A.A., Neely, M.D., Redha, R., Bauer, J.A., Odak, M., Weaver, C.D., Meiler, J., Aschner, M.*, et al.* (2014). Cellular manganese content is developmentally regulated in human dopaminergic neurons. Sci Rep *4*, 6801.

Lancaster, M.A., and Knoblich, J.A. (2014). Organogenesis in a dish: modeling development and disease using organoid technologies. Science *345*, 1247125.

Laprairie, R.B., Bagher, A.M., Kelly, M.E., and Denovan-Wright, E.M. (2015). Cannabidiol is a negative allosteric modulator of the cannabinoid CB1 receptor. Br J Pharmacol *172*, 4790-4805.

Lassuthova, P., Rebelo, A.P., Ravenscroft, G., Lamont, P.J., Davis, M.R., Manganelli, F., Feely, S.M., Bacon, C., Brozkova, D.S., Haberlova, J.*, et al.* (2018). Mutations in ATP1A1 Cause Dominant Charcot-Marie-Tooth Type 2. Am J Hum Genet *102*, 505-514.

Laughery, M., Todd, M., and Kaplan, J.H. (2004). Oligomerization of the Na,K-ATPase in cell membranes. J Biol Chem *279*, 36339-36348.

Laursen, M., Gregersen, J.L., Yatime, L., Nissen, P., and Fedosova, N.U. (2015). Structures and characterization of digoxin- and bufalin-bound Na+,K+-ATPase compared with the ouabain-bound complex. Proc Natl Acad Sci U S A *112*, 1755-1760.

Lee, S.J., Litan, A., Li, Z., Graves, B., Lindsey, S., Barwe, S.P., and Langhans, S.A. (2015). Na,K-ATPase beta1-subunit is a target of sonic hedgehog signaling and enhances medulloblastoma tumorigenicity. Mol Cancer *14*, 159.

Lensch, M.W., and Mummery, C.L. (2013). From stealing fire to cellular reprogramming: a scientific history leading to the 2012 Nobel Prize. Stem Cell Reports *1*, 5-17.

Leo, A., Russo, E., and Elia, M. (2016). Cannabidiol and epilepsy: Rationale and therapeutic potential. Pharmacol Res *107*, 85-92.

Levinsohn, E.A., and Hill, K.P. (2020). Clinical uses of cannabis and cannabinoids in the United States. J Neurol Sci *411*, 116717.

Li, L., Chao, J., and Shi, Y. (2018a). Modeling neurological diseases using iPSC-derived neural cells : iPSC modeling of neurological diseases. Cell Tissue Res *371*, 143-151.

Li, M., Jazayeri, D., Corry, B., Melodi, M.K., Heinzen, E.L., Goldstein, D.B., and Petrou, S. (2015). A functional correlate of severity in alternating hemiplegia of childhood. Neurobiol Dis *77*, 88-93.

Li, X., Tao, Y., Bradley, R., Du, Z., Tao, Y., Kong, L., Dong, Y., Jones, J., Yan, Y., Harder, C.R.K.*, et al.* (2018b). Fast Generation of Functional Subtype Astrocytes from Human Pluripotent Stem Cells. Stem Cell Reports *11*, 998-1008.

Li, Z., and Langhans, S.A. (2015). Transcriptional regulators of Na,K-ATPase subunits. Front Cell Dev Biol *3*, 66.

Ligresti, A., Petrosino, S., and Di Marzo, V. (2009). From endocannabinoid profiling to 'endocannabinoid therapeutics'. Curr Opin Chem Biol *13*, 321-331.

Lingrel, J.B. (2010). The physiological significance of the cardiotonic steroid/ouabain-binding site of the Na,K-ATPase. Annu Rev Physiol *72*, 395-412.

Liu, C., Oikonomopoulos, A., Sayed, N., and Wu, J.C. (2018). Modeling human diseases with induced pluripotent stem cells: from 2D to 3D and beyond. Development *145*.

Liu, Y., Liu, H., Sauvey, C., Yao, L., Zarnowska, E.D., and Zhang, S.C. (2013). Directed differentiation of forebrain GABA interneurons from human pluripotent stem cells. Nat Protoc *8*, 1670-1679.

Lo, B., and Parham, L. (2009). Ethical issues in stem cell research. Endocr Rev *30*, 204-213.

Lykken, E.A., Shyng, C., Edwards, R.J., Rozenberg, A., and Gray, S.J. (2018). Recent progress and considerations for AAV gene therapies targeting the central nervous system. J Neurodev Disord *10*, 16.

Maherali, N., Sridharan, R., Xie, W., Utikal, J., Eminli, S., Arnold, K., Stadtfeld, M., Yachechko, R., Tchieu, J., Jaenisch, R.*, et al.* (2007). Directly reprogrammed fibroblasts show global epigenetic remodeling and widespread tissue contribution. Cell Stem Cell *1*, 55-70.

Mahmoudi, S., and Brunet, A. (2012). Aging and reprogramming: a two-way street. Curr Opin Cell Biol *24*, 744-756.

Mandegar, M.A., Huebsch, N., Frolov, E.B., Shin, E., Truong, A., Olvera, M.P., Chan, A.H., Miyaoka, Y., Holmes, K., Spencer, C.I.*, et al.* (2016). CRISPR Interference Efficiently Induces Specific and Reversible Gene Silencing in Human iPSCs. Cell Stem Cell *18*, 541-553.

Markham, N.O., Cooper, T., Goff, M., Gribben, E.M., Carnahan, R.H., and Reynolds, A.B. (2012). Monoclonal antibodies to DIPA: a novel binding partner of p120-catenin isoform 1. Hybridoma (Larchmt) *31*, 246-254.

Maroof, A.M., Keros, S., Tyson, J.A., Ying, S.W., Ganat, Y.M., Merkle, F.T., Liu, B., Goulburn, A., Stanley, E.G., Elefanty, A.G.*, et al.* (2013). Directed differentiation and functional maturation of cortical interneurons from human embryonic stem cells. Cell Stem Cell *12*, 559-572.

Martin-Vasallo, P., Dackowski, W., Emanuel, J.R., and Levenson, R. (1989). Identification of a putative isoform of the Na,K-ATPase beta subunit. Primary structure and tissue-specific expression. J Biol Chem *264*, 4613-4618.

Masoud, M., Prange, L., Wuchich, J., Hunanyan, A., and Mikati, M.A. (2017). Diagnosis and Treatment of Alternating Hemiplegia of Childhood. Curr Treat Options Neurol *19*, 8.

Maussion, G., Rocha, C., Bernard, G., Beitel, L.K., and Durcan, T.M. (2019). Patient-Derived Stem Cells, Another in vitro Model, or the Missing Link Toward Novel Therapies for Autism Spectrum Disorders? Front Pediatr *7*, 225.

McDermott, J.P., Sanchez, G., Chennathukuzhi, V., and Blanco, G. (2012). Green fluorescence protein driven by the Na,K-ATPase alpha4 isoform promoter is expressed only in male germ cells of mouse testis. J Assist Reprod Genet *29*, 1313-1325.

Mechoulam, R., and Parker, L.A. (2013). The endocannabinoid system and the brain. Annu Rev Psychol *64*, 21-47.

Meier, S.D., Kovalchuk, Y., and Rose, C.R. (2006). Properties of the new fluorescent Na+ indicator CoroNa Green: comparison with SBFI and confocal Na+ imaging. J Neurosci Methods *155*, 251-259.

Mencacci, N.E. (2016). The Endless Expansion of the Phenotypic Spectrum of ATP1A3 Mutations: A True Diagnostic Challenge. Mov Disord Clin Pract *3*, 395-397.

Mertens, J., Reid, D., Lau, S., Kim, Y., and Gage, F.H. (2018). Aging in a Dish: iPSC-Derived and Directly Induced Neurons for Studying Brain Aging and Age-Related Neurodegenerative Diseases. Annu Rev Genet *52*, 271-293.

Mikati, M.A., Kramer, U., Zupanc, M.L., and Shanahan, R.J. (2000). Alternating hemiplegia of childhood: clinical manifestations and long-term outcome. Pediatr Neurol *23*, 134-141.

Mishra, N.K., Peleg, Y., Cirri, E., Belogus, T., Lifshitz, Y., Voelker, D.R., Apell, H.J., Garty, H., and Karlish, S.J. (2011). FXYD proteins stabilize Na,K-ATPase: amplification of specific phosphatidylserine-protein interactions. J Biol Chem *286*, 9699-9712.

Molnar, Z., Clowry, G.J., Sestan, N., Alzu'bi, A., Bakken, T., Hevner, R.F., Huppi, P.S., Kostovic, I., Rakic, P., Anton, E.S.*, et al.* (2019). New insights into the development of the human cerebral cortex. J Anat *235*, 432-451.

Mordasini, P., Schroth, G., Guzman, R., Barth, A., Seiler, R.W., and Remonda, L. (2005). Endovascular treatment of posterior circulation cerebral aneurysms by using Guglielmi detachable coils: a 10-year single-center experience with special regard to technical development. AJNR Am J Neuroradiol *26*, 1732-1738.

Moseley, A.E., Williams, M.T., Schaefer, T.L., Bohanan, C.S., Neumann, J.C., Behbehani, M.M., Vorhees, C.V., and Lingrel, J.B. (2007). Deficiency in Na,K-ATPase alpha isoform genes alters spatial learning, motor activity, and anxiety in mice. J Neurosci *27*, 616-626.

Murata, K., Kinoshita, T., Ishikawa, T., Kuroda, K., Hoshi, M., and Fukazawa, Y. (2020). Region- and neuronal-subtype-specific expression of Na,K-ATPase alpha and beta subunit isoforms in the mouse brain. J Comp Neurol.

Muratore, C.R., Srikanth, P., Callahan, D.G., and Young-Pearse, T.L. (2014). Comparison and optimization of hiPSC forebrain cortical differentiation protocols. PLoS One *9*, e105807.

Myers, A.K., Cunningham, J.G., Smith, S.E., Snow, J.P., Smoot, C.A., and Tucker, E.S. (2020). JNK signaling is required for proper tangential migration and laminar allocation of cortical interneurons. Development *147*.

Narsinh, K.H., Sun, N., Sanchez-Freire, V., Lee, A.S., Almeida, P., Hu, S., Jan, T., Wilson, K.D., Leong, D., Rosenberg, J.*, et al.* (2011). Single cell transcriptional profiling reveals heterogeneity of human induced pluripotent stem cells. J Clin Invest *121*, 1217-1221.

Neely, M.D., Litt, M.J., Tidball, A.M., Li, G.G., Aboud, A.A., Hopkins, C.R., Chamberlin, R., Hong, C.C., Ess, K.C., and Bowman, A.B. (2012). DMH1, a highly selective small molecule BMP inhibitor promotes neurogenesis of hiPSCs: comparison of PAX6 and SOX1 expression during neural induction. ACS Chem Neurosci *3*, 482-491.

Nehme, R., Zuccaro, E., Ghosh, S.D., Li, C., Sherwood, J.L., Pietilainen, O., Barrett, L.E., Limone, F., Worringer, K.A., Kommineni, S.*, et al.* (2018). Combining NGN2 Programming with Developmental Patterning Generates Human Excitatory Neurons with NMDAR-Mediated Synaptic Transmission. Cell Rep *23*, 2509-2523.

Neville, B.G., and Ninan, M. (2007). The treatment and management of alternating hemiplegia of childhood. Dev Med Child Neurol *49*, 777-780.

Nevsimalova, S., Dittrich, J., Havlova, M., Tauberova, A., Korsova, B., Hajek, M., Masopust, J., and Michalova, K. (1994). Alternating hemiplegia in childhood: a cross-sectional study. Brain Dev *16*, 189-194.

Nishimoto, K., Tomlins, S.A., Kuick, R., Cani, A.K., Giordano, T.J., Hovelson, D.H., Liu, C.J., Sanjanwala, A.R., Edwards, M.A., Gomez-Sanchez, C.E.*, et al.* (2015). Aldosterone-stimulating somatic gene mutations are common in normal adrenal glands. Proc Natl Acad Sci U S A *112*, E4591-4599.

Noguchi, S., Mutoh, Y., and Kawamura, M. (1994). The functional roles of disulfide bonds in the beta-subunit of (Na,K)ATPase as studied by site-directed mutagenesis. FEBS Lett *341*, 233-238.

Odawara, A., Katoh, H., Matsuda, N., and Suzuki, I. (2016). Physiological maturation and drug responses of human induced pluripotent stem cell-derived cortical neuronal networks in long-term culture. Sci Rep *6*, 26181.

Ohi, Y., Qin, H., Hong, C., Blouin, L., Polo, J.M., Guo, T., Qi, Z., Downey, S.L., Manos, P.D., Rossi, D.J.*, et al.* (2011). Incomplete DNA methylation underlies a transcriptional memory of somatic cells in human iPS cells. Nat Cell Biol *13*, 541-549.

Ohnishi, T., Yanazawa, M., Sasahara, T., Kitamura, Y., Hiroaki, H., Fukazawa, Y., Kii, I., Nishiyama, T., Kakita, A., Takeda, H.*, et al.* (2015). Na, K-ATPase alpha3 is a death target of Alzheimer patient amyloid-beta assembly. Proc Natl Acad Sci U S A *112*, E4465-4474.

Okita, K., Ichisaka, T., and Yamanaka, S. (2007). Generation of germline-competent induced pluripotent stem cells. Nature *448*, 313-317.

Okita, K., Matsumura, Y., Sato, Y., Okada, A., Morizane, A., Okamoto, S., Hong, H., Nakagawa, M., Tanabe, K., Tezuka, K.*, et al.* (2011). A more efficient method to generate integration-free human iPS cells. Nat Methods *8*, 409-412.

Oliveira, M.S., Furian, A.F., Rambo, L.M., Ribeiro, L.R., Royes, L.F., Ferreira, J., Calixto, J.B., Otalora, L.F., Garrido-Sanabria, E.R., and Mello, C.F. (2009). Prostaglandin E2 modulates Na+,K+-ATPase activity in rat hippocampus: implications for neurological diseases. J Neurochem *109*, 416-426.

Onos, K.D., Sukoff Rizzo, S.J., Howell, G.R., and Sasner, M. (2016). Toward more predictive genetic mouse models of Alzheimer's disease. Brain Res Bull *122*, 1-11.

Ormond, K.E., Bombard, Y., Bonham, V.L., Hoffman-Andrews, L., Howard, H., Isasi, R., Musunuru, K., Riggan, K.A., Michie, M., and Allyse, M. (2019). The clinical application of gene editing: ethical and social issues. Per Med *16*, 337-350.

Paciorkowski, A.R., McDaniel, S.S., Jansen, L.A., Tully, H., Tuttle, E., Ghoneim, D.H., Tupal, S., Gunter, S.A., Vasta, V., Zhang, Q.*, et al.* (2015). Novel mutations in ATP1A3 associated with catastrophic early life epilepsy, episodic prolonged apnea, and postnatal microcephaly. Epilepsia *56*, 422-430.

Palladino, M.J., Bower, J.E., Kreber, R., and Ganetzky, B. (2003). Neural dysfunction and neurodegeneration in Drosophila Na+/K+ ATPase alpha subunit mutants. J Neurosci *23*, 1276-1286.

Panagiotakaki, E., De Grandis, E., Stagnaro, M., Heinzen, E.L., Fons, C., Sisodiya, S., de Vries, B., Goubau, C., Weckhuysen, S., Kemlink, D.*, et al.* (2015). Clinical profile of patients with ATP1A3 mutations in Alternating Hemiplegia of Childhood-a study of 155 patients. Orphanet J Rare Dis *10*, 123.

Panagiotakaki, E., Gobbi, G., Neville, B., Ebinger, F., Campistol, J., Nevsimalova, S., Laan, L., Casaer, P., Spiel, G., Giannotta, M.*, et al.* (2010). Evidence of a non-progressive course of alternating hemiplegia of childhood: study of a large cohort of children and adults. Brain *133*, 3598-3610.

Paquet, D., Kwart, D., Chen, A., Sproul, A., Jacob, S., Teo, S., Olsen, K.M., Gregg, A., Noggle, S., and Tessier-Lavigne, M. (2016). Efficient introduction of specific homozygous and heterozygous mutations using CRISPR/Cas9. Nature *533*, 125-129.

Pasca, A.M., Park, J.Y., Shin, H.W., Qi, Q., Revah, O., Krasnoff, R., O'Hara, R., Willsey, A.J., Palmer, T.D., and Pasca, S.P. (2019). Human 3D cellular model of hypoxic brain injury of prematurity. Nat Med *25*, 784-791.

Pedemonte, C.H., and Kaplan, J.H. (1992). A monosaccharide is bound to the sodium pump alpha-subunit. Biochemistry *31*, 10465-10470.

Pedemonte, C.H., Sachs, G., and Kaplan, J.H. (1990). An intrinsic membrane glycoprotein with cytosolically oriented n-linked sugars. Proc Natl Acad Sci U S A *87*, 9789-9793.

Perel, P., Roberts, I., Sena, E., Wheble, P., Briscoe, C., Sandercock, P., Macleod, M., Mignini, L.E., Jayaram, P., and Khan, K.S. (2007). Comparison of treatment effects between animal experiments and clinical trials: systematic review. BMJ *334*, 197.

Peres, F.F., Lima, A.C., Hallak, J.E.C., Crippa, J.A., Silva, R.H., and Abilio, V.C. (2018). Cannabidiol as a Promising Strategy to Treat and Prevent Movement Disorders? Front Pharmacol *9*, 482.

Perrin, S. (2014). Preclinical research: Make mouse studies work. Nature *507*, 423-425.

Pisciotta, L., Gherzi, M., Stagnaro, M., Calevo, M.G., Giannotta, M., Vavassori, M.R., Veneselli, E., Consortium, I.B.A., and De Grandis, E. (2017). Alternating Hemiplegia of Childhood: Pharmacological treatment of 30 Italian patients. Brain Dev *39*, 521-528.

Pivovarov, A.S., Calahorro, F., and Walker, R.J. (2018). Na(+)/K(+)-pump and neurotransmitter membrane receptors. Invert Neurosci *19*, 1.

Post, R.L., Hegyvary, C., and Kume, S. (1972). Activation by adenosine triphosphate in the phosphorylation kinetics of sodium and potassium ion transport adenosine triphosphatase. J Biol Chem *247*, 6530-6540.

Poulsen, H., Khandelia, H., Morth, J.P., Bublitz, M., Mouritsen, O.G., Egebjerg, J., and Nissen, P. (2010a). Neurological disease mutations compromise a C-terminal ion pathway in the Na(+)/K(+)-ATPase. Nature *467*, 99-102.

Poulsen, H., Morth, P., Egebjerg, J., and Nissen, P. (2010b). Phosphorylation of the Na+,K+-ATPase and the H+,K+-ATPase. FEBS Lett *584*, 2589-2595.

Price, E.M., Rice, D.A., and Lingrel, J.B. (1990). Structure-function studies of Na,K-ATPase. Site-directed mutagenesis of the border residues from the H1-H2 extracellular domain of the alpha subunit. J Biol Chem *265*, 6638-6641.

Purcell, S.M., Moran, J.L., Fromer, M., Ruderfer, D., Solovieff, N., Roussos, P., O'Dushlaine, C., Chambert, K., Bergen, S.E., Kahler, A.*, et al.* (2014). A polygenic burden of rare disruptive mutations in schizophrenia. Nature *506*, 185-190.

Qi, Y., Zhang, X.J., Renier, N., Wu, Z., Atkin, T., Sun, Z., Ozair, M.Z., Tchieu, J., Zimmer, B., Fattahi, F.*, et al.* (2017). Combined small-molecule inhibition accelerates the derivation of functional cortical neurons from human pluripotent stem cells. Nat Biotechnol *35*, 154-163.

Qian, X., Song, H., and Ming, G.L. (2019). Brain organoids: advances, applications and challenges. Development *146*.

Ramme, A.P., Koenig, L., Hasenberg, T., Schwenk, C., Magauer, C., Faust, D., Lorenz, A.K., Krebs, A.C., Drewell, C., Schirrmann, K.*, et al.* (2019). Autologous induced pluripotent stem cell-derived four-organ-chip. Future Sci OA *5*, FSO413.

Ran, F.A., Hsu, P.D., Wright, J., Agarwala, V., Scott, D.A., and Zhang, F. (2013). Genome engineering using the CRISPR-Cas9 system. Nat Protoc *8*, 2281-2308.

Reinhard, L., Tidow, H., Clausen, M.J., and Nissen, P. (2013). Na(+),K (+)-ATPase as a docking station: protein-protein complexes of the Na(+),K (+)-ATPase. Cell Mol Life Sci *70*, 205-222.

Richards, K.S., Bommert, K., Szabo, G., and Miles, R. (2007). Differential expression of Na+/K+-ATPase alpha-subunits in mouse hippocampal interneurones and pyramidal cells. J Physiol *585*, 491-505.

Ridge, K.M., Dada, L., Lecuona, E., Bertorello, A.M., Katz, A.I., Mochly-Rosen, D., and Sznajder, J.I. (2002). Dopamine-induced exocytosis of Na,K-ATPase is dependent on activation of protein kinase C-epsilon and -delta. Mol Biol Cell *13*, 1381-1389.

Rose, E.M., Koo, J.C., Antflick, J.E., Ahmed, S.M., Angers, S., and Hampson, D.R. (2009). Glutamate transporter coupling to Na,K-ATPase. J Neurosci *29*, 8143-8155.

Rosewich, H., Ohlenbusch, A., Huppke, P., Schlotawa, L., Baethmann, M., Carrilho, I., Fiori, S., Lourenco, C.M., Sawyer, S., Steinfeld, R.*, et al.* (2014a). The expanding clinical and genetic spectrum of ATP1A3-related disorders. Neurology *82*, 945-955.

Rosewich, H., Thiele, H., Ohlenbusch, A., Maschke, U., Altmuller, J., Frommolt, P., Zirn, B., Ebinger, F., Siemes, H., Nurnberg, P.*, et al.* (2012). Heterozygous de-novo mutations in ATP1A3 in patients with alternating hemiplegia of childhood: a whole-exome sequencing gene-identification study. Lancet Neurol *11*, 764-773.

Rosewich, H., Weise, D., Ohlenbusch, A., Gartner, J., and Brockmann, K. (2014b). Phenotypic overlap of alternating hemiplegia of childhood and CAPOS syndrome. Neurology *83*, 861-863.

Roubergue, A., Philibert, B., Gautier, A., Kuster, A., Markowicz, K., Billette de Villemeur, T., Vuillaumier-Barrot, S., Nicole, S., Roze, E., and Doummar, D. (2015). Excellent response to a ketogenic diet in a patient with alternating hemiplegia of childhood. JIMD Rep *15*, 7-12.

Ryan, D., Drysdale, A.J., Lafourcade, C., Pertwee, R.G., and Platt, B. (2009). Cannabidiol targets mitochondria to regulate intracellular Ca2+ levels. J Neurosci *29*, 2053-2063.

Sabouraud, P., Riquet, A., Spitz, M.A., Deiva, K., Nevsimalova, S., Mignot, C., Lesca, G., Bednarek, N., Doummar, D., Pietrement, C.*, et al.* (2019). Relapsing encephalopathy with cerebellar ataxia are caused by variants involving p.Arg756 in ATP1A3. Eur J Paediatr Neurol *23*, 448-455.

Saha, K., and Jaenisch, R. (2009). Technical challenges in using human induced pluripotent stem cells to model disease. Cell Stem Cell *5*, 584-595.

Sances, S., Bruijn, L.I., Chandran, S., Eggan, K., Ho, R., Klim, J.R., Livesey, M.R., Lowry, E., Macklis, J.D., Rushton, D.*, et al.* (2016). Modeling ALS with motor neurons derived from human induced pluripotent stem cells. Nat Neurosci *19*, 542-553.

Sasaki, M., Ishii, A., Saito, Y., and Hirose, S. (2017). Progressive Brain Atrophy in Alternating Hemiplegia of Childhood. Mov Disord Clin Pract *4*, 406-411.

Sasaki, M., Ishii, A., Saito, Y., Morisada, N., Iijima, K., Takada, S., Araki, A., Tanabe, Y., Arai, H., Yamashita, S.*, et al.* (2014). Genotype-phenotype correlations in alternating hemiplegia of childhood. Neurology *82*, 482-490.

Sasaki, M., Sakuma, H., Fukushima, A., Yamada, K., Ohnishi, T., and Matsuda, H. (2009). Abnormal cerebral glucose metabolism in alternating hemiplegia of childhood. Brain Dev *31*, 20-26.

Sasaki, M., Sakuragawa, N., and Osawa, M. (2001). Long-term effect of flunarizine on patients with alternating hemiplegia of childhood in Japan. Brain Dev *23*, 303-305.

Sauter, E.J., Kutsche, L.K., Klapper, S.D., and Busskamp, V. (2019). Induced Neurons for the Study of Neurodegenerative and Neurodevelopmental Disorders. Methods Mol Biol *1942*, 101-121.

Schlingmann, K.P., Bandulik, S., Mammen, C., Tarailo-Graovac, M., Holm, R., Baumann, M., Konig, J., Lee, J.J.Y., Drogemoller, B., Imminger, K.*, et al.* (2018). Germline De Novo Mutations in ATP1A1 Cause Renal Hypomagnesemia, Refractory Seizures, and Intellectual Disability. Am J Hum Genet *103*, 808-816.

Schutte, R.J., Xie, Y., Ng, N.N., Figueroa, P., Pham, A.T., and O'Dowd, D.K. (2018). Astrocyte-enriched feeder layers from cryopreserved cells support differentiation of spontaneously active networks of human iPSC-derived neurons. J Neurosci Methods *294*, 91-101.

Schwinger, R.H., Bundgaard, H., Muller-Ehmsen, J., and Kjeldsen, K. (2003). The Na, K-ATPase in the failing human heart. Cardiovasc Res *57*, 913-920.

Scott, K.A., Dalgleish, A.G., and Liu, W.M. (2017). Anticancer effects of phytocannabinoids used with chemotherapy in leukaemia cells can be improved by altering the sequence of their administration. Int J Oncol *51*, 369-377.

Scudellari, M. (2016). How iPS cells changed the world. Nature *534*, 310-312.

Selvakumar, P., Owens, T.A., David, J.M., Petrelli, N.J., Christensen, B.C., Lakshmikuttyamma, A., and Rajasekaran, A.K. (2014). Epigenetic silencing of Na,K-ATPase beta 1 subunit gene ATP1B1 by methylation in clear cell renal cell carcinoma. Epigenetics *9*, 579-586.

Seok, J., Warren, H.S., Cuenca, A.G., Mindrinos, M.N., Baker, H.V., Xu, W., Richards, D.R., McDonald-Smith, G.P., Gao, H., Hennessy, L.*, et al.* (2013). Genomic responses in mouse models poorly mimic human inflammatory diseases. Proc Natl Acad Sci U S A *110*, 3507-3512.

Severino, M., Pisciotta, L., Tortora, D., Toselli, B., Stagnaro, M., Cordani, R., Morana, G., Zicca, A., Kotzeva, S., Zanaboni, C.*, et al.* (2020). White matter and cerebellar involvement in alternating hemiplegia of childhood. J Neurol.

Shafer, M.E., Mayfield, J.W., and McDonald, F. (2005). Alternating hemiplegia of childhood: a study of neuropsychological functioning. Appl Neuropsychol *12*, 49-56.

Shamraj, O.I., Grupp, I.L., Grupp, G., Melvin, D., Gradoux, N., Kremers, W., Lingrel, J.B., and De Pover, A. (1993). Characterisation of Na/K-ATPase, its isoforms, and the inotropic response to ouabain in isolated failing human hearts. Cardiovasc Res *27*, 2229-2237.

Sheridan, C. (2017). CRISPR therapeutics push into human testing. Nat Biotechnol *35*, 3-5.

Shi, Y., Inoue, H., Wu, J.C., and Yamanaka, S. (2017). Induced pluripotent stem cell technology: a decade of progress. Nat Rev Drug Discov *16*, 115-130.

Shi, Y., Kirwan, P., and Livesey, F.J. (2012a). Directed differentiation of human pluripotent stem cells to cerebral cortex neurons and neural networks. Nat Protoc *7*, 1836-1846.

Shi, Y., Kirwan, P., Smith, J., Robinson, H.P., and Livesey, F.J. (2012b). Human cerebral cortex development from pluripotent stem cells to functional excitatory synapses. Nat Neurosci *15*, 477-486, S471.

Shinoda, T., Ogawa, H., Cornelius, F., and Toyoshima, C. (2009). Crystal structure of the sodium-potassium pump at 2.4 A resolution. Nature *459*, 446-450.

Shrivastava, A.N., Redeker, V., Fritz, N., Pieri, L., Almeida, L.G., Spolidoro, M., Liebmann, T., Bousset, L., Renner, M., Lena, C.*, et al.* (2015). alpha-synuclein assemblies sequester neuronal alpha3-Na+/K+-ATPase and impair Na+ gradient. EMBO J *34*, 2408-2423.

Shrivastava, A.N., Redeker, V., Pieri, L., Bousset, L., Renner, M., Madiona, K., Mailhes-Hamon, C., Coens, A., Buee, L., Hantraye, P.*, et al.* (2019). Clustering of Tau fibrils impairs the synaptic composition of alpha3-Na(+)/K(+)-ATPase and AMPA receptors. EMBO J *38*.

Shrivastava, A.N., Triller, A., and Melki, R. (2018). Cell biology and dynamics of Neuronal Na(+)/K(+)-ATPase in health and diseases. Neuropharmacology, 107461.

Silver, K., and Andermann, F. (1993). Alternating hemiplegia of childhood: a study of 10 patients and results of flunarizine treatment. Neurology *43*, 36-41.

Simmons, C.Q., Thompson, C.H., Cawthon, B.E., Westlake, G., Swoboda, K.J., Kiskinis, E., Ess, K.C., and George, A.L., Jr. (2018). Direct evidence of impaired neuronal Na/K-ATPase pump function in alternating hemiplegia of childhood. Neurobiol Dis *115*, 29-38.

Sival, D.A., Vansenne, F., Van der Hout, A.H., Tijssen, M.A.J., and de Koning, T.J. (2018). Fever-Induced Paroxysmal Weakness and Encephalopathy (FIPWE)-Part of a Phenotypic Continuum in Patients With ATP1A3 Mutations? Pediatr Neurol *81*, 57-58.

Skou, J.C. (1957). The influence of some cations on an adenosine triphosphatase from peripheral nerves. Biochim Biophys Acta *23*, 394-401.

Smedemark-Margulies, N., Brownstein, C.A., Vargas, S., Tembulkar, S.K., Towne, M.C., Shi, J., Gonzalez-Cuevas, E., Liu, K.X., Bilguvar, K., Kleiman, R.J.*, et al.* (2016). A novel de novo mutation in ATP1A3 and childhood-onset schizophrenia. Cold Spring HarbMol CaseStud *2*, a001008.

Smith, N.A., Kress, B.T., Lu, Y., Chandler-Militello, D., Benraiss, A., and Nedergaard, M. (2018). Fluorescent Ca(2+) indicators directly inhibit the Na,K-ATPase and disrupt cellular functions. Sci Signal *11*.

Spiller, S., and Friedrich, T. (2014). Functional analysis of human Na(+)/K(+)-ATPase familial or sporadic hemiplegic migraine mutations expressed in Xenopus oocytes. World J Biol Chem *5*, 240-253.

Stadtfeld, M., and Hochedlinger, K. (2010). Induced pluripotency: history, mechanisms, and applications. Genes Dev *24*, 2239-2263.

Staerk, J., Dawlaty, M.M., Gao, Q., Maetzel, D., Hanna, J., Sommer, C.A., Mostoslavsky, G., and Jaenisch, R. (2010). Reprogramming of human peripheral blood cells to induced pluripotent stem cells. Cell Stem Cell *7*, 20-24.

Sternberger, L.A., and Sternberger, N.H. (1983). Monoclonal antibodies distinguish phosphorylated and nonphosphorylated forms of neurofilaments in situ. Proc Natl Acad Sci U S A *80*, 6126-6130.

Studer, L., Vera, E., and Cornacchia, D. (2015). Programming and Reprogramming Cellular Age in the Era of Induced Pluripotency. Cell Stem Cell *16*, 591-600.

Sugimoto, H., Ikeda, K., and Kawakami, K. (2014). Heterozygous mice deficient in Atp1a3 exhibit motor deficits by chronic restraint stress. Behav Brain Res *272*, 100-110.

Sweadner, K.J., Arystarkhova, E., Penniston, J.T., Swoboda, K.J., Brashear, A., and Ozelius, L.J. (2019). Genotype-structure-phenotype relationships diverge in paralogs ATP1A1, ATP1A2, and ATP1A3. Neurol Genet *5*, e303.

Sweadner, K.J., Herrera, V.L., Amato, S., Moellmann, A., Gibbons, D.K., and Repke, K.R. (1994). Immunologic identification of Na+,K(+)-ATPase isoforms in myocardium. Isoform change in deoxycorticosterone acetate-salt hypertension. Circ Res *74*, 669-678.

Sweadner, K.J., and Rael, E. (2000). The FXYD gene family of small ion transport regulators or channels: cDNA sequence, protein signature sequence, and expression. Genomics *68*, 41-56.

Sweney, M.T., Newcomb, T.M., and Swoboda, K.J. (2015). The expanding spectrum of neurological phenotypes in children with ATP1A3 mutations, Alternating Hemiplegia of Childhood, Rapid-onset Dystonia-Parkinsonism, CAPOS and beyond. Pediatr Neurol *52*, 56-64.

Sweney, M.T., Silver, K., Gerard-Blanluet, M., Pedespan, J.M., Renault, F., Arzimanoglou, A., Schlesinger-Massart, M., Lewelt, A.J., Reyna, S.P., and Swoboda, K.J. (2009). Alternating hemiplegia of childhood: early characteristics and evolution of a neurodevelopmental syndrome. Pediatrics *123*, e534-e541.

Szaflarski, J.P., and Bebin, E.M. (2014). Cannabis, cannabidiol, and epilepsy--from receptors to clinical response. Epilepsy Behav *41*, 277-282.

Takahashi, K., and Yamanaka, S. (2006). Induction of pluripotent stem cells from mouse embryonic and adult fibroblast cultures by defined factors. Cell *126*, 663-676.

Takata, A., Miyake, N., Tsurusaki, Y., Fukai, R., Miyatake, S., Koshimizu, E., Kushima, I., Okada, T., Morikawa, M., Uno, Y.*, et al.* (2018). Integrative Analyses of De Novo Mutations Provide Deeper Biological Insights into Autism Spectrum Disorder. Cell Rep *22*, 734-747.

Tang, Y., Liu, M.L., Zang, T., and Zhang, C.L. (2017). Direct Reprogramming Rather than iPSC-Based Reprogramming Maintains Aging Hallmarks in Human Motor Neurons. Front Mol Neurosci *10*, 359.

Taniguchi, K., Kaya, S., Abe, K., and Mardh, S. (2001). The oligomeric nature of Na/K-transport ATPase. J Biochem *129*, 335-342.

Tau, G.Z., and Peterson, B.S. (2010). Normal development of brain circuits. Neuropsychopharmacology *35*, 147-168.

Telias, M., Segal, M., and Ben-Yosef, D. (2014). Electrical maturation of neurons derived from human embryonic stem cells. F1000Res *3*, 196.

Thomas, A., Baillie, G.L., Phillips, A.M., Razdan, R.K., Ross, R.A., and Pertwee, R.G. (2007). Cannabidiol displays unexpectedly high potency as an antagonist of CB1 and CB2 receptor agonists in vitro. Br J Pharmacol *150*, 613-623.

Thomson, J.A., Itskovitz-Eldor, J., Shapiro, S.S., Waknitz, M.A., Swiergiel, J.J., Marshall, V.S., and Jones, J.M. (1998). Embryonic stem cell lines derived from human blastocysts. Science *282*, 1145-1147.

Tian, R., Gachechiladze, M.A., Ludwig, C.H., Laurie, M.T., Hong, J.Y., Nathaniel, D., Prabhu, A.V., Fernandopulle, M.S., Patel, R., Abshari, M.*, et al.* (2019). CRISPR Interference-Based Platform for Multimodal Genetic Screens in Human iPSC-Derived Neurons. Neuron *104*, 239-255 e212.

Tiziano, F.D. (2019). Human neuroblastoma model of AHC: towards a medium throughput screening of candidate therapeutic compounds. Paper presented at: 8th Symposium on ATP1A3 in Disesae (Reykjavik, Iceland).

Tokhtaeva, E., Clifford, R.J., Kaplan, J.H., Sachs, G., and Vagin, O. (2012). Subunit isoform selectivity in assembly of Na,K-ATPase alpha-beta heterodimers. J Biol Chem *287*, 26115-26125.

Tokhtaeva, E., Munson, K., Sachs, G., and Vagin, O. (2010). N-glycan-dependent quality control of the Na,K-ATPase beta(2) subunit. Biochemistry *49*, 3116-3128.

Torres, A., Brownstein, C.A., Tembulkar, S.K., Graber, K., Genetti, C., Kleiman, R.J., Sweadner, K.J., Mavros, C., Liu, K.X., Smedemark-Margulies, N.*, et al.* (2018). De novo ATP1A3 and compound heterozygous NLRP3 mutations in a child with autism spectrum disorder, episodic fatigue and somnolence, and muckle-wells syndrome. Mol Genet Metab Rep *16*, 23-29.

Toustrup-Jensen, M.S., Einholm, A.P., Schack, V.R., Nielsen, H.N., Holm, R., Sobrido, M.J., Andersen, J.P., Clausen, T., and Vilsen, B. (2014). Relationship between intracellular Na+ concentration and reduced Na+ affinity in Na+,K+-ATPase mutants causing neurological disease. J Biol Chem *289*, 3186-3197.

Toyoshima, C., Kanai, R., and Cornelius, F. (2011). First crystal structures of Na+,K+-ATPase: new light on the oldest ion pump. Structure *19*, 1732-1738.

Toyoshima, C., Nakasako, M., Nomura, H., and Ogawa, H. (2000). Crystal structure of the calcium pump of sarcoplasmic reticulum at 2.6 A resolution. Nature *405*, 647-655.

Uhlen, M., Bandrowski, A., Carr, S., Edwards, A., Ellenberg, J., Lundberg, E., Rimm, D.L., Rodriguez, H., Hiltke, T., Snyder, M.*, et al.* (2016). A proposal for validation of antibodies. Nat Methods *13*, 823-827.

Urayama, O., and Sweadner, K.J. (1988). Ouabain sensitivity of the alpha 3 isozyme of rat Na,K-ATPase. Biochem Biophys Res Commun *156*, 796-800.

Vaillend, C., Mason, S.E., Cuttle, M.F., and Alger, B.E. (2002). Mechanisms of neuronal hyperexcitability caused by partial inhibition of Na+-K+-ATPases in the rat CA1 hippocampal region. J Neurophysiol *88*, 2963-2978.

van den Ameele, J., Tiberi, L., Vanderhaeghen, P., and Espuny-Camacho, I. (2014). Thinking out of the dish: what to learn about cortical development using pluripotent stem cells. Trends Neurosci *37*, 334-342.

Vatine, G.D., Barrile, R., Workman, M.J., Sances, S., Barriga, B.K., Rahnama, M., Barthakur, S., Kasendra, M., Lucchesi, C., Kerns, J.*, et al.* (2019). Human iPSC-Derived Blood-Brain Barrier Chips Enable Disease Modeling and Personalized Medicine Applications. Cell Stem Cell *24*, 995-1005 e1006.

Vedovato, N., and Gadsby, D.C. (2014). Route, mechanism, and implications of proton import during Na+/K+ exchange by native Na+/K+-ATPase pumps. J Gen Physiol *143*, 449-464.

Venteo, S., Bourane, S., Mechaly, I., Sar, C., Abdel Samad, O., Puech, S., Blostein, R., Valmier, J., Pattyn, A., and Carroll, P. (2012). Regulation of the Na,K-ATPase gamma-subunit FXYD2 by Runx1 and Ret signaling in normal and injured non-peptidergic nociceptive sensory neurons. PLoS One *7*, e29852.

Vera, E., Bosco, N., and Studer, L. (2016). Generating Late-Onset Human iPSC-Based Disease Models by Inducing Neuronal Age-Related Phenotypes through Telomerase Manipulation. Cell Rep *17*, 1184-1192.

Verret, S., and Steele, J.C. (1971). Alternating hemiplegia in childhood: a report of eight patients with complicated migraine beginning in infancy. Pediatrics *47*, 675-680.

Vila-Pueyo, M., Pons, R., Raspall-Chaure, M., Marce-Grau, A., Carreno, O., Sintas, C., Cormand, B., Pineda-Marfa, M., and Macaya, A. (2014). Clinical and genetic analysis in alternating hemiplegia of childhood: ten new patients from Southern Europe. J Neurol Sci *344*, 37-42.

Vinciguerra, M., Deschenes, G., Hasler, U., Mordasini, D., Rousselot, M., Doucet, A., Vandewalle, A., Martin, P.Y., and Feraille, E. (2003). Intracellular Na+ controls cell surface expression of Na,K-ATPase via a cAMP-independent PKA pathway in mammalian kidney collecting duct cells. Mol Biol Cell *14*, 2677-2688.

Viollet, L., Glusman, G., Murphy, K.J., Newcomb, T.M., Reyna, S.P., Sweney, M., Nelson, B., Andermann, F., Andermann, E., Acsadi, G.*, et al.* (2015). Alternating Hemiplegia of Childhood: Retrospective Genetic Study and Genotype-Phenotype Correlations in 187 Subjects from the US AHCF Registry. PLoS One *10*, e0127045.

Virgadamo, S., Charnigo, R., Darrat, Y., Morales, G., and Elayi, C.S. (2015). Digoxin: A systematic review in atrial fibrillation, congestive heart failure and post myocardial infarction. World J Cardiol *7*, 808-816.

Vuillaumier-Barrot, S., Panagiotakaki, E., Le Bizec, C., El Baba, C., Consortium, E.N.f.S., Fontaine, B., Arzimanoglou, A., Seta, N., and Nicole, S. (2010). Absence of mutation in the SLC2A1 gene in a cohort of patients with alternating hemiplegia of childhood (AHC). Neuropediatrics *41*, 267-269.

Wang, G., Kawakami, K., and Gick, G. (2007). Divergent signaling pathways mediate induction of Na,K-ATPase alpha1 and beta1 subunit gene transcription by low potassium. Mol Cell Biochem *294*, 73-85.

Wang, J., Velotta, J.B., McDonough, A.A., and Farley, R.A. (2001). All human Na(+)-K(+)-ATPase alpha-subunit isoforms have a similar affinity for cardiac glycosides. Am J Physiol Cell Physiol *281*, C1336-1343.

Warren, L., Manos, P.D., Ahfeldt, T., Loh, Y.H., Li, H., Lau, F., Ebina, W., Mandal, P.K., Smith, Z.D., Meissner, A.*, et al.* (2010). Highly efficient reprogramming to pluripotency and directed differentiation of human cells with synthetic modified mRNA. Cell Stem Cell *7*, 618-630.

Weaver, C.D., Harden, D., Dworetzky, S.I., Robertson, B., and Knox, R.J. (2004). A thallium-sensitive, fluorescence-based assay for detecting and characterizing potassium channel modulators in mammalian cells. J Biomol Screen *9*, 671-677.

Weigand, K.M., Messchaert, M., Swarts, H.G., Russel, F.G., and Koenderink, J.B. (2014). Alternating hemiplegia of childhood mutations have a differential effect on Na + ,K + -ATPase activity and ouabain binding. BiochimBiophysActa *1842*, 1010-1016.

Wernig, M., Meissner, A., Foreman, R., Brambrink, T., Ku, M., Hochedlinger, K., Bernstein, B.E., and Jaenisch, R. (2007). In vitro reprogramming of fibroblasts into a pluripotent ES-cell-like state. Nature *448*, 318-324.

Williams, D.A. (2009). National Institutes of Health releases new guidelines on human stem cell research. Mol Ther *17*, 1485-1486.

Wilson, S.W., and Houart, C. (2004). Early steps in the development of the forebrain. Dev Cell *6*, 167-181.

Xiao, A.Y., Wei, L., Xia, S., Rothman, S., and Yu, S.P. (2002). Ionic mechanism of ouabain-induced concurrent apoptosis and necrosis in individual cultured cortical neurons. J Neurosci *22*, 1350-1362.

Xiao, B., Zhang, Y., Niu, W., Gao, P., and Zhu, D. (2009). Association of ATP1B1 single-nucleotide polymorphisms with blood pressure and hypertension in a Chinese population. Clin Chim Acta *407*, 47-50.

Xie, Y., Schutte, R.J., Ng, N.N., Ess, K.C., Schwartz, P.H., and O'Dowd, D.K. (2018). Reproducible and efficient generation of functionally active neurons from human hiPSCs for preclinical disease modeling. Stem Cell Res *26*, 84-94.

Yang, N., Chanda, S., Marro, S., Ng, Y.H., Janas, J.A., Haag, D., Ang, C.E., Tang, Y., Flores, Q., Mall, M.*, et al.* (2017). Generation of pure GABAergic neurons by transcription factor programming. Nat Methods *14*, 621-628.

Yang, X., Gao, H., Zhang, J., Xu, X., Liu, X., Wu, X., Wei, L., and Zhang, Y. (2014). ATP1A3 mutations and genotype-phenotype correlation of alternating hemiplegia of childhood in Chinese patients. PLoS One *9*, e97274.

Yano, S.T., Silver, K., Young, R., DeBrosse, S.D., Ebel, R.S., Swoboda, K.J., and Acsadi, G. (2017). Fever-induced parosysmal weakness and encephalopathy, a new phenotype of ATP1A3 mutation. Pediatr Neurol *73*, 101-105.

Ye, Q., Yan, L.Y., Xue, L.J., Wang, Q., Zhou, Z.K., Xiao, H., and Wan, Q. (2011). Flunarizine blocks voltage-gated Na(+) and Ca(2+) currents in cultured rat cortical neurons: A possible locus of action in the prevention of migraine. Neurosci Lett *487*, 394-399.

Zhang, D., Hou, Q., Wang, M., Lin, A., Jarzylo, L., Navis, A., Raissi, A., Liu, F., and Man, H.Y. (2009). Na,K-ATPase activity regulates AMPA receptor turnover through proteasome-mediated proteolysis. J Neurosci *29*, 4498-4511.

Zhang, Y., Pak, C., Han, Y., Ahlenius, H., Zhang, Z., Chanda, S., Marro, S., Patzke, C., Acuna, C., Covy, J.*, et al.* (2013a). Rapid single-step induction of functional neurons from human pluripotent stem cells. Neuron *78*, 785-798.

Zhang, Y., Pak, C., Han, Y., Ahlenius, H., Zhang, Z., Chanda, S., Marro, S., Patzke, C., Acuna, C., Covy, J.*, et al.* (2013b). Rapid Single-Step Induction of Functional Neurons from Human Pluripotent Stem Cells. Neuron *78*, 785-798.

Zhou, T., Benda, C., Dunzinger, S., Huang, Y., Ho, J.C., Yang, J., Wang, Y., Zhang, Y., Zhuang, Q., Li, Y.*, et al.* (2012). Generation of human induced pluripotent stem cells from urine samples. Nat Protoc *7*, 2080-2089.

Zirra, A., Wiethoff, S., and Patani, R. (2016). Neural Conversion and Patterning of Human Pluripotent Stem Cells: A Developmental Perspective. Stem Cells Int *2016*, 8291260.

Zou, S., and Kumar, U. (2018). Cannabinoid Receptors and the Endocannabinoid System: Signaling and Function in the Central Nervous System. Int J Mol Sci *19*.